The role of the sigma subunit of Adaptor Protein-2, AP2σ2,

in the regulation of calcium homeostasis

A thesis submitted to the University of Oxford



in candidature for the degree of Doctor of Philosophy

by

Angela Rogers MB BS BSc MRCP

Academic Endocrine Unit
Radcliffe Department of Medicine
University of Oxford

Green Templeton College
University of Oxford

Hilary Term 2016

The role of the sigma subunit of Adaptor Protein-2, AP2σ2, in the regulation of calcium homeostasis

A thesis submitted to the University of Oxford in candidature for the degree of Doctor of Philosophy by

Angela Rogers MB BS BSc MRCP
Green Templeton College
Radcliffe Department of Medicine

Hiliary Term 2016

Abstract

The calcium sensing receptor (CaSR), a G-protein coupled receptor (GPCR), and its downstream signalling pathways are essential for calcium homeostasis. Loss- or gain-of-function (LOF and GOF, respectively) mutations in components of these pathways result in disorders of calcium homeostasis including Familial hypocalciuric hypercalcaemia (FHH) and Autosomal dominant hypocalcaemia (ADH). FHH type 3 (FHH3) is due to LOF mutations in the σ2 subunit (AP2σ2) of adaptor protein-2 (AP-2). The FHH3-associated AP2σ2 mutations identified to date affect the Arg15 residue and comprise heterozygous Arg15Cys, Arg15Leu, and Arg15His mutations. AP-2 is a ubiquitously expressed heterotetrameric protein, with a central role in clathrin-mediated endocytosis of transmembrane proteins, such as GPCRs.

This thesis demonstrates that AP2σ2 mutations account for ~7% of all FHH mutations, only affect the Arg15 residue and show evidence of mutation bias, with only AP2σ2 Arg15Cys, Arg15Leu, and Arg15His mutations identified. Additionally, the study has identified *de novo* AP2σ2 mutations and revealed that FHH3 probands may present with a broader phenotype not seen in FHH1. The heterozygous missense AP2σ2 mutation was demonstrated to have no effect on the stability of the AP-2 complex *in vivo*. This thesis revealed that gain-of-function AP2σ2 mutations are unlikely to be a cause of ADH, which is due to GOF mutations in CaSR in >70% of cases.

The CaSR activates its downstream signalling pathways, including the mitogen-activated protein kinase (MAPK) pathway, through coupling with its associated G-proteins. The AP2σ2 mutations resulted in loss of activating phosphorylation events in the MAPK pathway suggesting a role for AP2σ2 in CaSR signalling. Additionally, the AP2σ2 Arg15Cys, Arg15His and Arg15Leu mutations were revealed to exert differential effects on the $G\alpha_{q/11}$ and MAPK signalling pathways, suggesting mutation-bias signalling.

Clathrin-mediated endocytosis is crucial for embryological development. This thesis has demonstrated that mice homozygous for an *Ap2s1* splice site mutation, predicted to produce a functional knock-out, were lethal before embryonic day 12.5 (E12.5), suggesting AP2σ2 is essential for cell viability in the developing embryo.

Thus, the work of this thesis has further elucidated the role of AP2σ2 in the biological pathways of CaSR signalling and clathrin-mediated endocytosis, and in the molecular pathology of disorders of calcium homeostasis.

Statement of Contribution

Treena Cranston from the Department of Clinical Genetics, Oxford University Hospitals NHS Trust performed *CASR* mutational analysis on the hypercalcaemic probands (section 4) and *CASR*, *GCMB*, and *PTH* mutational analysis on the hypocalcaemic probands (section 7). Nigel Rust at the Dunn School of Pathology, University of Oxford assisted in flow cytometry experiments (sections 3.2.5.2 and 4.1.5). Rosie Head from the University of Oxford performed the screen of the MRC Harwell ENU-mutagenised DNA archive (section 6.1.1). Sara Wells and her team at the Mary Lyon Centre, MRC Harwell performed the animal husbandry, metabolic cage studies and post-mortem preparation of tissue samples for the *Ap2s1* IVS 2+2T>C mutant mice (sections 3.2.6 and 6). Tertius Hough in the Biochemistry Department, Mary Lyon Centre, MRC Harwell analysed the murine blood and urine samples (sections 3.2.6 and 6). Lydia Tyboul and her team at the Mary Lyon Centre, MRC Harwell performed the TALENs and R15L donor matrix co-injection into the single cell BL/6J embryos and screening for potential founders, and performed the *Ap2s1* splice site homozygous mutant staged embryo analysis (sections 6.1.5.4.1 and sections 6.1.6).

Acknowledgements

I would like to thank Professor Raj Thakker for this wonderful opportunity to undertake my DPhil in the Academic Endocrine Unit. I have learnt so much from you, which I will take forward into my future career. I would like to thank Professor Roger Cox for his support and useful discussions regarding my DPhil project. I am grateful to Professors Graham Russell and Paul Wordsworth who provided invaluable feedback following my transfer viva and confirmation of status. I would also like to thank the Wellcome Trust for providing me with funding to undertake these studies.

This thesis would not have been possible were it not for the help and guidance of one fantastic scientist, Caroline M. Gorvin, to whom I will be eternally grateful. Thank you for rescuing me when I was lost in a sea of science. I would like to thank my family, especially my mum, Anna, who has always been there for me with unconditional love and support and my friends, Mimi, Jo and Simon (and gorgeous Thomas), who kept me sane. My college advisor, Lindy Castell, was always on hand with tremendously sage advice. And finally I must acknowledge two marvellous endocrinologists: Professor John Wass, who started me on the path of Endocrinology back in 2006. There are no words to express my gratitude to you; and Niki Karavitaki, your door was always open to me and you have been a pillar of support through it all.

Contents

1 Introduction 18
1.1 Distribution of calcium in the body 19
1.2 The physiological roles of calcium 21
1.3 Calcium homeostasis 23
1.4 The Calcium Sensing Receptor (CaSR) 28
1.4.1 Structure of the CaSR 28
1.4.2 The calcium sensing receptor gene, *CASR* 34
1.4.3 CaSR ligand binding and receptor activation 34
1.4.4 G-protein coupling 36
1.4.5 Orthosteric agonists and allosteric modulators of the CaSR 37
1.5 CaSR downstream signalling pathways 41
1.5.1 $G\alpha_{q/11}$ signalling 41
1.5.2 $G\alpha_{12/13}$ signalling 44
1.5.3 $G\alpha_{i/o}$ signalling 46
1.5.4 $G\alpha_{s}$ signalling 47
1.5.5 Allosteric modulators and ligand-biased signalling 48
1.5.6 Mutation-biased signalling 50
1.6 Inactivation of CaSR 52
1.7 Internalisation of CaSR 53
1.7.1 Role of Adaptor protein-2 (AP-2) in clathrin-mediated endocytosis 56
1.7.2 Role of clathrin in clathrin-mediated endocytosis 59
1.8 Trafficking of the CaSR 60
1.8.1 Post-endocytic trafficking of the CaSR 60
1.8.2 Biosynthesis of CaSR and Agonist-Driven Insertional Signalling (ADIS) 63
1.9 The physiological roles of the CaSR 65
1.9.1 The calciotropic roles of the CaSR 65
1.9.2 The non-calciotropic roles of the CaSR 72
1.9.3 The role of the CaSR in foetal development 74
1.10 Disorders of calcium homeostasis 75
1.10.1 Hypercalcaemic disorders 75
1.10.2 Hypocalcaemic disorders 80
1.11 Mouse models 84
1.11.1 Chemical mutagenesis using N-ethyl-N-nitrosourea 85
1.11.2 Targeted mutagenesis 86
1.11.3 Mouse models of disorders of calcium homeostasis associated with CaSR mutations 89

2 Study aim and objectives 94

3 Materials and methods 95
3.1 Materials 96
3.1.1 Chemicals 96
3.1.2 Oligonucleotides 96
3.1.3 Enzymes 96
3.1.4 Vectors 97
3.1.5 Buffers 97
3.2 Methods 99

3.2.1 Ethical approval for research 99
3.2.2 Protocols involving manipulation of DNA 99
3.2.3 Protocols involving manipulation of RNA 102
3.2.4 Protocols involving manipulation of protein 105
3.2.5 Protocols involving cells in culture 107
3.2.6 Protocols used for animal studies 116
3.2.7 Bioinformatic analyses 118
3.2.8 Statistical analyses 118

Genetics of AP2σ2 mutations in Familial hypocalciuric hypercalcaemia (FHH) 121

4 Genetics of AP2σ2 mutations in Familial hypocalciuric hypercalcaemia (FHH) 122
4.1.1 Biochemical features of probands investigated for AP2σ2 mutations 123
4.1.2 Identification of AP2σ2 mutations in probands with FHH 123
4.1.3 Identification of mutation bias in AP2σ2 mutations 126
4.1.4 Identification and investigation of kindreds with AP2σ2 mutations 133
4.1.5 Functional characterisation of a novel *GNA11* variant in an FHH3 proband 135
4.1.6 Identification of *GNA11* single nucleotide polymorphisms (SNPs) in hypercalcaemic probands 138
4.1.7 Effect of AP2σ2 mutation on the stability of the AP-2 complex 139
4.1.8 Discussion and future studies 144

5 The effects of AP2σ2 mutations on the mitogen-activated protein kinase (MAPK) signalling pathways 153
5.1.1 Characterisation of the functional effects of AP2σ2 mutations on phosphorylated ERK1/2 (pERK1/2) using an amplified luminescence proximity homogenous (AlphaScreen) assay 155
5.1.2 Characterisation of the functional effects of AP2σ2 mutations on target gene transcription 169
5.1.3 Characterisation of the effect of cinacalcet on the functional effects of AP2σ2 mutations 177
5.1.4 Discussion and future studies 184

***Ap2s1* mouse models 192**

6 *Ap2s1* mouse models 193
6.1.1 Strategy for the generation of *Ap2s1* mouse models 193
6.1.2 *Ap2s1* mutations identified from the MRC Harwell ENU-induced DNA archive screen 194
6.1.3 Prediction of the possible consequences of the *Ap2s1* mutations identified 195
6.1.4 Characterisation of the functional effects of the AP2σ2 Tyr20Asn mutation 198
6.1.5 Investigation of the functional effects of *Ap2s1* IVS 2+2T>C mutation *in vivo* 200
6.1.6 Generation of a knock-in mouse model harbouring a heterozygous *Ap2s1* R15L mutation 214
6.1.7 Discussion and future studies 215

7 Genetics of AP2σ2 mutations in ADH 222

7.1.1 Statistical analysis and determination of ADH proband sample size 222
7.1.2 Clinical and biochemical features of probands with ADH 224
7.1.3 Dideoxynucleotide sequence analysis in the ADH probands 226
7.1.4 Discussion and future studies.....228

8 Summary.....230

9 References.....235

10 Appendix.....254
10.1 Vector maps.....254
10.2 Primer sequences 256
10.2.1 Primers for PCR amplification and sequencing of human *AP2S1* 256
10.2.2 Primers for PCR amplification and sequencing of human *GNA11* 257
10.2.3 Primers for PCR of mouse *AP2S1* cDNA 257
10.2.4 Primers for genotyping of splice site *Ap2s1* mouse model 257
10.2.5 Primers for sequencing pCR-Blunt II-TOPO construct 258
10.2.6 Primers for sequencing pBI-CMV4 *AP2S1* construct.....258
10.2.7 Primers for sequencing pBI-CMV4 *GNA11* constructs 258
10.2.8 Primers used for site-directed mutagenesis in pBI-CMV4 *GNA11* construct.....259
10.3 Antibodies.....259
10.3.1 Primary 259
10.3.2 Secondary 260
10.4 Publications 260

List of Figures

Figure 1.1. Schematic representation of the regulation of intracellular calcium. 20
Figure 1.2. Schematic illustration of extracellular calcium homeostasis.....24
Figure 1.3. Relationship between PTH secretion and extracellular Ca^{2+} *in vivo* and *in vitro* 25
Figure 1.4. Vitamin D_3 metabolism. 27
Figure 1.5. Schematic representation of the interaction between GPCR and heterotrimeric G-protein. 30
Figure 1.6. Structure of the Class C GPCRs. 33
Figure 1.7. Schematic representation of ligand binding and activation of the CaSR. .35
Figure 1.8. Schematic representation of the secondary structure of the Gα subunit. ..37
Figure 1.9. Allosteric modulators of the CaSR and their binding sites. 40
Figure 1.10. CaSR signalling via $G\alpha_{q/11}$ coupling. 43
Figure 1.11. CaSR signalling via $G\alpha_{12/13}$ coupling. 45
Figure 1.12. CaSR signalling via $G\alpha_{i/o}$ coupling. 47
Figure 1.13. Schematic representation of multiple G-protein signalling pathways including $G\alpha_s$ coupling. 48
Figure 1.14. Schematic representation of ligand biased signalling. 49
Figure 1.15. Schematic representation of 70 naturally occurring CaSR mutations. 51
Figure 1.16. Clathrin-mediated endocytosis and retrograde trafficking. 55
Figure 1.17. Surface representation of the AP-2 core. 57
Figure 1.18. Schematic representation of the closed and open conformations of AP-2. 58
Figure 1.19. Schematic representation of the Adaptor Protein-related Complex 2 Sigma 1 Subunit gene, *AP2S1*. 59
Figure 1.20. Schematic representation of clathrin triskelia organised into a clathrin cage. 60
Figure 1.21. Non-canonical signalling of β_2-adrenergic receptor. 62
Figure 1.22. Agonist-driven insertional signalling (ADIS). 64
Figure 1.23. Schematic diagram showing the expression of CaSR in the kidney. 67
Figure 1.24. Schematic representation of an epithelial cell from the thick ascending limb of the loop of Henle. 69
Figure 1.25. Schematic representation of bone remodelling in an adult. 71
Figure 1.26. Chemical mutagenesis using N-ethyl-N-nitrosourea (ENU). 86
Figure 1.27. Genome editing using transcription activator-like effector nucleases (TALENs) technology 88
Figure 3.1. Schematic representation of flow cytometry using Indo-1-AM to measure intracellular Ca^{2+} in response to increasing concentrations of extracellular Ca^{2+}. 110
Figure 3.2. Schematic representation of the AlphaScreen mechanism of action. 112
Figure 4.1. Observed and predicted mutations at AP2σ2 R15 residue. 126
Figure 4.2. Detection of *de novo* AP2σ2 mutations. 128
Figure 4.3. Comparison of biochemical phenotypes between FHH1 and FHH3. 132
Figure 4.4. Detection of an AP2σ2 mutation in the FHHks family. 134
Figure 4.5. Multiple amino acid sequence alignment of Gα11 residue Met87 (M87) in orthologues and paralogues. 136
Figure 4.6. Intracellular calcium responses to changes in extracellular calcium in HEK293-CaSR cells transfected with Gα11 WT, M87V or empty vector, pBI-CMV4-RFP. 137
Figure 4.7. Detection of an AP2σ2 mutation in the FHH_{ok} family. 140

Figure 4.8. Quantitative RT-PCR analysis of the AP-2 subunit genes, *AP2A1, AP2B1, AP2M1* and *AP2S1,* in the lymphoblastic DNA of four affected and four unaffected members of the FHHok kindred to investigate RNA expression. 142
Figure 4.9. Western blot analysis showing expression of the AP-2 subunits in the lymphoblastoid cells from affected and unaffected members of the FHHok kindred. 143
Figure 4.10. The genetic causes of FHH.....144
Figure 5.1. Preliminary experiment to determine the effect of time interval between transfection and calcium treatment on pERK1/2 response assessed by AlphaScreen assay. 157
Figure 5.2. Preliminary experiment to determine the duration of extracellular calcium treatment required to induce maximal pERK1/2 response assessed by AlphaScreen assay. 158
Figure 5.3. Preliminary experiment to determine the effect of extracellular calcium concentration on pERK1/2 response assessed by AlphaScreen assay. 160
Figure 5.4. The effect of extracellular calcium concentration on pERK1/2 response in AP2σ2 WT and R15C cells assessed by AlphaScreen assay. 163
Figure 5.5. The effect of extracellular calcium concentration on pERK1/2 response in AP2σ2 WT and R15H cells assessed by AlphaScreen assay. 165
Figure 5.6. The effect of extracellular calcium concentration on pERK1/2 response in AP2σ2 WT and R15L cells assessed by AlphaScreen assay. 167
Figure 5.7. Normalisation of pERK1/2 responses for total ERK1/2 assessed by AlphaScreen assay. 169
Figure 5.8. The effect of extracellular calcium concentration on NFAT and SRE reporter gene expression in HEK293 cells stably expressing AP2σ2 WT assessed by dual-luciferase reporter gene assay. 171
Figure 5.9. The effect of extracellular calcium concentration on NFAT reporter activity in AP2σ2 WT and mutant cells assessed by luciferase reporter gene assay. 173
Figure 5.10. Western blot analysis of the expression of CaSR in AP2σ2 WT and AP2σ2 mutant cell lysates used in the luciferase reporter gene assays. 174
Figure 5.11. The effect of extracellular calcium concentration on SRE reporter activity in AP2σ2 WT and mutant cells assessed by luciferase reporter gene assay. 176
Figure 5.12. Preliminary experiment to determine the effect of cinacalcet concentration and duration of treatment on NFAT reporter gene expression in HEK293 cells transiently transfected with CaSR assessed by dual-luciferase reporter gene assay. 180
Figure 5.13. The effect of 20nM cinacalcet on NFAT and SRE reporter gene expression in AP2σ2 WT and mutant cells assessed by luciferase reporter gene assay. 183
Figure 5.14. Bias plot showing the effects of the AP2σ2 mutations on differential coupling of the CaSR. 187
Figure 6.1. Schematic diagram showing the *Ap2s1* mutations identified by a genotype-driven screen of the MRC Harwell ENU-induced DNA archive. 194
Figure 6.2. Structural modelling of AP2σ2 WT, AP2σ2 Tyr20Asn and AP2σ2 Ile123Asn. 195
Figure 6.3. Predicted consequences of the *Ap2s1* IVS 2+2T>C mutation. 197
Figure 6.4. Intracellular calcium responses to changes in extracellular calcium of HEK293-CaSR cells transfected with AP2σ2 WT, Y20N or empty vector, pBI-CMV4-RFP. 199

Figure 6.5. Outcome of the *Ap2s1* IVS 2+2T>C mutation at the genomic level in the heterozygous ENU-mutagenised mice. 201
Figure 6.6. Structural modelling of AP2σ2 WT and AP2σ2 splice site mutant proteins. 202
Figure 6.7. Pedigree of *Ap2s1* IVS 2+2T>C mice. 203
Figure 6.8. Plasma biochemistry of 12 week old *Ap2s1* IVS 2+2T>C $Ap2s1^{+/+}$ and $Ap2s1^{+/-}$ mice from metabolic cage studies. 207
Figure 6.9. Urinary biochemistry of *Ap2s1* IVS 2+2T>C $Ap2s1^{+/+}$ and $Ap2s1^{+/-}$ mice at 12 weeks of age obtained from metabolic cage studies. 208
Figure 6.10. RT-qPCR analysis of the AP-2 subunit genes, *Ap2a1*, *Ap2b1*, *Ap2m1* and *Ap2s1*, in the kidney lysates of four $Ap2s1^{+/+}$ and $Ap2s1^{+/-}$ mice to investigate RNA expression. 210
Figure 6.11. Western blot analysis showing expression of the AP-2 subunits in the kidney lysates of four $Ap2s1^{+/+}$ and $Ap2s1^{+/-}$ mice. 211
Figure 6.12. Gross morphological appearances of E12.5 $Ap2s1^{+/+}$ and $Ap2s1^{-/-}$ embryos. 213
Figure 6.13. Amino acid residue conservation between APσ orthologues and paralogues. 217
Figure 6.14. Structural modelling of mutant and WT AP2σ2 showing altered positions of the residues involved in binding to the dileucine motifs in transmembrane proteins. 218
Figure 7.1. Binomial probability analysis to predict sample size required to detect one or more *AP2S1* mutations for different mutation prevalences in hypocalcaemic probands. 223
Figure 10.1. Vector map for pBI-CMV4-RFP. 254
Figure 10.2. Vector map for pGL4.30[*luc2P*/NFAT-RE/Hydro]. 254
Figure 10.3. Vector map for pGL4.33[*luc2P*/SRE/Hydro] 255
Figure 10.4. Vector map for pCR-Blunt II-TOPO. 255
Figure 10.5. Vector map for pUC18. 256

List of Tables

Table 1. Physiological roles of extracellular and intracellular calcium.....22
Table 2. Classification system for the GPCR superfamily 31
Table 3. Cell lines used for experiments.....108
Table 4. Clinical and biochemical findings in 9 FHH probands with AP2σ2 mutations. 125
Table 5. Previously reported *GNA11* single nucleotide polymorphisms (SNPs) detected in hypercalcaemic probands. 138
Table 6. *GNA11* and *AP2S1* single nucleotide polymorphisms (SNPs) reported on the National Centre for Biotechnology Information (NCBI) database of short genetic variants (dbSNP) or identified by the Exome Sequencing Project of the National Heart, Lung, and Blood Institute (NHLBI-ESP). 152
Table 7. Differential effects of AP2σ2 mutations on signalling pathways and gene transcription relative to AP2σ2 WT.....185
Table 8. Differential effects of cinacalcet on AP2σ2 mutations.....190
Table 9. Evolutionary conservation of residues 20 and 123 of the AP2σ subunit across vertebrate orthologues and paralogues.....196
Table 10. Observed and expected numbers of mice as predicted by Mendelian inheritance of the *Ap2s1* IVS 2+2T>C mutation in the second generation of mice. .204
Table 11. Biochemistry of 12 week old $Ap2s1^{+/+}$ and $Ap2s1^{+/-}$ mice obtained through metabolic cage studies. 206
Table 12. Observed and expected numbers of mice as predicted by Mendelian inheritance of the *Ap2s1* IVS 2+2T>C mutation in the third generation of mice.....212
Table 13. Observed and expected numbers of E12.5 embryos as predicted by Mendelian inheritance of the *Ap2s1* IVS 2+2T>C mutation. 212
Table 14. Clinical and biochemical findings in the 19 hypocalcaemic probands.....225
Table 15. *CASR* and *GNA11* heterozygous SNPs identified in hypocalcemic probands. 227

Abbreviations

$1,25(OH)_2D_3$	1,25-dihydroxyvitamin D_3
Å	Angstrom
AC	Adenylyl cyclase
ADH	Autosomal dominant hypocalcaemia
ADH1	Autosomal dominant hypocalcaemia type 1
ADH2	Autosomal dominant hypocalcaemia type 2
ADH3	Autosomal dominant hypocalcaemia type 3
ADIS	Agonist driven insertional signalling
AH	Autoimmune hypoparathryroidism
AHH	Autoimmune hypocalciuric hypercalcaemia
AHO	Albright hereditary osteodystrophy
AlF_4	Aluminium fluoride
ALP	Alkaline phosphatase
ALT	Alkaline transferase
AMP	Adenosine monophosphate
AP2σ2	Adaptor protein 2 sigma subunit
APS	Autoimmune polyendocrinopathy syndrome
ATP	Adenosine triphosphate
ATPase	ATP hydrolase
BMC	Bone mineral content
BMD	Bone mineral density
BMSC	Bone marrow stromal cell
bp	Basepair
BSA	Bovine serum albumin
$Ca^{2+}{}_i$	Intracellular calcium
$[Ca^{2+}]_i$	Intracellular calcium concentration
$Ca^{2+}{}_o$	Extracellular calcium
$[Ca^{2+}]_o$	Extracellular calcium concentration
cAMP	Cyclic AMP
CAPS	Cyclohexylamino-1-propanesulfonic acid
CaSR	Calcium sensing receptor
CCCR	Urinary calcium: creatinine clearance ratio
CCVs	Clathrin-coated vesicles
CD	Collecting duct
cDNA	Complementary DNA
CI	Confidence interval
Cl^-	Chloride
Cldn	Claudin
CNS	Central nervous system
Cre	Cyclization recombinase enzyme
CTAL	Cortical thick ascending limb
DAG	Diacylglycerol
dbSNP	Database of short genetic variants

DCT	Distal convoluted tubule
ddNTPs	Dideoxy-nucleotide triphosphate
del	Deletion
DEXA	Dual-energy X-ray absorptiometry
dH_2O	Distilled H_2O
DMSO	Dimethyl sulfoxide
DNA	Deoxyribonucleic Acid
DNAse	Deoxyribonuclease
dNTPs	Deoxynucleotide triphosphates
E. coli	*Escherichia coli*
EBV	Epstein-Barr virus
ECD	Extracellular domain
EDTA	Ethylenediamine tetra-acetic acid
EGF	Epidermal growth factor
EMMA	European Mutant Mouse Archive
ENU	*N*-ethyl-*N*-nitrosourea
ER	Endoplasmic reticulum
ERK1/2	Extracellular signal-regulated kinases 1 and 2
ES	Embryonic stem cell
FCS	Foetal calf serum
FHH	Familial hypocalciuric hypercalcaemia
FHH1	Familial hypocalciuric hypercalcaemia type 1
FHH2	Familial hypocalciuric hypercalcaemia type 2
FHH3	Familial hypocalciuric hypercalcaemia type 3
FHH_{NI}	Familial hypocalciuric hypercalcaemia kindred from Northern Ireland
FHH_{OK}	Familial hypocalciuric hypercalcaemia kindred from Oklahoma
FLP	Flippase recombinase
$FrCa^{2+}$	Fractional excretion of calcium
FRET	Forster resonance energy transfer
FRT	Flippase recombinase target
Gcm2	Glial cells missing homolog 2
Gd^{3+}	Gadolinium
GDP	Guanosine diphosphate
GFP	Green fluorescent protein
GPCR	G-protein coupled receptor
GRK	GPCR kinases
GTP	Guanosine triphosphate
GTPase	GTP hydrolase
Gα	G-protein alpha-subunit
Gα11	G-protein subunit alpha 11
H^+	Hydrogen
$[H^+]$	Hydrogen ion concentration
HBSS	Hank's Balanced Salt Solution
HDR	Hypoparathyroidism, sensorineural deafness and renal disease
HEK293	Human Embryonic Kidney cell line 293
ICD	Intracellular domain

Indo-1-AM	Indo-1 acetoxymethylester
IP_3	Inositol-1,4,5-trisphosphate
iPMS	Isopropyl methane sulfonate
IRES	Internal ribosome entry sites
iU	International unit
JG	Juxtaglomerular
JGA	Juxtaglomerular apparatus
JNK	c-Jun N terminal kinase
K^+	Potassium
Kb	Kilo base pairs
Kda	Kilodaltons
lacZ	β-Galactosidase
LB	Luria Bertani
ln	Natural logarithm
luc2	Firefly luciferase gene
LOH	Loop of Henle
m	Mutant
M	Molar
MAPK	Mitogen-activated protein kinase
mg	Milligram
Mg^{2+}	Magnesium
$[Mg^{2+}]_o$	Extracellular magnesium concentration
mGluR1	Metabotropic glutamate receptor type 1
ml	Millilitre
mM	Millimolar
mmol	Millimoles
mod	Modification
MRC	Medical Research Council
mRNA	Messenger RNA
MTAL	Medullary thick ascending limb
n	Number
Na^+	Sodium
$[Na^+]$	Sodium ion concentration
NaCl	Sodium chloride
NaOH	Sodium hydroxide
NaPi-Iia	Type 2a sodium-phosphate co-transporters
NCBI	National Centre for Biotechnology Information
NCX	Na^+/Ca^{2+} exchangers
neo	Neomycin
NFAT	Nuclear Factor of Activated T cells
ng	Nanogram
NHE3	Sodium-hydrogen exchanger 3
NHLBI-ESP	National Heart, Lung, and Blood Institute Exome Sequencing Project
NKCC2	Na^+-K^+-$2Cl^-$ co-transporter
NSHPT	Neonatal severe hyperparathyroidism
p	Short arm of chromosome

pbFRET	Photobleach Forster resonance energy transfer
PBS	Phosphate buffered saline
PCR	Polymerase chain reaction
PDB	Protein Data Bank
PFA	Paraformaldehyde
PHPT	Primary hyperparathyroidism
PIP_2	Phosphatidylinositol-4,5-bisphosphate
PKA	Protein kinase A
PKC	Protein kinase C
PLC	Phospholipase C
PLCβ	Phospholipase C-beta
PMCA	Plasma membrane Ca^{2+}-ATPase
PO_4^-	Phosphate
PT	Proximal tubule
PTH	Parathyroid hormone
PTH1R	Type 1 PTH receptor
PTHrP	Parathyroid hormone related protein
PVDF	Polyvinylidene fluoride
q	Long arm of chromosome
RT-qPCR	Quantitative, real time polymerase chain reaction
RANK	Receptor activator of nuclear factor κB
RANKL	Receptor activator of nuclear factor κB ligand
RE	Restriction endonuclease
RFP	Red fluorescent protein
RGS	Regulators of G-protein signalling
RNA	Ribonucleic acid
RNAi	RNA interference
RNAse	Ribonuclease
ROMK	Renal outer medulllary potassium channel
rpm	Revolutions per minute
RT-PCR	Reverse transcriptase polymerase chain reaction
sdH_2O	Sterile distilled H_2O
SD	Standard deviation
SDM	Site directed mutagenesis
SDS-PAGE	Sodium dodecyl sulfate polyacrylamide electrophoresis
SEM	Standard error of the mean
siRNA	Short interfering RNA
SNV	Single nucleotide variant
SFO	Subfornical organ
SPR	Surface plasmon resonance
SRE	Serum response element
TAL	Thick ascending limb
Taq	*Thermus aquaticus*
TBE	Tris-Borate-EDTA
TBS	Tris buffered saline
TBS-T	TBS-Tween

TGS	Tris/Glycine/SDS
TIRF	Total internal reflection fluorescence
TMD	Transmembrane domain
Tris	Tris(hydroxymethyl)aminomethane
TRPV5	Transient receptor potential cation channel subfamily V member 5 channel
UCCR	Urinary calcium:creatinine ratio
UTR	Untranslated region
UV	Ultra violet radiation
V	Voltage (volts)
v/v	Volume/volume
w/v	Weight/volume
Wnt3A	Wingless-type integration site family, member 3A
WT	Wild-type
µg	Microgram
µl	Microlitre

Amino Acid Table

Amino acid	3-letter symbol	1-letter symbol
Alanine	Ala	A
Arginine	Arg	R
Asparagine	Asn	N
Aspartic acid	Asp	D
Cysteine	Cys	C
Glutamic acid	Glu	E
Glutamine	Gln	Q
Glycine	Gly	G
Histidine	His	H
Hydroxyproline	Hyp	O
Isoleucine	Ile	I
Leucine	Leu	L
Lysine	Lys	K
Methionine	Met	M
Phenylalanine	Phe	F
Proline	Pro	P
Pyroglutamatic acid	Glp	U
Serine	Ser	S
Threonine	Thr	T
Tryptophan	Trp	W
Tyrosine	Tyr	Y
Valine	Val	V

1 Introduction

1.1 Distribution of calcium in the body

Calcium is a divalent cation that is found within both the extracellular and intracellular compartments of complex, multicellular organisms.[1] The total human body content of calcium is approximately 1400mg, with over 99% stored in the insoluble, crystal form as hydroxyapatite [$Ca_{10}(PO_4)_6(OH)_2$] in bones and teeth, 0.9% stored in the crystal form in the plasma membrane and intracellular organelles, and 0.l% solubilised in the extracellular and intracellular fluid compartments.[1] Within the plasma, 50% of calcium is freely ionised (Ca^{2+}) whilst the remainder is predominantly protein-bound, mainly to albumin, and a small proportion is associated with ion complexes.[1] Regulation of the extracellular Ca^{2+} concentration is necessary as a constant supply of extracellular Ca^{2+} must be available to the cell for Ca^{2+}-regulated functions, described in section 1.2. Within the plasma, it is the ionised fraction that is physiologically active and under tight regulation by a complex homeostatic system, discussed in section 1.3. The normal ranges for total plasma albumin-adjusted and ionised calcium are 2.20 – 2.60 mmol/L and 1.10 – 1.30 mmol/L, respectively.[1]

The cytosolic Ca^{2+} concentration is 10,000 fold lower than that of the extracellular concentration and in resting cells is approximately 100 nM.[1] Ca^{2+} enters the cell via plasma membrane Ca^{2+} channels that may be voltage- or ligand-gated depending on the tissue type (Figure 1.1).[2] The low cytosolic concentration is achieved through active transport of Ca^{2+} into intracellular organelles, including the endoplasmic reticulum (ER), mitochondria and sarcoplasmic reticulum (SR)[2] and by movement of Ca^{2+} out of the cell through high-affinity/low-capacity plasma membrane Ca^{2+}

adenosine triphosphatases (PMCA) and low-affinity/high-capacity sodium (Na^+)/ Ca^{2+} exchangers (NCX) (Figure 1.1).[2] These cellular features enable intracellular Ca^{2+} to rapidly increase its concentration by up to 100-fold through the entry of extracellular Ca^{2+} into the cell and release of stored intracellular Ca^{2+} making it an efficient second messenger.[1]

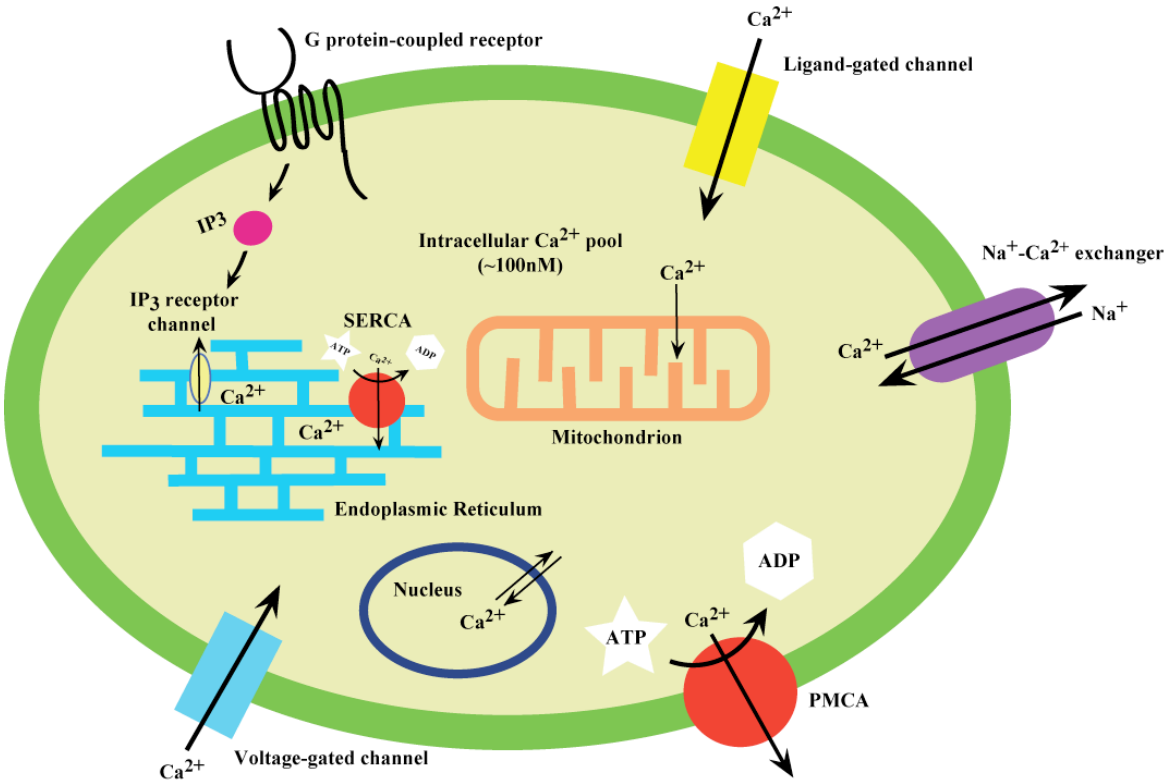


Figure 1.1. Schematic representation of the regulation of intracellular calcium.

The entry of extracellular Ca^{2+} into cells is mediated by voltage- and ligand-gated channels in the plasma membrane. The intracellular Ca^{2+} concentration is maintained at approximately 100nM[1] through the active transport of Ca^{2+} into organelles such as mitochondria for storage. This is achieved in the sarcoplasmic reticulum (SR, not shown) and endoplasmic reticulum (ER) by the sarcoendoplasmic reticulum Ca^{2+}-ATPase (SERCA).[3] Ca^{2+} can be released from intracellular stores by various mechanisms including activation of G-protein-coupled receptors in the plasma membrane which result in production of inositol 1,4,5-trisphosphate (IP3), discussed in detail in section 1.5. IP3 binds to receptor channels on the ER resulting in release of Ca^{2+} into the cytosol.[3] Ca^{2+} can be exchanged between the nucleus and cytosol. Intracellular Ca^{2+} is removed from the cell by the Na^+/Ca^{2+} exchanger and plasma membrane Ca^{2+}-ATPase (PMCA).[3] Adapted from Carafoli E, 2003.[3]

1.2 The physiological roles of calcium

Much has been discovered regarding the physiological roles of calcium since Sydney Ringer's accidental discovery that tap water containing calcium resulted in contraction of isolated rat hearts.[4] Both extracellular and intracellular calcium are essential for a variety of processes in complex, multicellular organisms (Table 1) and are essential for normal cellular function.[1] Insoluble extracellular calcium is vital for the integrity of the skeleton, protecting organs such as the brain, heart, and lungs, and enabling locomotion to occur.[1] The different proportions of hydroxyapetite in dentine and enamel contribute to their unique properties and thus, contribute to the effective ingestion of nutrients.[5] Insoluble extracellular calcium provides a vast mineral store supplying the extracellular fluid with soluble calcium in situations when extracellular levels fall.[1] Soluble extracellular calcium is required for processes such as blood clotting, maintenance of plasma membrane integrity and regulation of plasma membrane potential.[1]

A steady soluble extracellular calcium concentration is required to maintain intracellular calcium levels where calcium may be stored in its crystal form in organelles such as mitochondria, SR and ER and contributes to their structural integrity.[1] Additionally, the presence of these intracellular stores allow for rapid changes to occur in the level of intracellular soluble calcium, enabling it to act as a secondary messenger. Intracellular soluble calcium is involved in the generation of action potentials, cell contraction and motility, cell division, cytoskeletal function[1] and secretion of hormones including adrenaline, vasopressin, glucagon and insulin.[6]

Table 1. Physiological roles of extracellular and intracellular calcium.

Form		Location	Role
Extracellular	*Insoluble*	Bone and teeth	Organ protection Locomotion Ingestion of nutrients Mineral store and reserve
	Soluble	Extracellular fluid	Blood clotting Regulation of plasma membrane potential
Intracellular	*Insoluble*	Plasma membrane Organelles	Maintenance of structural integrity Storage
	Soluble	Cytosol Nucleus	Cytoskeletal function Generation of action potentials Cell contraction and motility Hormone secretion Cell division Oocyte fertilisation

Table adapted from Brown E.M 1991[1]

Cytosolic calcium plays critical roles during animal oocyte fertilisation.[7] Firstly, it is involved in the slow block of polyspermy, which is an inositol 1,4,5-trisphosphate (IP3)-mediated process, and involves cortical granule exocytosis.[8] The released cortical granule enzymes modify the oocyte's extracellular matrix.[8] The calcium signal generated following interaction between sperm and oocyte activates the metabolism of the fertilised oocyte and initiates development of the zygote.[7] In mammalian oocytes, the generation of fertilisation calcium waves following fusion of sperm and oocyte have been shown to control cell division and patterning in early embryos.[9]

1.3 Calcium homeostasis

A complex homeostatic system, comprising the calcium-sensing receptor (CaSR), a class C guanine-nucleotide protein-coupled receptor (GPCR), parathyroid hormone (PTH) and 1,25-dihydroxyvitamin D_3 ($1,25(OH)_2D_3$), tightly regulates extracellular Ca^{2+}, despite daily variations in calcium ingestion[10] (Figure 1.2). The extracellular Ca^{2+} concentration is constantly monitored by CaSRs expressed by the chief cells of the parathyroid and the parafollicular cells of the thyroid.[1] In the parathyroid, there is a steep inverse sigmoidal relationship between extracellular Ca^{2+} *in vivo* and *in vitro* (Figure 1.3) and secretion of PTH,[1] an 84-amino acid peptide.[10] This steep relationship ensures that plasma Ca^{2+} is tightly controlled within a narrow range.[1] This contrasts with the parafollicular cells of the thyroid which secrete calcitonin, a 32 amino acid peptide, in response to a rise in extracellular Ca^{2+}.[1] Calcitonin plays a significant role in Ca^{2+} homeostasis in rodents but its contribution to homeostasis in humans is relatively minor.[11] These calciotropic hormones exert their effects by acting on the following target organs either directly or directly: kidneys; bone; and intestine (Figure 1.2).

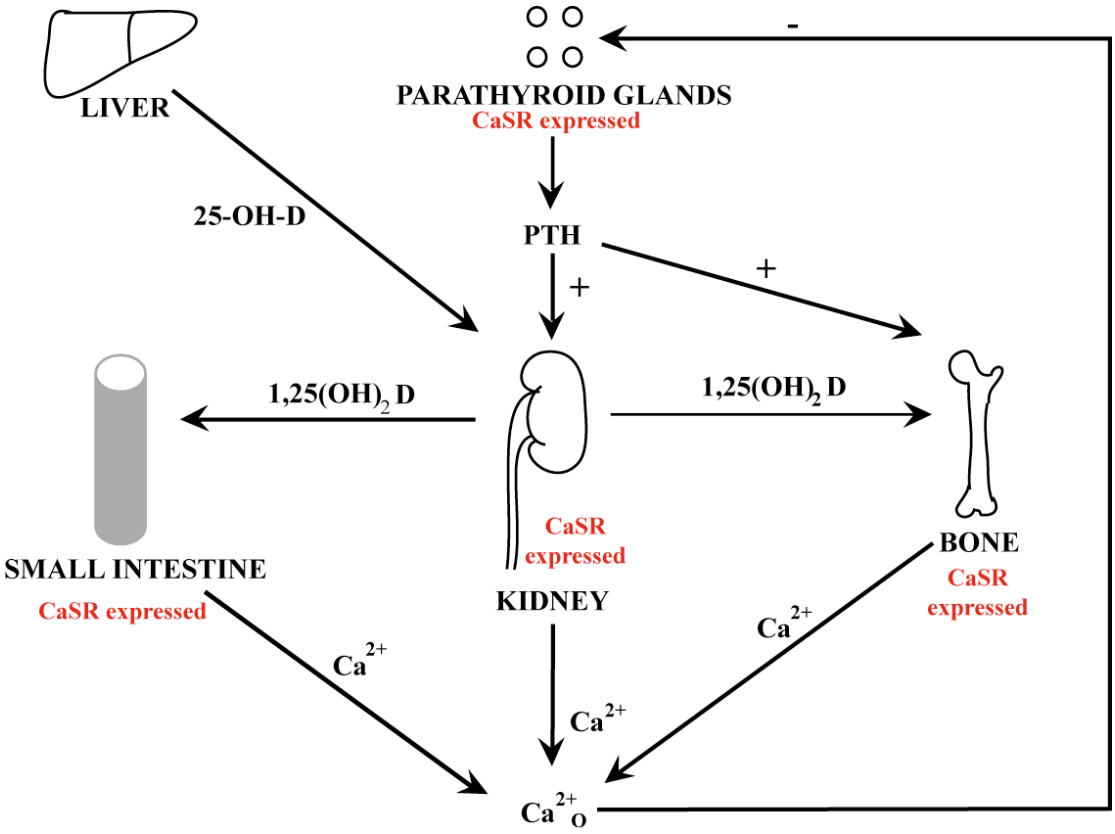


Figure 1.2. **Schematic illustration of extracellular calcium homeostasis**

In response to a fall in extracellular Ca^{2+} (Ca^{2+}_o), the chief cells of the parathyroid glands secrete parathyroid hormone (PTH). PTH promotes Ca^{2+} reabsorption and PO_4^{3-} excretion in the kidney, mobilises Ca^{2+} and PO_4^{3-} from the bone, and stimulates 1α-hydroxylase activity in the kidney. 1α-hydroxylase increases the production of 1,25-dihydroxyvitamin D_3 ($1,25(OH)_2D_3$) from 25-hydroxyvitamin D_3 (25-OH-D) and promotes Ca^{2+} and PO_4^{3-} absorption in the gut and the release of Ca^{2+} and PO_4^{3-} from the bone. +, stimulatory effect; -, inhibitory effect. Adapted from Brown E.M. 1993.[12]

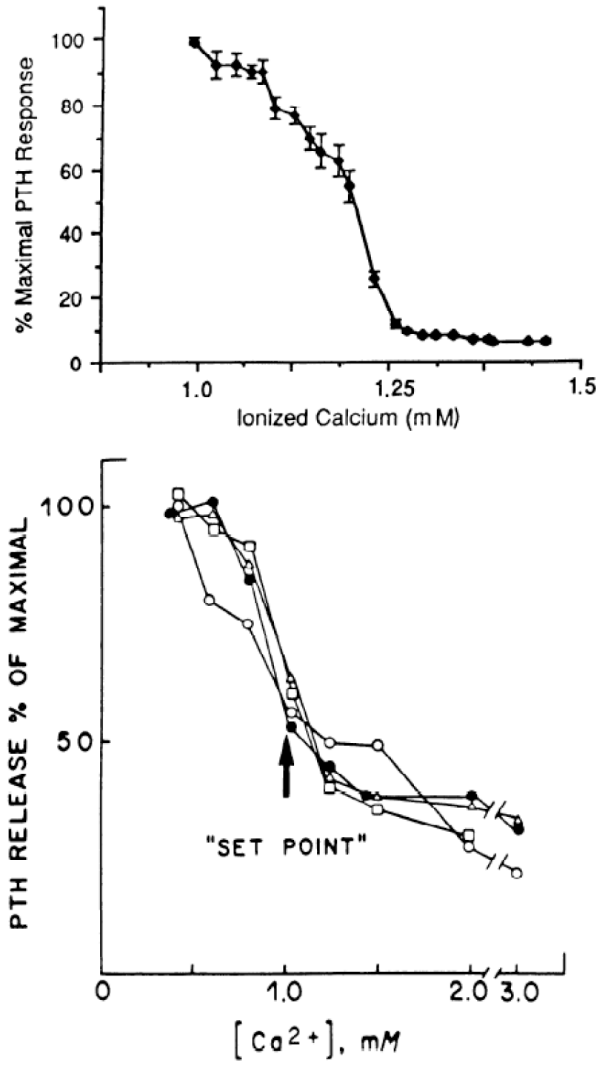


Figure 1.3. Relationship between PTH secretion and extracellular Ca^{2+} *in vivo* and *in vitro*

There is a steep inverse sigmoidal relationship between PTH secretion and extracellular Ca^{2+} *in vivo* (top) and *in vitro* (bottom). *In vitro* studies were performed using cells from several normal human parathyroid glands (shown by different symbols) and *in vivo* studies were performed by infusing EDTA or calcium in normal humans. Adapted from Brown E.M. 1991.[1]

PTH mediates its effects by binding to the PTH type 1 receptor,[13] expressed by cells in the kidney and bone. PTH acts in the kidney to induce distal tubular reabsorption of Ca^{2+}, promote excretion of phosphate (PO_4^{3-}) in the proximal tubule and stimulate proximal tubular production of $1,25(OH)_2D_3$, the most biologically active form of vitamin D_3, by activation of 1α-hydroxylase (Figure 1.2).[14] Within the bone, PTH

stimulates the mobilisation of Ca^{2+} and PO_4^{3-}. During a brief period of hypocalcaemia and hence, a transient rise in PTH, homeostasis will be achieved by renal reabsorption of Ca^{2+} and mobilisation of Ca^{2+} from the bone, both of which occur within minutes of the rise in PTH[15] and normocalcaemia is restored within minutes to a few hours (Figure 1.2).[14]

Vitamin D_3 is produced in the skin by the photolytic cleavage and isomerisation of cholesterol or absorbed in the small intestine (Figure 1.4). It is transported to the liver bound to vitamin D-binding protein where it undergoes 25-hydroxylation to 25-hydroxyvitamin D_3 [25-OH-D] (Figure 1.4), which is the predominant form of vitamin D_3 in the circulation.[16] 25-OH-D undergoes 1α-hydroxylation in the kidney to $1,25(OH)_2D_3$ (Figure 1.4).[17] This is the most biologically active form of vitamin D_3 and its synthesis by 1α-hydroxylase is stimulated by hypophosphataemia and hypocalcaemia in addition to PTH whilst hyperphosphataemia, hypercalcaemia, and $1,25(OH)_2D_3$ inhibit its production.[17] $1,25(OH)_2D_3$ enhances absorption of Ca^{2+} and PO_4^{3-} from the small intestine and promotes Ca^{2+} and PO_4^{3-} mobilisation from bone.[17] The increased synthesis of $1,25(OH)_2D_3$ requires several hours of exposure to an increased PTH level.[14] Thus, this mechanism enhances the PTH-mediated response in cases of prolonged hypocalcaemia, leading to increased small intestinal absorption of Ca^{2+} and further Ca^{2+} mobilisation from bone.[14]

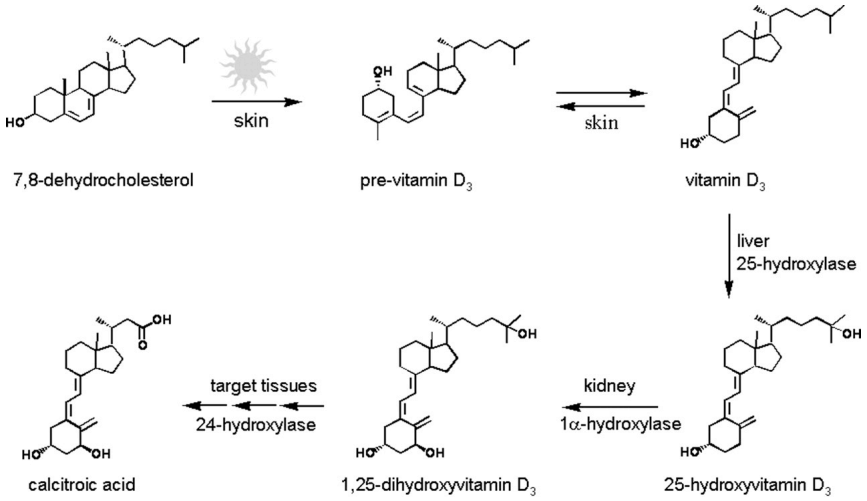


Figure 1.4. Vitamin D_3 metabolism.

Vitamin D_3 is produced in the skin from 7,8-dehydrocholesterol and transported to the liver by vitamin D-binding protein, where it undergoes conversion to 25-hydroxyvitamin D_3 by 25-hydroxylase. 1α-hydroxylation occurs in the kidney producing 1,25-dihydroxyvitamin D_3, the active form of the vitamin. 24-hydroxylase carries out catabolic inactivation in the target tissues. Adapted from Dusso A.S. *et al*. 2005.[16]

Thus, in response to a fall in extracellular Ca^{2+}, the parathyroid chief cells secrete PTH, which stimulates mobilisation of Ca^{2+} and PO_4^{3-} from bone, increases renal distal tubular reabsorption of extracellular Ca^{2+}, promotes proximal tubular PO_4^{3-} excretion and stimulates synthesis of $1,25(OH)_2D_3$.[14] $1,25(OH)_2D_3$ enhances absorption of Ca^{2+} and PO_4^{3-} from the small intestine and promotes Ca^{2+} and PO_4^{3-} mobilisation from bone.[14] The overall effect is a net rise in extracellular Ca^{2+}, correcting the hypocalcaemia. The extracellular homeostatic system provides an opposite response to hypercalcaemia. Hypercalcaemia produces a fall in circulating PTH levels which leads to reduced mobilization of Ca^{2+} and PO_4^{3-} from bone, decreases renal distal tubular reabsorption of extracellular Ca^{2+}, reduces proximal tubular PO_4^{3-} excretion and reduces synthesis of $1,25(OH)_2D_3$.[14] Additionally, in hypercalcaemia the CaSR in the cortical thick ascending limb of the nephron promotes renal calcium excretion (section 1.9.1.2).[18]

There is a steep inverse relationship between extracellular Ca^{2+} concentration and PTH secretion (Figure 1.3).[1] The set point of the cell is the extracellular Ca^{2+} concentration at which PTH secretion is half-maximally inhibited and in normal human parathyroid cells this is approximately 1mM Ca^{2+},[19] which is slightly lower than the extracellular Ca^{2+} concentration in humans of 1.1 – 1.3mM.[1] This results in a relatively low basal secretory rate of PTH maintaining normocalcaemia and provides a significant functional reserve for the system to respond to hypocalcaemia.[12] When hypocalcaemia is prolonged as seen in secondary hyperparathyroidism due to chronic renal failure, the set-point of the cell has been shown to increase.[20 21] Additionally, the stability of PTH mRNA increases due to post-transcriptional modification in states of prolonged hypocalcaemia,[22] resulting in increased PTH synthesis, secretion, and parathyroid cell hypertrophy. Over the course of time, persistent hypocalcaemia and hyperphosphataemia will result in parathyroid cell proliferation,[23] discussed in section 1.9.

1.4 The Calcium Sensing Receptor (CaSR)

1.4.1 Structure of the CaSR

The GPCR superfamily is the largest group of plasma membrane receptors in eukaryotes.[24] They consist of a single polypeptide with an extracellular domain (ECD) to which the agonist binds, a seven transmembrane-spanning domain and an intracellular domain (ICD) which interacts with G-proteins (Figure 1.5).[24] Their identification began with early studies performed on rhodopsin and the β_2-adrenergic receptor (β_2AR), which identified significant sequence homology between the amino

acid sequences of these receptors.[25] Additionally, functional studies using the purified receptors demonstrated that agonist binding coupled to activation of G-proteins (Figure 1.5), G_s for the β_2AR[26] and G_t for rhodopsin.[27] The G-proteins that interact with GPCRs are heterotrimeric and comprise α, β and γ subunits (Figure 1.5).[24] They are characterised by the ability of the α subunit to bind to guanosine diphosphate (GDP) in the inactive state and guanosine triphosphate (GTP) in the active state (Figure 1.5).[24] In the absence of an agonist stimulating the GPCR, the GDP-G-protein complex is bound to the GPCR (Figure 1.5). When an agonist binds to the ECD, a conformational change occurs in the receptor resulting in exchange of GDP for GTP on the Gα subunit and thus, its activation.[24] The Gα subunit is released from the receptor, dissociates from the βγ subunit and mobilises laterally in the plasma membrane (Figure 1.5) to activate downstream signalling pathways,[24 28] discussed in section 1.5. This is the accepted model for G-protein signalling, however it has been demonstrated that certain G-protein subunits undergo rearrangement rather than dissociation following activation *in vivo*,[28] such as $G\alpha_i$[29] and $G\alpha_s$.[30]

Following the discovery of rhodopsin and the β_2AR, many GPCRs have been cloned, their crystal structures solved and their effects functionally characterised. A classification system categorising GPCRs into 6 classes (A-F) based on sequence homology and functional similarity was established by Attwood and Findlay in 1994 [31] and more recently an alternative classification called GRAFS (Glutamate, Rhodopsin, Adhesion, Frizzled/Taste2, Secretin) was introduced (Table 2).[32]

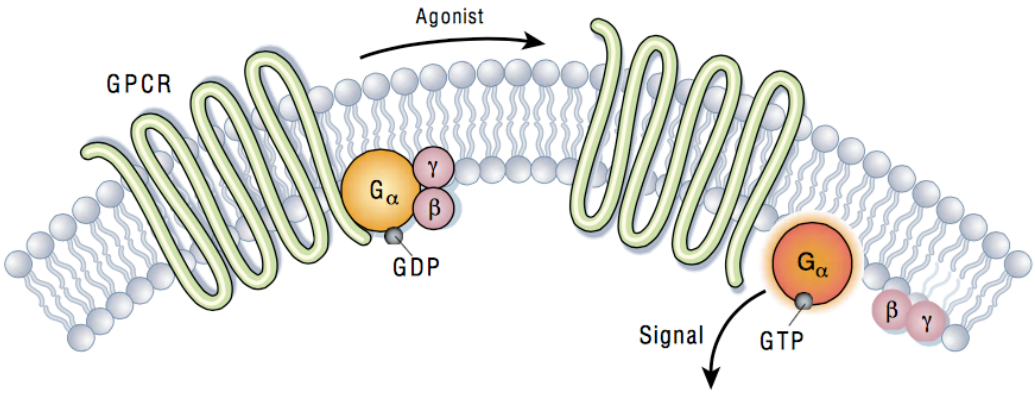


Figure 1.5. Schematic representation of the interaction between GPCR and heterotrimeric G-protein.

In the absence of agonist binding, the heterotrimeric G-protein is bound to the intracellular domain of a GPCR in its inactive state with GDP bound to the Gα subunit.[24] When an agonist stimulates the receptor, a conformational change occurs allowing exchange of GDP for GTP on the Gα subunit.[24] This releases the Gα subunit from the receptor and results in dissociation of the Gα and βγ subunits.[24]

Table 2. **Classification system for the GPCR superfamily**

Class	Examples (Receptors for)	Types of ligand	Type of functional domains in the N termini (excluding transmembrane)	Conserved cysteine residues in extracellular loops 1 and 2	Proteolytic processing of the N termini
Rhodopsin	Rhodopsin B_2-adrenergic (B_2AR) Luteinising hormone (LHR)	Peptides, proteins (including enzymes), small organic compounds, lipid-like substances, nucleotides	Proteolytic sites, leucine-rich repeat, low-density lipoprotein receptor class A	Yes	Yes
Secretin	Secretin PTH 1 & 2 Calcitonin	Peptides, proteins	Hormone-binding domain	Yes	No
Glutamate	Metabotropic glutamate CaSR Taste Gamma-aminobutyric acid B ($GABA_B$)	Amino acids, cations, small organic compounds, carbohydrates	Venus fly trap domain short consensus repeats (SUSHI)	Yes	No
Adhesion	Adhesion	Proteins, glycosaminoglycan	GPCR proteolytic site, thrombospondin domain, immunoglobulin domain	Yes	Yes
Frizzled	Frizzled	Proteins	Wnt binding domain	Yes	No
Taste2	Taste2	Small organic compounds	-	No	No

Adapted from Lagerström M.C and Schiöth. 2008. [33]

The CaSR was cloned from bovine parathyroid tissue in 1993 and identified as having sequence homology and functional similarity to the metabotropic glutamate (mGlu) receptor.[34] The crystal structure of the 1078 amino acid CaSR has not been determined unlike that of the extracellular domains of the mGlu1[35] and mGlu3 receptors[36] and the transmembrane domain of the mGlu5 receptor[37] (Figure 1.6A). Based on sequence homology, the 612 amino acid hydrophilic ECD of the CaSR is predicted to be organised into a venus fly trap domain (VFTD)[35] (Figure 1.6A). This is a bi-lobed structure with a cavity between the two lobes to accommodate ligand binding and thus is predicted to harbour multiple Ca^{2+} binding sites.[38 39] A cysteine rich domain (CRD) and a 14 amino acid linker connect the ECD to a 250 amino acid transmembrane domain (TMD)[34] (Figure 1.6B). The TMD consists of seven hydrophobic helical domains, connected by three extracellular loops and three intracellular loops, and connects to the 216 amino acid intracellular domain (ICD)[34] which binds to the heterotrimeric G-proteins, discussed further in section 1.4.4. Dimerisation is common within the GPCR superfamily with receptors forming homo- or heterodimers[40] (Figure 1.6C). Formation of a combination of non-covalent interactions[41] and disulphide bonds[42] between the VFTDs of two CaSR monomers within the ER results in dimerisation[43] such that the CaSR exists as a homodimer on the cell surface.[44]

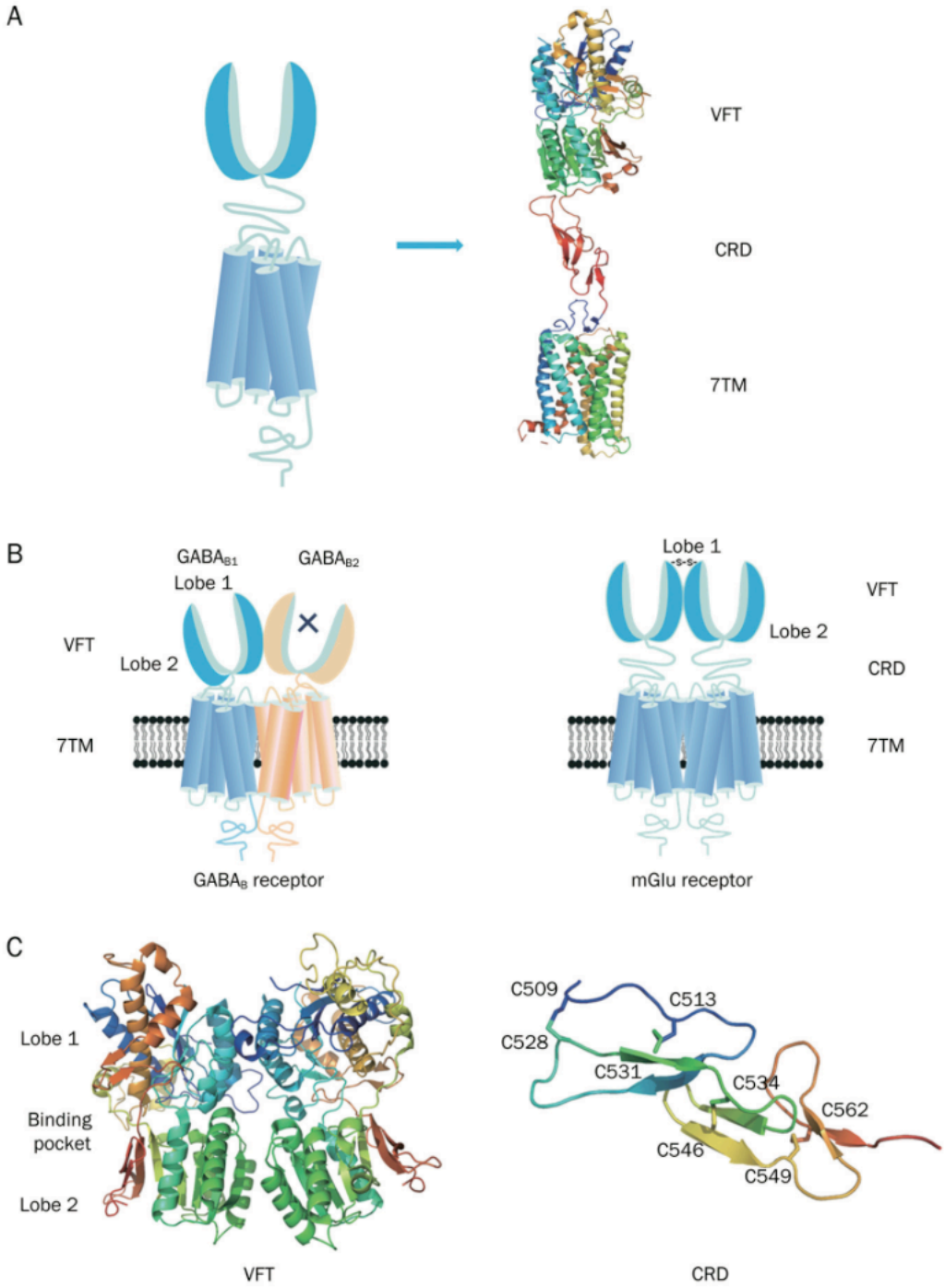


Figure 1.6. Structure of the Class C GPCRs.

(**A**) The extracellular domain of class C GPCRs is organised into a Venus fly trap (VFT) domain which comprises two lobes separated by a cleft for ligand binding. This is connected by a cysteine rich domain (CRD) to the seven transmembrane domain (7TM). The intracellular domain couples to heterotrimeric G-proteins (not shown). (**B**) Schematic representation of class C GPCRs present in the plasma membrane as a heterodimer (γ-aminobutyric acid B ($GABA_B$) receptor on left figure) or as homodimers (mGlu receptor on the right). The CaSR receptor forms homodimers in the endoplasmic reticulum prior to insertion into the plasma membrane. (**C**) Resolved crystal structure of the VFT showing the two lobes and cleft for agonist binding and CRD of the mGlu1 receptor. Figure adapted from Chun L. 2012.[45]

1.4.2 The calcium sensing receptor gene, *CASR*

The calcium sensing receptor gene, *CASR*, was mapped to human chromosome 3q21.1 shortly after cloning of the 1078 amino acid CaSR from bovine parathyroid.[34] [46] [47] It comprises 8 exons, with exons 1A and 1B encoding two distinct, alternate 5'untranslated regions (UTRs).[48] Exon 2 encodes the 242 nucleotides of the 3' end of the 5'UTR and the translation initiation codon whilst exons 3 to 7 code for the remainder of the CaSR protein.[48] In exon 7 two different polyadenylation signal sequences result in two 3'UTRs.[48] Two promotors, P1 and P2, control the transcription of *CASR*. P1 comprises a TATA box at nucleotide -26 and a CCAAT box at -110 relative to the transcriptional start site and P2 comprises an Sp1/3 site at the transcriptional start site.[49] Vitamin D response elements[49] and Glial Cells Missing (GCM)[50] elements are present in both promotors.

1.4.3 CaSR ligand binding and receptor activation

Determination of the crystal structure of the mGlu1 receptor bound and unbound to its agonist glutamate revealed how ligand binding resulted in activation of class C GPCRs.[35] [51] These studies revealed that two major conformational changes occur on ligand binding including the closure of at least one VFTD within the dimer and the rotation of one venus fly trap module (VFTM) relative to the other, bringing their C-terminal ends closer by more than 20Å (Figure 1.7).[35] [51] This produces a conformational change in the CRDs which is transferred to the TMDs[37] and subsequently the ICDs. This conformational change activates the bound Gα subunit of

the bound G-protein resulting in exchange of GDP for GTP and dissociation of the Gα subunit from the receptor and the βγ subunit.

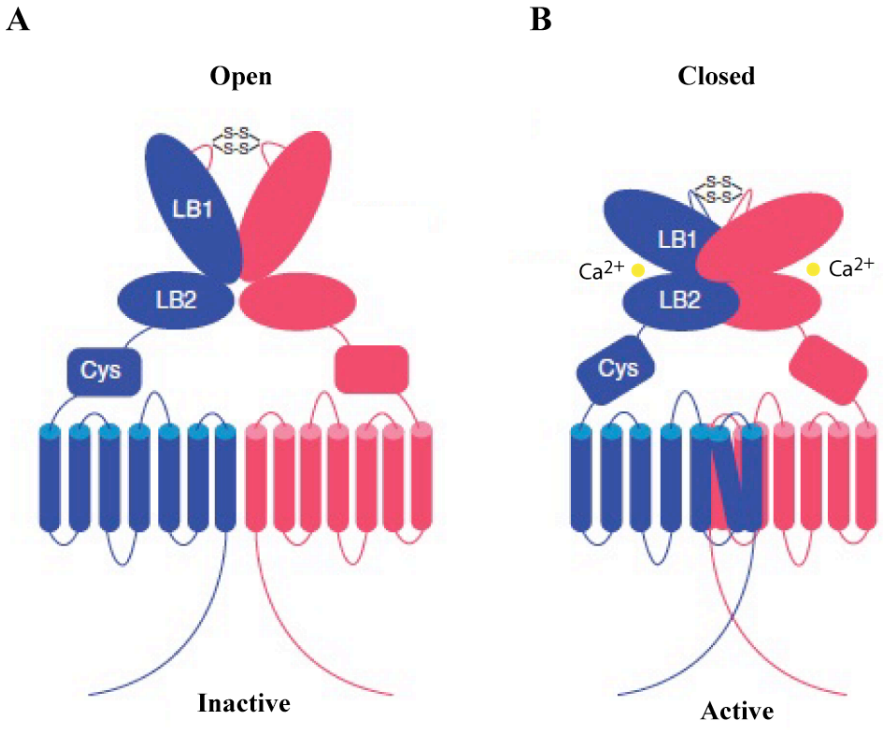


Figure 1.7. Schematic representation of ligand binding and activation of the CaSR.

The CaSR exists as a homodimer on the cell surface as a result of the formation of non-covalent interactions and disulphide bonds (represented by S-S) between the venus fly trap domains (VFTDs) of two CaSR monomers. Dimerisation occurs within the endoplasmic reticulum (ER). (A) In the absence of a ligand, lobe 1 and lobe 2 (LB1 and LB2, respectively) of the VFTD are open and binding sites for G-proteins within the intracellular loops of the CaSR are blocked preventing downstream signalling from occurring. Thus the CaSR is in an inactive conformation. (B) On ligand binding within the cavity of the VFTD, the lobes of the homodimer come together resulting in rotation of the VFT. This produces a conformational change in the cysteine-rich regions (Cys) which is transferred to the transmembrane domain. This activates the CaSR enabling the intracellular loops to interact with G-proteins and initiate downstream signalling. Adapted from Hendy *et al*. 2009. [52]

For the $GABA_B$ receptor (Figure 1.6) only one VFTD in the dimer needs to be in the closed conformation for G-protein coupling to occur[53] compared with the mGlu5 receptor (Figure 1.6) where open-closed and closed-closed dimer pairs work as partial and full agonists, respectively.[54] Thus as the CaSR shares sequence homology with the mGlu receptors,[34] it can be extrapolated that the CaSR homodimer may behave similarly to the mGlu5 receptor.

1.4.4 G-protein coupling

Despite the large number of GPCRs, they interact with a comparatively small number of G-proteins. In humans, Gα subunits are encoded by 16 genes, Gβ subunits are encoded by 5 genes and Gγ subunits are encoded by 12 genes.[55] GPCRs couple with heterotrimeric G-proteins (section 1.4) which are classified into four groups based on the primary sequence homology of the Gα subunit: $G\alpha_{q/11}$; $G\alpha_{12/13}$; $G\alpha_{i/o}$; and $G\alpha_{s}$.[56] Resolution of the crystal structures of many G-proteins in various conformations has revealed the Gα subunit to comprise a GTPase domain, conserved across all members of the G-protein superfamily connected through linker regions to a helical domain which is unique to the particular Gα subunit (Figure 1.8).[57] The GTPase domain is made up of six β-sheets surrounded by five α-helices.[57] Three flexible loops within the GTPase domain, known as the switch regions, are involved in stabilising the Gα complex (Figure 1.8).[57] The Gα-GDP complex is predicted to be unstable *in vivo* due to the exposure of hydrophobic surfaces by the switch regions.[57] On binding of GTP, the switch residues undergo a conformational change, collapsing inwards and burying the hydrophobic residues within the Gα-GTP complex.[57]

Early studies on bovine parathyroid cells demonstrated expression of $G\alpha_{q/11}$, $G\alpha_{12/13}$, $G\alpha_{i}$, and $G\alpha_{s}$ subunits, with highest levels of expression being that of $G\alpha_{11}$.[58] Unlike the mGlu receptors which tend to couple to a specific G-protein, the CaSR was revealed to be a pleiotropic receptor.[59] When stably expressed in human embryonic kidney 293 (HEK293) cells, the CaSR was demonstrated to couple to $G\alpha_{q/11}$,[60 61] $G\alpha_{12/13}$,[60] and $G\alpha_{i/o}$.[60 61] Amino acid residues in intracellular loops 2 and 3 of the CaSR were identified as critical for the coupling of the receptor to $G\alpha_{q/11}$ using

alanine mutagenesis.[62] The sites of coupling for $G\alpha_{12/13}$ and $G\alpha_i$ to the CaSR have not yet been identified.

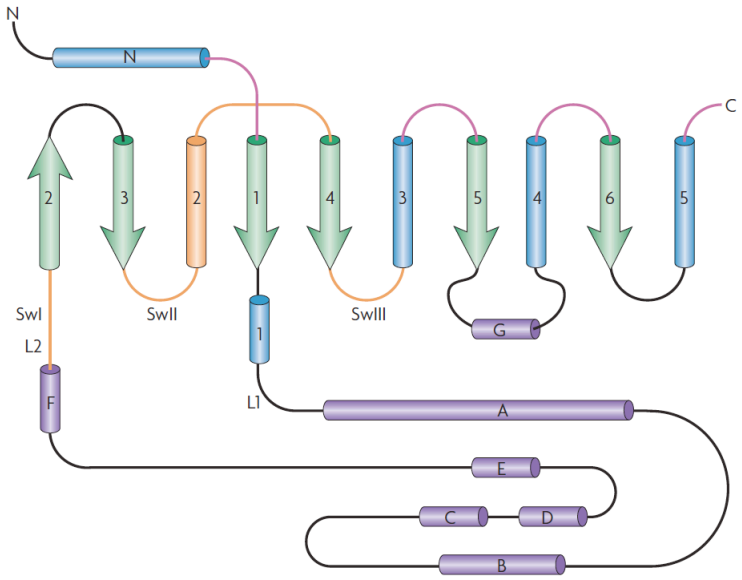


Figure 1.8. Schematic representation of the secondary structure of the Gα subunit.

The Gα subunit comprises a helical domain (purple) connected through linker regions (L1 and L2) to a GTPase domain (β-sheets in green and α-helices in blue). Switch regions (orange) within the GTPase domain are involved in receptor-mediated release of GDP from the subunit. Adapted from Oldham W.M and Hamm H.E. 2008. [57]

1.4.5 Orthosteric agonists and allosteric modulators of the CaSR

The CaSR is activated not only by extracellular Ca^{2+} but by an array of heterogenous positively charged orthosteric agonists including polycations such as extracellular Mg^{2+}, Gd^{3+}, and Sr^{2+} [34], polyvalent charged molecules such as spermine[63] and the highly charged, polycationic aminoglycoside antibiotics.[64] These are referred to as type I calcimimetics and bind to sites within the VFTD. Positive allosteric modulators (PAMS) of the CaSR, referred to as type II calcimimetics, act to increase the sensitivity of the receptor to its agonists and thus bind at a site which is distinct from the ligand.[65] They can be endogenous such as the aromatic L-amino acids[66] and γ-

glutamyl peptides, which bind in the ECD, or synthetic, which bind within the TMD (Figure 1.9). Negative allosteric modulators (NAMS) reduce the sensitivity of the CaSR to its agonists and include endogenous NAMs such as protons and Na^+ ions or synthetic molecules, referred to as calcilytics (Figure 1.9).

The CaSR is able to adopt several active conformations each of which is stabilised by different ligands enabling the CaSR to couple with different G-proteins.[67] This phenomenon is referred to as ligand-biased signalling. The particular G-protein with which the CaSR couples is thus both ligand- and cell-type-dependent.[68] Allosteric modulators have been shown to have further effects on the ligand-dependent coupling of the receptor with G-proteins, discussed in section 1.5.5.

The development of NPS R-568 (Figure 1.9), the first type II calcimimetic, followed the observation that the phenylalkylamine-type Ca^{2+} channel blockers such as verapamil increased the release of intracellular Ca^{2+} and PTH secretion in response to extracellular Ca^{2+} stimulation.[65] NPS R-568 was shown to potentiate the effects of extracellular Ca^{2+} on the CaSR expressed by the parathyroid cells on PTH secretion *in vitro* and *in vivo,*[69] and it was also shown to stimulate calcitonin release by the CaSR expressed by the parafollicular cells of the thyroid.[70] Many of the first-generation calcimimetics were not suitable for clinical use due to poor bioavailability. The second-generation calcimimetic, cinacalcet (Figure 1.9), was also shown to preferentially potentiate CaSR signalling in parathyroid cells compared to parafollicular cells and was more easily absorbed.[71] Cinacalcet is routinely used for the treatment of hypercalcaemia associated with end-stage renal failure.[72] It is also used in the treatment of primary hyperparathyroidism in severe cases where surgery is

contraindicated[73] and has been shown to reduce serum calcium levels in inoperable cases of parathyroid carcinoma.[74] Its use is restricted because of the potential side effect of severe hypocalcaemia associated with stimulation of both parathyroid and renal CaSRs.[65] Cinacalcet has additionally been demonstrated to be of clinical use in familial hypocalciuric hypercalcaemia,[75] discussed in section 1.10.1.1.

High throughput screening has been used to identify the majority of discovered calcilytics, most of which are analogues of the first calcilytic NPS 2143 (Figure 1.9) and comprise a *gem*-dimethyl amino alcohol motif.[65] It was postulated that calcilytics would be a treatment for osteoporosis due to their predicted acute inhibition of parathyroid CaSRs and the resultant transient PTH release which would stimulate osteoblast activity.[65] However no effect on bone density was seen.[65] Recently, calcilytics have shown beneficial results in autosomal dominant hypocalcaemia (ADH) *in vitro*[76-79] and *in vivo* [78 79], discussed in section 1.10.2.1.1.

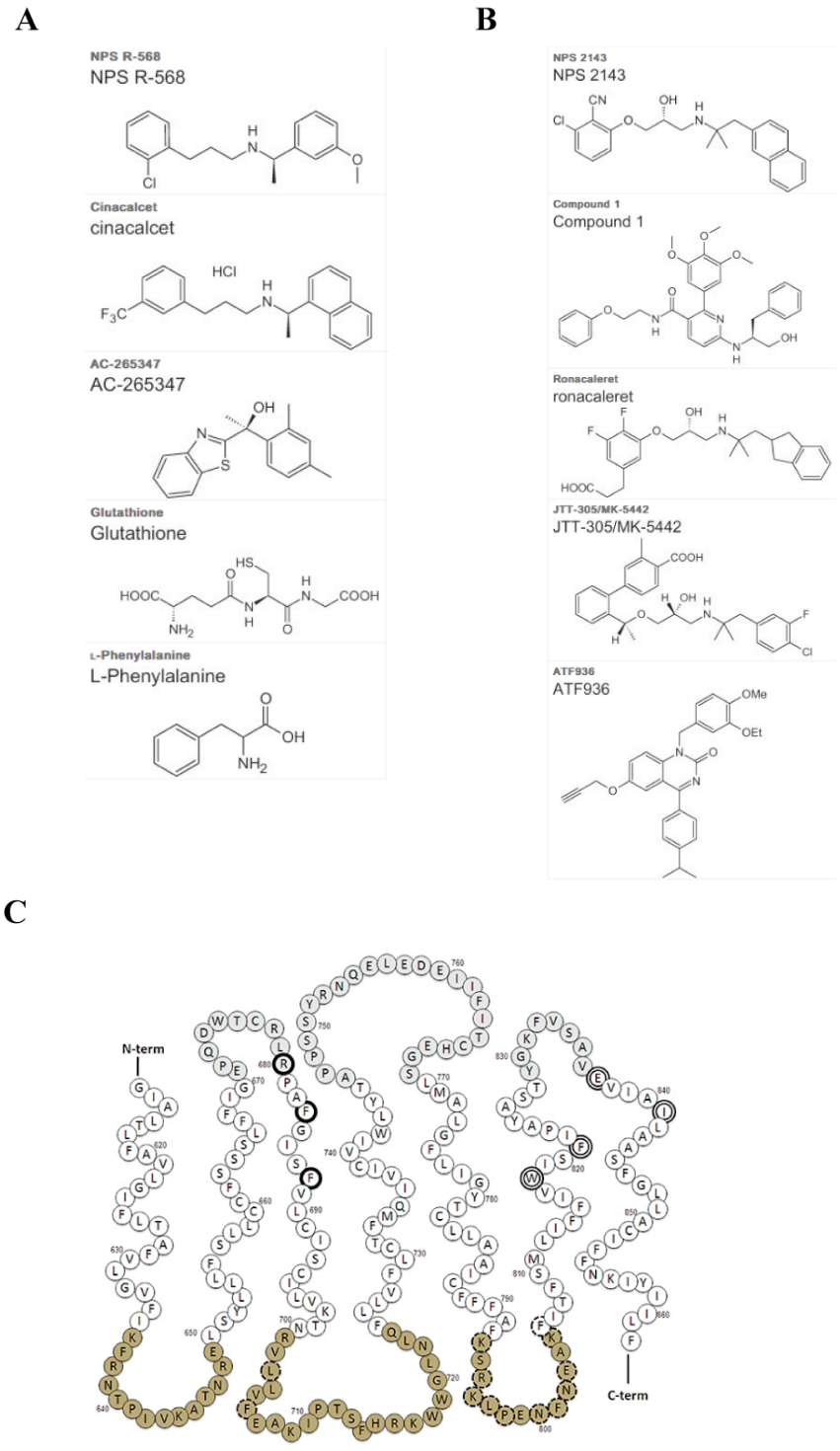


Figure 1.9. Allosteric modulators of the CaSR and their binding sites.

Chemical structure of (A) Positive allosteric modulators of the CaSR comprising NPS R-568, cinacalcet, AC- 265347, glutathione, and L-phenylalanine. (B) Negative allosteric modulators comprising the synthetic calcilytics NPS 2143, compound 1, ronacaleret, JTT-305/MK-5442, and ATF936. (C) Schematic representation of the heptahelical domain of the CaSR. The synthetic calcimimetics and calcilytics bind in the transmembrane domain whilst the naturally occurring amino acids and glutathione bind in the extracellular domain. Amino acid residues where both calcimimetics and calcilytics bind are represented by double-lined circles and those to which only calcilytics bind are represented by single, bold circles. Adapted from Nemeth E. F. 2013.[65] and Khan M. A. and Conigrave A. D. 2010.[59]

1.5 CaSR downstream signalling pathways

The particular G-protein with which the CaSR couples is both ligand- and cell-type-dependent (sections 1.4.4 and 1.4.5).[68] Early studies on bovine parathyroid cells demonstrated expression of $G\alpha_{q/11}$, $G\alpha_{12/13}$, $G\alpha_i$, and $G\alpha_s$ subunits with highest levels of expression being that of $G\alpha_{11}$.[58] The CaSR is a pleiotropic receptor which has been demonstrated to couple to $G\alpha_{q/11}$,[60 61] $G\alpha_{12/13}$,[60] and $G\alpha_{i/o}$.[60 61] and under certain circumstances, $G\alpha_s$[80] depending on the ligand activating the receptor and the cell type (section 1.4.4). The GTP-Gα subunit complexes are responsible for initiating an array of downstream intracellular signalling pathways. The $G\alpha_{q/11}$ pathway is the predominant intracellular signalling pathway in the parathyroid.[58]

1.5.1 $G\alpha_{q/11}$ signalling

The $G\alpha_{q/11}$ signalling pathway has been shown to be activated by extracellular Ca^{2+} in parathyroid cells,[60] osteoblasts[81] and CaSR-expressing HEK293 cells.[60] The GTP-$G\alpha_{q/11}$ complex dissociates from the CaSR and βγ subunit and moves laterally within the plasma membrane to activate phospholipase C (PLC) (Figure 1.10).[30] PLC hydrolyses the plasma membrane-bound phospholipid phosphatidylinositol 4,5-bisphosphate (PIP2) to inositol 1,4,5-trisphosphate (IP3) and diacylglycerol (DAG) (Figure 1.10).[82]

DAG remains bound to the plasma membrane whilst IP3 diffuses through the cytosol to the ER where it binds to IP3 receptors.[3] Binding to IP3 receptors stimulates a rapid rise in intracellular Ca^{2+} from ER stores (Figure 1.10), which acts as a second

messenger capable of interacting with numerous intracellular binding proteins to stimulate multiple signalling cascades.[82]

The intracellular Ca^{2+}-binding proteins act as Ca^{2+} sensors and are classified into two groups according to structure: those containing EF-hand motifs, comprising a helix-loop-helix structural domain, such as calmodulin and calcineurin; and those lacking this motif, including protein kinase C (PKC).[83] Calmodulin is a highly abundant, ubiquitously expressed protein with different subcellular locations depending on the cell type.[84] Binding of a Ca^{2+} ion to each of 4 EF-hand domains within calmodulin leads to a conformational change such that the Ca^{2+}–calmodulin complex is able to bind itself tightly around its target proteins due to the presence of a flexible linker region.[83] Its target proteins include calmodulin-dependent protein kinases, receptors, ion channels and other enzymes.[84]

DAG stimulates the mitogen activated protein kinase (MAPK) pathway through the activation of PKC[85] (Figure 1.10). MAPKs are serine/threonine-specific protein kinases which are evolutionarily conserved in eukaryotic cells.[86] Four MAPK subgroups are expressed in mammalian cells: Extracellular signal-regulated kinase 1/2 (ERK1/2); Jun amino-terminal kinases (JNK1/2/3); p38 MAPK; and ERK5.[87] Each subgroup comprises a MAPK kinase kinase, a MAPK kinase and a MAPK and signal transduction occurs through sequential dual tyrosine and threonine phosphorylation.[86] The MAPKs act on a diverse range of target proteins including transcription factors to influence gene expression and regulate cell differentiation, proliferation and apoptosis.[86] Extracellular Ca^{2+} was demonstrated to activate the ERK1/2 pathway

through a $G\alpha_{q/11}$-mediated activation of PKC in bovine parathyroid and HEK293 cells expressing the CaSR.[85]

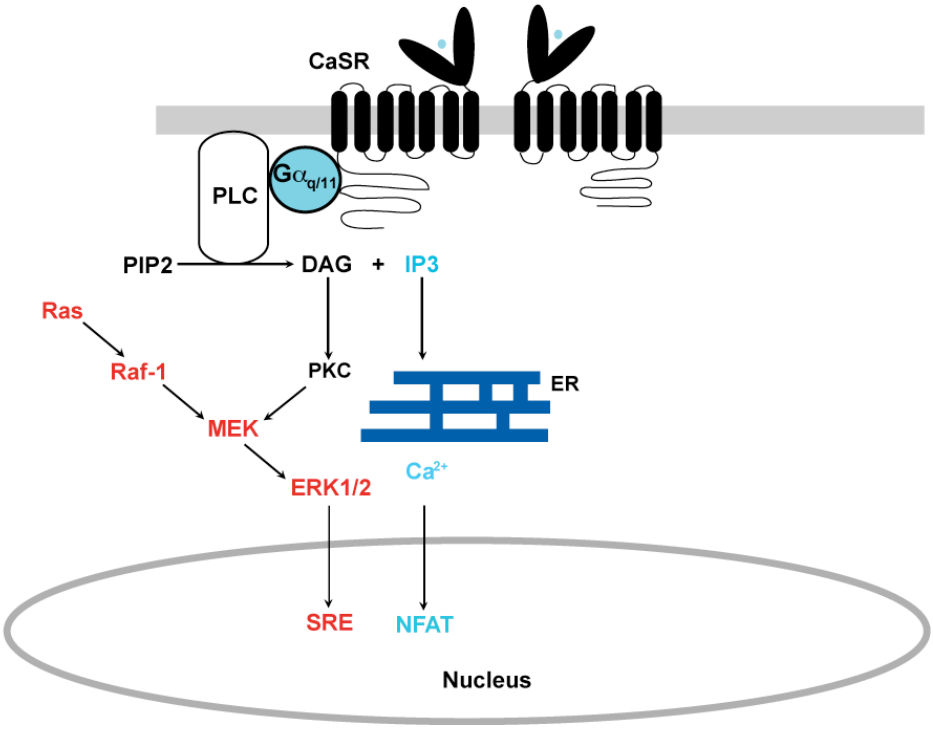


Figure 1.10. CaSR signalling via $G\alpha_{q/11}$ coupling.

Binding of Ca^{2+} to the extracellular domain (ECD) of the CaSR leads to a conformational change in the transmembrane domain[35 36] resulting in activation of the guanine nucleotide exchange function of the α subunit of $G_{q/11}$ with exchange of guanosine diphosphate (GDP) for guanosine triphosphate (GTP). This results in dissociation of the α subunit from the receptor and from the βγ subunit.[82] The Gα subunit activates phospholipase C (PLC) which hydrolyses phosphatidylinositol 4,5-bisphosphate (PIP2) to inositol trisphosphate (IP3) and diacylglycerol (DAG).[82] IP3 increases intracellular Ca^{2+} by stimulating the release of Ca^{2+} from stores in the endoplasmic reticulum (ER). Intracellular Ca^{2+} activates Ca^{2+}-regulated transcription factors such as nuclear factor of activated T-cells response element (NFAT) to induce gene transcription, in a calmodulin-calcineurin dependent pathway. DAG stimulates protein kinase C (PKC) which initiates a phosphorylation cascade (the mitogen-activated protein kinase (MAPK) pathway) involving Ras, Raf proto-oncogene serine/threonine-protein kinase (Raf-1), mitogen/extracelluar signal regulated kinase (MEK) and extracellular signal-regulated kinase 1/2 (ERK1/2). Downstream signalling activates transcription factors that bind to serum-response elements (SRE) in the promotors of MAPK target genes, thus SRE is often used as a reporter construct to study MAPK signalling. Adapted from Hofer A. M. and Brown E. M. 2003.[82]

Many genes can be activated downstream of $G\alpha_{q/11}$ and the MAPK signalling pathways. However, the precise targets of CaSR are unknown, or difficult to study *in vitro*. Thus, most studies of gene transcription downstream of $G\alpha_{q/11}$ have focused on

expression of the nuclear factor of activated T-cells (NFAT) (Figure 1.10) family of transcription factors which are regulated by intracellular Ca^{2+} through its binding with calmodulin and subsequent formation of a complex with calcineurin.[88] Once activated, calcineurin is responsible for the dephosphorylation and nuclear localisation of NFAT transcription complexes.[88] Additionally, the serum response element (SRE) (Figure 1.10) is a common regulatory element present in the promoters of many MAPK target genes.[89] Thus, SRE reporter activity is used as a measure of ERK1/2 signalling and represents a convergence pathway for several G-proteins, including $G\alpha_{q/11}$ and $G\alpha_{i/o}$.[90]

1.5.2 $G\alpha_{12/13}$ signalling

Extracellular Ca^{2+} has been shown to activate the $G\alpha_{12/13}$ signalling pathway in parathyroid cells and CaSR-expressing HEK293 cells.[60] $G\alpha_{12/13}$ signalling has been less extensively studied in bone[91] but has been demonstrated in osteoblasts.[91 92] The anti-fracture agent, Strontium ranelate, was demonstrated to mediate its effects on bone in part through activation of CaSR on osteoblasts[93] and this has been suggested to occur through activation of $G\alpha_{12/13}$ signalling.[68] The $G\alpha_{12/13}$ subunit activates RhoA, a member of the Ras superfamily, through Rho guanine nucleotide exchange factors (RhoGEF) (Figure 1.11).[94] The Ras superfamily comprises small GTPases which are similar in structure and function to the Gα subunits but function as monomeric G-proteins.[95] Activation of RhoA kinase by RhoA is essential for control of cell shape and migration by the formation and organisation of actin filaments, which produces membrane ruffling.[96] RhoA-mediated activation of phospholipase D results in generation of DAG, activation of PKC and initiation of the ERK1/2 signalling cascade (Figure 1.11). $G\alpha_{12/13}$ has been shown to activate adenylyl cyclase isoform-7[97]

resulting in elevated cAMP levels and providing a further layer of complexity to the intricate network of downstream signalling pathways.

The serum response factor (SRF) belongs to the MADS (MCM1, Agamous and Deficiens, SRF) box family of transcription factors and binds to the SRE in target genes.[98] Many genes can be activated downstream of $G\alpha_{12/13}$ and SRF has been shown to be activated by Rho and Ras mediated signals,[98] and thus, measures of $G\alpha_{12/13}$-mediated gene transcription often utilise reporter gene constructs of SRF-response elements (Figure 1.11).[90]

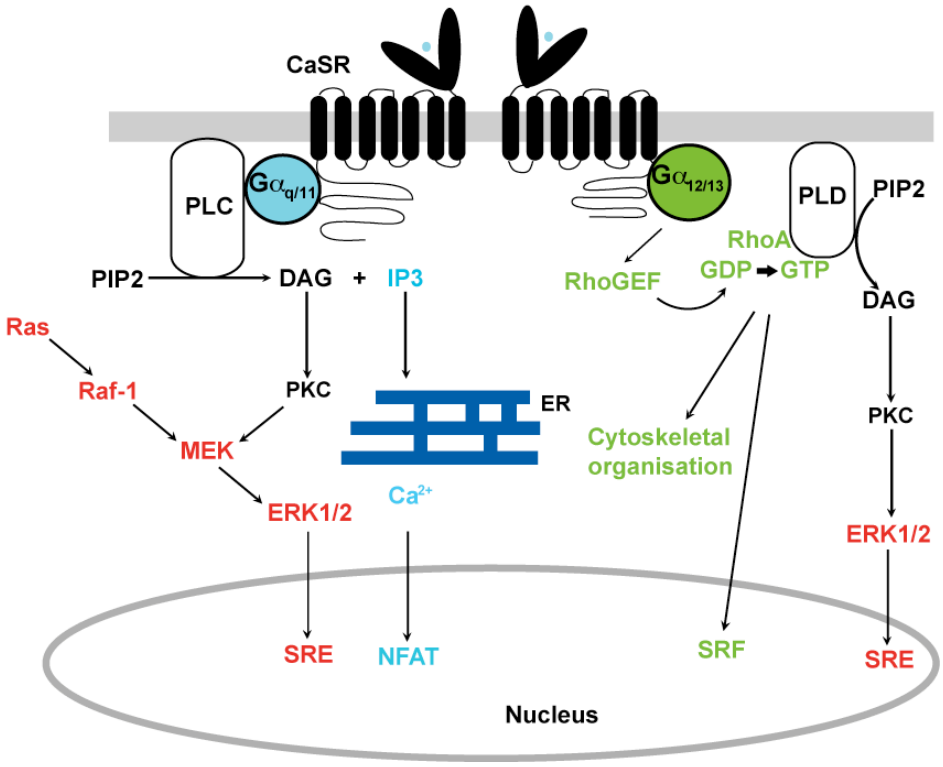


Figure 1.11. CaSR signalling via $G\alpha_{12/13}$ coupling.

Activation of $G\alpha_{12/13}$ leads to stimulation of the guanine exchange function of Rho (RhoGEF) resulting in the activation of RhoA, which exchanges GDP for GTP. Activated RhoA induces membrane-bound phospholipase D which hydrolyses phosphatidylcholine and phosphatidylinositol to diacylglycerol (DAG). DAG activates protein kinase C (PKC) and the MAPK signalling pathway as seen with CaSR signalling via $G\alpha_{q/11}$ coupling, indicating that more than one G-protein signal transduction pathway converges on the MAPK pathway. Additionally, activated RhoA is involved in cytoskeletal organization and membrane ruffling. Control of gene transcription is through activation of the serum response factor (SRF), which has been shown to be induced by Rho mediated signals, and SRE via the ERK1/2 signalling pathway. Adapted from Cheng Z. *et al*. 2010.[90]

1.5.3 $G\alpha_{i/o}$ signalling

Extracellular Ca^{2+} has been shown to mediate coupling of the CaSR to $G\alpha_{i/o}$ in parathyroid cells,[60] CaSR-expressing HEK293 cells,[60] and osteoblasts[99] (Figure 1.12). Activation of the $G\alpha_{i/o}$ subunit leads to inhibition of adenylyl cyclase resulting in a reduction in the conversion of adenosine triphosphate (ATP) to cyclic monophosphate (cAMP).[100] The fall in cAMP levels has an inhibitory effect on protein kinase A (PKA), which requires two cAMP molecules to bind to its regulatory subunit for activation.[100] There is complex crosstalk between the cAMP and ERK1/2 signalling pathways with interactions occurring through PKA-independent pathways, PKA-mediated inhibition of Raf-1 and PKA-mediated activation of the GTPase Rap1, which interferes with Ras-mediated activation of the MAPK pathway, depending on cell-type.[100] Gene transcription downstream of $G\alpha_{i/o}$ signalling is under the influence of the transcription factor cAMP response element-binding protein (CREB).[100] CREB binds to cAMP response elements (CRE) which are regulatory elements present in the promotors of target genes and thus CRE can be used as a measure of $G\alpha_{i/o}$–mediated gene expression.[90]

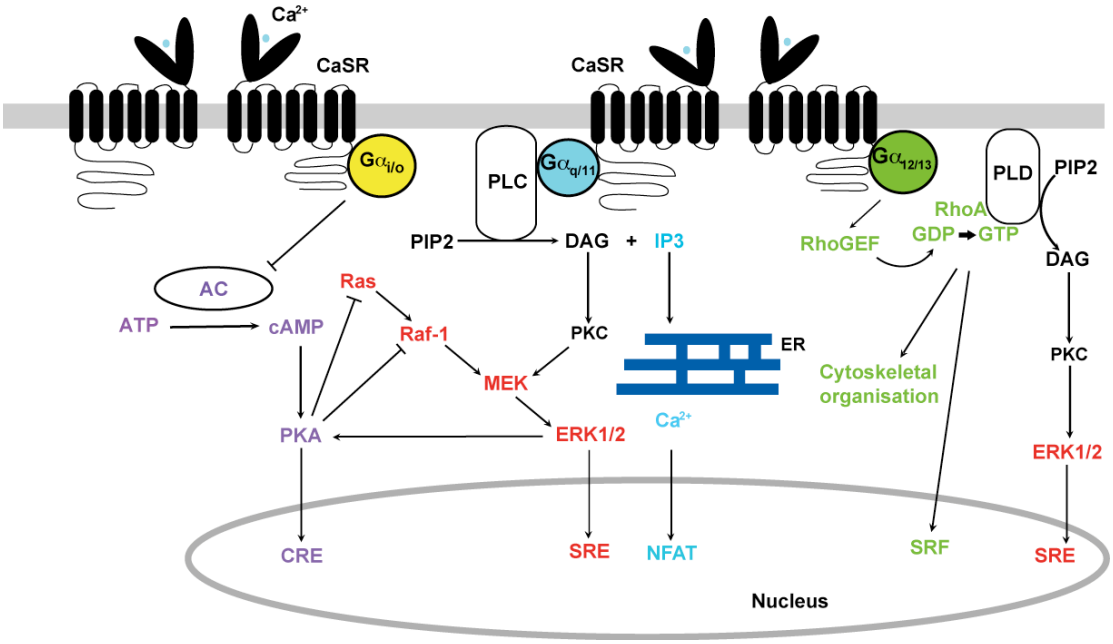


Figure 1.12. **CaSR signalling via $G\alpha_{i/o}$ coupling.**

Activation of the $G\alpha_{i/o}$ subunit leads to inhibition of adenylyl cyclase resulting in a reduction in the conversion of adenosine triphosphate (ATP) to cyclic monophosphate (cAMP). This reduction in cAMP levels has an inhibitory effect on protein kinase A (PKA) which itself has an inhibitory effect on the MAPK signalling pathway. Thus $G\alpha_{i/o}$ signalling can also influence gene transcription through SRE. Downstream of PKA, Gαi/o signalling can influence gene transcription through the cAMP response element-binding protein (CREB) (not shown). CREB binds to cAMP response elements (CRE) present in the promotors of target genes and thus CRE can be used as a measure of Gαi/o–mediated gene expression. Adapted from Cheng Z. *et al*. 2010.[90]

1.5.4 $G\alpha_s$ signalling

CaSR has been demonstrated to switch coupling from the $G\alpha_{i/o}$ to $G\alpha_s$ subunit in two breast cancer cell lines[80] and in a pituitary tumour cell line[101] therefore, stimulating cAMP synthesis (Figure 1.13). The mechanisms behind this switch in G-protein coupling are not understood and require further investigation.

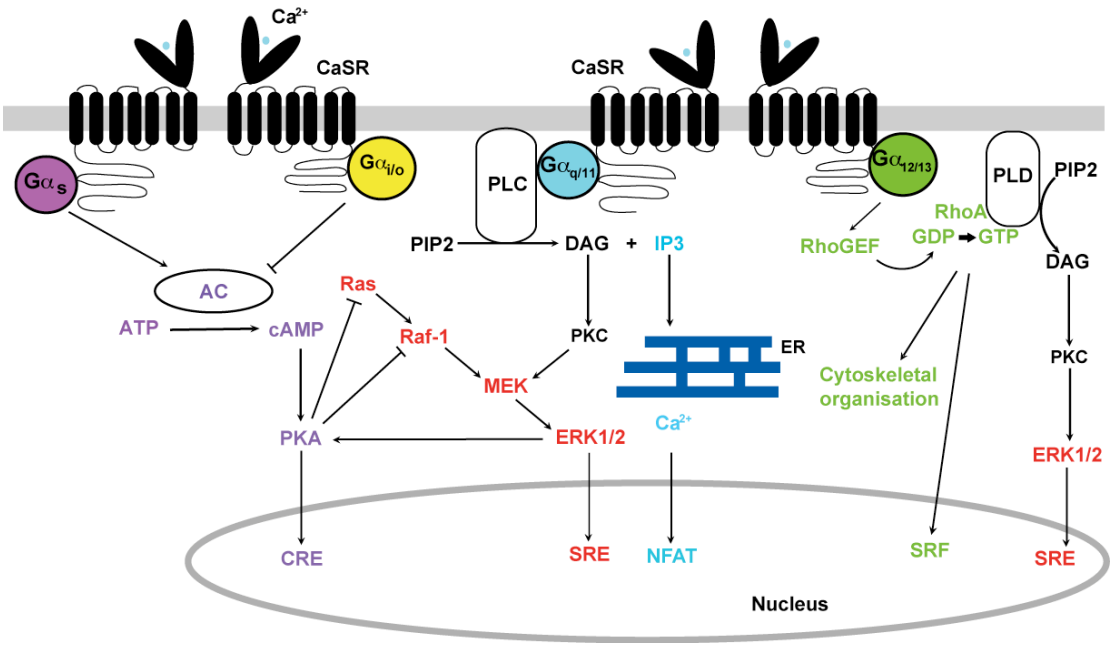


Figure 1.13. Schematic representation of multiple G-protein signalling pathways including $G\alpha_s$ coupling.

Coupling of the CaSR to $G\alpha_s$ has been demonstrated in certain tumour cell lines. This results in activation of adenylyl cyclase (AC) and hydrolysis of adenosine triphosphate (ATP) to cyclic adenosine monophosphate (cAMP). The mechanism underlying this switch in G-protein coupling is unknown. Coupling of the CaSR to the other heterotrimeric G-proteins, $G\alpha_{q/11}$, $G\alpha_{12/13}$, and $G\alpha_{i/o}$, is shown to demonstrate the pleiotropy of the receptor and the complexity of the downstream signalling pathways. Adapted from Cheng Z. *et al*. 2010.[90]

1.5.5 Allosteric modulators and ligand-biased signalling

Different ligands have varying capacities to activate the signalling pathways downstream of CaSR, a phenomenon referred to as biased signalling (section 1.4.5). For example, in CaSR-expressing HEK293 cells, it has been shown that extracellular Ca^{2+} preferentially mediates activation of the PLC-IP3 pathway and inhibition of cAMP pathway over phosphorylation of the ERK1/2 pathway (pERK1/2).[102] The signalling profile of extracellular Ca^{2+} contrasts with that of spermine which favours pERK1/2.[103] As allosteric modulators can either modify the affinity or efficacy of the orthosteric agonist or can induce a conformational change in the receptor in the

absence of the ligand, they have the capacity to alter the signalling profile of the bound receptor (Figure 1.14).

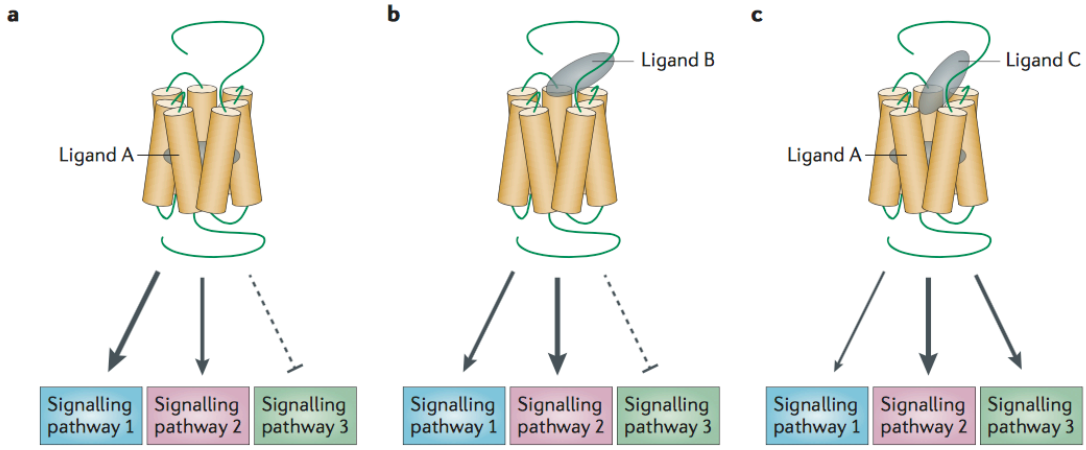


Figure 1.14. Schematic representation of ligand biased signalling.

The ability of different ligands to modulate the coupling of an agonist to downstream signalling pathways is shown in the following examples: (**a**) When ligand A binds to the transmembrane domain of the GPCR, signalling through pathway 1 is potentiated (bold arrow) whilst signalling through pathway 3 is blocked (dashed line); (**b**) Binding of ligand B to the VFTD potentiates signalling through pathway 2 (bold arrow) with inhibition of pathway 3 (dashed line); and (**c**) Co-binding of ligand C and ligand A potentiates signalling through pathway 2 (bold arrow) but reduces signalling through pathway 1 (thin arrow). Adapted from Wootten D *et al*. 2013.[104]

For example, L-amino acids which are endogenous PAM and bind in the VFTD inhibit cAMP production,[105] have limited effects on pERK1/2[102] and preferentially mediate intracellular Ca^{2+} release through a $G\alpha_{12/13}$-mediated pathway.[106] Studies have also shown the signalling bias of synthetic PAMs such as cinacalcet.[96] Cinacalcet is an effective treatment for various forms of hyperparathyroidism due to the suppression of PTH secretion in the parathyroid.[65] However, it is associated with hypocalcaemia which is due to a combination of: parathyroid PTH secretion; enhancement of extracellular Ca^{2+}-mediated activation of CaSRs in the renal thick ascending limb; and possibly, extracellular Ca^{2+}-mediated activation of CaSRs in thyroid parafollicular C-cells resulting in calcitonin release.[65 102] Calcimimetics that have no effects beyond the parathyroid are likely to have a broader application of clinical uses. The third-generation calcimimetics, *R,R*-calcimimetic B and AC-

265347, effectively suppressed PTH secretion and have been demonstrated to favour pERK1/2 over intracellular Ca^{2+} release in the parathyroid.[67] Calcitonin release in thyroid C-cell lines is independent of pERK1/2. In a rat model of chronic kidney disease, there was a reduced incidence of hypocalcaemia seen in affected rats treated with *R,R*-calcimimetic B.[107]

1.5.6 Mutation-biased signalling

Naturally occurring CaSR mutations are found throughout the length of the protein with 40% of disease-causing mutations located in the first 300 ECD residues[108] (Figure 1.15). Historically they have been functionally characterised as either global loss- or gain-of-function mutations and are associated with disorders characterised by hypercalcaemia and hypocalcaemia, respectively. For example, loss-of-function CaSR mutations result in familial hypocalciuric hypercalcaemia (FHH), neonatal severe primary hyperparathyroidism (NSHPT) and primary hyperparathyroidism (PHPT) whereas gain-of-function mutations result in autosomal dominant hypocalcaemia (ADH) and Bartter syndrome type V (discussed in section 1.10).[109]

Historically, the majority of studies functionally characterised CaSR mutations using measurements of $G\alpha_{q/11}$ –mediated signalling but recent studies have revealed that many mutations do not cause a global loss- or gain-of function in coupling of the CaSR to all its downstream signalling pathways.[102] The majority of these CaSR mutations are located in the ECD and TMD.[110] For example, Arg185Gln (R185Q) (Figure 1.15) is classified as a loss-of-function mutation located in the ECD which causes neonatal severe hyperparathyroidism (discussed in section 1.10).[110] It has been

demonstrated to result in a loss of preferential coupling to intracellular Ca^{2+} mobilisation relative to pERK1/2 rather than a global loss-of-function.[110] Detailed functional studies into the effects of naturally occurring mutations on the downstream signalling pathways not only give insight into the clinical phenotype but also have implications for the development of pathway-specific drug therapies.

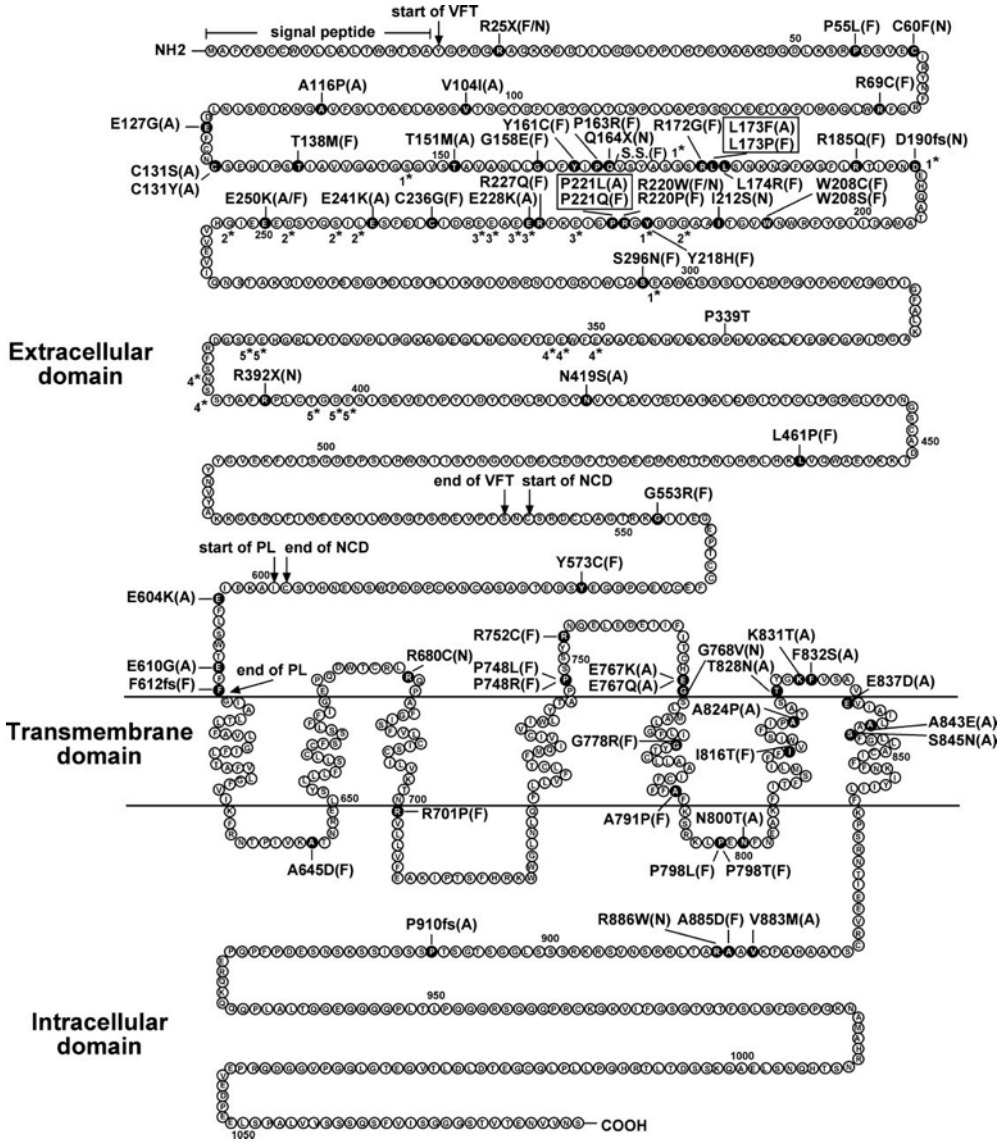


Figure 1.15. Schematic representation of 70 naturally occurring CaSR mutations.

Naturally occurring CaSR mutations are found in the extracellular, transmembrane and intracellular domains of the protein. The bracketed letter following the amino acid change indicates whether the variant was identified in an individual with familial hypocalciuric hypercalcaemia (F), neonatal severe hyperparathyroidism (N), autosomal dominant hypocalcaemia (A), or in both familial hypocalciuric hypercalcaemia and autosomal dominant hypocalcaemia (A/F) (section 1.10). Adapted from Hannan F.M. *et al*. 2012.[111]

1.6 Inactivation of CaSR

Following ligand binding, GPCRs undergo rapid phosphorylation by GPCR kinases (GRKs),[112] which are a family of protein kinases that phosphorylate serine and threonine residues in the ICD of their associated GPCR, or second-messenger protein kinases, such as PKC. This phosphorylation blocks G-protein binding hence inhibiting downstream signal transduction and has been shown to facilitate the binding of β-arrestin to the heptahelical domain.[113] The β-arrestins, β-arrestin-1 and β-arrestin-2, are ubiquitously expressed cytosolic proteins which bind specifically to ligand-bound GPCRs that have been phosphorylated.[114] β-arrestin-1 and β-arrestin-2 are themselves phosphorylated by ERK1/2[115] and casein kinase II,[116] respectively.

The CaSR undergoes phosphorylation by PKC at five residues within the ICD including Thr888,[117] resulting in recruitment of β-arrestin to the receptor. Additionally, a study examining the effects of GRK overexpression on CaSR downstream signal transduction using a SRE luciferase reporter assay, reported a reduction in CaSR-mediated signalling by GRKs 2, 4 and β-arrestin.[113] Inositol phosphate (IP) accumulation assays performed in cells expressing CaSR with the predicted PKC phosphorylation sites mutated to alanine demonstrated that overexpression of GRK2 significantly reduced extracellular Ca^{2+}-mediated IP accumulation whereas overexpression of β-arrestin-1 or β-arrestin-2 had no effect on IP accumulation.[118] This suggested that GRK2 predominantly binds to $G\alpha_q$.[118] In summary, these data suggest that GRKs and PKC phosphorylate CaSR resulting in its inactivation and that subsequent recruitment of β-arrestin may be PKC dependent for CaSR.

The CaSR is resistant to desensitisation, which is defined as loss of functional response in the receptors on exposure to continuous agonist stimulation, and consequently enables CaSR to evoke downstream signalling responses despite continuous exposure to extracellular Ca^{2+}.[59] Mechanisms of GPCR desensitisation can be either short- or long-term. Short-term desensitisation involves the phosphorylation of the receptor by GRKs or protein kinases and long-term desensitisation involves regulation of gene expression. It has been postulated that CaSR may avoid short-term desensitisation by undergoing repeated phosphorylation and dephosphorylation at PKC phosphorylation sites, including Thr888 where this phenomenon was demonstrated.[119] The lack of desensitisation is also likely to be a consequence of the unique mechanisms that regulate the cell surface expression and trafficking of the CaSR which are yet to be fully elucidated[120], discussed in section 1.8.

1.7 Internalisation of CaSR

Transmembrane proteins can be internalised by clathrin-mediated endocytosis (CME) (Figure 1.16)[121 122] or clathrin-independent endocytosis such as caveolae.[123] Studies have shown that GPCRs predominantly use CME,[123] as is the case for CaSR, and thus non-CME pathways will not be discussed further. CME is essential for the regulation of cell surface expression of receptors, control of activation of downstream signalling pathways, sampling of the extracellular environment to maintain cellular homeostasis and maintenance of the plasma membrane itself.[122] The process can be constitutive or agonist-induced and commences with invagination of the plasma membrane to form a coated pit.[121 122] For most GPCRs ligand binding commonly results in a GRK/protein kinase-mediated phosphorylation of the receptor and subsequent binding of β-

arrestin.[123] β-arrestin, in addition to blocking the G-protein-GPCR interaction, promotes the recruitment of adaptor protein-2 (AP-2) and clathrin (Figure 1.16) and in addition, facilitates receptor inclusion into the developing vesicles.[123] Studies on CME of CaSR have suggested that the process is rapid and constitutive rather than agonist-induced.[120 124]

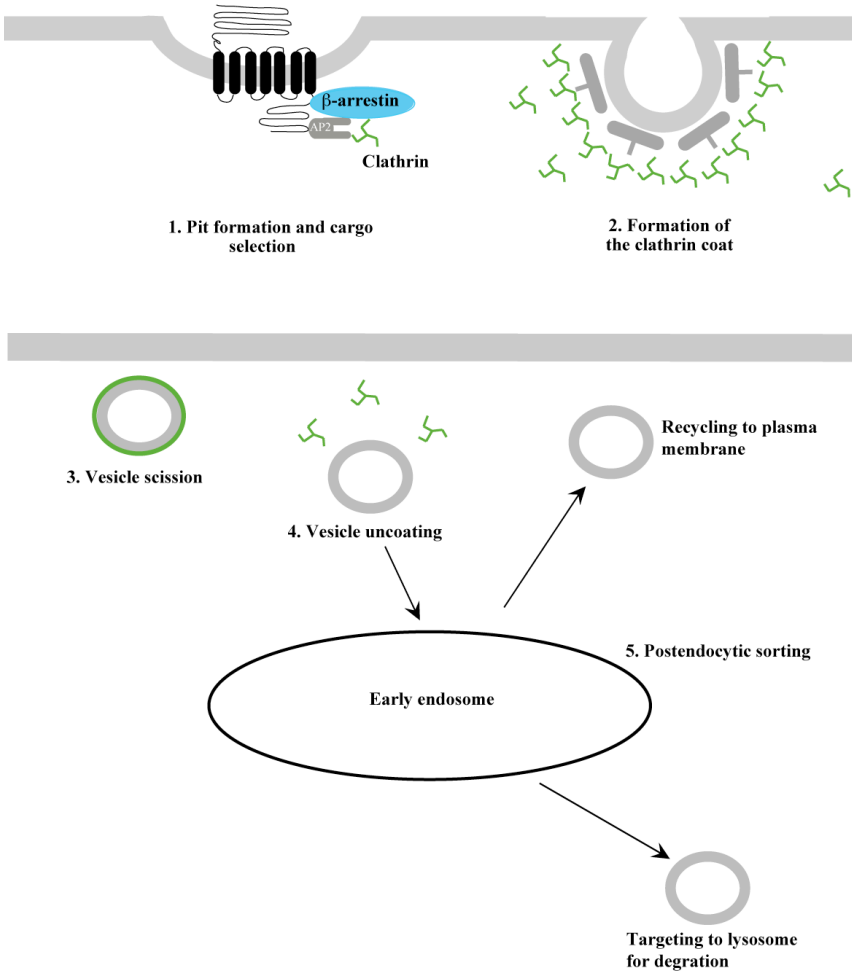


Figure 1.16. Clathrin-mediated endocytosis and retrograde trafficking.

Clathrin-mediated endocytosis commences with: (1) the formation of a coated pit in the plasma membrane.[122] AP-2 and other accessory proteins involved in cargo selection are recruited to the plasma membrane.[122] AP-2 recognises binding-motifs within the intracellular domain of plasma membrane proteins binding to them via the μ2 or σ2 subunits. The β2 subunit then interacts with clathrin triskelia.[122] (2) The clathrin triskelia polymerise to form the clathrin coat.[122] (3) Dynamin is recruited to the neck of the clathrin-coated vesicle, by Bin-Amphiphysin-Rvs (BAR) domain-containing proteins, and undergoes self-polymerisation inducing membrane scission.[122] However, CME of CaSR has been suggested to be dynamin-independent.[125] (4) The coated vesicle travels into the cell, the clathrin coat disassembles, and the uncoated vesicle fuses with its target endosome.[122] (5) The endocytosed GPCRs are then sorted between divergent downstream pathways which has distinct effects on downstream signalling. Rapid recycling of receptors to the plasma membrane results in return of functional receptors to the cell surface enabling ligand binding, receptor activation, and downstream signalling to occur. Recycling of the CaSR to the plasma membrane has been shown in some studies[124] but not in others.[120] Targeting of endocytosed GPCRs to the lysosomes, however, prevents those receptors from being used for further signaling events and results in proteolytic degradation. Adapted from McMahon H. T. and Boucrot. 2011.[122]

1.7.1 Role of Adaptor protein-2 (AP-2) in clathrin-mediated endocytosis

AP-2 is a member of the family of ubiquitously expressed cytosolic heterotetrameric adaptor protein complexes involved in cellular trafficking. They are all composed of two large subunits of 100-130kDa, one medium subunit of ~50kDa and a small subunit of 17-20kDa.[126] AP-2 is an ~250kDa complex consisting of a central core domain comprising two smaller subunits, the μ2 and σ2 subunits, which are 50kDa and 17kDa, respectively, and two larger appendage domains of ~100kDa, the α and β2 subunits (Figure 1.17).[126] The α and β2 subunits form a compact core around the N-terminal domain of μ2 (N-μ2) and σ2 subunits (Figure 1.17), which together form a ridge on which the C-terminal domain of μ2 (C-μ2) is positioned.[126] The N-μ2 and σ2 subunits, which are structurally similar, are considered to stabilise the AP-2 complex and both comprise a 5-stranded β-sheet with α helices on both sides.[126] Each subunit is in contact with all the other subunits within the complex (Figure 1.17) and large/small subunit heterodimers form with hydrophobic interfaces between α/σ2 and β2/N-μ2 subunits.[126] If a subunit is deleted, the complex becomes insoluble due to exposure of the hydrophobic surface.[126]

The μ2 subunit is able to bind β-arrestin[127] and this may be involved in recruitment of AP-2 to the plasma membrane. The recruitment of AP-2 to the plasma membrane triggers transition from a closed to open conformation which involves movement of the μ2 subunit (Figure 1.18).[128] This leads to exposure of PIP2- and peptide-binding motifs on AP-2.[128] The μ2 subunit recognises tyrosine-based motifs (YXXØ, where Y= tyrosine, X= any amino acid, and Ø= amino acid with a bulky hydrophobic side

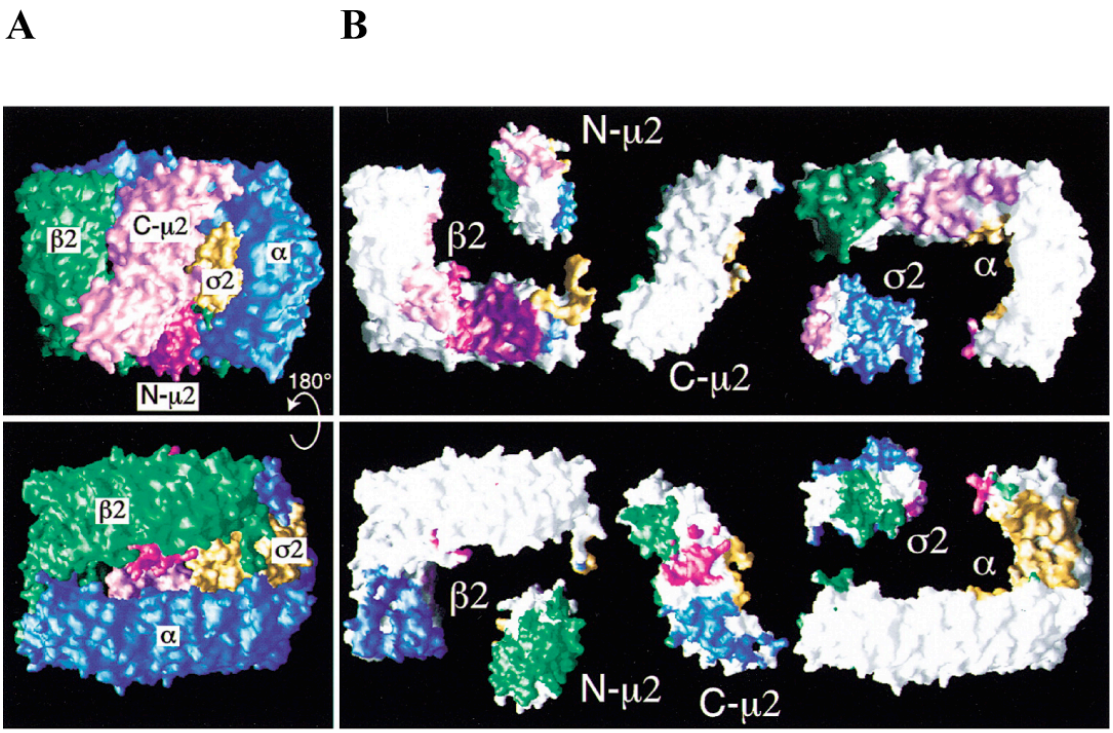


Figure 1.17. Surface representation of the AP-2 core.

(A) Surface representation of the AP-2 core (α subunit, blue; β2 subunit, green; σ2 subunit, yellow; N-terminal domain of μ2 (N- μ2) subunit, dark purple; C-terminal domain of μ2 (C-μ2) subunit, pink) with front (upper image) and back (lower image) views. (B) Surface representation of the individual subunits of AP-2 showing regions of interaction. Front (upper image) and back (lower image) views are shown. Regions that interact with the α subunit are shown in blue, those that interact with the β2 subunit are shown in green, those that interact with σ2 subunit are shown in yellow, those that interact with N-μ2 subunit are dark purple and those that interact with C-μ2 subunit are shown in pink. Image taken from Collins B. M. 2002.[126]

chain) in the cytoplasmic tails of transmembrane proteins and the σ2 subunit recognises acidic dileucine motifs (E/DxxxLL, where E/D= glutamic acid or aspartic acid, x= any amino acid, and L=leucine).[129] Dileucine motifs have been shown to form polar contacts with key residues in the AP-2 complex, Arg15 in the σ2 subunit and Arg21 in the α subunit.[129] There is a putative dileucine motif in the ICD of the CaSR (Leu1013Leu1014) which when mutated to Ala1013Ala1014 is associated with a reduction in intracellular Ca^{2+} release compared to WT CaSR,[130] however this motif has an Arg in the -4 position (RxxxLL, rather than E/D). However, it is possible that plasma membrane proteins with such non-canonical sorting motifs may bind to the

AP-2 core, such as the low-density lipoprotein (LDL) receptor.[126] Presentation of PIP2 in combination with a peptide motif in the ICD of a plasma membrane protein, such as the CaSR, leads to over-competition of side chains of the β2 subunit for cargo-binding sites on the μ2 or σ2 subunit, resulting in cargo binding.[128]

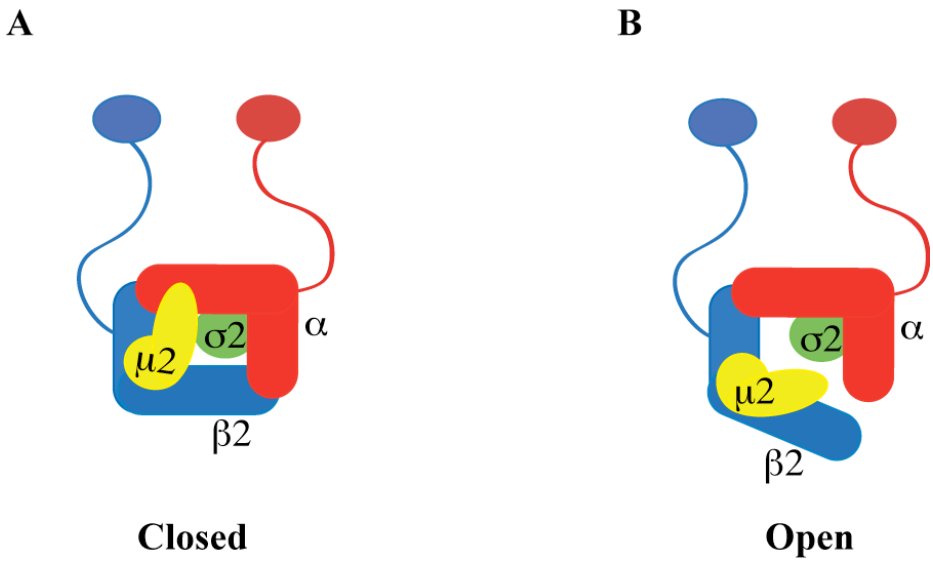


Figure 1.18. Schematic representation of the closed and open conformations of AP-2.

(A) In the closed, inactive state, the α (red) and β2 (blue) subunits of the AP-2 complex form a puckered ring around the μ2 (yellow) and σ2 (green) subunits.[128] (B) On recruitment to the plasma membrane, AP-2 adopts an open conformation.[128] The ring structure divides between the N termini of the α and β2 subunits whilst the C terminus of μ2 rotates about its long axis.[128] This leads to exposure of PIP2-binding sites on the α subunit and peptide-binding motifs on σ2 and μ2 subunits.[128] Presentation of PIP2 and peptide motif in the intracellular domain of cargo leads to over-competition of side chains of β2 subunit for cargo-binding sites on μ2 or σ2, such that cargo-binding occurs. Adapted from Jackson *et el.* 2010.[128]

1.7.1.1 The Adaptor Protein-related Complex 2 Sigma 1 Subunit gene (*AP2S1*)

The Adaptor Protein-related Complex 2 Sigma 1 Subunit gene (*AP2S1*) encodes the 142kDa σ2 subunit of AP-2 (AP2σ2). *AP2S1* is located at 19q13.3-19q.13.2 and comprises 5 exons (Figure 1.19). The 229bp of exon 1 are predominantly untranslated except for the translation initiation codon, ATG. Exon 2 is 150bp in length and contains the Arg15 residue (Figure 1.19), mutations of which to Cys, His and Leu are

associated with familial hypocalciuric hypercalcaemia type 3 (FHH3),[130] discussed in section 1.10.1.1. FHH3 is the only human disorder to be associated to date with a mutation in a gene encoding an AP-2 subunit. Exons 3 and 4 are 174bp combined whilst exon 5 is 382bp in length, with 102bp of coding sequence terminated by the stop codon, TGA (Figure 1.19). The gene has ten transcripts of which seven are protein-coding.

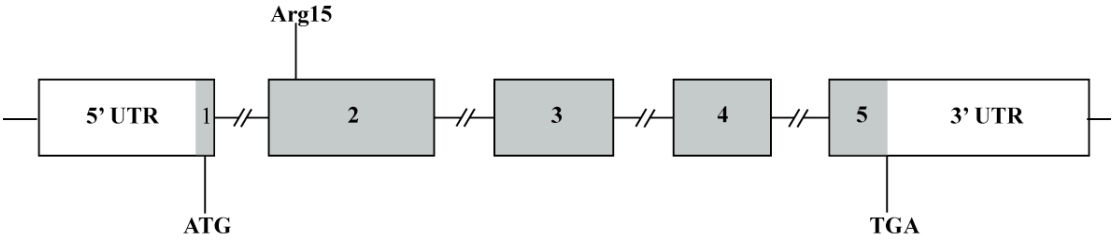


Figure 1.19. Schematic representation of the Adaptor Protein-related Complex 2 Sigma 1 Subunit gene, *AP2S1*.

AP2S1 encodes the 142 amino acid σ2 subunit of AP-2 and comprises 5 exons (shown by the boxes). Exon 1 is 229bp in length and is predominantly comprised of 5'UTR (shown by the unshaded region) followed by the translation initiation codon (represented by the shaded region). Exon 2 is 150bp in length and contains the Arg15 residue, mutations in which are associated with familial hypocalciuric hypercalcaemia type 3.[130] Exons 3 and 4 are 114bp and 60bp in length, respectively. Exon 5 comprises 102bp of coding sequence (represented by the shaded region) terminated by the stop codon TGA and the remainder is 3'UTR.

1.7.2 Role of clathrin in clathrin-mediated endocytosis

After AP-2 has bound to PIP2 and its cargo, the β2 subunit interacts with clathrin triskelia.[122 128] A clathrin triskelion consists of three ~190kDa clathrin heavy chains, each of which is bound to a light chain of ~25kDa. Clathrin triskelia polymerise to form a lattice-like, clathrin-coated vesicle (CCV) (Figure 1.20) which stabilises the curvature of the enlarging vesicle.[122] Recruitment of dynamin, a large GTPase, to the neck of CCVs by Bin-Amphiphysin-Rvs (BAR) domain-containing proteins such as amphiphysin and endophilin has been demonstrated for CME of GPCRs.[131]

Polymerisation around the neck of the vesicle promotes GTP hydrolysis, leading to a conformational change in dynamin resulting in vesicle scission (Figure 1.16).[132] However, vesicle budding has been shown to be dynamin-independent for CaSR.[125] The CCV is subsequently internalised into the cell where the clathrin coat is disassembled by proteins including the ATPase heat shock cognate 70 (HSC70) and auxilin.[133] The uncoated vesicle is then trafficked to its target endosome.

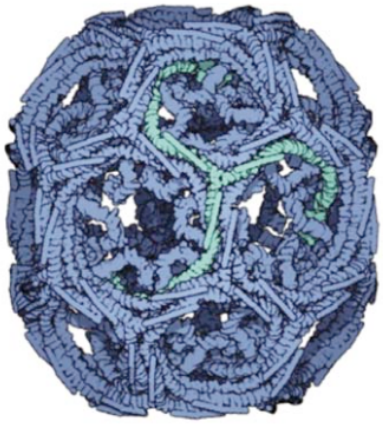


Figure 1.20. Schematic representation of clathrin triskelia organised into a clathrin cage.

Individual clathrin triskelions (light green) polymerise to form a clathrin cage-like lattice (blue) which surrounds and supports the developing vesicle. The clathrin-coated vesicles range in size from 30-100nm and are 100-fold stiffer than the typical liposome.[134] Adapted from Vitaliano G.D. *et al*. 2012.[134]

1.8 Trafficking of the CaSR

1.8.1 Post-endocytic trafficking of the CaSR

Once GPCRs are internalised, they are trafficked to distinct endosomal compartments such as the pre-early or early endosomes for post-endocytic sorting (Figure 1.16).[135] Whilst the post-endocytic sorting of the CaSR is yet to be fully elucidated, the trafficking of other GPCRs, such as the class A GPCRs β_2AR and luteinising

hormone receptor (LHR), has been characterised more precisely. β_2AR is trafficked to the early endosome and a key protein involved in its endosomal localisation is Rab5, a member of the Rab GTPase family of Ras-like small GTP binding proteins involved in various stages of trafficking.[123] Contrastingly, LHR is trafficked to the pre-early endosome and localisation to this compartment requires the postsynaptic density protein (PSD95), *Drosophila* disc large tumour suppressor (Dlg1), zonula occludens-1 protein (zo-1) (PDZ) domain containing protein GAIP-interacting protein C terminus (GIPC).[135]

GPCR signalling occurs via G-protein coupling (section 1.5) and this can be referred to as canonical signalling, as they were the first signal transduction pathways to be elucidated. Subsequently, it has been revealed that GPCRs can signal via additional signalling pathways referred to as non-canonical pathways. For example, it has been revealed that some GPCRs continue to signal following endocytosis such that trafficking and signalling rather than being two discrete processes are interconnected.[135 136] The β-arrestins have been demonstrated to activate signalling pathways downstream of β_2AR independently of G-protein activation by acting as a scaffold for the assembly of proteins including those involved in the ERK1/2 pathway (Figure 1.21).[137] Dephosphorylated β-arrestin-1 stimulates ERK1/2 activation and subsequently, pERK1/2 phosphorylates β-arrestin-1 resulting in a negative feedback effect on the function of β-arrestin-1.[115] The interactions between β-arrestins and the ERK1/2 pathway for CaSR are yet to be elucidated.

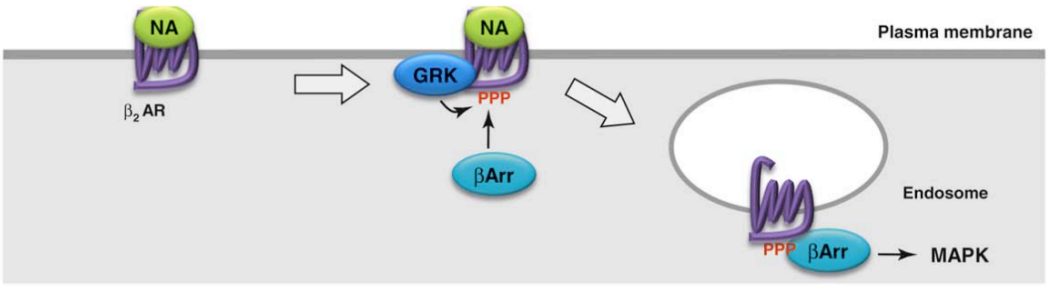


Figure 1.21. Non-canonical signalling of β_2-adrenergic receptor.

Noradrenaline (NA) binding to the β_2-adrenergic receptor (β_2AR) results in receptor activation and subsequent phosphorylation by GPCR related kinase (GRK). β-arrestin (βArr) is recruited to the phosphorylated receptor and internalisation occurs. Following internalisation, β_2AR complexed with βArr can activate the MAPK signalling cascade from endosomes via a G-protein-independent mechanism. Adapted from Calebrio D et al. 2010.[138]

Additionally, the post-endocytic sorting of receptors has been revealed to have effects on their downstream signalling activity.[135] It has been shown that redirection of the LHR from the pre-early endosome to the early endosome is associated with a reduction in the duration of the ERK1/2 signal generated.[135] Thus, the trafficking network of GPCRs is involved in the regulation of downstream signalling events.[135]

Once sorted to the pre-early or early endosomes, GPCRs can be trafficked to either the late endosome for lysosomal-mediated degradation via the multi-vesicular body (MVB) or recycled back to the plasma membrane (Figure 1.16).[136] Dorfin-mediated ubiquitination[139] of CaSR was shown to be involved in targeting the internalised receptor for lysosomal degradation. Many proteins that are targeted for rapid degradation contain a long sequence rich in proline, glutamine, serine, and threonine (PEST-like sequence)[124] and such a sequence is present in the ICD of the CaSR, which is likely to target it for lysosomal degradation. Recycling of the CaSR to the plasma membrane has been shown in one study[124] but not in another.[120]

1.8.2 Biosynthesis of CaSR and Agonist-Driven Insertional Signalling (ADIS)

The CaSR is targeted to the ER by a signal peptide following synthesis by the ribosome and here it undergoes dimerisation by formation of disulphide bonds between the VFTDs of individual CaSR momomers (Figure 1.7).[42 43] The homodimers are trafficked from the ER to the Golgi apparatus (Figure 1.22) by chaperones, including p24A[140] and receptor-activity-modifying proteins (RAMPs)[141], where they are heavily glycosylated.[43] The glycosylated homodimers traverse through the trans-Golgi network (TGN) before being incorporated into secretory vesicles and trafficked to the cell surface (Figure 1.22), which requires chaperones such as Rab1[142] and calmodulin.[143]

Vesicles containing fully mature CaSR are retained intracellularly at the TGN or near-membrane location.[120] Increases in the concentration of extracellular Ca^{2+} lead to rapid insertion of these vesicles into the plasma membrane, increasing the concentration of cell surface CaSR.[120] This process is known as agonist-driven insertional signalling (ADIS)[120] (Figure 1.22). A possible explanation for this process could be that key chaperones may be responsive to changes in intracellular Ca^{2+} or other downstream effectors and following ligand binding to cell surface CaSR and signal transduction, activation of chaperones results in increased anterograde trafficking of intracellular CaSR with increased cell surface receptor expression. This may explain the finding that calmodulin binding domain mutations in the CaSR are associated with abnormal intracellular calcium oscillations.[143]

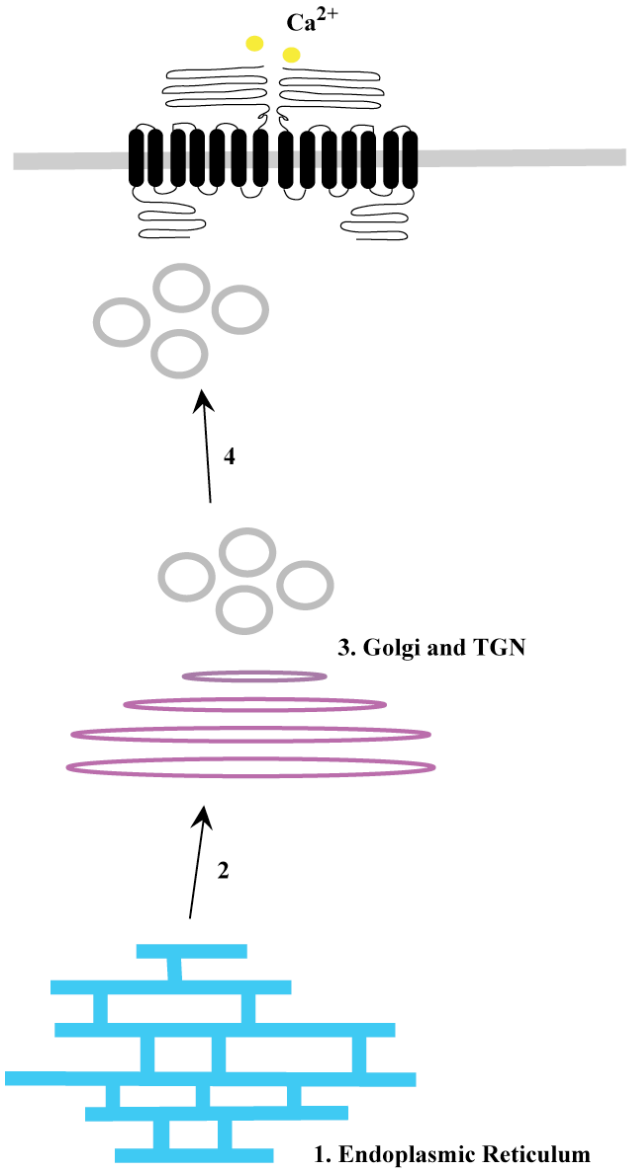


Figure 1.22. Agonist-driven insertional signalling (ADIS).

The anterograde trafficking of CaSR has been shown to be responsive to the extracellular concentration of Ca^{2+}. (1) Newly synthesized CaSR monomers undergo dimerisation in the endoplasmic reticulum (ER).[42 43] (2) The homodimers are trafficked from the ER to the Golgi apparatus by chaperones.[141] (3) Glycosylation occurs within the Golgi apparatus[43] before the receptors are packaged into secretory vesicles within the trans-Golgi network (TGN). (4) The vesicles are then trafficked to the cell surface where vesicles containing mature CaSR are retained intracellularly in a peri-membrane location.[120] Increases in the concentration of extracellular Ca^{2+} lead to rapid insertion of these vesicles into the plasma membrane, increasing the concentration of cell surface CaSR.[120] This process is known as agonist-driven insertional signalling (ADIS).[120] Adapted from Grant M. P. *et al*. 2011.[120]

1.9 The physiological roles of the CaSR

The role of the CaSR in the regulation of calcium in blood and bone, referred to as its calciotropic role, is well established and the role of the CaSR in calcium homeostasis has been described in detail in section 1.3. The CaSR expressed within the parathyroid-kidney-bone axis has additional calciotropic roles, which are discussed in sections 1.9.1.1, 1.9.1.2, and 1.9.1.3. The CaSR is also expressed in the gastrointestinal tract, vasculature, lung, and central and peripheral nervous systems where it has been demonstrated to have non-calciotropic roles[144] (section 1.9.2). Furthermore, the CaSR has been demonstrated to be involved in organogenesis in the developing embryo in addition to mineral homeostasis[145] (section 1.9.3).

1.9.1 The calciotropic roles of the CaSR

1.9.1.1 The role of the CaSR in the parathyroid

In addition to the control of PTH secretion (section 1.3), the CaSR in the parathyroid glands controls PTH gene expression and parathyroid gland proliferation,[18] both of which are stimulated by hypocalcaemia and inhibited by hypercalcaemia. The mechanism by which activation of CaSR downstream signalling pathways regulates PTH secretion is incompletely understood. However, the polymerisation of the F-actin cytoskeleton has been shown to be involved in the inhibition of PTH secretion in response to increased extracellular Ca^{2+} in polarised parathyroid cells and is likely to prevent trafficking of PTH secretory vesicles to the plasma membrane.[146]

The regulation of PTH gene expression by CaSR is predominantly post-transcriptional, regulating PTH mRNA stability through post-translational modifications of *trans*-acting proteins which bind to a *cis*-acting AU-rich element (ARE) in the PTH mRNA 3'UTR.[147] AU-rich binding factor 1 (AUF1) is a stabilising protein whereas K homology (KH) domain splicing regulatory protein (KSRP) destabilises PTH mRNA.[147] The balanced interaction between PTH mRNA and these proteins thus determine serum PTH levels.[147] Expression of CaSR in HEK293 cells causes the PTH mRNA to interact with KSRP rather than AUF1 resulting in PTH mRNA instability and reduced PTH synthesis.[147] Hypocalcaemia attenuates the effect of CaSR expression on PTH mRNA instability.[147]

In normal adults, cellular proliferation within the parathyroid gland is controlled at very low levels[148] whereas parathyroid hyperplasia is seen in secondary hyperparathyroidism due to chronic renal failure,[23] in mice homozygous for loss-of-function mutations of the calcium sensing receptor gene (*Casr*)[149] and in individuals with homozygous loss-of-function mutations of *CASR*.[150] Suppression of parathyroid gland proliferation by the calcimimetic NPS R-568 (Figure 1.9) was demonstrated in a rodent model of chronic renal failure.[148] The mechanisms by which the CaSR regulate parathyroid gland hyperplasia remain uncertain but may involve cyclin D1,[151] a member of the highly conserved cyclin family required for progression through the G1 phase of the cell cycle, and the cyclin-dependent kinase inhibitors.[152]

1.9.1.2 The role of the CaSR in kidney

The CaSR has been shown to be expressed throughout much of the nephron (Figure 1.23) at the mRNA[153] and protein[154] level. Expression of CaSR on the apical and basolateral membranes of the tubules allows for sensing of Ca^{2+} in the lumen and the interstitial plasma, respectively providing a coordinated renal response to disturbances in extracellular Ca^{2+} homeostasis (section 1.3).

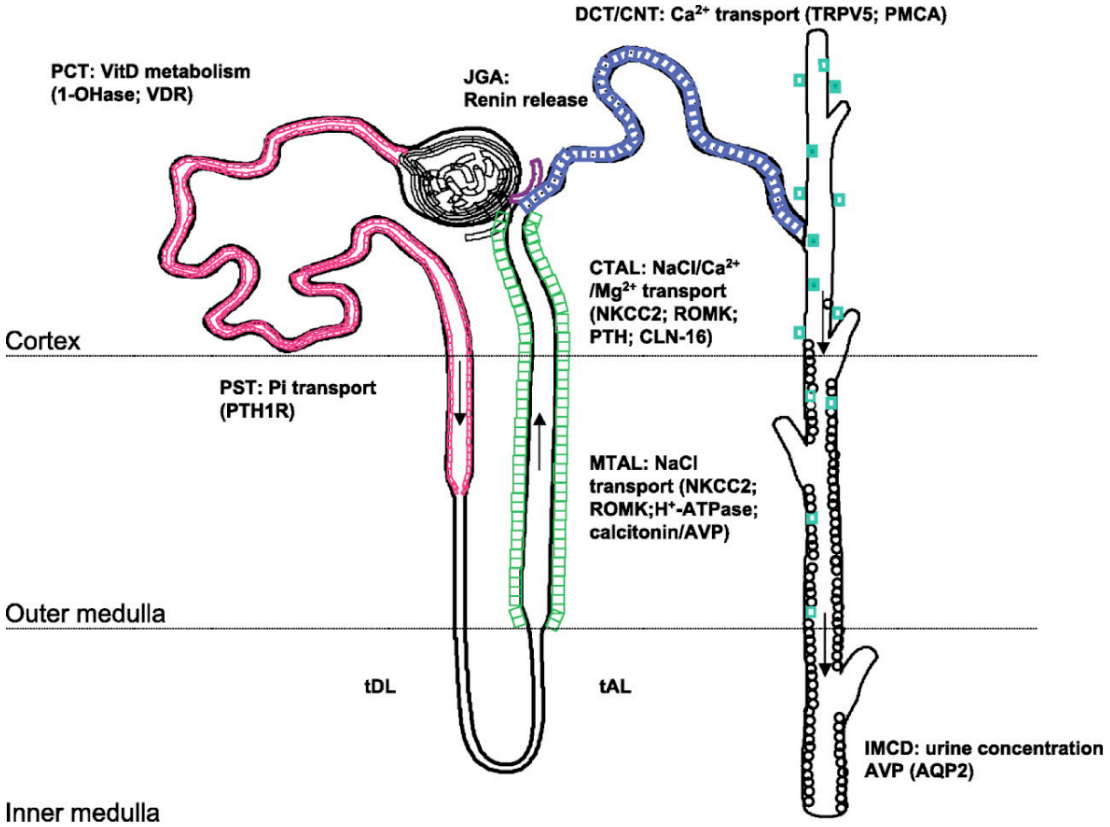


Figure 1.23. Schematic diagram showing the expression of CaSR in the kidney.

In the proximal convoluted tubule (PCT), the CaSR is expressed apically (represented by the pink shading) compared with the medullary and cortical thick ascending limbs (MTAL and CTAL, respectively) where the CaSR is expressed basolaterally (represented by the green shading). In the distal convoluted tubule (DCT)/connecting segment (CNT), CaSR expression can be detected apically, basolaterally or intracellularly depending on the particular species (shown by purple shading). Within the inner medullary collecting duct (IMCD), CaSR expression is apical and the receptor has been shown to co-localise with vasopressin-regulated aquaporin 2 (AQP2) water channels. PST, proximal straight tubule; tDL/tAL, thin descending/ascending limb; JGA: juxtaglomerular apparatus; TRPV5, transient receptor potential vanilloid 5; PMCA, plasma membrane Ca^{2+}-ATPase; VitD, vitamin D; VDR, vitamin D receptor; NKCC2, Na^{+}-K^{+}-$2Cl^{-}$ cotransporter 2; ROMK, renal outer medullary potassium K^{+} channel; PTH, parathyroid hormone. Adapted from Riccardi D and Brown E. M. 2009.[18]

Within the proximal tubule, CaSR is expressed in the subapical region[154] (Figure 1.23). The CaSR in this region controls circulating $1,25(OH)_2D_3$ as demonstrated by studies performed in proximal tubule-derived cell lines where high concentrations of luminal Ca^{2+} inhibited 1α-hydroxylase activity.[155] $1,25(OH)_2D_3$ modulates CaSR gene expression in the proximal tubule.[49] Additionally, CaSR regulates PO_4^{3-} excretion through the PTH receptor 1 (PTH1R) within the proximal tubule.[156]

In the thick ascending limb (TAL), reabsorption of cations such as Ca^{2+} and Mg^{2+} occurs by the transcellular or paracellular routes (Figure 1.24).[18] This process is driven by maintenance of a positive charge within the lumen of the TAL generated by the actions of: the apical Na^+-K^+-$2Cl^-$ co-transporter (NKCC2) (Figure 1.24), which actively transports 1 Na^+, 1 K^+ and 2 Cl^- ions into the cell from the lumen; and the apical renal outer medullary potassium K^+ (ROMK) channel (Figure 1.24), which allows K^+ to passively diffuse back into the lumen.[18] The basolateral Na^+/K^+-ATPase and Cl^- channels (Figure 1.24) then move the intracellular Na^+ and Cl^- into the interstitial plasma, respectively.[18]

During states of hypercalcaemia, activation of the CaSR on the basolateral surface of the TAL (Figure 1.23) inhibits ROMK channels[157] resulting in loss of the positive charge in the lumen and a subsequent reduction in paracellular Na^+, Ca^{2+} and Mg^{2+} transport.[158] Additionally, the CaSR controls Ca^{2+} reabsorption in the cortical TAL and in response to hypercalcaemia. Thus, the PTH-mediated apical transcellular passage of Ca^{2+} is inhibited[159] as is the active transport of Ca^{2+} across the basolateral membrane by the Ca^{2+}-ATPase into the bloodstream.[160]

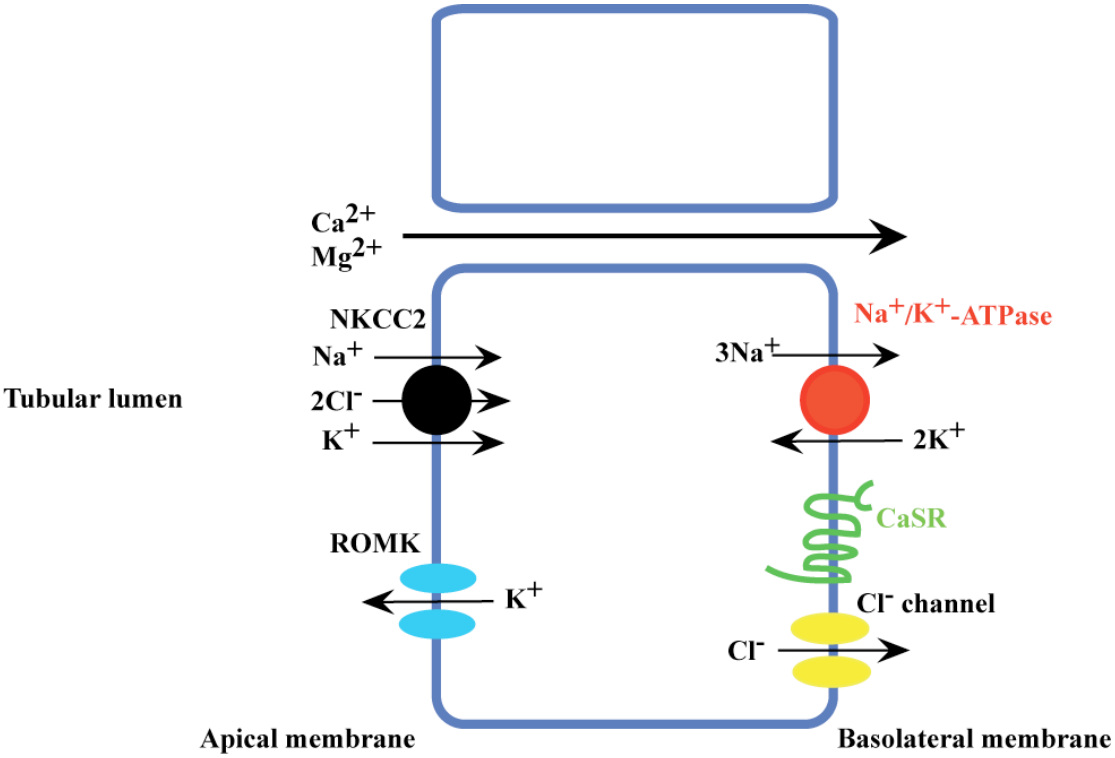


Figure 1.24. Schematic representation of an epithelial cell from the thick ascending limb of the loop of Henle.

Within the thick ascending limb of the loop of Henle, reabsorption of cations such as Ca^{2+} and Mg^{2+} occurs by the transcellular or paracellular routes.[18] This process is driven by the maintenance of a positive charge within the lumen, which is generated by the Na^{+}-K^{+}-$2Cl^{-}$ co-transporter (NKCC2) and the apical renal outer medullary potassium K^{+} (ROMK) channel.[18] The basolateral Na^{+}/K^{+}-ATPase and voltage-gated Cl^{-} channels then move the intracellular Na^{+} and Cl^{-} into the interstitial plasma, respectively.[18]

In the distal convoluted tubule (DCT), the CaSR may be involved in preventing excessive loss of Ca^{2+} in the urine in states of renal Na^{+} wasting.[18] The epithelial Ca^{2+} channel transient receptor potential vanilloid member 5 (TRPV5) and CaSR have been shown to co-localise at the apical membrane in the DCT (Figure 1.23) and activation of the CaSR in cells overexpressing TRPV5 resulted in increased TRPV5 activity.[161] In states of renal Na^{+} wasting, the associated increased urinary Ca^{2+} is hypothesised to activate the apical CaSR resulting in increased TRPV5 activity and reduced urinary Ca^{2+} excretion.[18]

The inner medullary collecting duct is responsible for regulating the final production of urine.[18] In hypercalciuric states it has been shown that activation of apical CaSR, which co-localises with vasopressin-regulated aquaporin 2 (AQP2) water channels,[162] results in reduced cell surface expression of AQP2 channels.[162] This results in reduced water reabsorption and thus hypercalcaemia can result in nephrogenic diabetes insipidus.[18]

1.9.1.3 The role of the CaSR in bone

Bone remodelling is a tightly regulated process which comprises a sequence of events commencing with resorption of mineralised matrix by osteoclasts and deposition of new bone matrix by osteoblasts to replace the resorbed bone (Figure 1.25).[163] Osteoblastogenesis is the process by which mesenchymal stem cells (MSCs) under the influence of a variety of signalling and transcription factors differentiate to osteoblast precursors and mature into osteoblasts (Figure 1.25).[164] Mature osteoblasts secrete osteoid, which mineralises to form bone. During osteoblast activation, receptor activator of nuclear factor κ-light-chain-enhancer of activated B cells ligand (RANKL) expression increases whereas expression of osteoprotegerin, the RANKL decoy receptor, decreases.[164] RANKL rapidly activates nuclear factor κ-light-chain-enhancer of activated B cells (NF-κB), a transcription factor involved in the regulation of many genes involved in cell proliferation and survival, on binding. This promotes osteoclastogenesis, which commences with a haematopoietic progenitor cell (HPC) committing to differentiation to an osteoclast precursor and maturing into an osteoclast (Figure 1.25). Extracellular Ca^{2+} is involved in the control of this process through its actions on PTH secretion in the parathyroid (section 1.3). Additionally,

extracellular Ca^{2+} has been demonstrated to directly activate CaSR expressed on bone cells and modulate bone remodelling at a local level (Figure 1.25).

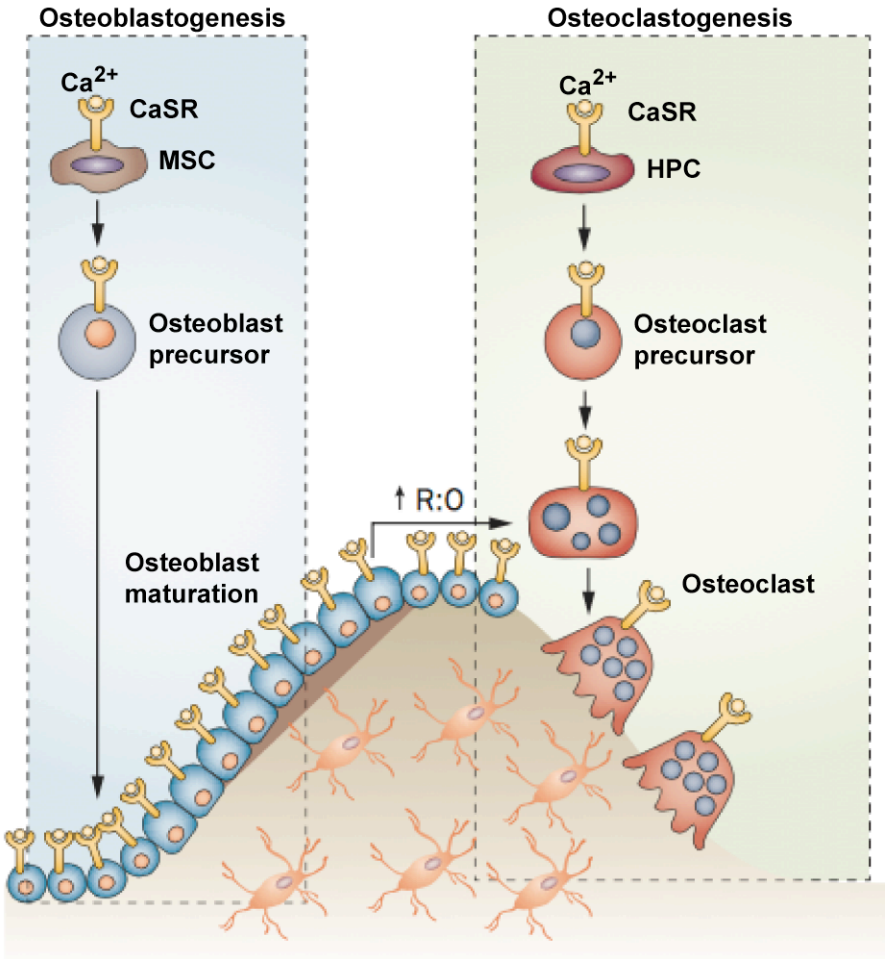


Figure 1.25. Schematic representation of bone remodelling in an adult.

Bone remodelling consists of cycles of bone formation and resorption. Osteoblastogenesis is the process by which mesenchymal stem cells (MSCs) expressing the CaSR undergoing differentiation to osteoblast precursors and mature into osteoblasts.[164] This is dependent upon a variety of signalling and transcription factors but extracellular Ca^{2+} has been shown to be involved. Mature osteoblasts secrete osteoid which mineralises to form bone. During osteoblast activation, RANKL (R) expression increases whereas expression of osteoprotegerin (O) decreases.[164] This promotes osteoclastogenesis which commences with a haematopoietic progenitor cell (HPC) committing to differentiation to an osteoclast precursor and maturing into an osteoclast. Adapted from Goltzman D *et al*. 2015.[164]

Osteoblast and osteoblast lineages have been demonstrated to express CaSR[165] and activation of CaSR on osteoblasts by extracellular Ca^{2+}[166] results in $G\alpha_{q/11}$ and $G\alpha_{i/o}$–mediated signalling (section 1.4.4), leading to production of PKC, PKA, and activation of the MAPK cascade.[163] Increased extracellular Ca^{2+} mediates osteoblast

proliferation and differentiation in *in vitro* osteoblast models.[167] Thus in the setting of bone remodelling, release of Ca^{2+} at sites of bone resorption stimulates osteoblastogenesis and deposition of new bone matrix (Figure 1.25).

Extracellular Ca^{2+} activates CaSR expressed on osteoclast precursors *in vitro*[168] suggesting a role for the CaSR in osteoclastogenesis (Figure 1.25). Activation of the CaSR on osteoclasts by extracellular Ca^{2+} may play a role in stimulating apoptosis through activation of PLC and NF-κB.[169] Adult mice expressing a constitutively active mutant CaSR in osteoblasts demonstrated increased bone resorption, which was associated with increased levels of RANKL, decreased bone volume and reduced bone mineral density (BMD).[170] Additionally, studies performed in *ex vivo* bone marrow cells from Parathyroid hormone gene (*Pth*) null and *Casr* null mice revealed that PTH-stimulated RANKL expression and osteoclastogenesis were reduced in the *Pth* null mice compared with the *Casr* null mice.[171]

1.9.2 The non-calciotropic roles of the CaSR

1.9.2.1 The role of the CaSR in the vasculature

Within the vasculature, the CaSR is expressed in the vascular smooth muscle and vascular endothelium where it is involved in blood pressure control.[172] Mice with isolated CaSR ablation from vascular smooth muscle cells demonstrate hypotension due to a reduction in peripheral vascular resistance whilst activation of the CaSR on the vascular endothelium results in nitric oxide-mediated relaxation.[144] In the setting of vascular calcification, CaSR expression is reduced on vascular smooth muscle

cells.[173] Vascular calcification is commonly seen in patients with end-stage chronic kidney disease and is associated with increased cardiovascular morbidity and mortality.[174] Many of these patients have received calcimimetic treatment over the last decade to treat the hyperparathyroidism associated with their renal disease. The calcimimetic R-568 (Figure 1.9) was shown to increase CaSR expression on vascular smooth cells *in vitro*[173] whilst a recent randomised, control study suggested that cinacalcet reduced the risk of cardiovascular events in elderly patients receiving haemodialysis compared to placebo.[72]

1.9.2.2 The role of the CaSR in the lungs

The CaSR is expressed on the epithelial and smooth muscle cells of both the human and mouse respiratory tract.[175] Recently, mouse and human *ex vivo* studies have revealed increased CaSR expression in asthma with consequent increases in downstream signalling pathways.[175] Interestingly, the sputum of asthmatics contains cationic proteins and polyamines.[144] Human airway smooth muscle cells from healthy individuals exposed to tumour-necrosis factor-α and interleukin-13 for 48 hours showed significantly increased CaSR protein expression.[175] The calcilytic NPS 2143 (Figure 1.5) was associated with a reduction in airway hyperresponsiveness and inflammation in a mouse model of asthma.[175]

1.9.3 The role of the CaSR in foetal development

The CaSR has been shown to play key roles in the developing foetus not only in calcium homeostasis via regulation of PTH-related peptide (PTHrP) and PTH secretion but also in the optimal development of other viscera and tissues such as the skeleton, lungs[176] and nervous system.[177] The CaSR is widely expressed throughout the developing foetus with highest levels of expression seen in the bone, cartilage, lung, kidney, intestine and nervous system.[178]

Approximately 30g of calcium is actively transported across the human placenta to the developing foetus, predominantly during the last trimester.[179] Fetal mammals are hypercalcaemic compared to their mothers and this hypercalcaemia is maintained irrespective of the concentrations of maternal extracellular Ca^{2+} or $1,25(OH)_2D_3$.[145] The CaSR is critical for normal skeletal development as demonstrated by mice with tissue-specific homozygous deletion of *Casr* in osteoblasts and chrondrocytes.[180] Mice with homozygous deletion of *Casr* in osteoblasts had smaller and under mineralized skeletons with reduced expression of genes encoding markers of osteoblast differentiation compared to control mice.[180] Mice with homozygous deletion of *Casr* in chondrocytes were lethal before embryonic day 13 (E13).[180] Viability was achieved by induction of the chrondrocyte-specific deletion at E16 to E18 with these mice showing delayed growth plate development.[180]

During embryogenesis, lung epithelial cells secrete fluid into the lumen to act as a template around which branching can occur.[145] It has been demonstrated that CaSR expression in the developing mouse lung is confined to the branching morphogenesis

period[181] and that activation of the CaSR with foetal concentrations of extracellular Ca^{2+} stimulates Cl^--driven lung fluid secretion which results in suppression of branching morphogenesis.[176] Within the developing nervous system, the CaSR is highly expressed in both peripheral and central nervous systems, with a peak between E18 and postnatal day 0.[145] In the peripheral nervous system, regulated expression of the CaSR occurs at the time point when the sympathetic axons innervate their peripheral tissues.[177] In the central nervous system, CaSR expression has been identified throughout the postnatal rat brain and spinal cord and its distribution is suggestive of a role in myelinisation and oligodendrocyte maturation.[182]

1.10 Disorders of calcium homeostasis

Disorders of calcium homeostasis can result in either hypercalcaemia or hypocalcaemia.

1.10.1 Hypercalcaemic disorders

The hypercalcaemic disorders attributable to CaSR abnormalities include familial hypocalciuric hypercalcaemia (FHH), neonatal severe hyperparathyroidism (NSHPT), and autoimmune hypocalciuric hypercalcaemia (AHH).

1.10.1.1 Familial hypocalciuric hypercalcaemia

Familial hypocalciuric hypercalcaemia (FHH) is an autosomal dominant syndrome with a population prevalence of 1 in 50,000, which is characterised by hypercalcaemia

and inappropriately low urinary calcium excretion.[130] FHH is genetically heterogeneous with 3 types identified: FHH type 1 (described in section 1.10.1.1.1); FHH type 2 (described in section 1.10.1.1.2); and FHH type 3 (described in section 1.10.1.1.3).

1.10.1.1.1 Familial hypocalciuric hypercalcaemia type 1

An autosomal dominant syndrome of hypercalcaemia affecting 17 members of a kindred was first described in 1966.[183] The index case remained hypercalcaemic following three and a half gland parathyroidectomy.[183] In 1972 this autosomal dominant disorder of calcium homeostasis was named as FHH[184] and characterised biochemically by elevated serum calcium concentrations and inappropriately low urinary calcium excretion in the presence of normal circulating PTH levels.[184] Some affected individuals also had modestly elevated or high normal serum magnesium levels and low or low normal serum phosphate levels.[184] By the 1980s more than 30 kindreds had been identified with the disorder.[185 186] Some of those affected developed pancreatitis[187] or chondrocalcinosis[130] later in life.

Genetic linkage analysis studies using FHH kindreds revealed evidence of locus heterogeneity with mapping of FHH loci to DNA sequence polymorphic markers on chromosome 3q[188 189], 19p13.3,[189] and 19q13.[190 191] The CaSR was cloned from bovine parathyroid tissue[34] at approximately the same time that human *CASR* was located on chromosome 3q21.1 making it a candidate gene for FHH.[46 192] Subsequently, mutational analysis of *CASR* has identified >130 different mutations associated with FHH (Figure 1.15) and this is referred to as FHH type 1 (FHH1).[111 193]

The FHH-associated *CASR* mutations are predominantly missense substitutions but nonsense, deletion, insertion and splice-site mutations have also been reported (Figure 1.15).[111 193] Functional characterisation of these mutations revealed them to result in loss-of-function in the receptor causing a rightward shift in the dose-response curve of the mutant CaSR compared to that of the wild-type (WT) receptor such that the concentration of extracellular Ca^{2+} required to produce a half-maximal response in the cell (EC_{50}) was increased.[187] The majority of mutations are located within the ECD of CaSR (Figure 1.15).[111] Functional studies of several missense *CASR* mutations such as Gly778Asp and Leu174Arg (Figure 1.15) have revealed them to exert dominant negative effects on the WT receptor[194] and patient studies have established these mutations to be associated with more severe phenotypes.[195] Mutations resulting in truncated receptors such as IVS2-1Gly>Thr[196] and Arg25stop[194] (Figure 1.15) produce milder clinical phenotypes.

1.10.1.1.2 Familial hypocalciuric hypercalcaemia type 2

Loss-of-function *CASR* mutations now account for more than 65% of cases of FHH.[111] Studies performed in a kindred with FHH and unrelated probands who did not have a *CASR* mutation identified two loss-of-function mutations in guanine nucleotide binding protein, alpha 11 gene (*GNA11*), which encodes $G\alpha_{11}$ and which maps to 19p13.3.[197] The mutations comprised an in-frame deletion (Ile200del) located within the conserved switch region of the Gα subunit (section 1.4.4 and Figure 1.8) and a missense mutation (Leu135Gln), located within the helical domain.[197] FHH due

to mutations in *GNA11* is referred to as FHH type 2 (FHH2).[197] The phenotype of affected individuals was similar to that seen in FHH1.[197]

1.10.1.1.3 Familial hypocalciuric hypercalcaemia type 3

Using genetic linkage studies, the FHH locus on 19q13 was narrowed down to an approximately 3.5Mbp region.[130 191] Subsequently, exome capture and high-throughput sequence analysis of DNA from an affected individual from each of two unrelated families with FHH mapping to this locus identified an *AP2S1* c.269C>T (p.Arg15Cys) variant present in both individuals.[130] DNA sequence analysis of >50 affected FHH probands identified the AP2σ2 mutations to all involve the Arg15 residue and consisted of missense mutations to Cys, Leu and His. Functional characterisation of the AP2σ2 mutations *in vitro* by measurement of intracellular Ca^{2+} responses to increasing concentrations of extracellular Ca^{2+} revealed the mutations to result in loss-of-function of the receptor.[130] FHH associated with AP2σ2 mutations is referred to as FHH type 3 (FHH3).

1.10.1.1.4 Management of familial hypocalciuric hypercalcaemia

The majority of affected individuals with FHH are asymptomatic and require no treatment. However, for symptomatic probands with CaSR mutations, cinacalcet has been demonstrated to reduce hypercalcaemia and associated symptoms and reduce the frequency of episodes of pancreatitis.[198-200] Additionally, cinacalcet therapy normalised serum calcium and provided symptom control in a proband with an AP2σ2 Arg15Leu mutation.[75] The long-term sequelae of cinacalcet therapy in these

patients is unknown. Hypocalcaemia has limited the use of cinacalcet thus far and long-term data in FHH patients is lacking. Drug development is now focusing on production of targeted calcimimetics that restore the natural bias of the mutant receptor and tissue-specific responses.

1.10.1.2 Neonatal severe primary hyperparathyroidism

Neonatal severe primary hyperparathyroidism (NSHPT) is a rare disorder characterised by severe hypercalcaemia which typically manifests within the first 6 months of life, bone demineralisation and parathyroid hyperplasia.[201] [192] The most severely affected infants present with dehydration, renal impairment, failure to thrive, and multiple fractures,[202] [192] including rib fractures and ribcage deformities [203] which result in respiratory distress. It is most commonly due to homozygous loss-of-function *CASR* mutations (Figure 1.15).[46] [192] It can also occur due to *de novo* heterozygous *CASR* mutations.[192] [204] The majority of NSHPT-associated *CASR* mutations (>40%) are either nonsense or frameshift mutations (Figure 1.15) predicted to result in a truncated CaSR.[111]

The most severely affected patients are treated with aggressive hydration, bisphosphonates, and if there is no response or the clinical condition is life-threatening, urgent total parathyroidectomy is performed.[205] Cinacalcet has been shown to have an effect in an infant harbouring a *de novo* heterozygous Arg185Gln mutation (Figure 1.15) eliminating the need for parathyroidectomy.[206] However, when used in an individual harbouring a homozygous deletion-frameshift mutation (222_226delGATAT) of the CaSR, no effect was seen.[207] It can be postulated that the

lack of response is due to the presence of non-functional mutant CaSR and thus, cinacalcet was an ineffective treatment option in this case. This highlights the need for personalised medicine with prompt mutational analysis to aid decision-making regarding calcimimetic therapy versus parathyroidectomy.

1.10.1.3 Autoimmune hypocalciuric hypercalcaemia

Autoimmune hypocalciuric hypercalcaemia is characterised by the presence of circulating antibodies to the ECD of the CaSR, which presumably inactivate CaSR and result in increased PTH secretion.[208] Thus patients present with the clinical manifestations of FHH in the absence of CaSR mutations.[208] Additionally, they may have features of other autoimmune disorders such as thyroid dysfunction and coeliac disease.[208]

1.10.2 Hypocalcaemic disorders

The hypocalcaemic disorders attributable to CaSR abnormalities include autosomal dominant hypocalcaemia (ADH) and Bartter syndrome type V.

1.10.2.1 Autosomal dominant hypocalcaemia

ADH is a rare disorder and the exact prevalence is unknown. Like FHH, ADH is also genetically heterogeneous and can be classified into two types: ADH type 1 (section 1.10.2.1.1); and ADH type 2 (section 1.10.2.1.2).

1.10.2.1.1 Autosomal dominant hypocalcaemia type 1

It is characterised by mild to moderate hypocalcaemia which is symptomatic in ~50% of patients associated with normal circulating PTH levels in more than 40% and low PTH levels in the remainder. [197 209-212] Symptomatic individuals can suffer with paraesthesia, carpopedal spasm and seizures. [209 210] The serum phosphate level is typically mildly elevated or in the upper normal range whilst serum magnesium level is either reduced or in the low normal range.[209 210 212] An absolute hypercalciuria is seen in approximately 10% of those affected which may be associated with nephrocalcinosis or kidney stones.[210 213]

Following the discovery that FHH1 was caused by heterozygous loss-of-function *CASR* mutations, it was identified that heterozygous gain-of-function *CASR* mutations were associated with ADH. The ADH-associated *CASR* mutations produced a leftward shift in the dose-response curve of the mutant receptor and a reduction on the EC_{50} for extracellular Ca^{2+} compared to WT.[210 214] Less than 100 different ADH-associated *CASR* mutations have been identified and the associated ADH referred to as ADH type 1 (ADH1).[111 209-211 214-228] Approximately 95% of mutations are missense substitutions (Figure 1.15).[111]

1.10.2.1.2 Autosomal dominant hypocalcaemia type 2

ADH1 due to *CASR* mutations accounts for more than 70% of cases.[111 209-211] Thus, studies of probands with ADH and no *CASR* mutation revealed two gain-of-function *GNA11* mutations, referred to ADH type 2 (ADH2).[197] Both mutations were missense

substitutions, Arg181Gln and Phe341Leu.[197] Affected individuals had phenotypes similar to ADH1.[197]

1.10.2.1.3 Management of Autosomal dominant hypocalcaemia

The mainstay of treatment is calcium supplementation and vitamin D preparations. However, it has been shown that active $1,25(OH)_2D_3$ enhances renal CaSR expression inhibiting the reabsorption of calcium by the renal tubules resulting in hypercalciuria.[49] Therefore, vitamin D preparations can worsen the renal manifestations of ADH [49 210] and physicians need to titrate doses carefully to avoid worsening of nephrocalcinosis and renal stones. Recombinant PTH (1,34) therapy has been used in cases of ADH to normalise serum calcium levels.[229 230] However, in one case who received long-term recombinant PTH (1,34) therapy from age 6 years, nephrocalcinosis developed at the age of 19 years.[230] On the horizon are calcilytics[76] which have been shown to rectify the gain-of-function mutations associated with ADH *in vitro*[79 110] and and improve the hypercalcaemia[78 79], hypercalciuria[78] and renal calcification[78] seen in mouse models of ADH.

1.10.2.2 Bartter syndrome type V

Barrter syndrome is a group of autosomal disorders of electrolyte homeostasis characterised by renal salt wasting resulting in volume depletion and subsequent hyperreninaemic hyperaldosteronism and hypokalaemic alkalosis. The syndrome is classified into five types based on the associated mutation in the ion transporter or channel within the TAL of the loop of Henle (Figure 1.24): type 1 is due to mutations

involving NKCC2; type 2 is due to mutations involving ROMK; type 3 is due to mutations in the voltage-gated chloride channel type b (CLC-Kb); type IV is due to mutations in the β subunit (Barttin) of CLC-Kb and CLC-Ka; and type V is due to gain-of-function mutations of the CaSR.[109]

Barrter syndrome type V has been described in association with several gain-of-function mutations, Lys29Glu,[231] Leu125Pro,[158] Cys131Trp[232] and Ala843Glu.[232] Affected individuals presented with the classical features of Bartter syndrome and functional characterisation of the CaSR mutations showed severe gain-of-function with EC_{50} values lower than those of ADH mutations.[158 231 232] Additionally, Leu125Pro and Ala843Glu were demonstrated to activate the CaSR in the absence of extracellular Ca^{2+} thus making the mutant receptors constitutively active.[158 232] The activation of the basolateral CaSR in the TAL inhibits ROMK and NKCC2 resulting in renal salt wasting.

1.11 Mouse models

Mouse models have been used to study human diseases since the 1920s when European 'fancy' mice were inbred to generate new strains and investigate Mendelian inheritance.[233] These mating programs generated many of the laboratory strains used today. Subsequently, whole-genome sequencing of inbred strains, through the Mouse Genomes Project, has shown that many inbred strains have genomic DNA derived from more than one subspecies of *Mus musculus*.[234] Comparison of the coding regions of mouse and human genomes reveals approximately 85% sequence homology making mouse genetic research applicable to human diseases.[235] Additionally, mice are cost-effective and efficient to use due to their short reproductive cycle (~4-6 days), short gestational period (~20 days) and large litters (~6-8 pups) with breeding occurring throughout the year. Advantages of an *in vivo* model over an *in vitro* system include: the ability to study the pleiotropic effects of the disease on the organism; study the efficacy of novel compounds on diseases; and establish primary cell cultures from a variety of parental tissues containing the mutation of interest for *ex vivo* studies.

Mouse models harbouring the desired gene mutation can be generated using non-targeted or targeted strategies.[236] Non-targeted strategies include chemical mutagenesis utilising N-ethyl-N-nitrosourea (ENU) and targeted strategies include traditional gene targeting by modification of embryonic stem (ES) cells and gene editing technology using transcription activator-like effector nucleases (TALENs) and clustered regularly interspaced short palindromic repeats (CRISPR)-Cas9 system.

1.11.1 Chemical mutagenesis using N-ethyl-N-nitrosourea

The Mary Lyon Centre at MRC Harwell has established a chemical mutagenesis programme by injecting male BALB/c mice with the alkylating agent, ENU.[237] ENU transfers its ethyl group to the DNA base resulting in mispairing of DNA nucleotides during the first round of replication and following a subsequent round of replication, a point mutation is introduced at this site[236] (Figure 1.26). The ENU-treated male mice are mated with C3H females and the first generation of progeny (G1) are screened for new mutations.[237] DNA from over 12,000 individual G1 ENU-mutagenised mice is held within the archive with parallel frozen embryo and sperm samples, allowing for genotype-driven screens of the archive to be performed. A mouse line harbouring a gene mutation of interest can then be re-derived by *in vitro* fertilisation of a C3H line with spermatozoa harbouring the mutation of interest[237] or by transfer of the cryopreserved embryo into a pseudopregnant C3H mouse and *in vivo* studies performed.

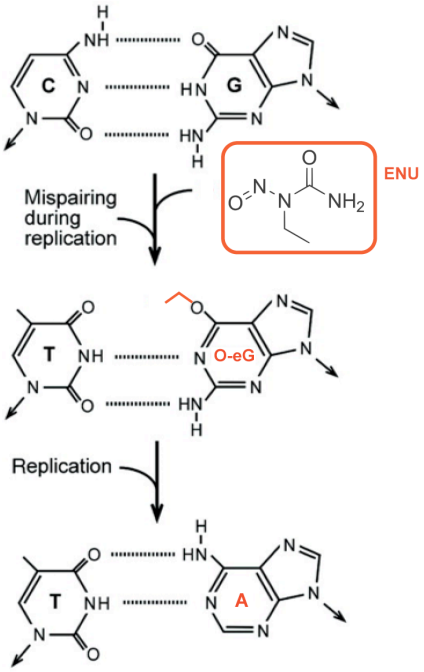


Figure 1.26. Chemical mutagenesis using N-ethyl-N-nitrosourea (ENU).

ENU (red box) transfers its ethyl group to DNA bases leading to mispairing of DNA nucleotides during replication. A point mutation (c.G>A) is then introduced into the genome following a subsequent round of replication. Adapted from Piret S. E and Thakker R. V. 2011.[236]

1.11.2 Targeted mutagenesis

Historically, targeted strategies have involved gene targeting by modification of ES cells and generation of chimeric mice which can take up to one year for the desired mutation to become germline.[238] Recently, gene editing technology using transcription activator-like effector nucleases (TALENs) and clustered regularly interspaced short palindromic repeats (CRISPR)-Cas system have been used to generate mouse models of human disease.[239 240] These both involve injection directly into one cell embryos and thus, eliminate the chimera stage, saving time and breeding costs.[241]

A TALEN is generated by the fusion of a transcriptor activator-like effector (TALE) DNA binding domain to the endonuclease, *Fok*I (Figure 1.27).[242] TALEs were originally discovered in *Xanthomonas* and contain a DNA binding domain which consists of 10-30 repeat modules, each of which is made up of approximately 35 amino acids.[242] The amino acids within the repeat modules are highly conserved except for the amino acids at positions 12 and 13,[242] referred to as the variable di-residue (Figure 1.27). Each variable di-residue recognises one nucleotide allowing for targeting of DNA with precision. TALENs are designed to operate such that when they bind to the DNA a spacer region is generated allowing the endonuclease domains to dimerise and create a double-stranded break in the DNA (Figure 1.27).[242] By co-injection of the TALEN pair with a repair template containing the mutation of interest to be inserted into the genome, homology-directed repair occurs with generation of a knock-in mutant mouse model (Figure 1.27).[238 242] Injection of the TALEN pair alone will result in non-homologous end-joining and generation of a knock-out mouse model of the gene of interest.[238 242] TALENs technology has been used to successfully generate rodent models of a range of disorders including epilepsy[243], Duchenne muscular dytrophy[244], and colitis.[245]

The CRISPR-Cas9 system, a component of the immune system of prokaryotes first identified in *Streptococcus pyogenes*, uses a combination of short guide RNAs to recognize and bind to specific DNA sequences, known as protospacer adjacent motifs.[241 246 247] The guide RNA sequence also contains the mutation of interest to be introduced into the genome. [241 246 247] Cas9, the CRISPR-associated nuclease, creates a double-stranded break in the DNA 3bp upstream of the protospacer adjacent motif sequence enabling homology-directed repair to occur. [241 246 247] A major advantage of

the CRISPR-Cas9 system over TALENs is the ability to introduce several mutations of interest into the genome at one time. [241 246 247]

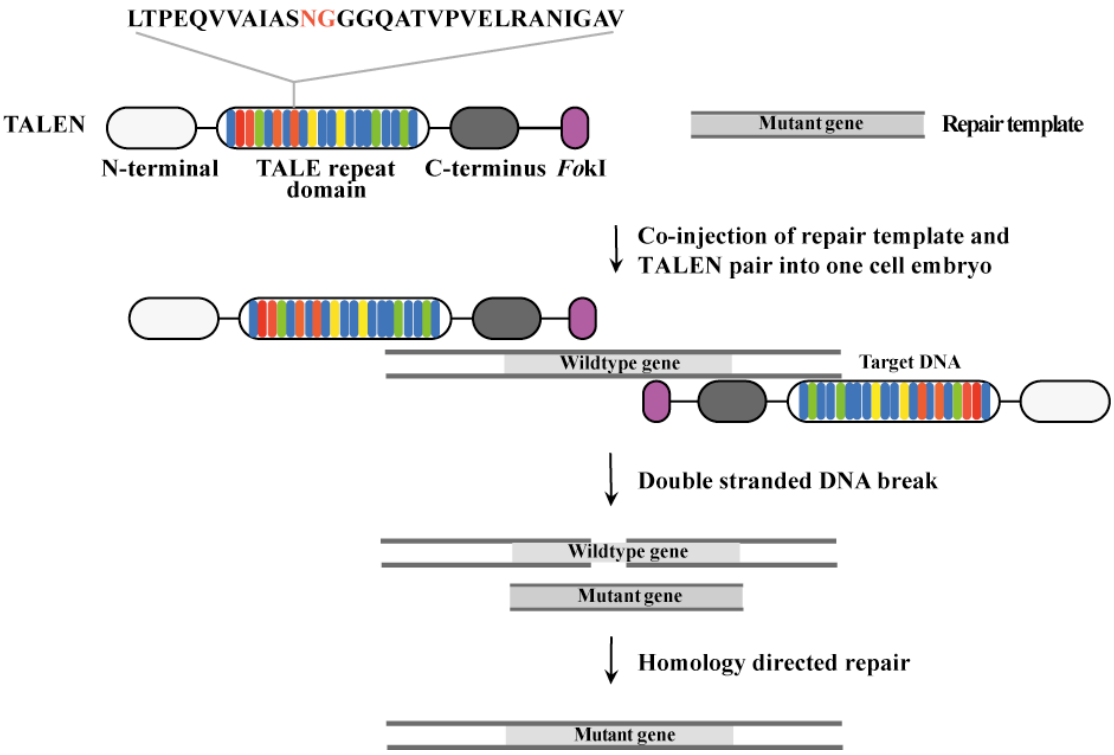


Figure 1.27. Genome editing using transcription activator-like effector nucleases (TALENs) technology

A transcription activator like effector nuclease (TALEN) comprises an N-terminal, a transcription activator like effector (TALE) DNA binding domain, a C-terminus and the endonuclease, *Fok*I.[238] The TALE domain consists of 10-30 repeat modules, each of which comprises approximately 33-35 amino acids.[242] These amino acids are highly conserved except for those at positions 12 and 13, referred to as the variable di-residue, (shown in red).[242] Each variable di-residue recognises one nucleotide allowing for specific DNA binding.[242] For genome editing using TALENs technology, co-injection of a pair of TALENs, in combination with a repair template containing the mutation to be incorporated into the genome is performed in a single cell embryo.[238] The TALENs bind to the DNA in pairs creating a spacer region, and allowing the endonucleases to create a double-stranded break in the DNA.[242] This is followed by homology-directed repair and generation of a knock-in mutation in the gene of interest. Adapted from Joung J. K and Sander J. D. 2013.[242]

1.11.3 Mouse models of disorders of calcium homeostasis associated with CaSR mutations

Mouse models of FHH1, NSHPT and ADH1 have been generated using chemical mutagenesis and targeted strategies to characterise the role of the CaSR in these pathological states *in vivo* and study the effects of novel compounds.

1.11.3.1 Mouse models of familial hypercalciuric hypercalcaemia type 1 (FHH1) and neonatal severe hyperparathyroidism (NSHPT)

1.11.3.1.1 Global *Casr* null mouse model

The global *Casr* null mouse model was generated through homologous recombination and knockout of exon 5.[149] Mice heterozygous for inactivation of *Casr* had a phenotype similar to that of patients with FHH type 1 with moderately elevated serum calcium, magnesium and PTH concentrations and hypocalciuria.[149] When both copies of *Casr* were inactivated, the mice had a phenotype consistent with NSHPT with severely elevated serum calcium and PTH concentrations, parathyroid hyperplasia, growth retardation, difficulty weaning and premature death in the perinatal period.[149]

1.11.3.1.2 Conditional *Casr* null mouse model

Tissue-specific *Casr* knockout mice were generated using Cre-lox technology which involves the introduction of two loxP sites flanking the gene to be knocked out and

Cre, which encodes Cre recombinase using homologous recombination and the activity of which can be controlled by tissue-specific promotors. Renal-specific *Casr* null mice demonstrated increased expression of activated NKCC2 in the TAL (Figure 1.24) and reduced expression of claudin-14, a membrane protein and component of tight junctions.[248] Mutant mice showed baseline biochemistry similar to that of WT littermates but when challenged with dietary calcium supplementation developed significantly lower urinary calcium excretion.[248] This data suggested the renal CaSR regulated Ca^{2+} reabsorption in the TAL (section 1.9.1.2).[248] Separate tissue-specific homozygous knockouts of *Casr* in the parathyroid gland and bone demonstrated marked impairment of skeletal development at birth with severely undermineralised osteoid on staining and reduced expression of genes encoding regulators of osteoblast differentiation.[180] Additionally, the majority of mice from both tissue-specific knockouts died within 3 weeks of birth.[180] These models demonstrated the role of parathyroid and bone CaSR in embryogenesis and early skeletal development.[180]

1.11.3.2 Mouse models of autosomal dominant hypocalcaemia type 1 (ADH1)

1.11.3.2.1 The *Nuf* mouse model

The Nuf mouse was identified due to the presence of cataracts through a phenotype-driven screen of a chemical mutagenesis (isopropyl methane sulfonate)-induced archive.[249] The mouse was identified to harbour a homozygous missense Leu723Gln mutation located in the fourth transmembrane domain of *Casr* and functional characterisation revealed the mutation to result in a gain-of-function in the mutant CaSR compared to the WT CaSR.[249] Affected homozygous and heterozygous mice

were found to be hypocalcaemic and hyperphosphataemic with reduced plasma PTH levels.[249] Recently, the calcilytic NPS 2143 was demonstrated to correct the gain-of-function mutation *in vitro* as determined by intracellular Ca^{2+} response and shifted the dose-response curve of HEK293 cells expressing the mutant CaSR rightward such that the EC_{50} of the mutant CaSR increased.[79] The calcilytic improved the hypocalcaemia and PTH level in the *Nuf* mice without elevating urinary calcium excretion (section 1.5.5).[79]

1.11.3.2.2 The Act-CaSR mouse model

A mouse model with a constitutively active mutant CaSR (Act-CaSR) expressed in mature osteoblasts under the control of the osteocalcin promotor demonstrated increased expression of RANKL.[170] This resulted in increased numbers and activity of osteoclasts with consequent reduction in bone volume and density compared to WT littermates.[170] This mouse model provided the first *in vivo* data that osteoblasts respond to extracellular Ca^{2+} within the bone microenvironment independent of PTH.[170]

1.11.3.1 Adaptor protein complex subunit mouse models

There are currently no published mutant mouse models for AP2σ2, encoded by *Ap2s1* or *Ap2s1* knockout mouse models. The phenotypes of these two models are predicted to be different with the mouse model harbouring an Arg15 *Ap2s1* mutation expected to have a phenotype consistent with FHH3. However, the *Ap2s1* homozygous knockout mouse would be predicted to display a phenotype consistent with a disorder

of endocytosis. Knockout mouse models have been generated for the AP2μ2 and AP2β2 subunits.[250 251] In both these models, mice with heterozygous deletion of one allele were phenotypically normal.[250 251] Mice with homozygous deletion of AP2μ2 were embryonic lethal dying before E3.5[250] suggesting the subunit is essential for cell viability, as opposed to organogenesis. Mice with homozygous deletion of AP2β2 died in the postnatal period due to cleft palate deformities,[250 251] suggesting this subunit is important for development. These different effects highlight the different roles for endocytosis in development, where CME is required for nutrient uptake, but also has a major role in patterning, by mediating morphogen gradients. During embryogenesis, cells identify their position within tissues by the concentrations of local levels of secreted molecules known as morphogens.[252] The sensing and subsequent activation of signal transduction pathways in cells is dependent upon normal signalling and trafficking.[252] Thus, defects in these mechanisms can result in patterning defects and impair cell viability.[252]

By studying either knockout mouse models of proteins involved in the internalisation of GPCRs or those causing human disorders associated with mutations in adaptor protein complex subunits, valuable insights have been gained. For example, the β-arrestin-1 and β-arrestin-2 knockout mouse models yielded information regarding the desensitisation of the B_2AR which was not provided by *in vitro* studies on purified proteins.[114] Fibroblast cell lines derived from mouse embryos (MEFs) that were single or double allele knock-outs for β-arrestin demonstrated functional specialisation.[114] Desensitisation of the B_2AR was not impaired in the single or double β-arrestin-1 knockouts but was severely impaired in both the single and double β-arrestin-2 knockouts with B_2AR sequestration seen.[114] Thus, the relative contributions of the β-

arrestins in desensitisation of B_2AR were demonstrated.[114] Another example is the adaptor protein-3 (AP-3) knockout mouse model which was used to study the human disease of Hermanksy-Pudlak syndrome, which is due to mutations in the β3A subunit of AP-3 and is characterised by oculocutaneous albinism, platelet abnormalities and pulmonary fibrosis.[253] AP-3 is another member of the adaptor protein family and is involved in trafficking of proteins to the lysosomes for degradation. Cells taken from double knockout mice were generated to express WT and mutant β3A subunits and trafficking studies performed.[254] These studies showed that WT β3A subunit rescued the phenotype as did a mutant which lacked a functional clathrin binding site indicating that clathrin was not needed for normal AP-3 function.[254] Thus, although an AP2σ2 homozygous knockout mouse may be predicted to be embryonic lethal, MEFs could be used for *in vitro* signalling and trafficking studies to understand the internalisation and trafficking of the CaSR, discussed further in section 6.1.7. This eliminates the need for knockdown studies using RNA interference (siRNA) in which a small quantity of the endogenous subunit usually persists due to the limitation of the technique.[255] Therefore, mouse models of *Ap2s1* could provide critical insights into its role in endocytosis, and in calcium homeostasis.

2 Study aim and objectives

The aim of this thesis is to increase the understanding of the role of AP2σ2 in the regulation of calcium homeostasis. The introduction describes the studies preceding this thesis and in this setting, the study objectives are:

1. Identify additional AP2σ2 mutations associated with FHH3.
2. Identify novel AP2σ2 mutations associated with non-CaSR ADH.
3. Investigate the effect of AP2σ2 mutations on CaSR downstream signalling pathways.
4. Establish mouse models of FHH3 to study the pleiotropic effect of AP2σ2 mutations and novel compounds.

3 Materials and methods

3.1 Materials

3.1.1 Chemicals

All chemicals were purchased from Santa Cruz Biotechnology, Inc., Sigma-Aldrich, BioRad and Merck Millipore.

3.1.2 Oligonucleotides

Primers for polymerase chain reaction (PCR) and DNA sequencing were synthesised by Sigma Aldrich-Genosys. Quantitect primers for quantitative real-time PCR (qPCR) were obtained from Qiagen and used with the Quantitect SYBR Green PCR Kit.

3.1.3 Enzymes

Proteinase K was purchased from Roche, DNA *Taq* polymerase and deoxynucleotide triphosphates (dNTPs) were purchased from Thermo Fisher Scientific and reverse transcriptase from Qiagen. T4 DNA ligase from Promega, and restriction endonucleases from New England Biolabs (NEB).

3.1.4 Vectors

The pBI-CMV4-RFP vector was purchased from Clontech Laboratories Ltd. The pGL4.30[*luc2P*/NFAT-RE/hydro] and pGL4.33[*luc2P*/SRE/hydro] vectors were obtained from Promega. The pCR-Blunt II-TOPO and pUC18 vectors were purchased from Thermo Fisher Scientific. All vector maps are shown in the appendix, section 10.1.

3.1.5 Buffers

1x CAPS buffer	10mM *N*-cyclohexyl-3-aminopropanesulfonic acid (CAPS) (SigmaAldrich), 10% (v/v) methanol, pH 11
Coomassie De-stain	10% methanol, 10% acetic acid
Coomassie Stain	50% methanol, 10% acetic acid, 0.05% brilliant blue R-250
DNA loading buffer for agarose gel	30% (v/v) glycerol, 20µM EDTA (w/v), 0.25% (w/v) bromophenol blue
LB agar	Agar added to LB broth at 1.5% (w/v), autoclaved
LB broth	1% (w/v) bactotryptone, 1% (w/v) yeast select extract, 0.5% (w/v) NaCl, autoclaved
NP-40 buffer	50mM Tris pH 7.7, 150mM NaCl, 0.5% NP-40, 1mM DTT, 1x protease inhibitor cocktail
NZY^+ broth	1% (w/v) casein hydrolysate, 0.5% (w/v) yeast extract, 0.5% (w/v) NaCl, pH 7.5, autoclaved, plus 12mM $MgCl_2$, 12.5 mM $MgSO_4$, 20mM glucose

Phosphate buffered saline (PBS)	140mM NaCl, 10mM phosphate, 3mM KCl, pH 7.4, autoclaved (PBS tablets, Invitrogen)
RIPA Buffer	50mM Tris, 150mM NaCl, 1% (v/v) Igepal-CA630, 0.5% (w/v) Na-deoxycholate, 1% (w/v) Sodium dodecyl sulfate (SDS), PMSF (10mg/ml), aprotinin (30µl/ml), Na-orthovanadate (10µl/ml), filter sterilised
Sodium dodecyl sulfate polyacrylamide gel electrophoresis (SDS-PAGE) gels	30% acrylamide mix (v/v), 1.5M Tris (pH 8.8), 10% (v/v) SDS, 0.2% (w/v) Ammonium persulfate (APS), 0.0016% (v/v) Tetramethylethylenediamine (TEMED)
1x Tris-EDTA (TE) buffer	10mM Tris/HCl pH 7.5, 0.1mM EDTA, filter sterilised
1x TBS-T	150mM NaCl, 100mM Tris pH 7.5, 0.1% (v/v) Tween-20
10x Tris-Borate-EDTA (TBE)	0.89M Tris base, 0.89M boric acid, 20mM EDTA; pH 8
1x Tris/Glycine/SDS (TGS)	25mM Tris, 192mM glycine, 0.1% (w/v) SDS (10X TGS solution BioRad)

3.2 Methods

3.2.1 Ethical approval for research

Informed consent was obtained from patients with disorders of calcium homeostasis, and where appropriate the parents or guardians of affected children, using protocols approved by local or national ethics committees (MREC/02/2/93). Clinical and biochemical details of probands included in studies are described in sections 4, 4.1.1, 4.1.2, 7 and 7.1.2.

Mice were maintained at the Mary Lyon Centre, MRC Harwell, UK and all animal experiments were performed in accordance with UK Home Office welfare guidelines and Home Office Project License restrictions (Project License number: 30/2752; Personal Licence number: IE789250B).

3.2.2 Protocols involving manipulation of DNA

3.2.2.1 Extraction of DNA from mouse tissue

Mouse ear sections of ~2mm diameter were lysed in 100µl of DNA extraction buffer with the addition of 200µg/ml of proteinase K. Biopsies were incubated at 55°C for 2 hours followed by a 15 minute incubation at 95°C to inactivate proteinase K.[168]

3.2.2.2 Amplification of DNA by Polymerase Chain Reaction

The polymerase chain reaction (PCR) is a method used to synthesise new complementary strands of DNA containing a target sequence from template strands. The reaction requires: oligonucleotide primers, which are short lengths of single-stranded DNA that complement the target sequence to be amplified (listed in the appendix, section 10.2); DNA polymerase, the most commonly used is *Taq* DNA polymerase from *Thermus aquaticus* which synthesises the new strand using the primers; deoxynucleotides (dNTPs), the components of DNA; and the template DNA.[256] A standard PCR reaction comprised: 1xPCR buffer; 200mM dNTPs; 1.5mM $MgCl_2$, 300nM of each primer, 1 unit of *Taq* Polymerase and 50-200ng of genomic DNA, as described previously.[256] Standard cycling conditions were as follows:

Cycles		Temp	Time
1		96°C	3 minutes
35	[	94°C	30 seconds
		55-60°C	30 seconds
		72°C	1 minute
1		72°C	10 minutes

Annealing temperatures were optimised for primers where appropriate. The PCR products were analysed by agarose gel electrophoresis and imaged using ethidium bromide.[256]

3.2.2.3 Automated DNA sequencing

PCR products were purified by Sureclean (Bioline), and DNA sequence analysis was performed using the BigDye Terminator v3.1 Cycle Sequencing Kit (Applied Biosciences) and ABI 3730xI and 3130 machines (Applied Biosystems). This sequencing system is based on the chain termination method first developed by Frederick Sanger *et al* in 1977.[257] During the sequencing reaction, fluorescently-labelled dideoxynucleotides (ddNTPs) are used, which terminate the reaction. The reaction products can be separated by polyacrylamide gel electrophoresis (PAGE) and the emission spectra of excited fluorescent tags detected by the sequencer. The electropherogram generated was analysed using DNA Dynamo sequence analysis software (BlueTractorSoftware Ltd). Reference sequences for comparison were obtained from the Ensembl Genome Browser.[258]

3.2.2.4 Incorporation and amplification of plasmid DNA

Molecular cloning involves a sequence of methods by which recombinant DNA is incorporated into a commercially available vector, and the vector is then transformed into bacterial cells for amplification and transfection into mammalian cells for expression studies.[259] Many vectors comprise small circular double stranded DNA and may have genes for antibiotic resistance allowing growth selection, and expression tags for detection by antibodies in Western blot or immunofluorescence studies. A number of vectors were used in these studies as follows; pBI-CMV4-RFP; pGL4.30[*luc2P*/NFAT-RE/hydro]; pGL4.33[*luc2P*/SRE/hydro]; pCR-Blunt II-TOPO; and pUC18 (vectors maps displayed in section 10.1).

DNA products were PCR amplified using cDNA as template and gel purified using the Geneclean kit (Qbiogene), as previously described.[130] DNA was incorporated into pCR-Blunt II-TOPO as an entry vector, by cutting both the vector and DNA with restriction enzymes at sequence-specific sites. DNA was ligated into the linearised vector in a 10μl reaction volume in a 3:1 insert:vector ratio, including 0.5μl vector, appropriate amount of insert, 1x ligation buffer and 1μl of T4 DNA ligase.[130] Reactions were incubated at room temperature for ~1 hour. Following ligation, constructs were transformed into XL10-Gold Ultracompetent *E.coli* bacterial cells, plated on LB-agar plates with the appropriate antibiotic and incubated overnight at 37°C, as described previously.[130] Colonies from these plates were amplified in overnight cultures and vector constructs isolated using the Wizard *Plus* SV Minipreps DNA Purification System (Promega). The DNA template was then sub-cloned into the desired mammalian expression vector using similar techniques.

3.2.3 Protocols involving manipulation of RNA

3.2.3.1 Extraction of RNA

RNA was extracted from homogenised mouse tissue (ear biopsies and kidneys) and lysed cells using the RNeasy Mini Kit (Qiagen), as previously described.[260] This process involved the addition of 1 volume of 70% ethanol to the lysate, which was loaded onto a silica membrane and any contaminants washed through the membrane using a sequence of buffers supplied with the kit, that remove protein and DNA contaminants, followed by purification of the RNA product. The RNA was eluted in

RNAse-free water, and its quantity and purity was assessed using the NanoDrop ND-2000 Spectrophotometer (Thermo Fisher Scientific). A 260/280 nm absorbance ratio of ~2.0 and a 260/230 nm absorbance ratio of >2.0 was accepted as 'pure' for RNA.[261]

3.2.3.2 Reverse transcription (RT) of RNA

Reverse transcription (RT) of RNA was used to convert the total RNA to copy DNA (cDNA) prior to qPCR, described in section 3.2.3.3. The Quantitect RT Kit (Qiagen) was used for this process.[260] The method involved removal of genomic DNA by addition of 1µg of RNA to 7x gDNA wipeout buffer and nuclease-free water in a 14µl reaction and incubation at 42°C for 2 minutes. Then RT of RNA and amplification of cDNA was achieved by addition of 5x quantiscript RT buffer, RT primer mix and quantiscript RT to the reaction mix up to a final volume of 20µl. The reaction mix was incubated at 42°C for 15 minutes, and 95°C for 3 minutes, then made up to a 50µl volume with nuclease-free water.

3.2.3.3 Quantitative PCR (qPCR)

qPCR was used to provide quantitative information on the levels of mRNA.[262] qPCR reactions were carried out using the Rotorgene SYBR Green Kit (Qiagen) using the two-step qPCR method. In this method, cDNA was synthesised as described in section 3.2.3.2. During the qPCR reaction, the SYBR green dye is incorporated into the amplified product and when bound to dsDNA emits a detectable fluorophore signal. qPCR reactions were carried out using the following standard cycling conditions in triplicate for the samples on a Rotor-Gene Q analyser (Qiagen):

Cycles	Temp	Time
1	95°C	30 minutes
40	95°C	5 seconds
	58°C	15 seconds
	72°C	10 seconds
	Melt curve analysis	

As the fluorophore binds to any dsDNA, a negative control was included alongside the test samples to ensure the amplified product was the desired one.[263] Primers used are listed in the appendix (section 10.2).

3.2.3.4 Analysis of qPCR data

The Rotor-Gene converts the raw data into a sigmoidal-shaped melt curve using the Rotorgene Q Series Software and all melt curves were examined to determine that primers only amplified a single gene product. Threshold cycle (C_T) values were obtained from the start of the log phase and C_T values were analysed in Microsoft Excel 2010-2013 using the Pfaffl method.[264] All qPCR experiments for *AP2A1*, *AP2B1, AP2M1,* and *AP2S1* samples were normalised to a geometric mean of the housekeeper genes *PGK1*, *TBP1*, and *GAPDH*. qPCR experiments for *Ap2a1*, *Ap2b1*, *Ap2m1* and *Ap2s1* were normalised to a geometric mean of *Gapdh* and *Act* genes. Pairwise comparisons of expression data were performed using the two-tailed Student's t-test.

3.2.4 Protocols involving manipulation of protein

3.2.4.1 Protein isolation from cultured cells

Protein was extracted from cultured cells by incubation with NP-40 buffer for 10 minutes on ice.[265] Lysed cells were pelleted by centrifugation at 14000 x g for 10 minutes and supernatant containing the soluble proteins was retained.[265] Sonication using an ultrasonic probe was used to fragment molecules of DNA prior to Western blot analysis,[266] described in section 3.2.4.3.

3.2.4.2 Protein isolation from snap frozen kidneys

Kidney samples were snap frozen and homogenised on dry ice to prevent sample degradation and protein was extracted using RIPA buffer for 10 mins at 4°C.[266 267] The lysed sample was pelleted by centrifugation at 14000xg for 10 minutes at 4°C and supernatant containing the soluble proteins was retained.[266 267] Sonication using an ultrasonic probe was used to fragment molecules of DNA prior to Western blot analysis,[266] described in section 3.2.4.3.

3.2.4.3 Western blot

Western blot analysis is a method used to detect a protein within a sample by use of a specific antibody.[266] The method comprises three key steps: separation of proteins within a sample according to their molecular weight by sodium dodecyl sulphate-

polyacrylamide gel electrophoresis (SDS-PAGE); transfer of separated proteins onto a polyvinylidene fluoride (PVDF) membrane; and detection of the target protein by probing the membrane with an antibody of interest. This primary antibody can then be detected by addition of an horseradish peroxidase (HRP)-labelled secondary antibody allowing for detection by chemiluminescence.[268]

Protein samples were mixed in a 1:1 ratio with Laemmli loading buffer (BioRad) and denatured at 80°C for 3 mins.[266] Equal protein concentrations were loaded onto 6-12% SDS-PAGE gels as appropriate and run in TGS buffer at 120V for one hour.[266] Following transfer onto a PVDF membrane in cold CAPS buffer at 100V for one hour, the blot was blocked in 5% non-fat milk in TBS-T for 1 hour at room temperature and then treated with a primary antibody diluted in milk/TBS-T for 1 hour at room temperature.[266] The blot was washed four times in TBS-T and the appropriate HRP-conjugated secondary antibody applied.[266] Following a further four TBS-T washes of the blot, proteins were detected using the Clarity Western ECL Kit (Biorad) on a BioRad Chemidoc XRS+ system. All antibodies and concentrations used in Western blot analysis are listed in the appendix (section 10.3). A housekeeper protein, such as calnexin, was used as a loading control for the amount of cellular protein content on all blots.[130] Densitometry was performed using BioRad Chemidoc XRS+ and Image J software.[130] Statistical analysis involved Student's t-test (two-tailed).

3.2.5 Protocols involving cells in culture

All cell culture work was undertaken under sterile conditions using a TriMAT2 Class 2 Microbiological Safety Cabinet (BioQuell) and with sterile reagents. Aliquots of cells were removed from liquid nitrogen and warmed to 37°C in a water bath. The contents of the vial were transferred to a sterile falcon tube and diluted slowly in 5ml of the appropriate medium. Cells were pelleted by centrifugation at 1000rpm for 3 minutes and the pellet resuspended in medium with 10% foetal calf serum (FCS) prior to seeding into a 75cm^2 flask and placed in the incubator.[130] The cell-lines used, and conditions for maintenance of the cells for these studies are summarised in Table 3. The HEK293 cells used for experiments were as follows: HEK293 cells transiently expressing genes of interest; HEK293 cells stably expressing the CaSR generated by Dr Andrew Nesbit[130]; and HEK293 cells stably expressing AP2σ2 generated by Dr Caroline M. Gorvin (unpublished data). Blood lymphocyte cell lines from the FHH_{ok} kindred underwent Epstein-Barr virus (EBV) transformation under the supervision of Professor R V Thakker previously.[269] Briefly, this process involved the use of freshly drawn samples of venous blood stored in ethylene diamine tetraacetic acid (EDTA) sample bottles.[270] Blood was diluted 1:1 with RPMI-1640 medium and layered onto a Histopaque-1077 Hybrimax gradient (Sigma-Aldrich).[270] Centrifugation was performed to obtain the lymphocyte layer, which was resuspended in antibiotic-free RPMI-1640 medium containing EBV and phytohemagglutinin (Sigma-Aldrich) in a 75cm^2 flask.[270] The medium was replenished every 3 days, and the cultures were monitored for signs of transformation such as clumping.[270] Transformed cultures were grown to approximately 1×10^8 cells and then cryopreserved in liquid nitrogen.[270] Successful transformations were viable following cryopreservation.[270]

Table 3. Cell lines used for experiments.

Cell line	Incubation conditions	Medium	Supplements	Passage confluency
HEK293	37°C, 5% CO_2	DMEM with GlutaMAX supplement	10% heat-inactivated FCS, geneticin 400μg/ml*	80%
FHH_{ok} kindred EBV-transformed lymphoblastoid	37°C, 5% CO_2	RPMI-1640	10% heat-inactivated FCS, penicillin-streptomycin 100U/ml	80%

*geneticin only added to medium when a gene was to be stably expressed in the cells

3.2.5.1 Transfection of DNA into cells

Transfection involves the incorporation of plasmid DNA into cells using cationic liposomes that complex with negatively charged nucleic acids to form DNA-containing liposomes.[271] These liposomes can fuse with the plasma membrane enabling the plasmid DNA to enter the cytoplasm.[271] Cells were not trypsinised prior to transfection in 75cm^2 flasks for the flow cytometry assay described in section 3.2.5.2. However, cells were trypsinised and plated into 24-, or 48-well plates as required before transfection for the amplified luminescence proximity homogenous (AlphaScreen) and luciferase reporter gene assays described in sections 3.2.5.3 and 3.2.5.4, respectively. Lipofectamine 2000 (Thermo Fisher Scientific) was used for transfecting all cells[272] and was incubated with serum-free medium prior to incubation with plasmid DNA (200ng/well and 16μg/75cm^2 flask) for 20 mins. Cells were exposed to transfection mixtures for 24 hours at 37°C, then growth medium with 10% FCS added for 24-48 hours before harvesting for the relevant *in vitro* assay.

3.2.5.2 Measurement of intracellular calcium concentrations using flow cytometry with Indo-1-acetoxymethylester (Indo-1-AM)

The effects of mutations in the CaSR or proteins involved in the signal transduction pathway on the receptor can be functionally assessed by measuring intracellular Ca^{2+} release in response to stimulation with extracellular Ca^{2+}.[130] This can be achieved through calcium flux assays which utilise fluorescent calcium-binding dyes, such as Indo-1 acetoxymethylester (Indo-1-AM) (Molecular Probes).[192 273] Indo-1-AM is cell-permeant and on entering the cell, the –AM group is cleaved from the molecule, thereby preventing the dye from leaving the cell.[274] It is excited by UV light, with an emission at ~475nm when unbound and at ~400nm when bound to Ca^{2+}.[274] As described in section 3.2.5.1, HEK293 cells stably expressing the CaSR (HEK293-CaSR) were transfected in 75cm^2 flasks and 24 hours later were plated into 175cm^2 flasks.[130] Cells were dissociated 48 hours following transfection with Hank's Balanced Salt Solution (HBSS) enzyme-free Cell Dissociation Buffer (Gibco).[130] The cell suspension was centrifuged at 1000rpm for 3 mins, pellet resuspended in ~4mls of Ca^{2+}- and Mg^{2+}-free HBSS (Gibco) and this cycle repeated.[130] Cells suspended in ~4mls of Ca^{2+}- and Mg^{2+}-free HBSS were loaded with 1μg/ml of Indo-1-AM (Figure 3.1) for 1 hour at 37°C in the dark.[130] The cell suspension was centrifuged at 1000rpm for 3 mins, pellet resuspended in ~4mls of Ca^{2+}- and Mg^{2+}-free HBSS and this cycle repeated 4 times to remove any extracellular dye.[130] Cells were resuspended in a final volume of 4mls of Ca^{2+}- and Mg^{2+}-free HBSS and maintained at 37°C for flow cytometry.[130]

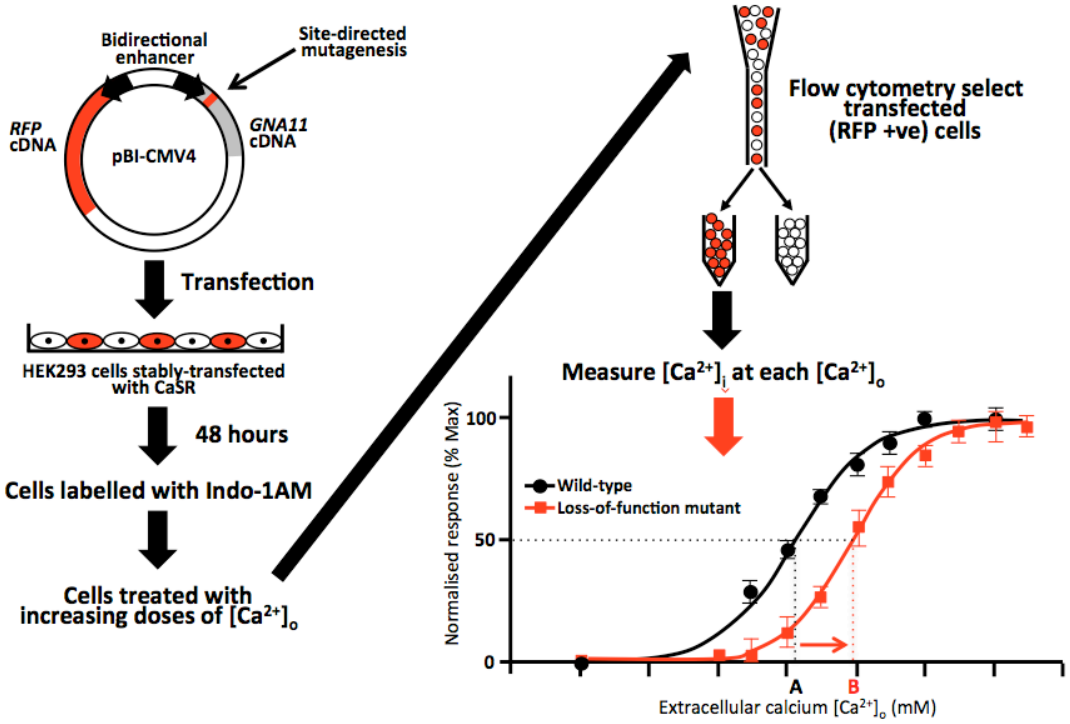


Figure 3.1. Schematic representation of flow cytometry using Indo-1-AM to measure intracellular Ca^{2+} in response to increasing concentrations of extracellular Ca^{2+}.

HEK293 cells stably expressing the CaSR were transfected with a bidirectional vector, pBI-CMV4-RFP, resulting in expression of the gene of interest and red fluorescent protein (RFP). Cells were exposed to increasing concentrations of extracellular Ca^{2+} ($[Ca^{2+}]_o$) as they passed through the flow cytometer, which selected the cells expressing RFP and thus, reduced signal from untransfected cells and cell debris. Intracellular Ca^{2+} measurements ($[Ca^{2+}]_i$) were used to construct concentration-response curves for WT and mutant cells, with illustration of the expected rightward shift and increase in EC_{50} seen following transfection with a loss-of-function mutation as seen in FHH (section 1.10.1.1). Adapted with permission of Dr F M Hannan.

A Beckman Coulter MoFlo XDP equipped with JDSU Xcyte UV Laser and a Coherent Sapphire 488nm Laser was used for flow cytometry.[130] Due to transfection of HEK293-CaSR cells with a bidirectional vector (pBI-CMV4-RFP) (Figure 3.1), they expressed the gene of interest and red fluorescent protein (RFP), allowing for the positive selection of transfected cells for analysis (Figure 3.1). The cells were treated with increasing concentrations of extracellular Ca^{2+} (Figure 3.1) and the fluorescence ratio versus time was recorded and data collected at 2 minutes intervals at each extracellular Ca^{2+} concentration.[130] Cytomation SUMMIT software (Beckmann Coulter) was used to determine the peak mean fluorescence ratio of the transient

response after each stimulus and the data normalised to a maximum 100% response.[130] Non-linear regression of normalised data using GraphPad Prism (GraphPad Software, Inc.) generated a concentration-response curve (Figure 3.1) and EC_{50} with 95% CI.[130]

3.2.5.3 Amplified luminescence proximity homogenous (AlphaScreen) assay

A range of methods can be used to study protein-protein interactions. The amplified luminescence proximity homogeneous (AlphaScreen) assay (PerkinElmer) has been validated for the study of cellular phosphorylation events and provides quantitative results.[275 276] The phosphokinase AlphaScreen assay is a bead-based assay, in which the unphosphorylated form of the substrate is captured by streptavidin-coated Alpha Donor Beads (Figure 3.2).[276] Protein A conjugated Acceptor beads will only bind to the phosphorylated form of the substrate of interest (Figure 3.2)[276] and thus, the two beads are brought into close proximity by a phosphorylation reaction. When excited by light at 680nm, the Donor bead donates a reactive oxygen species to the Acceptor bead, which then emits light at 520-620nm (Figure 3.2).[276] This signal can be detected allowing for quantitative data outputs.[276] The phosphorylated ERK1/2 (pERK1/2) and total ERK1/2 AlphaScreen assay kits (PerkinElmer) were used for studies.[276]

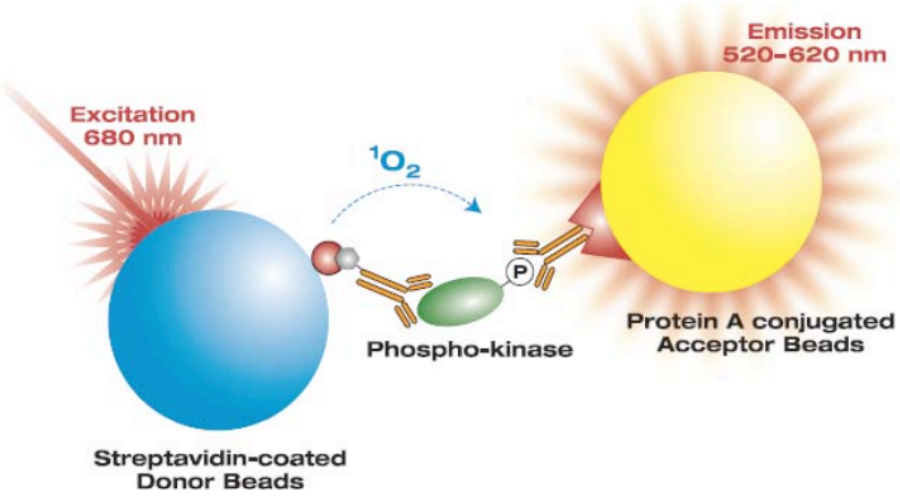


Figure 3.2. Schematic representation of the AlphaScreen mechanism of action.

A cellular phosphorylation event (white circle) brings the Acceptor (yellow) and Donor (blue) beads into close proximity through antibody binding. Excitation of the Donor beads with 680nm light stimulates them to donate a reactive oxygen species ($^1O_2$) to the Acceptor bead, which fluoresces, emitting light at 520-620nm. This signal can then be detected. Reproduced from PerkinElmer AlphaScreen SureFire ERK1/2 Assay Kit Manual, December 2010.

3.2.5.3.1 Phosphorylated ERK1/2 (pERK1/2) AlphaScreen assay

HEK293 cells stably expressing WT or mutant AP2σ2 were transiently transfected in 48-well plates as described in section 3.2.5.1 with WT CaSR. The following day, cells were exposed to overnight serum starvation. Forty-eight hours following transfection, medium was removed from the wells, cells were treated with 0-10mM calcium in serum-free medium for 5 mins at 37°C, medium was removed, and cells were lysed using 1x Surefire lysis buffer (PerkinElmer). The pERK1/2 AlphaScreen assay was performed using a 4µ aliquot of the lysate plated into a 384-well OptiPlate (PerkinElmer), as previously described.[276] A reaction mixture comprising 0.1µl acceptor beads, 0.05µl donor beads, 1ul activation buffer and 5.9µl reaction buffer was added to the cell lysate under low-light conditions at 4°C. The plate was sealed, wrapped in foil and incubated at 37°C for 2 hours. The fluorescence signal was measured using the PHERAstar *FS* microplate reader (BMG Labtech). Fold changes

were generated from the read-outs, data normalised and non-linear regression performed using GraphPad Prism to generate dose-response curves. Statistical analysis was performed by two-way test in analysis of variance (ANOVA) with the use of Tukey's multiple-comparisons comparing fold-changes. Expression of CaSR in the transfected cells was confirmed by Western blot analysis. A minimum of 3 independent biological replicates was performed in each experiment.

3.2.5.3.2 Total ERK1/2 AlphaScreen assay

HEK293 cells stably expressing WT or mutant AP2σ2 were transiently transfected in 48-well plates as described in section 3.2.5.1 with WT CaSR. The following day, cells were exposed to overnight serum starvation. Forty-eight hours following transfection, medium was removed from the wells, cells were treated with 0-10mM calcium in serum-free medium for 5 mins at 37°C, medium was removed, and cells were lysed using 1x Surefire lysis buffer (PerkinElmer). The Total ERK1/2 AlphaScreen assay was performed using a 4µl aliquot of the cell lysate plated into a 384-well OptiPlate. An acceptor mix comprising 0.04µl acceptor beads, 0.5ul activation buffer B and 2µl reaction buffer was added to the cell lysate under low-light conditions at 4°C. The plate was sealed, wrapped in foil and incubated at 37°C for 2 hours. A donor mix comprising 0.08µl donor beads and 2.4µl dilution buffer was added to the incubating mixture under low-light conditions. The plate was sealed, wrapped in foil and incubated for a further 2 hours at 37°C. The fluorescence signal was measured using the PHERAstar *FS* microplate reader. The read-out generated was used to normalise the corresponding pERK1/2 read-outs relative to total ERK1/2. Statistical analysis

was performed by two-way ANOVA with the use of Tukey's multiple-comparisons comparing fold-changes.

3.2.5.4 Dual-luciferase reporter gene assay

Reporter gene assays are used to study gene expression and utilise enzymes that display bioluminescence, such as the luciferases, to obtain a quantitative read-out.[277] In a dual reporter assay two individual reporter enzymes are simultaneously expressed and measured within the same system.[277] The experimental reporter is then normalised to the activity of the control reporter.[277] This normalisation helps to eliminate variability caused by limitations such as transfection efficiency, cell viability, and cell lysis efficiency.[277] In the Dual-Luciferase Reporter (DLR) assay system (Promega), the activity of Firefly (*Photinus pyralis*) and *Renilla* (*Renilla reniformis*) luciferases are measured sequentially from a single sample.[277] For experiments described below and in section 3.2.5.4.1, Firefly and *Renilla* were the experimental and control reporters, respectively.

HEK293 cells stably expressing WT or mutant AP2σ2 were transiently co-transfected in 24-well plates using Lipofectamine 2000 (Invitrogen) with 200ng of either pGL4.30[*luc2P*/NFAT-RE/hydro] or pGL4.33[*luc2P*/SRE/hydro] reporter gene constructs (vector maps shown in Appendix, Figure 10.2 and Figure 10.3, respectively), 10ng of *Renilla* control vector, and 200ng of CaSR receptor vector. One day following transfection, cells were incubated in serum-free media supplemented overnight. Cells were then treated with 0mM or 5mM calcium for 6 hours in serum-free media at 37°C. Cells were lysed using 100µl passive lysis buffer and a 20µl

aliquot of the cell lysate plated into a 96-well luminometer plate. The cell lysate was assayed for luciferase activity using a Veritas Turner Biosystems dual-injector luminometer and the Dual-Luciferase Reporter (DLR) assay system (Promega), as previously described.[276] Within the luminometer 100µl of LAR II (Promega) was dispensed into the well and firefly luciferase activity measured followed by 100µl of Stop & Glo reagent (Promega) and *Renilla* luciferase activity measured. The Firefly luciferase activity was adjusted for *Renilla* luciferase activity (Firefly/*Renilla* ratio) and ratios were expressed as fold changes relative to cells treated with 0mM calcium and WT, as previously described.[276] Statistical analysis was performed as for the AlphaScreen assays, described in section 3.2.5.3.1. Expression of CaSR in the transfected cells was confirmed by Western blot analysis, as described in section 3.2.4.3. A minimum of 3 independent biological replicates was performed in each experiment.

3.2.5.4.1 Dual-luciferase reporter gene assay examining the effects of cinacalcet on gene transcription

HEK293 cells stably expressing WT or mutant AP2σ2 were transiently co-transfected in 24-well plates using Lipofectamine 2000 (Invitrogen) with 200ng of either pGL4.30[*luc2P*/NFAT-RE/hydro] or pGL4.33[*luc2P*/SRE/hydro] reporter gene constructs (vector maps shown in Appendix, Figure 10.2 and Figure 10.3, respectively), 10ng of *Renilla* control vector, and 200ng of CaSR receptor vector. One day following transfection, cells were incubated in serum-free media supplemented overnight. Cells were treated with 10, 20 or 30nM cinacalcet in serum-free media or

5mM calcium for 6 or 24 hours at 37°C. Cells were lysed using 100µl passive lysis buffer and a 20µl aliquot of the cell lysate plated into a 96-well luminometer plate. The cell lysate was assayed for luciferase activity using a Veritas Turner Biosystems dual-injector luminometer and the Dual-Luciferase Reporter (DLR) assay system (Promega), as described in section 3.2.5.4. Data analysis was performed as described in section 3.2.5.4. Expression of CaSR in the transfected cells was confirmed by Western blot analysis, as described in section 3.2.4.3. A minimum of 3 independent biological replicates was performed in each experiment.

3.2.6 Protocols used for animal studies

3.2.6.1 Metabolic cage protocol

Twelve-week-old mice were individually housed in metabolic cages (Techniplast) for 3 days to enable acclimatisation prior to any measurements.[278] Mice were given water and expanded rat and mouse no.3 breeding diet containing 1.24% calcium, 0.83% total phosphorus, and 2948.01IU/kg vitamin D (Special Diet Services) *ad libitum*. All mice underwent a 24-hour period of assessment involving measurement and recording of: animal weight at 0 and 24 hours; 24-hour water and food consumption; 24-hour urine volume.[278] Urine samples were taken for analysis during the 24-hour period and each sample was centrifuged at 800×*g* for 10 minutes at 4°C and aliquots stored at −20°C prior to analysis.

3.2.6.2 Measurement of blood and urine biochemistry

Blood samples were obtained at the end of the metabolic cage study described in section 3.2.6.1 via the retro-orbital vein under isoflurane terminal anaesthetic. Plasma samples were analysed for calcium, magnesium, sodium, potassium, chloride, inorganic phosphate, urea, creatinine, glucose, total cholesterol, total protein, albumin, total bilirubin, alanine transaminase, alkaline phosphatase, glucose, vitamin D and PTH using an Olympus AU400 analyser, as described previously.[260] Urine samples obtained were analysed for calcium, magnesium, sodium, potassium, chloride, inorganic phosphate, urea, creatinine, glucose and total protein.

3.2.6.2.1 Analysis of blood and urine biochemistry

Plasma calcium was adjusted for plasma albumin concentration using the formula:

$$\text{Adjusted } Ca^{2+} = \text{plasma } Ca^{2+} \text{ (mmol/l) - [(plasma albumin (g/l) - 30) x 0.017]}$$ [182]

Fractional excretion of calcium, also known as the urinary calcium: creatinine clearance ratio (CCCR), was calculated using the formula:

$$\text{CCCR} = \frac{\text{urinary } Ca^{2+} \text{(mmol/l) x plasma creatinine (mmol/l)}}{\text{corrected plasma } Ca^{2+} \text{(mmol/l) x urinary creatinine (mmol/l)}}$$ [183]

Fractional excretion of phosphate, sodium, potassium and chloride was calculated in a similar manner. Statistical analysis was performed using Mann-Whitney test with Welch's correction and Bonferroni posttest in GraphPad Prism.

3.2.7 Bioinformatic analyses

3.2.7.1 Densitometry analysis of Western blots

Quantitative analysis of Western blots was performed by densitometry using ImageJ software (National Institute of Health) to calculate the relative density of each protein band relative to the equivalent loading control.[184]

3.2.8 Statistical analyses

All statistical analyses were performed in GraphPad Prism. For *in vitro* functional expression studies, non-linear regression of results was performed and data analysed for statistical significance using two-way ANOVA with Tukey's multiple comparison test.[276] Statistical comparisons of mean EC_{50} values from multiple transfections and technical replicates were undertaken using the *F* test.[12,118] For proband and *in vivo* studies, unpaired Mann-Whitney tests with Welch's correction were used to compare two groups.[260] Unpaired two-tailed Student's *t*-tests were used to assess the statistical significance of qPCR expression data.[260] A value of $p \leq 0.05$ was considered to be statistically significant for all analyses.

3.2.8.1 Web Resources

Program	Web Address
Berkeley Drosphilia Genome Project	http://www.fruitfly.org
Database of short genetic variants (dbSNP)	http://www.ncbi.nlm.nih.gov/projects/SNP/
Ensembl Genome Browser	http://www.ensembl.org
Exome Sequencing Project of the National Heart, Lung, and Blood Institute (NHLBI-ESP)	http://evs.gs.washington.edu
GeneSplicer	http://ccb.jhu.edu
Phyre2	http://www.sbg.bio.ic.ac.uk/phyre2/
Polyphen-2	http://genetics.bwh.harvard.edu/pph2/
Primer 3	http://bioinfo.ut.ee/primer3/
PubMed	http://www.ncbi.nlm.nih.gov/pubmed
Webcutter 2.0	http://rna.lundberg.gu.se/cutter2/

Results

Genetics of AP2σ2 mutations in Familial hypocalciuric hypercalcaemia (FHH)

4 Genetics of AP2σ2 mutations in Familial hypocalciuric hypercalcaemia (FHH)

Familial hypocalciuric hypercalcaemia (FHH) is a genetically heterogeneous disorder with three variants reported: FHH1 is due to loss-of-function CaSR mutations and accounts for more than 60% of FHH cases;[111] FHH2 is due to loss-of-function Gα11 mutations of which two cases have been reported;[197] and FHH3 is due to loss-of-function AP2σ2 mutations and may account for more than 5% of FHH cases,[130] as described in section 1.10.1.1. At the time of commencement of my DPhil studies, 3 different AP2σ2 mutations had been reported in 13 individuals and families with FHH.[130] The mutations all comprised heterozygous missense substitutions of the Arg15 residue (Arg15Cys (R15C), Arg15His (R15H) and Arg15Leu (R15L)). To further investigate the spectrum of AP2σ2 mutations in FHH3, I performed genetic and phenotypic characterisation of a sample of 56 hypercalcaemic probands who were found not to harbour CaSR mutations following referral to the Oxford Centre for Clinical Genetics for CaSR mutational analysis by their physician. These hypercalcaemic probands simultaneously underwent sequence analysis of the 1,077 bp coding region, 12 exon-intron boundaries and UTRs of *GNA11* to identify any mutations.

4.1.1 Biochemical features of probands investigated for AP2σ2 mutations

Fifty-six unrelated hypercalcaemic probands, in whom CaSR mutations were excluded, were investigated for the presence of AP2σ2 mutations. The cohort comprised 19 males and 37 females with ages at referral for mutational analysis that ranged from the neonatal period to 86 years, with an average age of 53 years. Approximately 94% of the hypercalcaemic probands had adjusted serum calcium levels <3.0 mmol/L (mean ± standard error of the mean (SEM): 2.75±0.02 mmol/L; normal range: 2.10-2.60 mmol/L). Serum PTH concentrations were elevated above the upper limit of normal in 76% of probands and within the normal range in the remainder (normal range: 10-65 ng/L; 1.3-7.6 pmol/L). Hypophosphataemia was found in 4% of probands with serum phosphate levels below the lower limit of normal (normal range: 0.70-1.40 mmol/L) and the remainder had serum phosphate levels within the normal range (mean±SEM: 1.00±0.06 mmol/L). Additionally, the hypercalcaemic probands demonstrated inappropriately low renal calcium excretion (mean CCCR±SEM: 0.01± 0.001; normal range> 0.02).

4.1.2 Identification of AP2σ2 mutations in probands with FHH

DNA sequence analysis of the 429 bp coding region, eight exon-intron boundaries and UTRs of *AP2S1* in the 56 unrelated probands identified *AP2S1* nucleotide changes in 9 probands (Table 4). Proband 19/12a harboured a c.269C>T mutation predicted to result in a missense amino acid change at codon 15 in AP2σ2 from Arg to Cys (R15C). Probands 08/11, 03/12 and 19/12b harboured a c.270G>A mutation predicted to result in a missense amino acid change at codon 15 in AP2σ2 from Arg to

His (R15H). Probands 02/03, 02/11, 09/12, 06/13b and 02/14 had harboured a c.270G>T mutation predicted to result in a missense amino acid change at codon 15 in AP2σ2 from Arg to Leu (R15L). Thus, 1 R15C, 3 R15H, and 5 R15L AP2σ2 mutations were identified in 9 FHH probands (Table 4). The identified FHH3-associated mutations all affected the R15 residue of the AP2σ2 subunit and had been previously reported as pathogenic loss-of-function mutations.[130] These 9 mutations, in combination with the 13 AP2σ2 mutations previously reported,[130] bring the total number of mutations to 7 R15C, 6 R15H and 9 R15L AP2σ2 mutations. This represents an AP2σ2 mutation detection rate of greater than 20% in this cohort of hypercalcaemic probands in whom CaSR mutations have been excluded. Additionally, one proband (19/12) harbouring an AP2σ2 R15H mutation was found to also harbour a novel *GNA11* c.501A>G variant which is predicted to result in an amino acid missense substitution of Met for Val at codon 87 in Gα11 (M87V) (described in section 4.1.5).

Table 4. Clinical and biochemical findings in 9 FHH probands with AP2σ2 mutations.

Mutation	Proband	Sex	Family history	Age[+] (years)	Clinical features	Serum Ca[a,b]	Serum Pi[c]	Serum Mg[d]	Serum ALP[e-f]	Serum PTH[h,i]	Urine CCCR[j,k]	Bone Mineral Density Lumbar Spine	Bone Mineral Density Femoral Neck
Arg15Cys													
	19/12a	M	Yes	48	Nil	2.94[a]	-	0.82	110[e]	45.0[h]	0.009[j]	-0.3[i]	-2.9[l]
Arg15His													
	08/11	F	Yes	33	H	2.76[a]	1.0	0.99	74[e]	7.4[i]	0.010	-2.6[l]	-2.3[l]
	03/12	F	Yes	44	Nil	2.80[a]	0.86	-	65[e]	5.2[i]	0.009[j]	-1.1[l]	-0.7[l]
	19/12b	F	-	19	Nil	2.74[a]	0.65	-	104[e]	4.6[i]	0.005[j]	-	-
Arg15Leu													
	02/03	F	No	15	A, L, S	2.90[a]	0.86	1.03	-	4.7[i]	0.015[j]	-4.6[m]	-
	02/11	F	-	14	L, P, S	3.20[a]	1.2	1.02	88[e]	31.0[h]	0.005[j]	-3.0[m]	-2.5[m]
	09/12	F	-	9	-	2.81[a]	1.0	0.97	298[f]	96[h]	0.002[j]	-	-
	06/13b	F	No	7	Nil	3.03[a]	0.87	0.95	285[f]	40.5[h]	0.001[j]	-1.3[m, n]	N
	02/14	F	No	26	H	2.95	1.17	0.98	-	4.0[i]	0.008[j]	-	-

Age [+]at presentation or diagnosis. Normal serum ranges[192]: albumin-adjusted calcium [a]2.10-2.60 mmol/L; ionized calcium [b]1.19-1.35 mmol/L; phosphate, [c]0.70-1.40 mmol/L; magnesium, [d]0.70-1.0 mmol/L; total alkaline phosphatase (ALP) activity, [e]50-130 U/L, [f]70-330 U/L; PTH, [h]10-65 ng/L; [i]1.3-7.6 pmol/L. Normal urine ranges; calcium-to-creatinine clearance ratio (CCCR) [j]>0.02; calcium-to-creatinine ratio, [k]0.3-0.7; [l]Bone mineral density (BMD) T-scores are provided for subjects >20 years old and [m]BMD Z-scores provided for subjects <20 years old; [n]whole body BMD Z-score = -2.0 for proband 06/13b; A, atrial septal defect; H, hypercalcaemic symptoms; L, learning disability; N, normal; S, short stature; P, pancreatitis; -, not known.

4.1.3 Identification of mutation bias in AP2σ2 mutations

The FHH3-associated AP2σ2 mutations identified to date[130 279 280] are all missense substitutions of the R15 residue, comprising R15C, R15H and R15L. Analysis of the nucleotide sequence of the R15 codon in unaffected individuals on the National Centre for Biotechnology Information (NCBI) database of short genetic variants (dbSNP) shows it to be CGC (Figure 4.1). The GC to AT nucleotide change is the most frequent mutation found in the human genome[281] and transition mutations in codon 15 giving rise to C>T and G>A changes result in R15C and R15H mutations, respectively. A transversion mutation at codon 15 gives rise to a G>T mutation resulting in an R15L mutation. However, the other possible outcomes of transversion mutations at codon 15 include R15G, R15P, and R15S, which have not been detected to date in hypercalcaemic probands (Figure 4.1). Thus, there is evidence of mutation bias at the R15 residue, demonstrated by the significant difference in observed versus expected frequencies of AP2σ2 R15 mutants ($p < 0.0001$, χ^2 test).

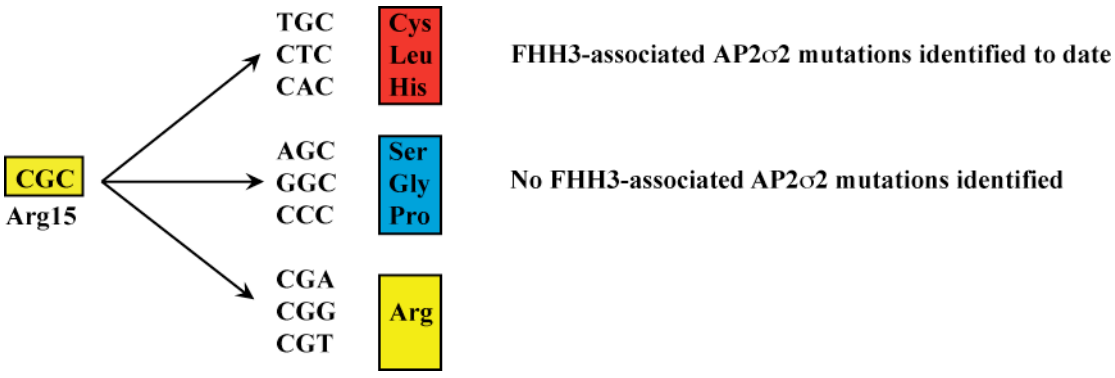


Figure 4.1. Observed and predicted mutations at AP2σ2 R15 residue.

Schematic representation of the possible nucleotide and amino acid substitutions affecting codon 15 of AP2σ2. Substitutions affecting the first or second nucleotide of R15 (CGC) are predicted to result in one of six possible non-synonymous mutations or variants, comprising Cys (TGC), Gly (GGC), His (CAC), Leu (CTC), Pro (CCC) or Ser (AGC). Substitutions affecting the third nucleotide of the codon are predicted to result in synonymous variants only.

Structural modelling studies within the group have recently demonstrated that mutation of the R15 residue to G, P, or S would result in loss of the interaction between a putative dileucine motif in the CaSR C-terminal and the AP2σ2 subunit.[282] Additionally, *in vitro* studies measuring intracellular Ca^{2+} release in response to extracellular Ca^{2+} have revealed the R15G, R15P and R15S AP2σ2 variants to be associated with a loss-of-function in the CaSR.[282] Studies of cell growth demonstrated a reduced number of cells expressing R15G, R15P and R15S compared with R15C, R15H and R15L AP2σ2 mutants, from 48 to 72 hours, which led to the hypothesis that the variants are not detected in patients as embryos would not be viable. However, further studies of proliferation and cellular senescence are required to better understand the differences between R15 mutations.

4.1.3.1 Identification of *de novo* AP2σ2 mutations in probands with FHH3

At the commencement of my studies, all familial AP2σ2 mutations reported showed an autosomal dominant pattern of inheritance. I identified two FHH probands, 06/13b and 02/03 (Table 4), harbouring AP2σ2 R15L mutations. In both cases these mutations were shown to be absent in their parents (Figure 4.2) and therefore likely to be arising *de novo*. During the course of my studies, a further *de novo* AP2σ2 mutation was identified in a case of FHH providing further evidence for *de novo* mutations as a cause of FHH3.[279] Genetic maternity and paternity was assumed due to ethical constraints.

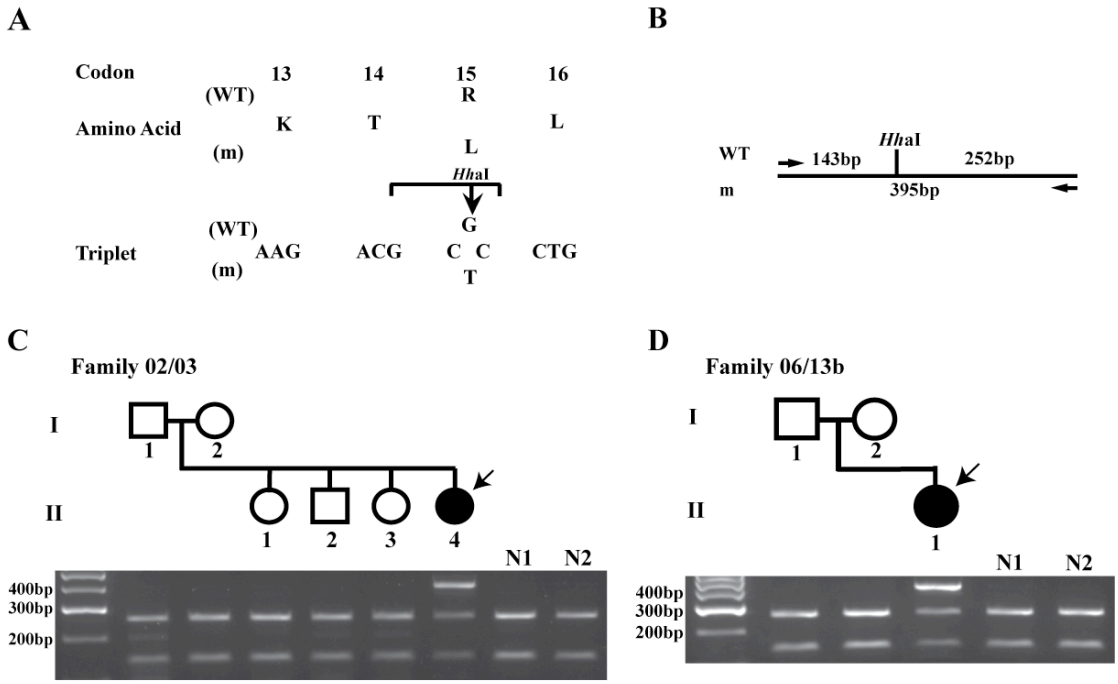


Figure 4.2. Detection of *de novo* AP2σ2 mutations.

(**A**) DNA sequence analyses of the probands (arrowed) revealed a G to T substitution at codon 15, predicted to result in a missense amino acid substitution of Arg (R) to Leu (L), and loss of a *Hha*I restriction endonuclease site. (**B**) *Hha*I restriction map showing that the endonuclease digests the 395bp wild-type (WT) product into 143bp and 252bp fragments but fails to digest the mutant (m) product. PCR and *Hha*I digestion revealed the probands (individual II.4 of family 02/03 (**C**) and individual II.1 of family 06/13b (**D**)) to be heterozygous for the R15L mutation. The absence of the R15L mutation in the unaffected parents of both probands is consistent with the mutation arising de *novo*.

4.1.3.2 Phenotypic characterisation of nine probands with AP2σ2 mutations

The 9 probands identified with AP2σ2 mutations comprised 1 male and 8 females with ages at diagnosis or presentation ranging from 7 years to 48 years old (Table 4). Two (02/03 and 02/11) of 7 probands were symptomatic due to their hypercalcaemia at diagnosis or presentation, and both harboured AP2σ2 R15L mutations. The level of hypercalcaemia was more severe compared to that seen in the unselected hypercalcaemic sample group investigated for AP2σ2 mutations (mean adjusted serum calcium±SEM for FHH3 vs hypercalcaemic patients: 2.90±0.05 vs 2.75±0.02 mmol/L; $p<0.01$; normal range: 2.10-2.60 mmol/L). Serum PTH concentrations were

within the normal range in 8 probands and elevated in 1 proband (09/12) whereas serum phosphate concentrations were within the normal range for all but 1 proband (19/12b) in whom it was low (mean±SEM: 0.95±0.06 mmol/L; normal range: 0.70-1.40 mmol/L). Hypermagnesaemia was present in 2 (02/03 and 02/11) of 7 probands and serum alkaline phosphatase activity was within the normal range in all probands for which data were available. All probands demonstrated reduced urinary calcium excretion with CCCR consistent with a diagnosis of FHH (mean CCCR±SEM: 0.007 ± 0.001).

Two of the probands harbouring R15L mutations (02/03 and 02/11) were identified as suffering with learning disabilities. One of these probands (02/03) was found to harbour an atrial septal defect, whilst the other proband (02/11) suffered from recurrent episodes of acute pancreatitis. The pancreatitis was unrelated to gallstones and sequence analysis, undertaken by the regional clinical genetics unit, for serine protease inhibitor, kazal-type, 1 (*SPINK1*), cystic fibrosis transmembrane conductance regulator (*CFTR*), protease, serine, 1 (*PRSS1*), and chymotrypsin C (*CTRC*), which are known to be associated with pancreatitis, did not reveal any mutations.

In addition to the features described above, probands 02/03 and 02/11 had short stature with height at or below the third centile and dual-energy x-ray absorptiometry (DXA) revealed reduced bone mineral density (BMD) (Z-scores at the lumbar spine: 02/03, -4.6; 02/11, -3.0; Paediatric Z-score < 2.5 suggests osteoporosis[283]). An additional 5 FHH3 probands harbouring AP2σ2 R15C, R15H and R15L mutations

demonstrated reduced BMD at the lumbar spine or femoral neck on DXA that was not associated with renal impairment, gonadal dysfunction, hyperthyroidism or vitamin D deficiency (adult T-score: 19/12a, -2.9; 08/11, -2.6; osteoporosis defined as T-score <2.5 by the World Health Organisation; paediatric lumbar spine Z-score: 02/03, -4.6; 02/11, -3.0; osteoporosis defined as paediatric Z-score <2.5[283]). These skeletal findings are suggestive of bone remodelling abnormalities.

A multi-generational kindred from Oklahoma (referred to as FHH_{ok}) has been extensively characterised phenotypically[190 269 284] and includes thirty-eight members spanning five generations. The FHH locus associated with this kindred mapped to 19q13[190 191] and affected members were found to harbour AP2σ2 R15C mutations.[130] Affected members have FHH as demonstrated by hypercalcaemia associated with hypocalcuria[190 269 284] and additionally, some develop hypophosphataemia, elevations in serum PTH and osteomalacia in later life.[284] The bone abnormalities were suggested from the radiological findings of 3 of 5 affected adults over the age of 40 years and an iliac crest biopsy from a 51 year old affected female, which demonstrated defective skeletal mineralisation.[284] The study identified that the proposita's brother was diagnosed with hypoparathyroidism complicated by severe osteomalacia associated with pseudofractures at age 20 years.[284] Osteomalacia can present as reduced BMD on DXA.[285] Skeletal radiographs and bone biopsies were not available on my cohort of probands with AP2σ2 mutations identified with reduced BMD.

4.1.3.3 Comparison between the phenotypes of FHH1 and FHH3

To determine whether FHH3 is associated with any differences in the biochemical phenotype when compared to FHH1, serum and urine biochemistry from the 9 FHH3 probands was compared with that of 9 previously reported FHH1 probands who harboured CaSR mutations (Figure 4.3).[192] This revealed that FHH3 probands have elevated serum magnesium levels compared to FHH1 probands (mean serum magnesium ± SEM: FHH3 probands, 0.97±0.03 mmol/L; FHH1 probands, 0.84±0.07 mmol/L; $p<0.05$). There were no significant differences in the serum concentrations of calcium, phosphate, or PTH or CCCR between the FHH3 and FHH1 probands. This result is however based on analysis of a small sample size and no data was available on the fractional excretion of magnesium and thus it cannot be suggested whether the difference in serum magnesium concentration is due to differences in the renal reabsorption of magnesium between FHH1 and FHH3.

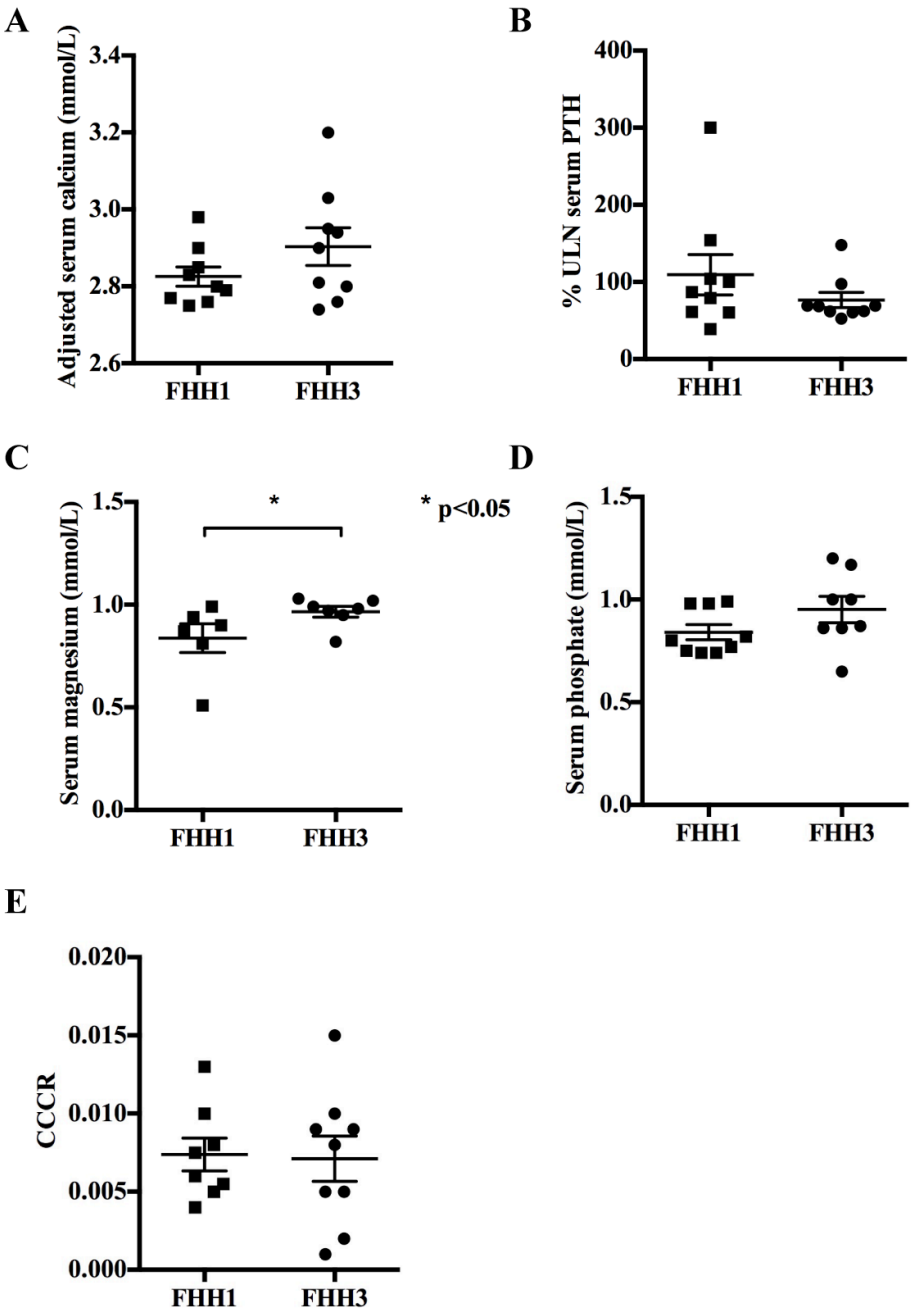


Figure 4.3. Comparison of biochemical phenotypes between FHH1 and FHH3.

Scatter plots of serum concentrations of (**A**) adjusted calcium, (**B**) PTH represented as % upper limit of normal (ULN), (**C**) magnesium, (**D**) phosphate, (**E**) urinary calcium: creatinine clearance ratio (CCCR) for FHH3 probands and a cohort of previously reported FHH1 probands with CaSR mutations.[192] FHH3 probands to have elevated serum magnesium levels compared to FHH1 probands ($p<0.05$). Mean values are represented by horizontal lines and error bars represent SEM. There were no significant differences in the serum concentrations of calcium, phosphate, or PTH or CCCR between the FHH3 and FHH1 probands.

4.1.4 Identification and investigation of kindreds with AP2σ2 mutations

A 16 year old female proband from Kansas, Missouri presenting with psychiatric and gastrointestinal symptoms was found to have an elevated serum ionised calcium (6.0 mg/dl, normal range: 4.5-5.3 mg/dl), normal serum PTH concentration (44 pg/mL; normal range: 10-69 pg/dL) and hypocalcuria (CCCR: 0.004; normal >0.02). DXA revealed no evidence of reduced bone density (whole body Z-score: -0.9). Family studies identified relatives noted to suffer with psychiatric and gastrointestinal symptoms, who were found to be hypercalcaemic and hypocalciuric.

DNA sequence analysis of the 429 bp coding region, 8 exon-intron boundaries and UTRs of *AP2S1* of the kindred (referred to as FHH_{ks} due to their location in the Midwest), consisting of the proband and four family members (two males and two females), identified an AP2σ2 R15C mutation in affected members (Figure 4.4).

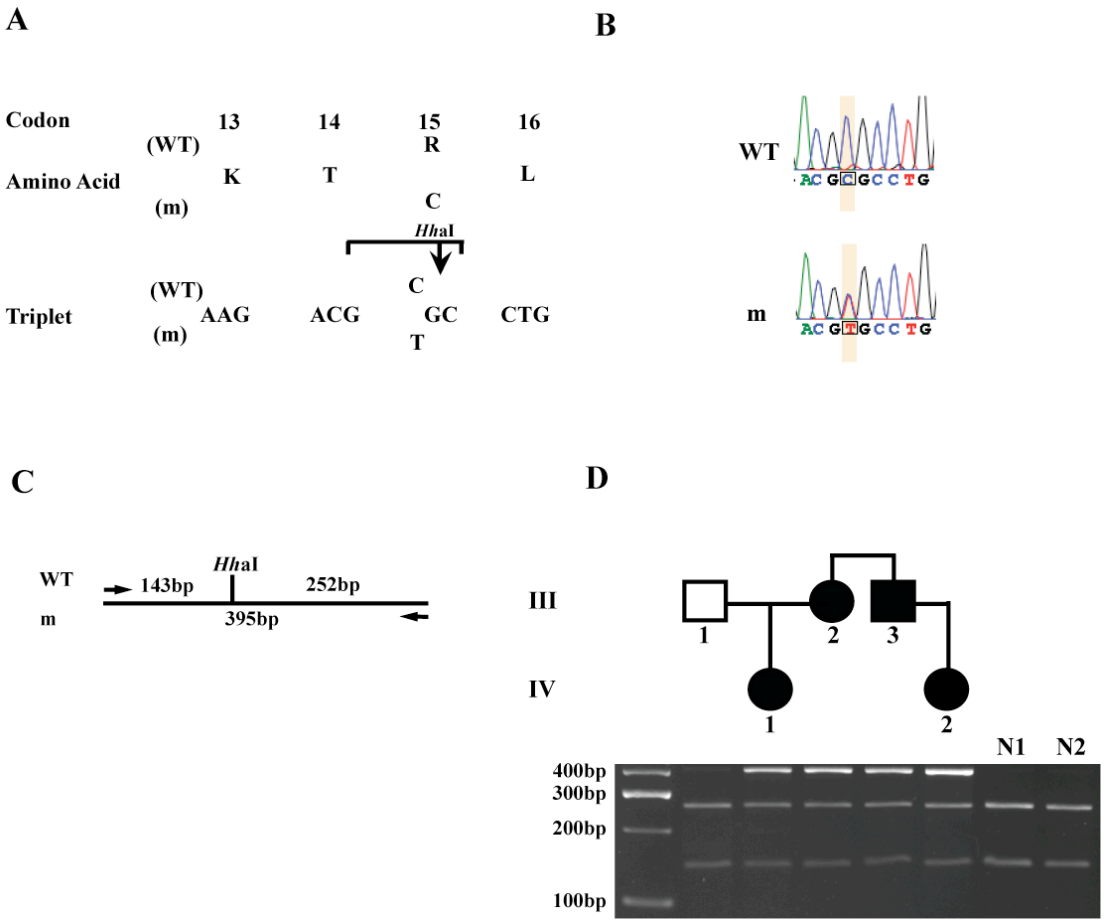


Figure 4.4. Detection of an AP2σ2 mutation in the FHHks family.

(**A**) DNA sequencing revealed a C-to-T substitution at codon 15, predicted to result in a missense amino acid transversion of R to C, and loss of a *Hha*I restriction endonuclease site. (**B**) DNA sequence analysis from an unaffected (WT) and affected (m) individual from the FHHks family. (**C**) Restriction map showing that *Hha*I digestion would result in two products of 143 bp and 242bp from the wild-type (WT) sequence, but would not affect the mutant (m) sequence. (**D**) PCR and *Hha*I digestion revealed individuals III.2, III.3, IV.1 and IV.2 of family FHH_{ks} to be heterozygous for an AP2σ2 R15C mutation.

4.1.5 Functional characterisation of a novel *GNA11* variant in an FHH3 proband

All the hypercalcaemic probands underwent simultaneous sequence analysis of the intron-exon boundaries and UTRs of *AP2S1* and *GNA11*, as previously described.[130] [197] One 19 year-old female proband (19/12b) was found to harbour an AP2σ2 R15H mutation and a novel *GNA11* c.501A>G variant, predicted to result in an amino acid missense substitution of Met for Val at codon 87 in Gα11 (M87V). The proband was asymptomatic and diagnosed due an incidental finding of hypercalcaemia (adjusted serum calcium: 2.74 mmol/L; normal range: 2.10-2.60 mmol/L) with a serum PTH concentration within the reference range and hypocalciuria (CCCR: 0.0005; normal >0.02) (Table 4). Two loss-of-function Gα11 mutations (Ile200del and Leu135Gln)[197] have previously been reported in probands with FHH who did not have CaSR or AP2σ2 mutations, described in section 1.10.1.1.2. Thus, this proband was unusual in having a pathogenic AP2σ2 mutation and a Gα11 variant of unknown significance, which I further investigated.

Residue M87 is highly conserved across vertebrate Gα11 subunit orthologues and Gα paralogues (Figure 4.5) with no variants identified. Although the Gα11 M87V variant was predicted to be benign by Polyphen-2,[286] an online software programme which predicts the possible effects of amino acid substitutions on the protein, the variant was not reported by dbSNP or found in approximately 6,500 exomes held by the Exome Sequencing Project of the National Heart, Lung, and Blood Institute (NHLBI-ESP) whose coverage included this region (databases accessed on 1 June 2015). It was

therefore predicted that the Gα11 M87V variant may represent a loss-of-function mutation and could be contributing to the FHH phenotype of the proband.

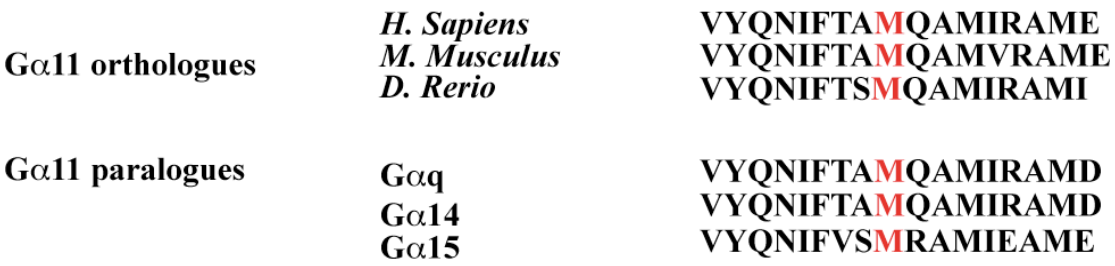
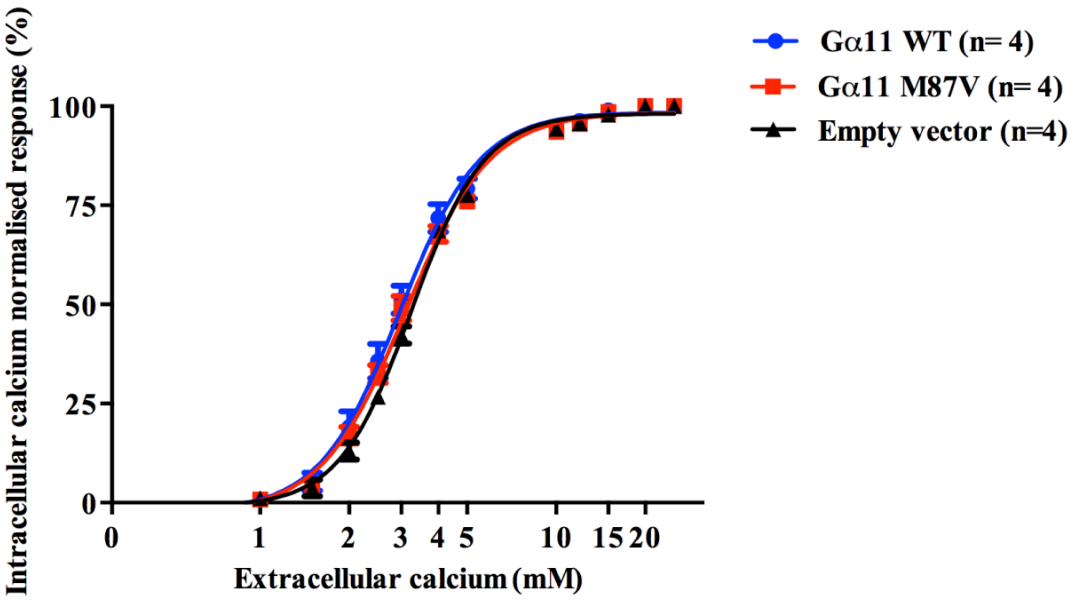


Figure 4.5. Multiple amino acid sequence alignment of Gα11 residue Met87 (M87) in orthologues and paralogues.

The M87 residue (red) is conserved in both orthologues and paralogues.

To investigate the functional effects of the Gα11 M87V variant, a flow cytometry assay using the calcium-binding dye, Indo-1-AM to detect intracellular Ca^{2+} release in response to increasing concentrations of extracellular Ca^{2+} was used to generate dose-response curves (Figure 4.6). Studies were performed in HEK293-CaSR cells transiently expressing either pBI-CMV4-Gα11-WT or pBI-CMV4-Gα11-M87V wild-type Gα11. Cells expressing either WT or Gα11 M87V responded to extracellular Ca^{2+} in a dose-dependent manner and there was no significant difference in the EC_{50} values (Gα11 WT EC_{50} = 2.96 (95% confidence interval (CI) = 2.83-3.10), Gα11 M87V EC_{50} = 3.09 (95% CI = 2.99-3.26), empty-pBI-CMV4-RFP EC_{50} = 3.24 (95% CI = 3.16-3.34), WT vs. M87V p= 0.14, n = 4 biological replicates) (Figure 4.6). Therefore, as the Gα11 M87V variant demonstrated no difference compared to WT expressing cells, it is unlikely to be pathogenic and contributing to the phenotype of the proband. Thus, the Gα11 M87V variant is likely to be a rare polymorphic variant.

A



B

	EC_{50}	95% CI
Gα11 WT	2.96	2.83-3.10
Gα11 M87V	3.09	2.99-3.26
Empty vector	3.24	3.16-3.34

Figure 4.6. Intracellular calcium responses to changes in extracellular calcium in HEK293-CaSR cells transfected with Gα11 WT, M87V or empty vector, pBI-CMV4-RFP.

(**A**) HEK293-CaSR cells were transiently transfected with either Gα11 WT (blue), M87V (red) or empty vector, pBI-CMV4-RFP (black). Forty-eight hours later, cells were labelled with Indo-1-AM and treated with increasing doses of extracellular calcium (0-10mM). Transfected cells were selected by flow cytometry and the intracellular calcium measured at extracellular calcium concentrations between 0 and 20mM. Mean ± SEM of n = 4 biological replicates are shown. (**B**) There was no significant difference in the concentration of calcium required to produce a half maximal response (EC_{50}) in WT and M87V transfected cells.

4.1.6 Identification of *GNA11* single nucleotide polymorphisms (SNPs) in hypercalcaemic probands

In addition to the novel *GNA11* variant identified whilst sequencing the 56 unrelated hypercalcaemic probands, five previously reported *GNA11* single nucleotide polymorphisms (SNPs) were detected in the probands (Table 5). These included: 3 intronic SNPs (rs143987260, rs116848044 and rs73527836), predicted to have no effect on splicing by splice site prediction programs (Berkeley Drosophila Genome Project (BDGP)[287] and GeneSplicer[288]); and two coding, synonymous SNPs (rs141926949 and rs4900), the predicted effects of which on Gα11 protein function are unknown, according to Polyphen-2[286].

Table 5. Previously reported *GNA11* single nucleotide polymorphisms (SNPs) detected in hypercalcaemic probands.

rs ID	Exon/Intron	cDNA change	Protein change	Frequency in hypercalcaemic probands	MAF	Polyphen-2 prediction
rs143987260	Intron 1	c.321+9G>A	-	0.02	<0.01	-
rs141926949	Exon 4	c.489C>T	Asp163Asp	0.02	<0.01	Unknown
rs116848044	Intron 5	c.736-6C>T	-	0.02	<0.01	-
rs4900	Exon 6	c.771C>T	Tyr257Tyr	0.66	0.35	Unknown
rs73527836	Intron 6	c889+8G>C	-	0.09	0.06	-

Variants are numbered in relation to the *GNA11* cDNA reference sequence (GenBank accession numbers NM_002067.3), whereby nucleotide +1 corresponds to A of the ATG-translation initiation codon. Information on mean allelic frequency (MAF) obtained from on the National Centre for Biotechnology Information (NCBI) database of short genetic variants (dbSNP) or the Exome Sequencing Project of the National Heart, Lung, and Blood Institute (NHLBI-ESP). Databases accessed on 18 July 2015.

4.1.7 Effect of AP2σ2 mutation on the stability of the AP-2 complex

Within the AP-2 complex, each subunit is in contact with all the other subunits (Figure 1.9) and it has been demonstrated *in vitro* that the stability of the AP-2 complex can be disrupted through the use of siRNA to knock down specific AP-2 subunits in HeLa cells.[255 289] Deletion of any one of the subunits has been shown *in vitro* to lead to exposure of a hydrophobic surface resulting in the mutant complex becoming insoluble.[126] To investigate the effect of a point mutation in an AP-2 subunit on the stability of the AP-2 complex, I sought to study cells derived from probands expressing AP2σ2 mutations. The effect of a point mutation in an AP-2 subunit on the stability of the complex had not previously been studied.

To investigate the effect of harbouring an AP2σ2 mutation on the stability of the AP-2 complex, lymphoblastoid cells derived from members of the FHH_{ok} kindred, a multi-generational kindred with FHH due to AP2σ2 R15C mutations,[130 269 284] were used. RNA and protein extracted from the lymphoblastoid cells of affected (two males and two females) and unaffected (two males and two females) members was analysed for the expression of all AP-2 subunits.

The genotype of the family members was identified using RT-PCR and restriction endonuclease analysis (Figure 4.7) and corresponded to the phenotype in all but one individual (V-21). Individual V-21 was a 13 year old male who developed end-stage renal failure secondary to medullary cystic disease and accelerated hypertension.[284] He was known to be hypercalcaemic prior to the onset of renal failure and remained

hypercalcaemic following a renal transplant.[284] His mother (IV-13) was normocalcaemic and no biochemistry was available on the father.[284] As the female subject (IV-13) had a normal serum calcium level with a hypercalcaemic child, she was originally classified as a carrier of FHH.[284] No lymphoblastoid cells were available from subject IV-13 for study. The findings of the restriction endonuclease analysis (Figure 4.7) confirm that the hypercalcaemia in individual V-21 is not due to an AP2σ2 mutation.

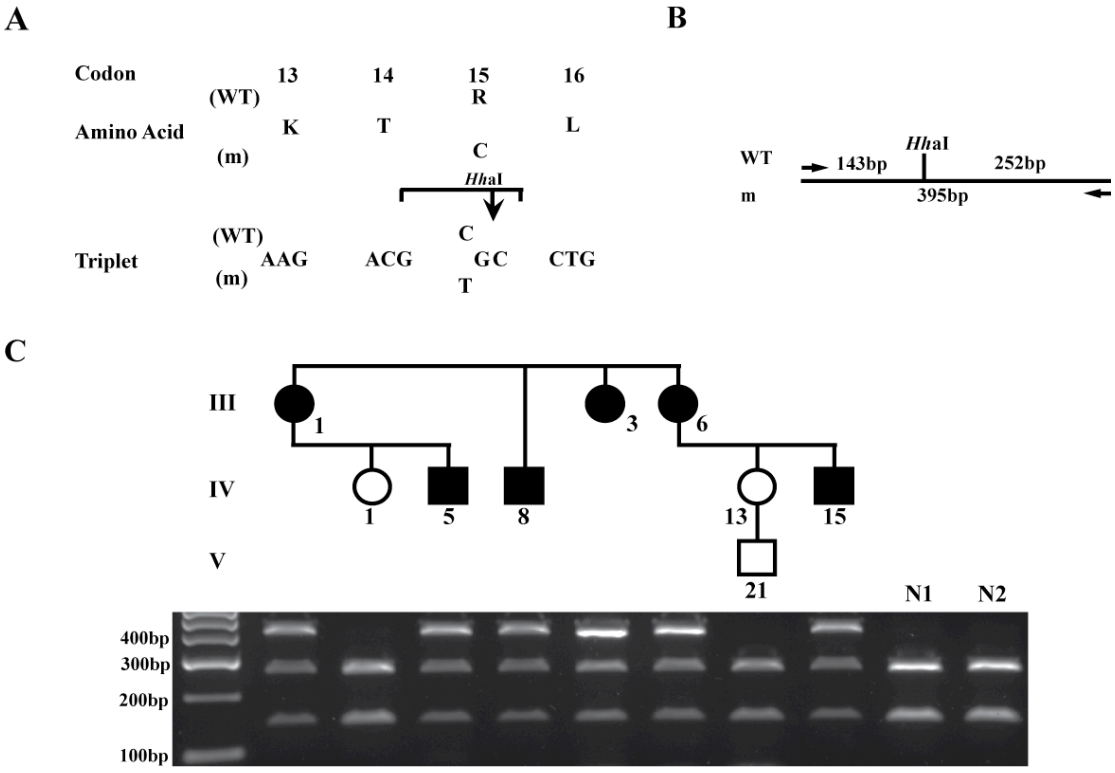


Figure 4.7. Detection of an AP2σ2 mutation in the FHH_{ok} family.

(**A**) DNA sequencing had previously reported a c.269C>T mutation in *AP2S1* predicted to result in a missense amino acid substitution of R to C at codon 15 in AP2σ2,[130] and loss of a *Hha*I restriction endonuclease site. (**B**) Restriction map showing that *Hha*I digestion would result in two products of 143bp and 242bp from the wild-type (WT) sequence, but would not affect the mutant (m) sequence. (**C**) PCR and *Hha*I digestion revealed individuals III.1, III.3, III.6, IV.5, IV.8 and IV.15 of family FHH_{ok} to be heterozygous for the AP2σ2 R15C mutation. Individual V.21 had previously been reported as affected on the basis of phenotype[284] but does not harbour an AP2σ2 mutation. No sample was available for analysis on individual IV.13.

To determine if the presence of a point mutation in AP2σ2 affected the expression of other AP-2 subunits, RT-qPCR was performed using RNA derived from lymphoblastoid cells of four affected and four unaffected individuals. Similar levels of RNA expression of the AP-2 subunit genes, *AP2A1* encoding AP2α*, AP2B1* encoding AP2β2, *AP2M1* encoding AP2μ2*,* and *AP2S1*, were identified in the affected and unaffected cells (Figure 4.8). Western blot analysis also showed similar levels of protein expression in affected and unaffected cells (Figure 4.9). These results suggest that the AP2σ2 R15C mutation does not affect the stability of the AP-2 complex *in vivo*.

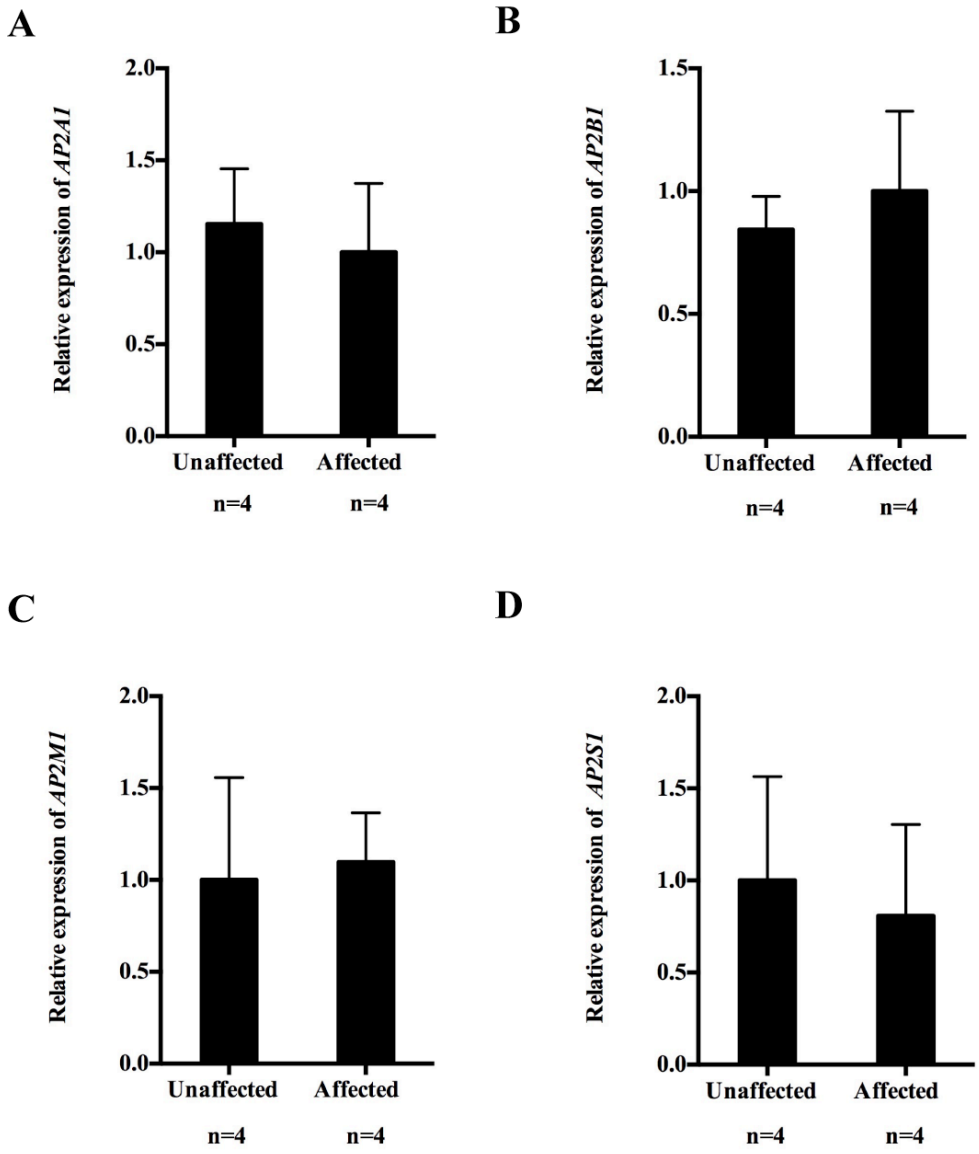


Figure 4.8. Quantitative RT-PCR analysis of the AP-2 subunit genes, *AP2A1, AP2B1, AP2M1* and *AP2S1,* in the lymphoblastic DNA of four affected and four unaffected members of the FHHok kindred to investigate RNA expression.

The target gene Ct value was expressed relative to the geometric mean Ct value of three housekeeper genes (*GAPDH, PGK1* and *TBP1*), and normalized to the mean target gene-to-housekeeper gene from the four unaffected members. (**A**) *AP2A1* (**B**) *AP2B1* (**C**) *AP2M1* (**D**) *AP2S1*. (**A-D**) The mean normalised target gene-to-housekeeper gene values obtained from a triplicate analysis of each affected and unaffected sample are shown expressed relative to unaffected. SEM is shown by the error bar. Results for affected and unaffected individuals were compared using a two-tailed unpaired Student's *t*-test. A value of $p<0.05$ was considered to be statistically significant. No significant difference was identified between affected and unaffected individuals for any of the AP-2 subunit genes analysed.

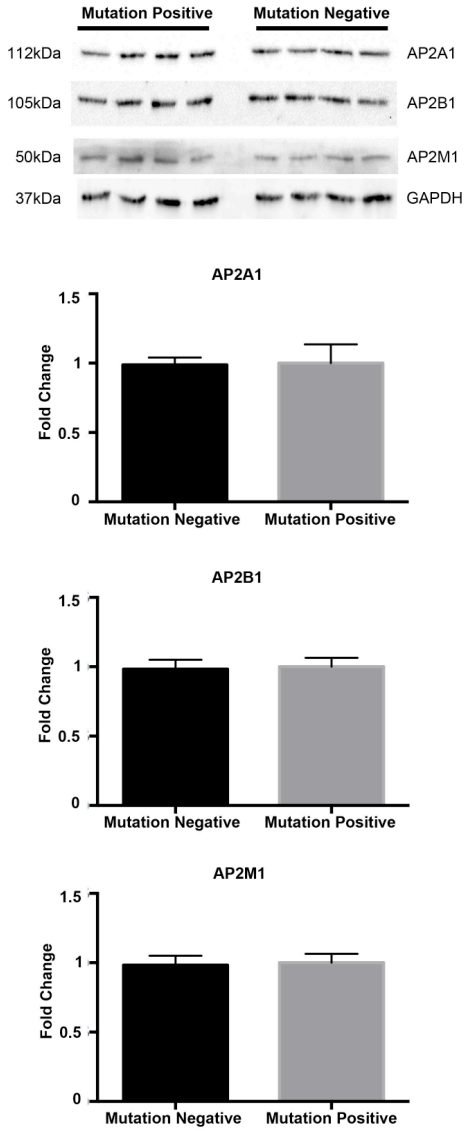


Figure 4.9. Western blot analysis showing expression of the AP-2 subunits in the lymphoblastoid cells from affected and unaffected members of the FHHok kindred.

Expression of the α, β2, and μ2 subunits of AP-2 in lymphoblastoid cells from unaffected (confirmed mutation negative) and affected (confirmed AP2σ2 R15C mutation positive) (n=4 each genotype) are shown. GAPDH is used as a loading control for the amount of cellular protein content. Figure used with permission of Dr Caroline M. Gorvin.

4.1.8 Discussion and future studies

My findings have shown that AP2σ2 mutations account for >20% of FHH in probands without CaSR mutations and thus, account for ~7% of all FHH, assuming CaSR mutations account for ~65% of all cases of FHH[111 212] (Figure 4.10). AP2σ2 mutations may account for a slightly greater proportion of FHH as over the course of my DPhil studies, 37 cases of FHH3 were reported in the literature.[130 279 280 282 290] Conversely, only two cases of FHH due to Gα11 mutations have been reported to date[197], thus suggesting that sequence analysis of genes associated with disorders of calcium homeostasis should proceed in the following order from first to last in clinical genetics laboratories: CaSR; AP2σ2; and Gα11.

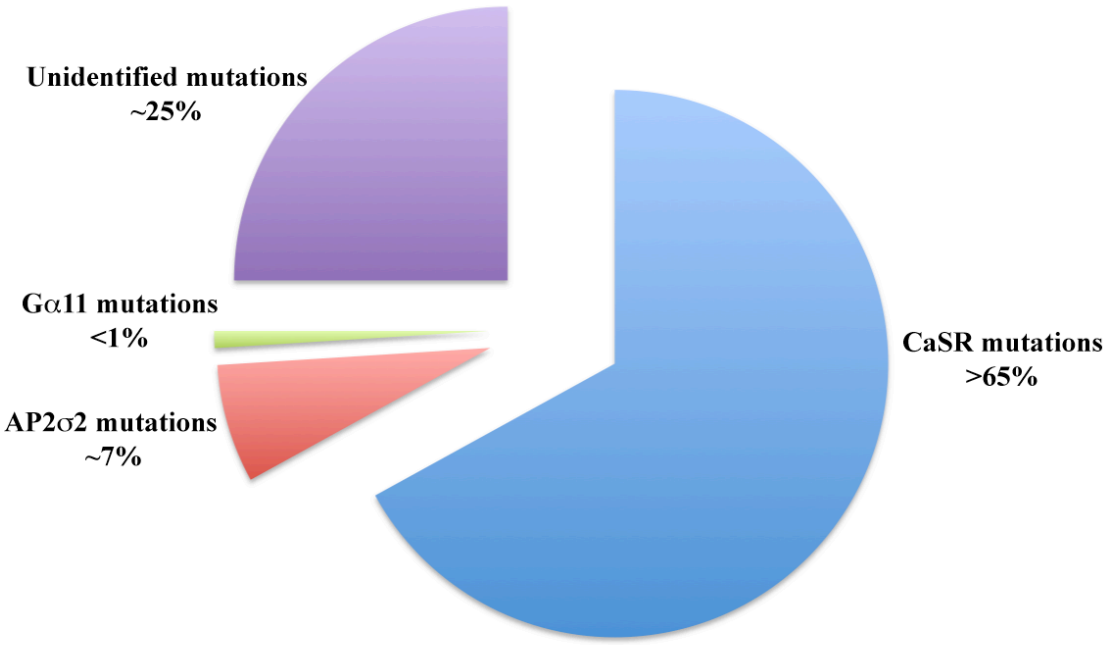


Figure 4.10. The genetic causes of FHH.

This pie chart illustrates the genetic heterogeneity of FHH. Since FHH was first described in the 1970s, ~75% of the genetic causes have subsequently been identified and functional characterisation of the mutations performed. However, in ~25% of cases of FHH the genetic cause remains unknown.

To identify the genetic causes in the remaining ~25% of FHH probands, unrelated individuals and families with FHH without CaSR, AP2σ2, and Gα11 mutations require further mutational analysis. As the families are not large enough for gene localisation using linkage analysis, a candidate gene approach is unfeasible given the large number of potential pathway components. Thus whole exome or whole genome sequencing studies are likely the most feasible options to identify the currently unknown genetic causes.

In comparison to CaSR, where disease-causing mutations are found throughout the protein (section 1.10.1.1.1 and Figure 1.15), FHH3-causing mutations are only associated with the R15 residue. This observation may be explained by co-crystallisation experiments using the 200kDa AP-2 core and a dileucine peptide, from a known clathrin-mediated endocytic cargo receptor CD4, which showed the 2 Leu residues from the cargo protein binding in two adjacent hydrophobic pockets of AP2σ2.[129] Residues within these hydrophobic pockets are highly conserved in AP2σ2 orthologs and APσ paralogs.[130] Mutation of these hydrophobic residues to hydrophilic ones (Leu65Ser, Val88Asp, Val98Ser, and Leu103Ser) inhibited binding.[129] Additionally, mutation of both Arg15 in AP2σ2 and Arg21 in AP2α resulted in reduced binding.[129] Thus, point mutations occurring elsewhere within AP2σ2 that do not disrupt the interaction between the dileucine motif in cargo proteins, such as CaSR, and the hydrophobic pockets are unlikely to give rise to a disease-causing phenotype. Two non-synonymous AP2σ2 SNPs, rs76488045 (Tyr59Ser) and rs11550738 (Cys68Ser), are reported by dbSNP and both are predicted to have damaging effects on AP2σ2 by Polyphen-2.[286] It is unknown if these changes affect binding of dileucine motif-containing cargo proteins. In addition, no phenotyping data

is available on the individuals in which these variants were identified, thus they may have disorders of calcium homeostasis. Functional characterisation of such variants with flow cytometry assays using Indo-1-AM to detect intracellular Ca^{2+} release in response to increasing concentrations of extracellular Ca^{2+} could be performed to identify which residues are important in calcium homeostasis.

The FHH3-associated AP2σ2 mutations identified to date[130 279 280] are all missense substitutions of the R15 residue, comprising R15C, R15H and R15L. Functional characterisation of the remaining possible AP2σ2 R15 variants, R15G, R15P and R15S, (Figure 4.1) demonstrated them to result in loss-of-function, reducing the release of extracellular Ca^{2+}-mediated intracellular Ca^{2+} release.[282] Additionally, cells expressing R15G, R15P and R15S did not replicate as rapidly as cells expressing R15C, R15H and R15L AP2σ2 mutants, which led to the hypothesis the variants are not detected in patients due to possible embryonic lethality.[282] However, embryonic lethality cannot be extrapolated from *in vitro* data and requires the generation of an *in vivo* model expressing one of the AP2σ2 R15 variants to investigate this hypothesis further.

This work has demonstrated that FHH3 occurs in association with *de novo* AP2σ2 mutations, consistent with a recently published case,[279] thereby indicating that probands may not have a family history of the disorder. FHH1 due to *de novo* CaSR mutations have been reported.[204 291] Probands with FHH3 are more likely to be symptomatic than those with FHH1. FHH1 is typically regarded as asymptomatic but rarely those affected may suffer with hypercalcaemic symptoms.[193] My studies

revealed that ~29% of FHH3 probands presented with hypercalcaemic symptoms. This finding may be associated with the higher serum calcium levels found in FHH3.

I have demonstrated AP2σ2 mutations to be associated with short stature and reduced BMD. When the FHH_{ok} kindred was first extensively characterised an iliac crest biopsy from a 51 year old affected female showed defective skeletal mineralisation and several affected adults had radiological findings consistent with osteomalacia.[284] Probands with NSHPT due to loss-of-function CaSR mutations have severe skeletal demineralisation present at birth.[186 204 292] However, no differences in skeletal development, as measured by DXA, have been identified in patients with FHH1 compared to age- and sex-matched controls.[293-296] Conversely, a kindred with a germline novel gain-of-function Gα11 (Arg60Leu) mutation displayed short stature and reduced BMD in conjunction with activation of the ERK1/2 signalling pathway.[297] These findings suggest that downstream signalling resulting in abnormalities of bone remodelling may contribute to the skeletal phenotype seen in FHH3 and warrants further investigation. To explore this hypothesis, an AP2σ2 R15L mouse model could be generated and the skeletal mineralisation of the mice examined, in conjunction with analysis of gene expression of regulators of osteoblast differentiation.[180] Use of primary bone cell lines expressing the AP2σ2 R15L mutant for *in vitro* signalling studies is discussed further in section 5.1.4.

One FHH3 proband experienced recurrent episodes of pancreatitis. Heterozygous CaSR mutations have been identified in probands with chronic pancreatitis and known *SPINK1* mutations.[298] The FHH3 proband did not harbour a *SPINK1* mutation

suggesting that the AP2σ2 mutation in isolation may be sufficient to produce the pathology. Recurrent pancreatitis has been reported in 3 probands with FHH1 but sequence analysis of CaSR only was performed.[187] Thus it cannot be concluded if the CaSR mutations identified alone contributed to the pathology and these probands are likely to harbour *SPINK1* mutations. The recurrent pancreatitis could be a manifestation of severe hypercalcaemia (serum adjusted calcium at presentation: 3.20 mmol/L; normal range: 2.10-2.60 mmol/L) but to study the role of AP2σ2 in the pancreas, a conditional knock-in mouse model expressing AP2σ2 R15L under a pancreas-specific promotor could be generated. Mice could be studied for the development of pancreatitis and histopathological analysis of the pancreas performed. Additionally, studies using primary pancreatic cell lines expressing AP2σ2 R15L examining the effects of extracellular Ca^{2+} on CaSR-coupled signalling pathways could be performed (sections 5.1.4 and 6.1.7).

Probands harbouring AP2σ2 mutations may additionally present with cognitive dysfunction, which has not been reported in association with CaSR mutations. Two of seven probands, both of whom harboured AP2σ2 R15L mutations were diagnosed with learning disabilities. The CaSR plays an important role during the development of the central nervous system, where it is thought to be involved in myelination and is highly expressed throughout rodent brains.[182] However, as this phenotype has not be seen in association with CaSR mutations, it can be postulated that the AP2σ2 mutations may be exerting an effect beyond those related to the downstream signalling pathways of the CaSR within the CNS during development. To explore this hypothesis, an AP2σ2 R15L mouse model could be generated and the developing

brains of embryos and young mice examined using immunohistochemistry. Older mice could be subjected to behavioural tasks to test learning and memory such as the Morris water maze and the novel object recognition test.[299] Primary neuronal cell lines could be established for *in vitro* experiments to examine the effect of the AP2σ2 mutations on the downstream signalling pathways (sections 5.1.4 and 6.1.7).

The AP-2 complex was demonstrated to be stable in lymphoblastoid cells derived from members of the FHH_{ok} kindred harbouring AP2σ2 R15C mutations. The mutant σ2 subunit had no effect on the expression of the other subunits of the AP-2 complex. This finding is consistent with that observed in fibroblasts derived from a proband with learning disabilities and autism, harbouring a nonsense mutation in the σ1 subunit of adaptor protein-1 (AP-1).[300] Western blot analysis showed similar levels of expression of the AP-1 complex subunits compared to control.[300] These findings suggests that point mutations do not affect the stability of adaptor proteins *in vivo* and hence downregulation of the other adaptor protein subunits does not occur, as it does in *in vivo* models of adaptor protein subunit knock-outs[250 251] and in *in vitro* cell systems using siRNA to knock down adaptor protein subunits.[255 289 301]

It is intriguing that a mutation in a ubiquitously expressed protein involved in such a fundamental cellular process as clathrin-mediated endocytosis, has such a limited phenotype in man. It has previously been hypothesised that the R15 residue of AP2σ2 is important in binding to cargo proteins, based on structural studies of CD4 receptor internalisation.[129] In these studies it was demonstrated that combined mutation of the R15 residue of AP2σ and the R21 residue of AP2α resulted in reduced binding of the

AP2 complex to cargo dileucine motifs. This indicates that R15 is important in protein interactions with cargo, although the contribution made by this residue alone is unclear as data was only presented on double AP2σ-R15 and AP2α-R21 mutations. Furthermore, the loss of interaction was not as great as that observed with other residues that bind to dileucine motifs. The CaSR harbours a putative non-canonical dileucine motif within its C-terminus (section 1.7). It has previously been hypothesised that mutations in the AP2σ-R15 residue reduce binding of the AP2 complex to dileucine motifs in select transmembrane receptors, of which CaSR is one. Further studies are required to determine if this is the case. Such studies could involve mutation of the dileucine motif and assessment of its effect on receptor trafficking using multiwavelength total internal reflection fluorescence (TIRF) microscopy, and direct assessment of the binding capability of AP2 to the CaSR C-terminus using surface plasmon resonance.

The Gα11 M87V variant was found to have no effect on intracellular calcium release and hence CaSR signal transduction compared to wild type. This demonstrates that the M87V variant is unlikely to represent a pathogenic mutation contributing to the FHH phenotype in the proband and is likely to be a novel SNP. Whilst residue M87 is highly conserved across vertebrate Gα11 subunit orthologues and Gα paralogues, the substitution of methionine for valine is unlikely to have an effect on the tertiary structure of AP2σ2 as both have hydrophobic side chains. Twelve non-synonymous SNPs are reported in *GNA11* on the NHLBI-ESP and dbSNP compared with two non-synonymous SNPs reported in the coding region of *AP2S1* (Table 6), none of which were identified in the probands. No phenotypic data is available in association with the genotype data provided on the databases and thus, some of the non-synonymous

SNPs which occur at very low or unknown frequencies due to low numbers of carriers and predicted by Polyphen-2[286] to be damaging, may represent mutations, particularly in the setting of FHH where affected individuals can be asymptomatic.

Five previously reported *GNA11* single nucleotide polymorphisms (SNPs) were detected in the hypercalcaemic probands. Associations between the identified SNPs and hypercalcaemia cannot be inferred from the data due to the insufficient sample size. However, *CASR* SNPs have been associated with serum calcium levels in genome wide association studies (GWAS).[302] The CaSR variant rs17251221 (MAF 14%) was shown to be associated with elevated levels of serum calcium and magnesium, and lower serum phosphate, similar to FHH.[302]

Table 6. ***GNA11*** **and** ***AP2S1*** **single nucleotide polymorphisms (SNPs) reported on the National Centre for Biotechnology Information (NCBI) database of short genetic variants (dbSNP) or identified by the Exome Sequencing Project of the National Heart, Lung, and Blood Institute (NHLBI-ESP).**

	rs ID	Exon	cDNA change	Protein change	MAF (%)	Polyphen-2 prediction
GNA11						
	rs141078172	1	c.23C>T	A8V	0.0077	Benign
	rs377224539	2	c.151G>A	G51R	0.0077	Probably damaging
	rs147528228	2	c.193G>A	A65T	0.7381	Benign
	rs140301317	2	c.217C>T	R73C	0.0077	Probably damaging
	rs374089777	2	c.256G>A	A86T	0.0077	Probably damaging
	rs371712160	3	c.643C>A	T134N	-	Benign
	rs191421665	4	c.750T>A	L170M	-	Benign
	rs144829732	6	c.1047G>A	V269I	-	Benign
	rs139538868	7	c.1146A>T	A302T	-	Possibly damaging
	rs386352309	7	c.1185G>A	D315N	<0.01	Benign
	rs201368515	7	c.1212A>G	I324V	<0.01	Benign
	rs376124717	7	c.1297A>G	N352S	-	Benign
AP2S1						
	rs76488045	3	c.405A>C	Y59S	-	Probably damaging
	rs11550738	3	c.432G>C	C68S	-	Probably damaging

Variants are numbered in relation to the *GNA11* and *AP2S1* cDNA reference sequence (GenBank accession numbers NM_002067.3 and NM_004069.4, respectively), whereby nucleotide +1 corresponds to A of the ATG-translation initiation codon. Databases accessed on 1 July 2015.

5 The effects of AP2σ2 mutations on the mitogen-activated protein kinase (MAPK) signalling pathways

Functional work studying the effect of AP2σ2 mutations on downstream signalling pathways has focussed on the $G\alpha_{q/11}$-mediated signal transduction pathway to date.[130] AP2σ2 mutations have been demonstrated to result in a loss-of-function, reducing the release of extracellular Ca^{2+}-mediated intracellular Ca^{2+} release.[130] Thus the AP2σ2 mutations were associated with a rightward shift in the dose-response curve compared to WT, such that the EC_{50} value of AP2σ2 R15C expressing cells was greater than that of AP2σ2 R15L expressing cells, which in turn was greater than that of AP2σ2 R15H expressing cells.[130] To further characterise the functional effects of AP2σ2 mutations on the CaSR, the MAPK pathway was selected for investigation. The MAPK pathway has been shown to be impaired in cells with CaSR and Gα11 mutations,[110 297 303] as it is a convergence pathway for multiple G-protein signal transduction pathways (Figure 1.13). Thus, as AP-2 is involved in clathrin-mediated endocytosis (CME) of CaSR,[304] it was postulated that cells expressing AP2σ2 mutations may demonstrate aberrant MAPK signalling. Additionally, loss- and gain-of function CaSR mutations have been shown to induce signalling bias at the CaSR[110] and thus it was postulated the AP2σ2 mutations may induce such bias.

Characterisation of the functional effects of AP2σ2 mutations on phosphorylated ERK1/2 (pERK1/2) using an amplified luminescence proximity homogenous (AlphaScreen) assay

5.1.1 Characterisation of the functional effects of AP2σ2 mutations on phosphorylated ERK1/2 (pERK1/2) using an amplified luminescence proximity homogenous (AlphaScreen) assay

To investigate the effects of the AP2σ2 mutations on the MAPK signalling pathway, phosphorylated ERK1/2 (pERK1/2) was measured using an amplified luminescence proximity homogenous (AlphaScreen) assay (section 3.2.5.3). Previously qualitative assessment of the MAPK signalling pathway in HEK293-CaSR cells was achieved using Western blot analysis of pERK1/2.[85] The pERK1/2 AlphaScreen assay provided quantitative results enabling generation of dose-response curves.

5.1.1.1 Optimisation of AlphaScreen assay conditions

The pERK1/2 AlphaScreen assay has been optimised for high-throughput screening in 384-well plates for various cell types. Prior to embarking on these studies the optimal conditions for assessment of pERK1/2 responses in the cell type I was using needed to be identified. Therefore, in order to determine the optimal assay conditions, preliminary experiments were performed in HEK293 cells transiently transfected with CaSR to identify: time interval between transfection and calcium treatment; duration of extracellular calcium treatment required to induce maximal pERK1/2 response; and effect of extracellular calcium concentration on pERK1/2 response.

To identify the optimal time interval between transfection and calcium treatment, HEK293 cells were transiently transfected with CaSR either 24 or 48 hours prior to calcium treatment and pERK1/2 responses were measured by AlphaScreen assay.

While pERK1/2 responses were elevated in CaSR-transfected cells compared with untransfected control at both time points, pERK1/2 responses were significantly higher in cells treated 48 hours post-transfection (fold increase relative to control: 24 hours, 2.4; 48 hours, 6.2; $p<0.01$) (Figure 5.1A). Expression of CaSR in all transfected cells was confirmed by Western blot analysis (Figure 5.1B). Therefore, subsequent studies used CaSR transfection 48 hours before AlphaScreen assays were performed.

To identify the optimal time point at which to assess pERK1/2 responses, HEK293 cells transiently transfected with CaSR were treated with 5mM calcium chloride for 0 – 30mins and pERK1/2 responses measured by AlphaScreen assay. The pERK1/2 responses were significantly higher in cells treated with 5mM calcium compared to cells treated with 0mM calcium after 5 minutes (fold increase relative to baseline: 0mM, 0.17; 5mM, 6.7; $p<0.0001$) and after 30 minutes (fold increase relative to baseline: 0mM, 0.19; 5mM, 2.3; $p<0.0001$) (Figure 5.2A). Expression of CaSR in all transfected cells was confirmed by Western blot analysis (Figure 5.2B). The early and late peaks in pERK activity suggest that CaSR, like many other GPCRs (Section 1.8.1 and Figure 1.21), may activate ERK1/2 through two different pathways. PTH activates ERK1/2 through the PTH1R via a G-protein-dependent pathway, which occurs early resulting in a peak pERK response at 5 minutes and a non-canonical, β-arrestin-dependent pathway, which occurs late with a peak pERK response after 30 to 60 minutes.[305] Thus, to study the activation of the ERK1/2 pathway by the G-protein-dependent pathway, a time interval of 5 minutes was adopted for subsequent AlphaScreen studies.

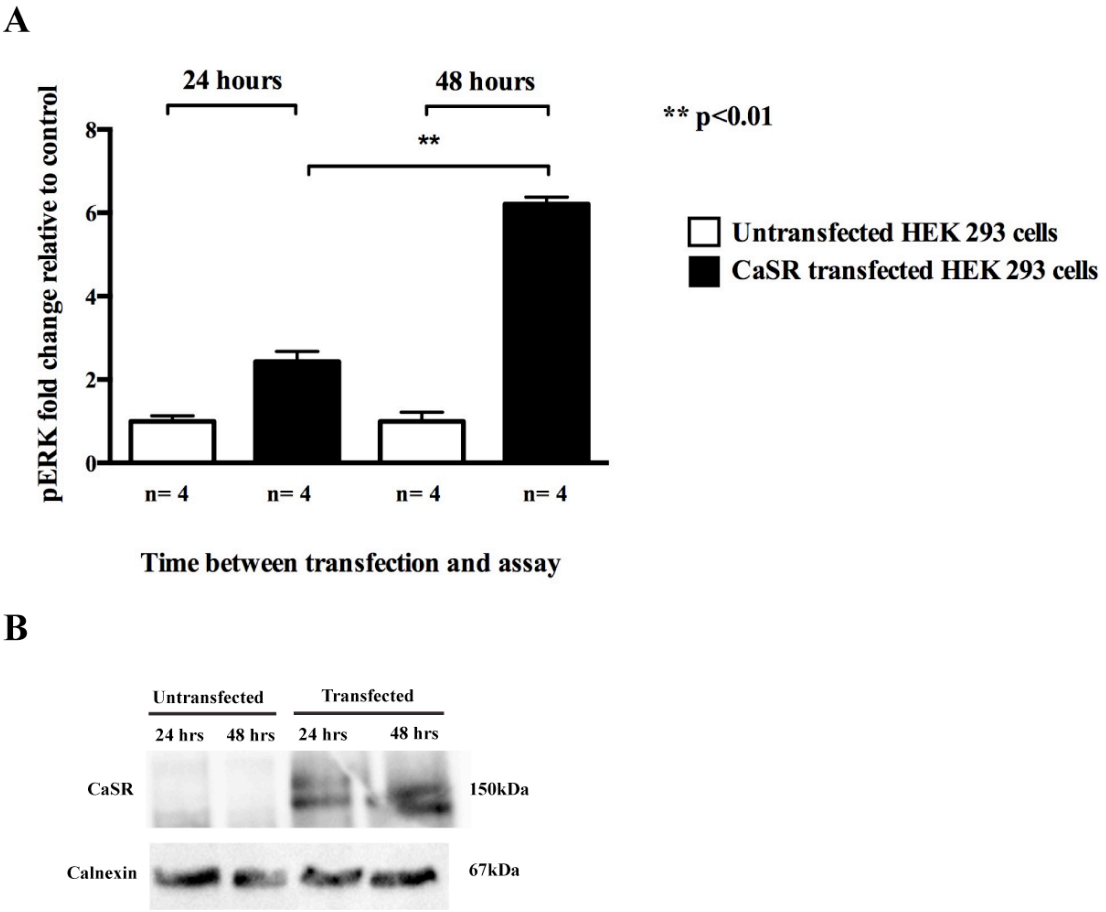


Figure 5.1. Preliminary experiment to determine the effect of time interval between transfection and calcium treatment on pERK1/2 response assessed by AlphaScreen assay.

HEK293 cells were transfected with CaSR either 24 or 48 hours prior to treatment with 5mM calcium for 5 minutes. Untransfected HEK293 cells were used as control. (**A**) Mean change in pERK response assessed by AlphaScreen assay. N= 4 biological replicates for each data set. Error bars indicate SEM. There was a significant increase in pERK1/2 response when HEK293 cells were transfected with CaSR 48 hours prior to calcium treatment compared with those transfected at 24 hours (fold increase relative to control: 24 hours, 2.4; 48 hours, 6.2; $p<0.01$). Two-way ANOVA used with Tukey's multiple comparison test to calculate statistical significance. (**B**) Representative Western blot analysis showing absence and detection of CaSR in untransfected and transfected cells, respectively and calnexin, used as a loading control for the amount of cellular protein content.

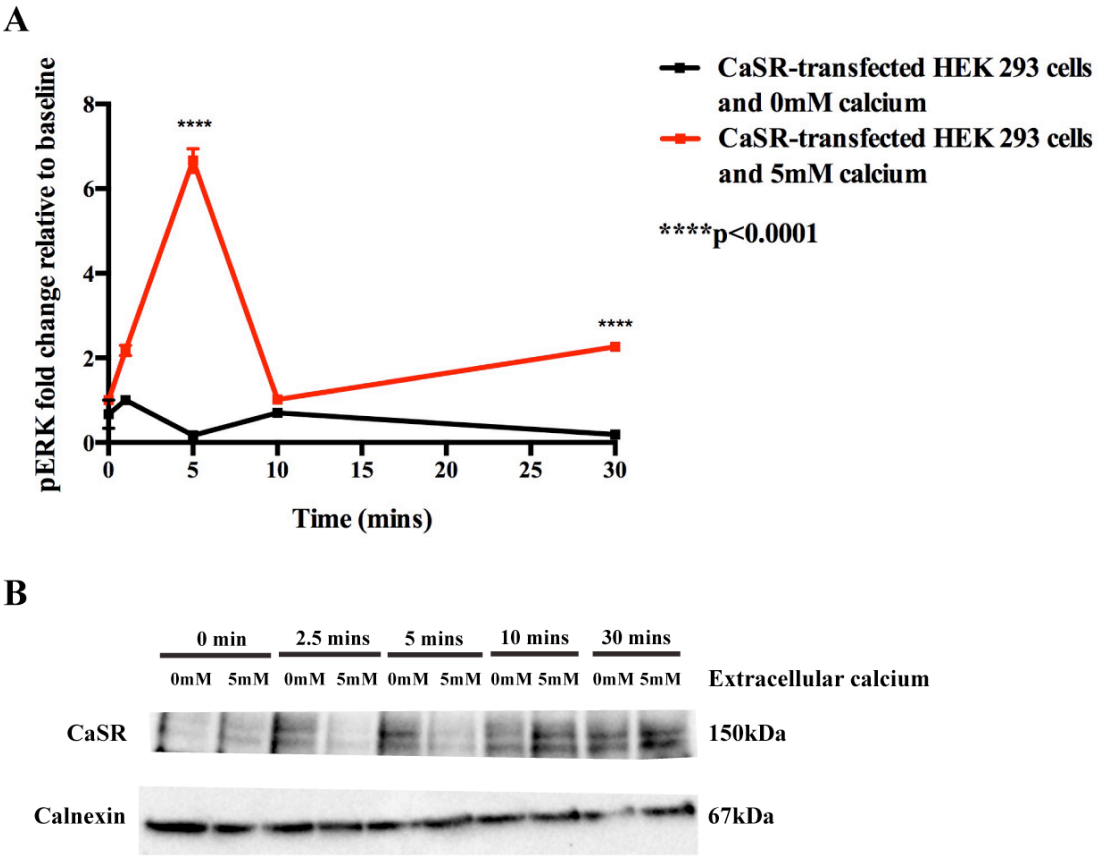


Figure 5.2. Preliminary experiment to determine the duration of extracellular calcium treatment required to induce maximal pERK1/2 response assessed by AlphaScreen assay.

HEK293 cells transiently transfected with CaSR were treated with 0 or 5mM calcium for 0-30 mins. (**A**) Mean pERK1/2 responses assessed by Alphascreen assay following treatment with 0 or 5mM calcium for 0-30 minutes. There was a significant increase in the pERK1/2 response after 5 mins treatment with 5mM calcium compared to those exposed to 0mM (fold increase relative to baseline: 0mM, 0.17; 5mM, 6.7; $p<0.0001$) and in cells treated for 30 mins with 5mM calcium (fold increase relative to baseline: 0mM, 0.19; 5mM, 2.3; $p<0.0001$). N= 4 biological replicates for each data set. Error bars indicate SEM. Two-way ANOVA used with Tukey's multiple comparison test to calculate statistical significance. (**B**) Representative Western blot analysis showing detection of CaSR in cells and calnexin, used as a loading control for the amount of cellular protein content.

To confirm that elevations in extracellular calcium concentration increased pERK1/2 responses in a dose-dependent manner, HEK293 cells transiently transfected with CaSR were treated with 0-10mM extracellular calcium for 5 minutes prior to cell lysis and pERK1/2 responses measured by AlphaScreen assay. Cells transfected with CaSR showed a concentration-dependent increase in pERK1/2 response following treatment with 0-10mM calcium, with pERK1/2 responses in transfected cells significantly elevated compared to untransfected cells between 5-10mM (fold increase relative to control, CaSR vs untransfected: 5mM, 1.14 vs 6.32, $p<0.05$; 7.5mM, 1.20 vs 6.90, $p<0.05$; 10mM, 1.21 vs 8.83; $p<0.01$) (Figure 5.3A). Expression of CaSR in all transfected cells was confirmed by Western blot analysis (Figure 5.3B).

The findings from these preliminary experiments were used to develop a protocol for subsequent studies (section 5.1.1.2). Briefly, cells were transfected 48 hours prior to treatment with 0-10mM calcium for 5 mins, cells lysed and AlphaScreen assay performed (section 3.2.5.3).

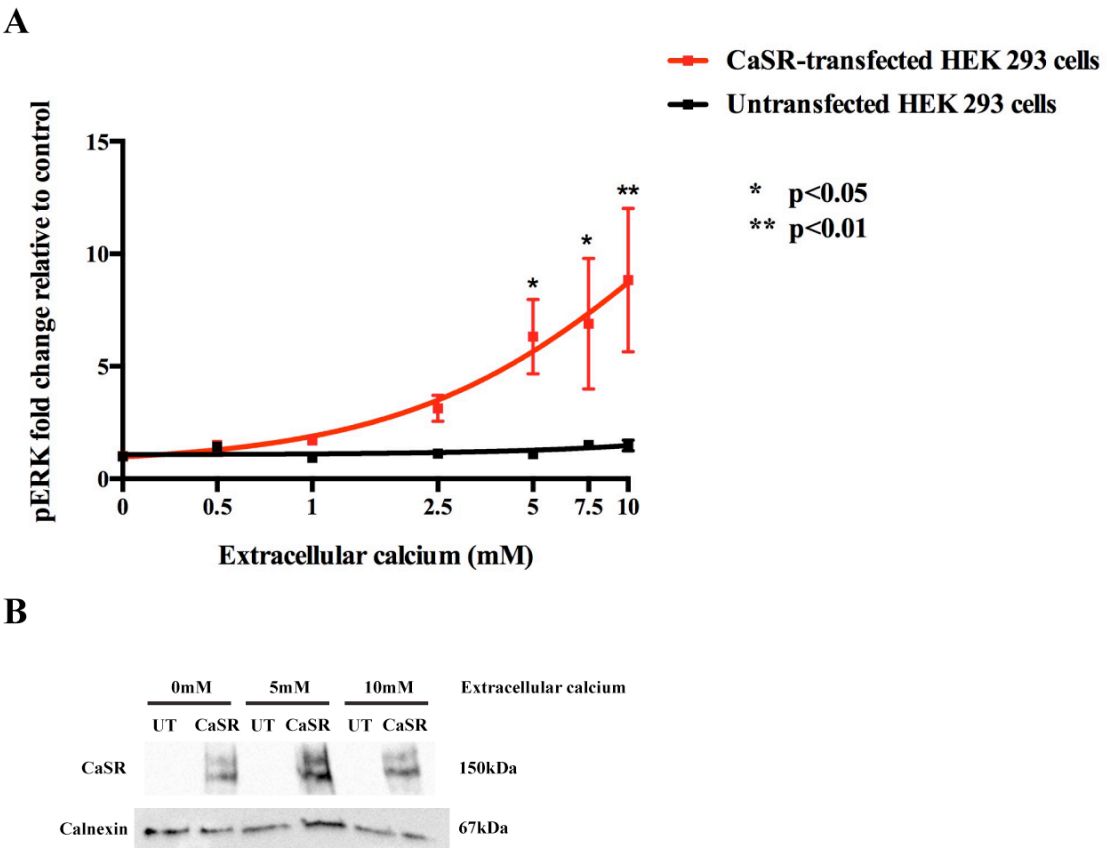


Figure 5.3. Preliminary experiment to determine the effect of extracellular calcium concentration on pERK1/2 response assessed by AlphaScreen assay.

HEK293 cells transfected with CaSR were treated with 0-10mM calcium for 5 minutes. Untransfected HEK293 cells were used as control. (**A**) Dose-response curve demonstrating pERK1/2 responses assessed by AlphaScreen assay in response to treatment with 0-10mM calcium. Transfected cells showed a concentration-dependent increase in pERK1/2 in response to treatment with increasing concentrations of calcium between 5-10mM compared to untransfected cells. N=4 biological replicates and error bars indicate SEM. (**B**) Representative Western blot analysis showing absence and detection of CaSR in untransfected and transfected cells, respectively and calnexin, used as a loading control for the amount of cellular protein content.

5.1.1.2 Effects of AP2σ2 mutations on pERK1/2 responses

To investigate the effects of the AP2σ2 mutations on the pERK1/2 signalling pathway, HEK293 cells stably expressing AP2σ2 WT or mutant constructs (R15C, R15H and R15L) (section 3.2.5) were used for AlphaScreen assays to reduce the variability in expression associated with transient transfection of the gene of interest. The AP2σ2 stable cells did not express CaSR and thus were transfected 48 hours prior to calcium stimulation. Following on from my preliminary studies, pERK1/2

responses were assessed following 5 minutes stimulation with extracellular calcium doses between 0-10mM. Activation of the MAPK pathway was measured using the pERK1/2 AlphaScreen assay (section 3.2.5.3.1). To assess how pERK1/2 responses occurred in AP2σ2 WT and mutant cells, data was analysed in the following ways: comparison to its own response at 0mM calcium (baseline); comparison to WT response at 0mM calcium; and comparison to vector-only control at 0mM calcium. This allowed for detection of differences between groups and identification of constitutive activity.

5.1.1.2.1 Effects of AP2σ2 R15C cells on pERK1/2 responses

As the concentration of extracellular calcium increased from 0-10mM, mean pERK1/2 responses in AP2σ2 WT cells rose significantly compared to their own baseline whereas AP2σ2 R15C cells failed to respond to increasing doses of extracellular calcium (mean pERK1/2 fold change relative to baseline: WT, 0mM=1.0, 10mM=52.6, $p<0.0001$, n=4; R15C, 1mM=1.0, 10mM=5.8, p=ns, n=4; Figure 5.4A). This can be partly explained by examination of the data compared to WT, in which basal levels of AP2σ2 R15C activity are elevated compared to WT but these are not significantly different (mean pERK1/2 fold change relative to WT at 0mM: WT, 1.0; R15C, 5.1; p=ns; n=4; Figure 5.4B). Thus, when R15C responses are expressed relative to WT only pERK1/2 responses at 7.5 and 10mM extracellular calcium are significantly different. Levels of pERK1/2 increase with exposure to extracellular calcium in a concentration-dependent manner in AP2σ2 WT and R15C cells relative to WT (Figure 5.4B). However, pERK1/2 responses were significantly reduced in AP2σ2 R15C cells at 7.5-10mM compared to WT (mean pERK1/2 fold

change: 7.5mM, WT = 20.0, R15C=7.9, $p<0.01$, n=4; 10mM, WT= 52.6, R15C=29.7, $p<0.0001$, n=4; Figure 5.4B), consistent with a loss-of-function phenotype. Cells transfected with vector only failed to demonstrate a dose-dependent increase in pERK1/2 (mean pERK1/2 fold change: 0mM, 1.0; 10mM, 1.4; p=ns; n=4; Figure 5.4C). When compared to control cells, both WT and R15C cells produced significantly increased pERK1/2 responses in a dose-dependent manner, although responses >5mM extracellular calcium were reduced in R15C cells compared to WT. Thus, responses in R15C expressing cells are consistent with a loss-of-function. Expression of CaSR in all transfected cells was confirmed by Western blot analysis (Figure 5.4D).

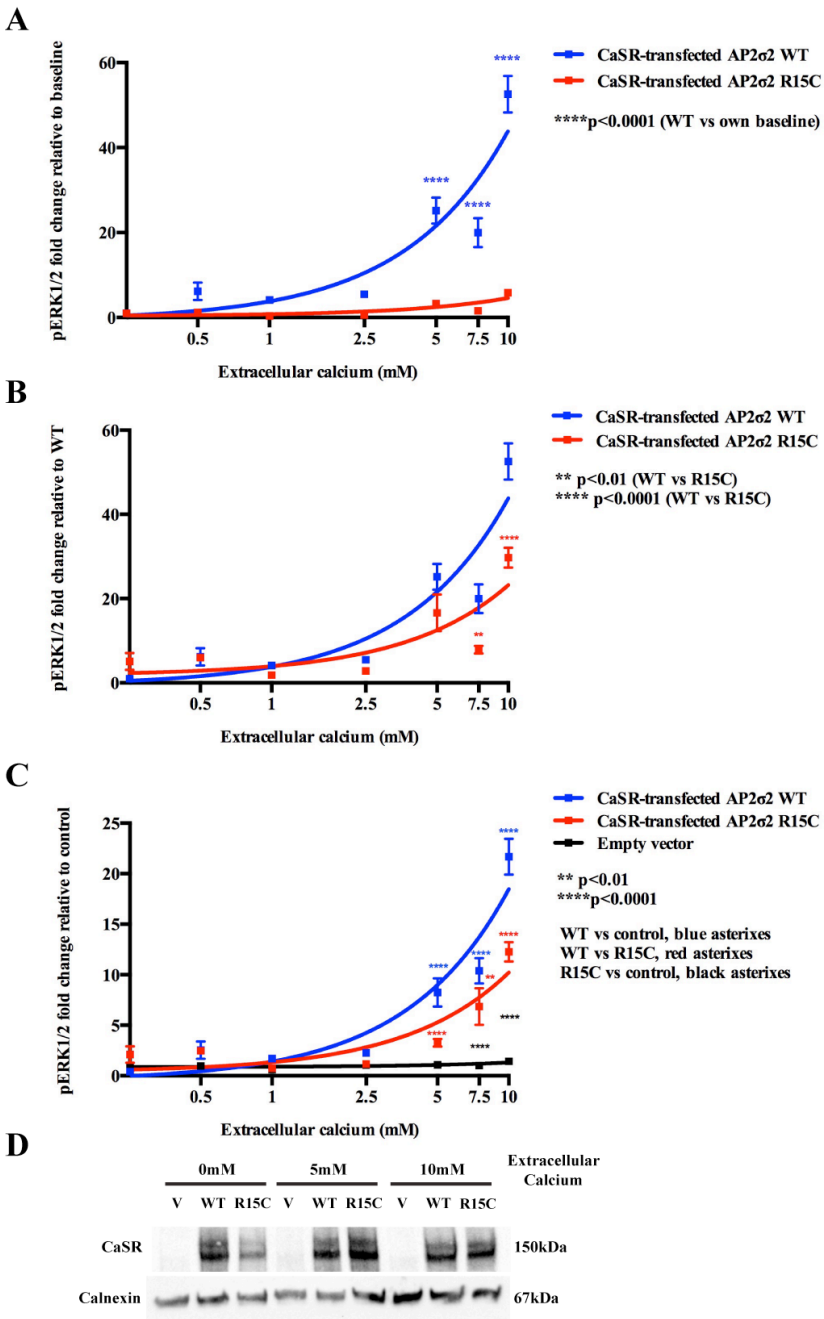


Figure 5.4. The effect of extracellular calcium concentration on pERK1/2 response in AP2σ2 WT and R15C cells assessed by AlphaScreen assay.

HEK293 cells expressing AP2σ2 WT or R15C were transfected with CaSR 48 hours prior to treatment with 0-10mM calcium for 5 mins. AP2σ2 WT cells transiently transfected with pcDNA3.1 were used as control. (**A-C**) Dose-response curves demonstrating pERK1/2 responses assessed by AlphaScreen assay following treatment with calcium 0-10mM. (**A**) AP2σ2 R15C cells fail to respond as the extracellular calcium concentration increased from 0-10mM unlike WT cells when compared to their errtebaseline activity (mean pERK1/2 fold change relative to baseline: WT, 0mM=1.0, 10mM=52.6, p<0.0001, n=4; R15C, 1mM=1.0, 10mM=5.8, p=ns, n=4). (**B**) AP2σ2 WT and R15C cells showed a concentration-dependent increase in pERK1/2 response between 0-10mM calcium when their activity was compared to that of WT at baseline. This response was significantly reduced in R15C cells at 7.5-10mM calcium compared to wild type (mean pERK1/2 fold change: 7.5mM, WT = 20.0, R15C=7.9, p<0.01, n=4; 10mM, WT= 52.6, R15C=29.7, p<0.0001, n=4). (**C**) Cells transfected with vector only failed to demonstrate a pERK1/2 response as the concentration of extracellular calcium increased from 0-10mM. (**D**) Representative Western blot analysis showing presence of CaSR in transfected cells and calnexin, used as a loading control for the amount of cellular protein content. N=4 and error bars indicate SEM.

5.1.1.2.2 Effect of AP2σ2 R15H mutation on pERK1/2 responses

AP2σ2 R15H cells failed to respond to increasing doses of extracellular calcium as the concentration increased from 0-10mM whilst mean pERK1/2 responses of AP2σ2 WT cells were seen to rise significantly from baseline (mean pERK1/2 fold change relative to baseline: WT, 0mM=1.0, 10mM=10.0, $p<0.05$, n=4; R15H, 1mM=1.0, 10mM=2.9, p=ns, n=4; Figure 5.5A). The basal activity of AP2σ2 R15H was reduced compared to WT but this difference was not significant (mean pERK1/2 fold change at 0mM relative to WT: WT=1.0; R15H=0.4; n=4; p=ns; Figure 5.5B). Levels of pERK1/2 increased with exposure to extracellular calcium in a concentration-dependent manner in AP2σ2 WT whereas pERK1/2 responses were significantly reduced in AP2σ2 R15H cells from 0.5-10mM calcium compared to WT (mean pERK1/2 fold change: 0.5mM, WT=3.8, R15H=0.5, $p<0.01$; 2.5mM, WT=7.2, R15H=0.8, $p<0.0001$; 10mM, WT=10.0, R15H=1.2, $p<0.0001$; n=4; Figure 5.5B), consistent with a loss-of-function phenotype. Cells transfected with vector only failed to demonstrate a pERK1/2 response as the concentration of extracellular calcium increased from 0-10mM (mean pERK1/2 fold change: 0mM=1.0; 10mM=1.7; p=ns; n=4; Figure 5.5C). Thus, responses in R15C expressing cells are consistent with a loss-of-function. Expression of CaSR in all transfected cells was confirmed by Western blot analysis (Figure 5.5D).

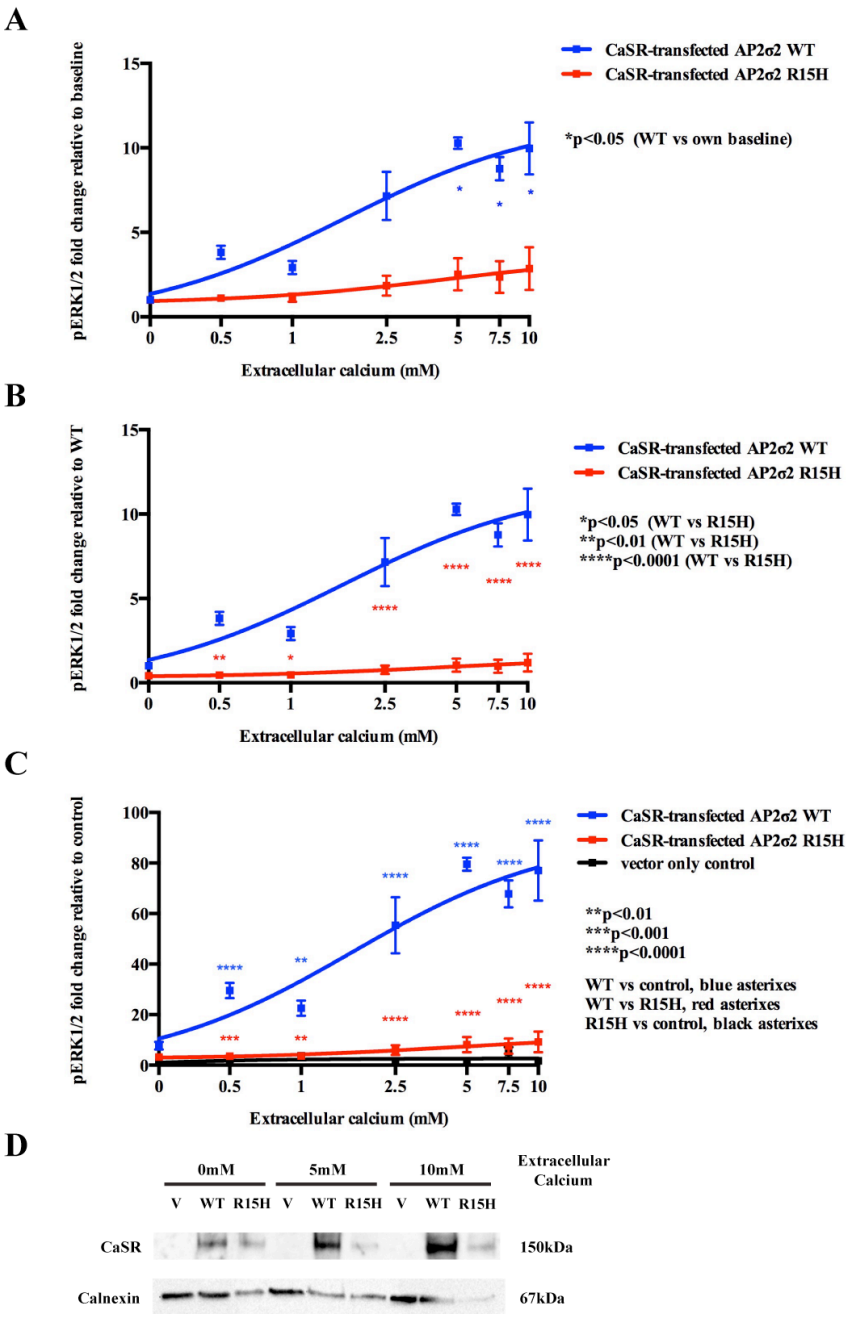


Figure 5.5. The effect of extracellular calcium concentration on pERK1/2 response in AP2σ2 WT and R15H cells assessed by AlphaScreen assay.

HEK293 cells expressing AP2σ2 WT or R15H were transfected with CaSR 48 hours prior to treatment with 0-10mM calcium for 5 mins. AP2σ2 WT cells transiently transfected with pcDNA3.1 were used as control. (**A-C**) Dose-response curves demonstrating pERK1/2 responses assessed by AlphaScreen assay following treatment with calcium 0-10mM. (**A**) AP2σ2 R15H cells fail to respond as the extracellular calcium concentration increased from 0-10mM unlike WT cells when compared to their baseline activity (mean pERK1/2 fold change relative to baseline: WT, 0mM=1.0, 10mM=10.0, $p<0.05$, n=4; R15H, 1mM=1.0, 10mM=2.9, p=ns, n=4). (**B**) AP2σ2 WT cells showed a concentration-dependent increase in pERK1/2 response between 0-10mM calcium. This response was significantly reduced in R15C cells between 0.5-10mM calcium compared to WT (mean pERK1/2 fold change: 0.5mM, WT=3.8, R15H=0.5, $p<0.01$; 2.5mM, WT=7.2, R15H=0.8, $p<0.0001$; 10mM, WT=10.0, R15H=1.2, $p<0.0001$; n=4). (**C**) Cells transfected with vector only failed to demonstrate a pERK1/2 response as the concentration of extracellular calcium increased from 0-10mM. (**D**) Representative Western blot analysis showing presence of CaSR in transfected cells and calnexin, used as a loading control for the amount of cellular protein content. N=4 and error bars indicate SEM.

5.1.1.2.3 Effect of AP2σ2 R15L mutation on pERK1/2 responses

Mean pERK1/2 responses of AP2σ2 R15L cells failed to increase significantly from baseline compared with AP2σ2 WT cells, which were seen to rise significantly from baseline as the extracellular calcium concentration increased from 0-10mM (mean pERK1/2 fold change relative to baseline: WT, 0mM=1.0, 10mM=10.7, $p<0.0001$, n=4; R15L, 1mM=1.0, 10mM=4.6, p=ns, n=4; Figure 5.6A). When assessed against WT cells, R15L cells demonstrated no difference in basal activity (mean pERK1/2 fold change at 0mM relative to WT: WT=1.0; R15L= 1.6; n=4; p=ns; Figure 5.6B). Levels of pERK1/2 increased with exposure to extracellular calcium in a concentration-dependent manner in AP2σ2 WT and R15L cells relative to WT (Figure 5.6B). However, pERK1/2 responses were significantly reduced in AP2σ2 R15L cells at 10mM compared to WT (mean pERK1/2 fold change at 10mM: WT=10.7, R15L=7.5; $p<0.05$; n=4; Figure 5.6B), consistent with a loss-of-function phenotype. Cells transfected with vector only failed to demonstrate a pERK1/2 response as the concentration of extracellular calcium increased from 0-10mM (mean pERK1/2 fold change: 0mM=1.0; 10mM=1.5; p=ns; n=4; Figure 5.6C). When compared to control cells, WT and R15L cells had increased pERK1/2 responses in a dose-dependent manner but R15L responses were reduced at 10mM consistent with a loss-of-function phenotype. Expression of CaSR in all transfected cells was confirmed by Western blot analysis (Figure 5.6D).

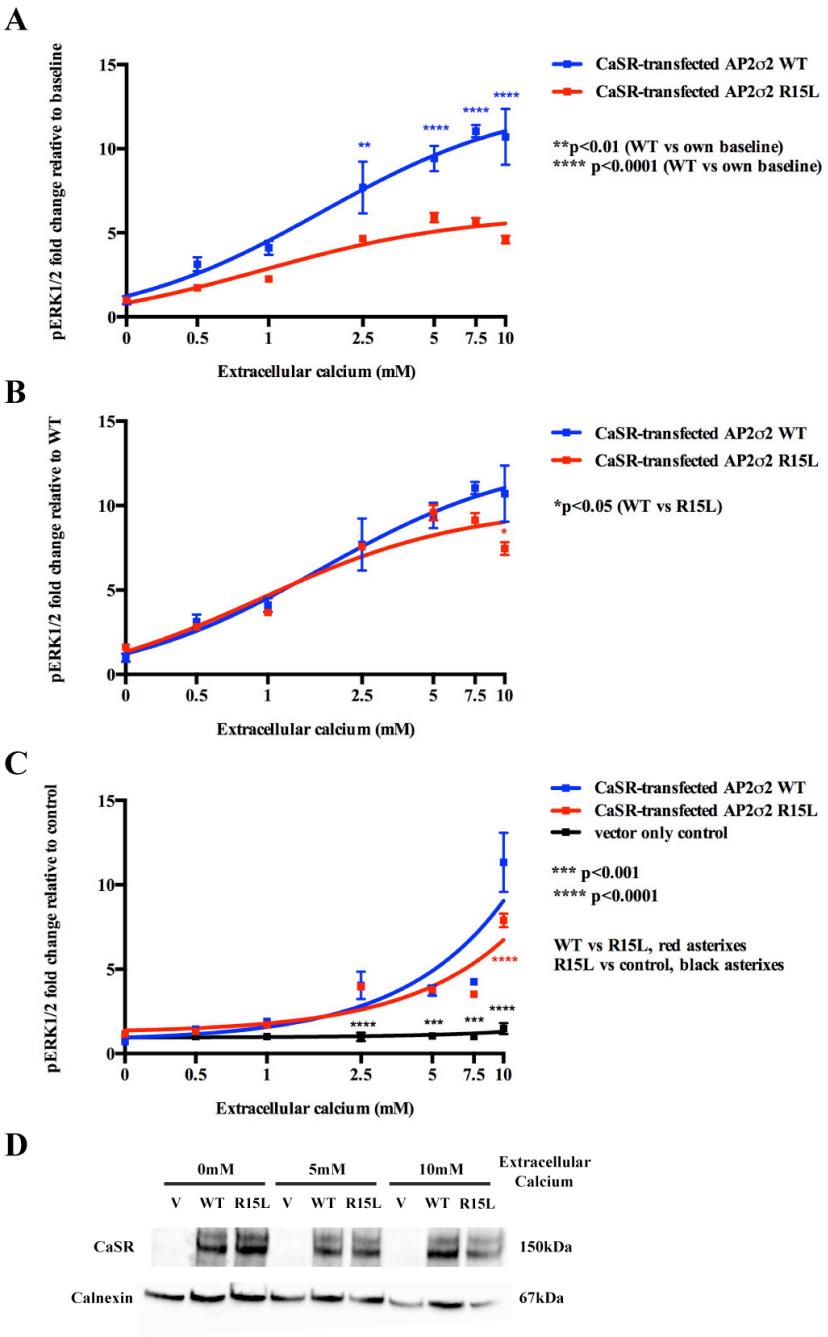


Figure 5.6. The effect of extracellular calcium concentration on pERK1/2 response in AP2σ2 WT and R15L cells assessed by AlphaScreen assay.

HEK293 cells expressing AP2σ2 WT or R15L were transfected with CaSR 48 hours prior to treatment with 0-10mM calcium for 5 mins. AP2σ2 WT cells transiently transfected with pcDNA3.1 were used as control. (**A-C**) Dose-response curves demonstrating pERK1/2 responses assessed by Alphascreen assay following treatment with 0-10mM calcium. (**A**) AP2σ2 R15L responses failed to increase significantly from baseline as the extracellular calcium concentration increased from 0-10mM unlike WT cells when compared to their baseline activity (mean pERK1/2 fold change relative to baseline: WT, 0mM=1.0, 10mM=10.7, $p<0.0001$, n=4; R15L, 1mM=1.0, 10mM=4.6, p=ns, n=4.) (**B**) AP2σ2 WT and R15L cells showed a concentration-dependent increase in pERK1/2 in response to treatment with increasing concentrations of calcium between 0-10mM. However, pERK1/2 responses were significantly reduced in R15L cells at 10mM compared to WT (mean pERK1/2 fold change at 10mM: WT=10.7, R15L=7.5; $p<0.05$, n=4), consistent with a loss-of-function. (**C**) Cells transfected with vector only failed to demonstrate a pERK1/2 response as the concentration of extracellular calcium increased from 0-10mM. (**D**) Representative Western blot analysis showing presence of CaSR in transfected cells and calnexin used as a loading control for the amount of cellular protein content. N=4 and error bars indicate SEM.

5.1.1.2.4 Normalisation of AlphaScreen assay results for cellular protein content

Western blot analysis confirmed the expression of CaSR in all transfected cells used in the AlphaScreen assays comparing AP2σ2 WT and mutant cells (Figure 5.4D, Figure 5.5D and Figure 5.6D). However, on visual comparison of the blots there is a difference in the protein content between the samples of cell lysate used. This may have been due to human loading error or differential protein transfer. Thus, to normalise the pERK1/2 responses for the amount of cellular protein in the AP2σ2 WT and mutant AlphaScreen lysates, total ERK1/2 was measured in the cell lysates using a total ERK1/2 AlphaScreen assay (section 3.2.5.3.2).

AP2σ2 R15C, R15H and R15L cells showed a significant reduction in pERK1/2-to-total ERK1/2 response in comparison to AP2σ2 WT cells treated with 5mM calcium (mean normalised pERK1/2 fold change: AP2σ2 WT=7.0, R15C=2.4, R15H=1.0; R15L=1.4; WT vs R15C, $p<0.001$; WT vs R15H, $p<0.0001$; WT vs R15L, $p<0.001$; n=4, Figure 5.7). These findings confirm that AP2σ2 R15C, R15H and R15L mutants cause loss of phosphorylation events in the MAPK pathway compared with WT, and are therefore predicted to result in the downregulation of MAPK-mediated gene transcription.

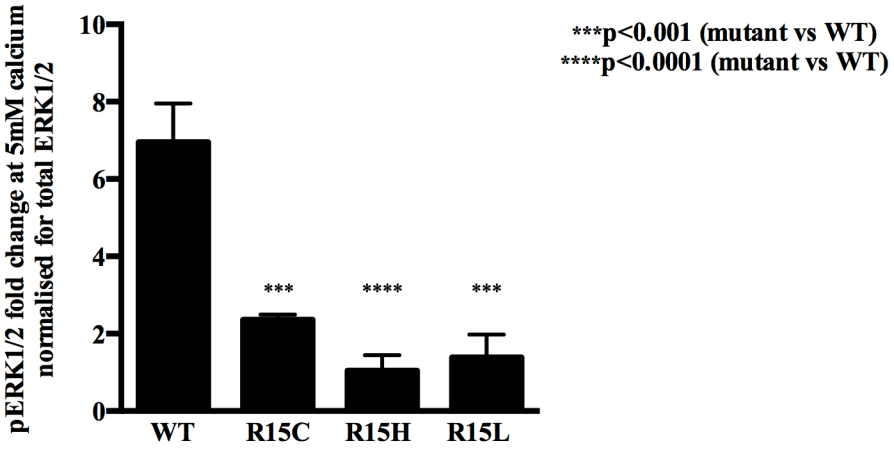


Figure 5.7. Normalisation of pERK1/2 responses for total ERK1/2 assessed by AlphaScreen assay.

Mean fold change in pERK1/2 responses of AP2σ2 WT and mutant cells at 5mM extracellular calcium normalised to total ERK1/2 assessed by AlphaScreen assay. Lysates of AP2σ2 R15C, R15H and R15L cells showed a significant reduction in normalised pERK1/2 response in comparison to AP2σ2 WT cells treated with 5mM calcium (mean normalised pERK1/2 fold change: AP2σ2 WT=7.0, R15C=2.4, R15H=1.0; R15L=1.4; WT vs R15C, $p<0.001$; WT vs R15H, $p<0.0001$; WT vs R15L, $p<0.001$). N=4 biological replicates for each data set. Error bars indicate SEM.

5.1.2 Characterisation of the functional effects of AP2σ2 mutations on target gene transcription

A complex cascade of Gα-mediated downstream signalling events mediates CaSR-regulated gene transcription (Figure 1.13). As AP2σ2 mutations result in loss of activating phosphorylation events in the ERK1/2 pathway compared to WT, it was hypothesised that this may result in reduced ERK1/2-mediated gene transcription with consequent disturbances in CaSR-regulated events. The effects of AP2σ2 mutations on gene transcription downstream of $G\alpha_{q/11}$ signalling were investigated using an NFAT dual-luciferase reporter assay (Sections 1.5 and 3.2.5.4). Target gene transcription downstream of the ERK1/2 pathway, a point of convergence for multiple

G-protein signalling pathways, was studied using a SRE dual-luciferase reporter assay (Sections 1.5 and 3.2.5.4).

5.1.2.1 Preliminary experiment to determine conditions for the dual-luciferase reporter assays

Dual-luciferase assays (section 3.2.5.4) have been used to study extracellular Ca^{2+}-mediated NFAT and SRE responses in mouse osteoblasts.[306] [307] Additionally, assessment of prolactin-induced activation of gene transcription via the Janus kinase 2(JAK2)-signal tranducer and activator of transcription 5 (STAT5) pathway using dual-luciferase reporter assays has been optimised in the Academic Endocrinology Unit.[276] However, these protocols required optimisation for the present cell system and conditions. In order to determine the assay conditions, a preliminary experiment was performed in HEK293 cells stably expressing AP2σ2 WT to determine the concentration of extracellular calcium required to induce gene transcription.

As a significant difference between AP2σ2 WT and mutant cells had been observed for the normalised pERK1/2 responses at 5mM calcium, this concentration was selected for the preliminary experiment. AP2σ2 WT expressing cells were transiently transfected with CaSR and 48 hours later, stimulated with 0-5mM calcium for 6 hours prior to analysing NFAT and SRE reporter gene activity. Stimulation with 5mM extracellular calcium resulted in increased NFAT and SRE reporter activity in AP2σ2 WT expressing cells (mean fold change in reporter activity: NFAT, 0mM =1.0, 5mM=5.2, $p<0.001$, Figure 5.8A; SRE, 0mM=1.0, 5mM=23.5, $p<0.001$, Figure

5.8B). Thus a concentration of 5mM calcium was used for subsequent dual-luciferase reporter assays.

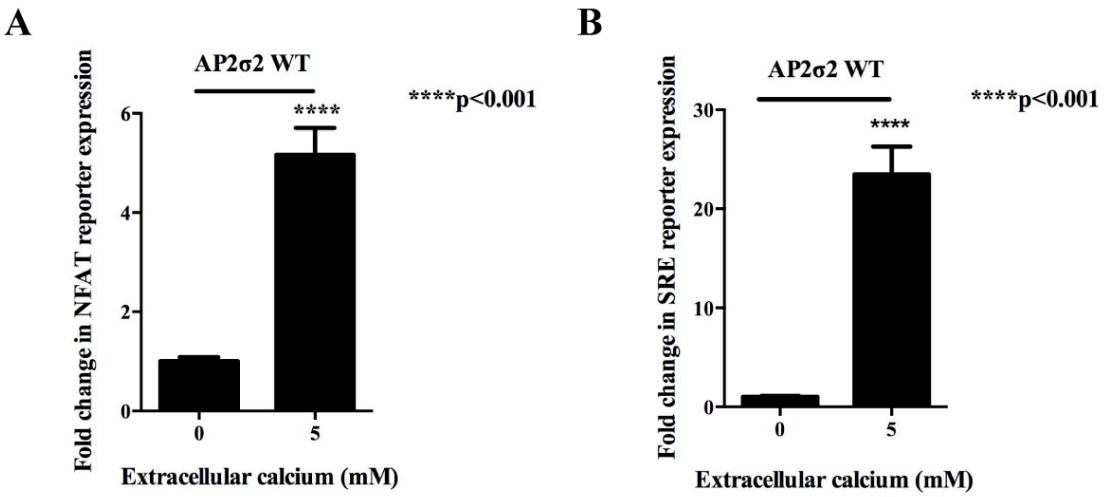


Figure 5.8. The effect of extracellular calcium concentration on NFAT and SRE reporter gene expression in HEK293 cells stably expressing AP2σ2 WT assessed by dual-luciferase reporter gene assay.

HEK293 cells stably expressing AP2σ2 WT were transfected with CaSR 48 hours prior to treatment with 0- 5mM calcium for 6 hours. (**A-C**) Bar charts represent mean fold change in luciferase reporter activity relative to WT, n=4 biological replicates, error bars indicate SEM. (**A**) NFAT reporter activity increased following treatment with 5mM extracellular calcium in AP2σ2 WT cells (mean fold change in reporter activity: NFAT, 0mM =1.0, 5mM=5.2, $p<0.001$). (**C**) Treatment with 5mM extracellular calcium resulted in increased SRE reporter gene activity by in AP2σ2 WT expressing cells (mean fold change: 0mM=1.0, 5mM=23.5, $p<0.001$).

5.1.2.2 Effects of AP2σ2 mutations on target gene transcription

5.1.2.2.1 Effects of AP2σ2 mutations on NFAT reporter activity assessed by dual-luciferase reporter assay

To investigate the effects of AP2σ2 mutations on target gene transcription, AP2σ2 WT or mutant (R15C, R15H or R15L) stable cells transiently transfected with CaSR were stimulated with 5mM calcium for 6 hours prior to analysing NFAT reporter gene activity. Stimulation with 5mM calcium resulted in increased NFAT reporter activity

in AP2σ2 WT and R15C expressing cells compared to 0mM (mean fold change in reporter activity: WT, 0mM=1.0, 5mM=3.0, $p<0.0001$; R15C, 0mM=1.0, 5mM=2.1, $p<0.001$; n=4; Figure 5.9A). However, NFAT reporter gene expression was significantly reduced in cells expressing AP2σ2 R15C compared to those expressing WT (mean fold change in reporter activity at 5mM calcium: WT=3.0, R15C=2.1, $p<0.0001$, n=4, Figure 5.9A). This finding suggests that the AP2σ2 R15C mutation is resulting in a loss-of-function in the $G\alpha_{q/11}$ signalling pathway as previously demonstrated,[130] with subsequent effects on NFAT-regulated gene transcription.

Following treatment with 5mM calcium, NFAT reporter activity failed to increase from baseline in AP2σ2 R15H expressing cells compared with WT (mean fold change in reporter activity at: WT, 0mM=1.0, 5mM=3.8, $p<0.0001$; R15H, 0mM=1.0, 5mM=1.1; p=ns; n=4; Figure 5.9B). A similar response was observed in AP2σ2 R15L cells compared to WT when stimulated with 5mM calcium (mean fold change: WT, 0mM=1.0, 5mM=2.5, $p<0.0001$; R15L, 0mM=1.0, 5mM=1.0; $p<0.0001$; n=4; Figure 5.9B). These findings indicate that the $G\alpha_{q/11}$ signalling pathway may be severely impaired in these cells with consequent downstream effects on NFAT-mediated regulation of gene transcription.

Western blot analysis was performed as all AP2σ2 expressing cells were transiently transfected with CaSR. This showed no significant difference in the amount of CaSR transfected relative to calnexin, used as a loading control for the amount of the total cellular protein content, between AP2σ2 WT and mutant expressing cells (Figure 5.10) used in the dual-luciferase reporter assays.

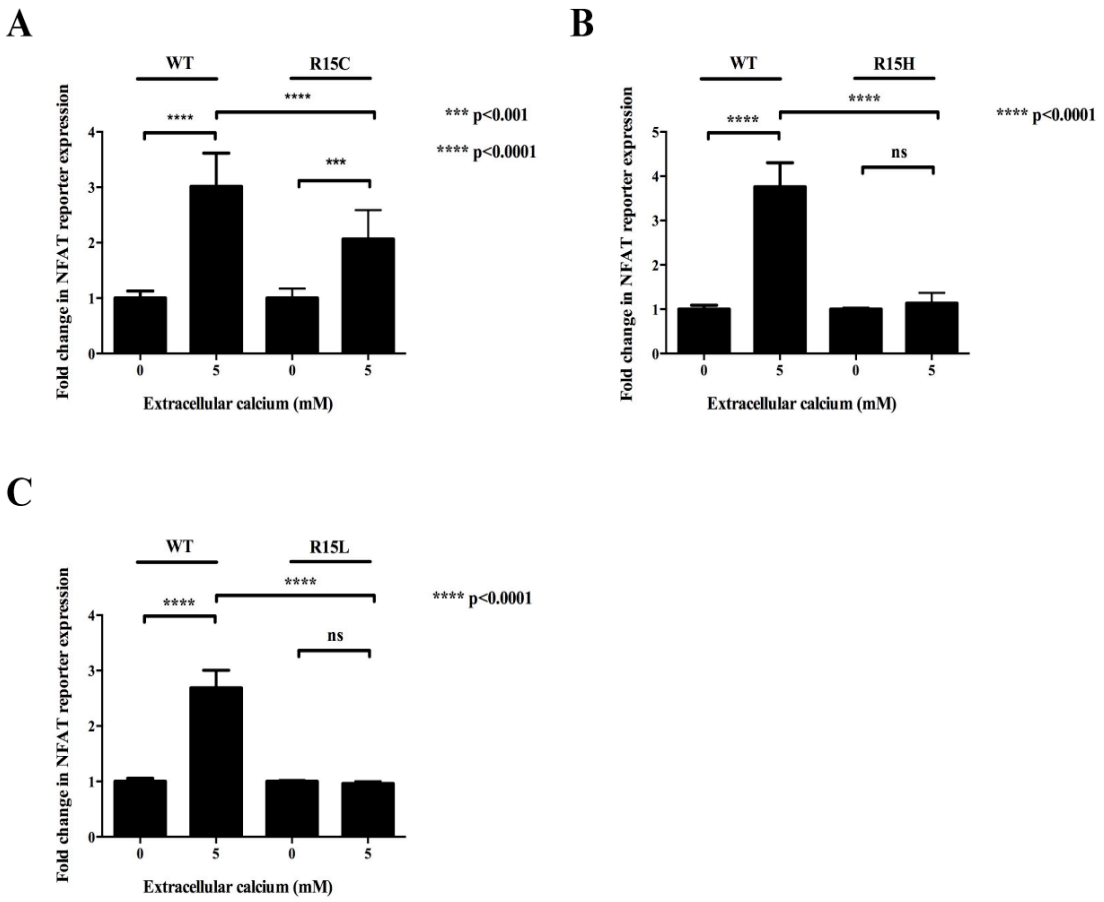


Figure 5.9. The effect of extracellular calcium concentration on NFAT reporter activity in AP2σ2 WT and mutant cells assessed by luciferase reporter gene assay.

HEK293 cells stably transfected with AP2σ2 WT or mutant (R15C, R15H or R15L) were transfected with CaSR 48 hours prior to treatment with 0mM or 5mM calcium for 6 hours. (**A-C**) Bar charts represent mean fold change in luciferase reporter activity relative to WT, n=4 biological replicates, error bars indicate SEM. (**A**) AP2σ2 WT and R15C cells showed an increase in NFAT reporter activity in response to treatment with 5mM extracellular calcium. However, NFAT reporter activity was significantly reduced in AP2σ2 R15C compared to WT (mean fold change at 5mM calcium: WT=3.0, R15C=2.0, $p<0.0001$, n=4). Both AP2σ2 R15H cells (**B**) and AP2σ2 R15L cells (**C**) failed to demonstrate an NFAT reporter gene response following stimulation with 5mM extracellular calcium compared to baseline.

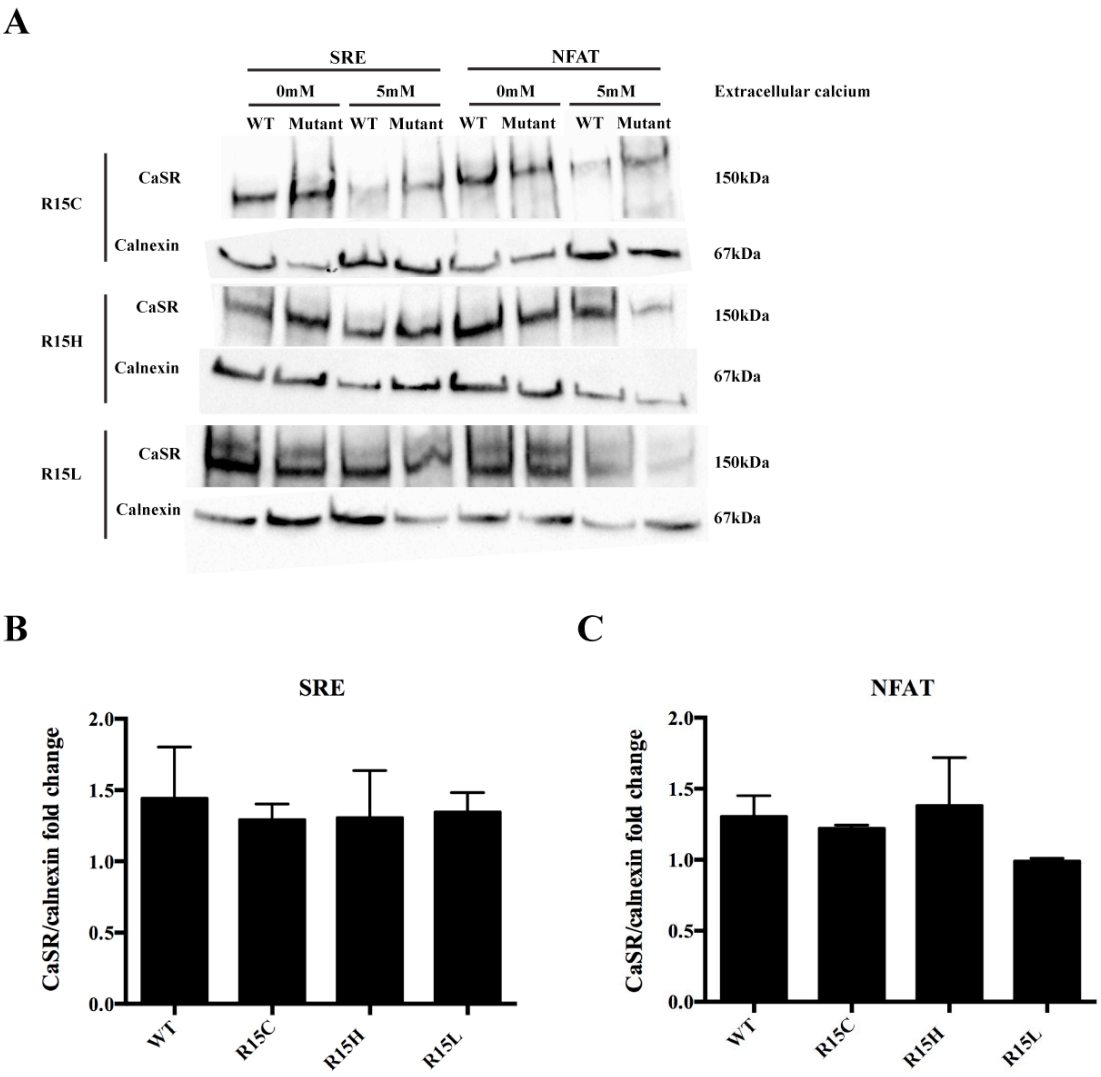


Figure 5.10. Western blot analysis of the expression of CaSR in AP2σ2 WT and AP2σ2 mutant cell lysates used in the luciferase reporter gene assays.

(**A**) Western blot analysis showing detection of CaSR in transfected cells and calnexin, used as a loading control for the amount of total cellular protein content. (**B-C**) Bar charts represent mean fold change in CaSR expression normalised for calnexin, n=4 biological replicates, error bars indicate ± SEM. When CaSR expression data from 4 biological replicates was normalised for calnexin, there was no significant difference in the amount of CaSR expressed by AP2σ2 WT, R15C, R15H and R15L expressing cells used for the (**B**) NFAT luciferase reporter gene assays or (**C**) SRE luciferase reporter gene assays.

5.1.2.2.2 Effects of AP2σ2 mutations on SRE reporter activity assessed by dual-luciferase reporter assay

To investigate the effects of AP2σ2 mutations on target gene transcription, AP2σ2 WT or mutant (R15C, R15H or R15L) stable cells transiently transfected with CaSR were stimulated with 5mM calcium for 6 hours prior to analysing SRE reporter gene activity. Stimulation with 5mM calcium resulted in increased SRE reporter activity in AP2σ2 WT and R15C expressing cells compared to 0mM (mean fold change in reporter activity: WT, 0mM=1.0, 5mM=14.1, $p<0.0001$; R15C, 0mM=1.0, 5mM=6.4, $p<0.001$; n=4; Figure 5.11A). However, SRE reporter activity was significantly reduced in cells expressing AP2σ2 R15C at 5mM calcium compared to WT (mean fold change at 5mM calcium: WT=14.1, R15C=6.4, $p<0.0001$, n=4, Figure 5.11A). These findings suggest that the AP2σ2 R15C mutation is resulting in downregulation in the ERK1/2 signalling cascade, with subsequent effects on SRE-regulated gene transcription.

Stimulation with 5mM extracellular calcium resulted in increased SRE reporter activity in AP2σ2 WT and R15H expressing cells (mean fold change in reporter activity: WT, 0mM=1.0, 5mM=18.3, $p<0.0001$; R15H, 0mM=1.0, 5mM=21.2, $p<0.0001$; n=4; Figure 5.11B). However, there was no significant difference observed in the level of SRE reporter activity between R15H and WT expressing cells at 5mM calcium (mean fold change in reporter activity at 5mM calcium: WT=18.3, R15H=21.2, p=ns, n=4, Figure 5.11B). This is in contrast to responses seen for NFAT indicating that cells with R15H mutations may exhibit mutation bias, favouring an increase in one G-protein pathway compared to others. This observation suggests the

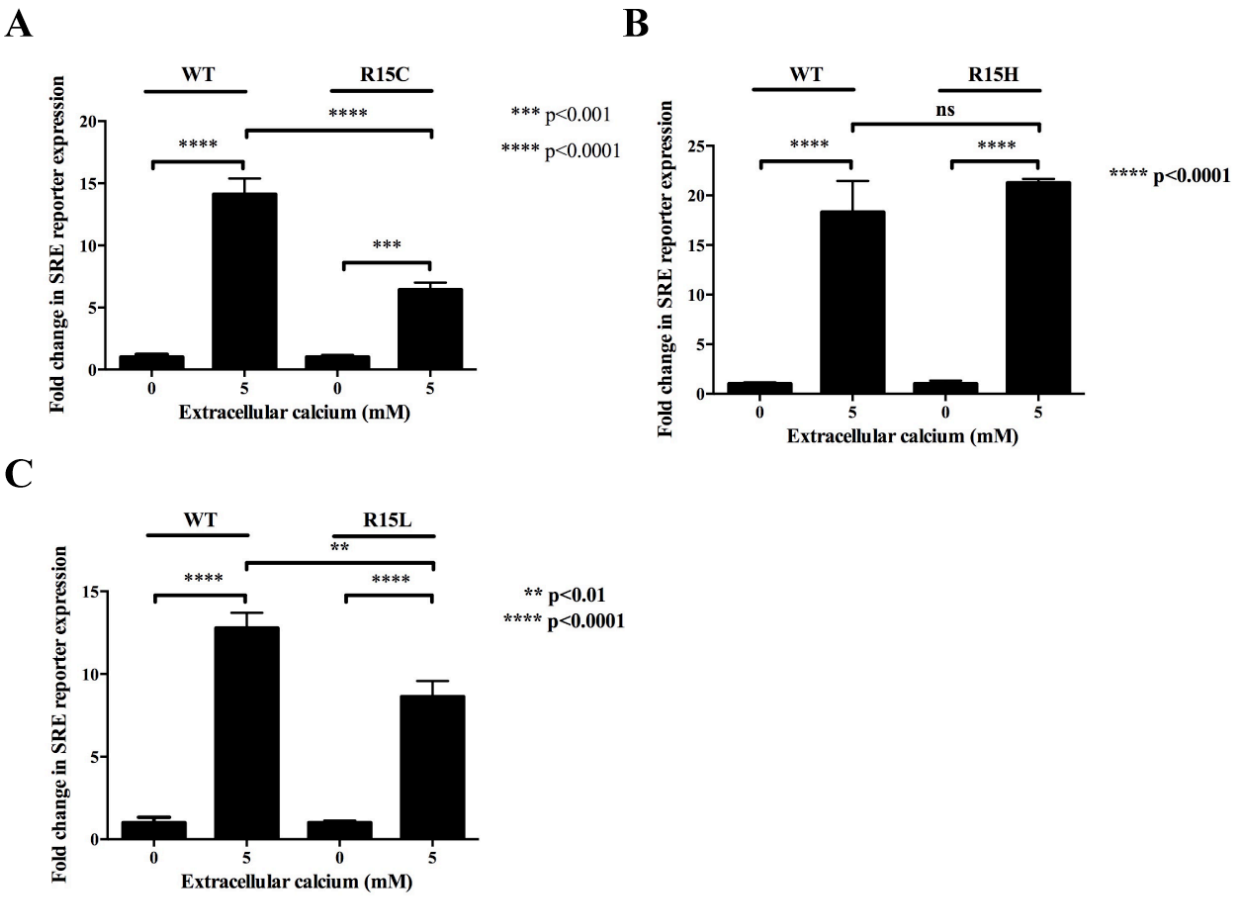


Figure 5.11. The effect of extracellular calcium concentration on SRE reporter activity in AP2σ2 WT and mutant cells assessed by luciferase reporter gene assay.

HEK293 cells stably transfected with AP2σ2 WT, R15C, R15H or R15L were transfected with CaSR 48 hours prior to treatment with 0mM or 5mM calcium for 6 hours. (**A-C**) Bar charts represent mean fold change in luciferase reporter activity relative to WT, n=4 biological replicates, error bars indicate SEM. (**A**) AP2σ2 WT and R15C cells showed an increase in SRE reporter activity in response to treatment with 5mM extracellular calcium. However, SRE reporter gene expression was significantly reduced in AP2σ2 R15C compared to WT (mean fold change at 5mM calcium: WT=14.1, R15C=6.4, $p<0.0001$, n=4). (**B**) SRE reporter activity increased on 5mM extracellular calcium treatment in AP2σ2 R15H and there was no significant difference in the level of SRE reporter gene expression between AP2σ2 WT and AP2σ2 R15H at 5mM extracellular calcium. (**C**) Treatment with 5mM extracellular calcium resulted in increased SRE reporter gene expression in AP2σ2 WT and R15L. However, SRE reporter gene expression was significantly reduced in AP2σ2 R15L compared to WT (mean fold change in SRE activity at 5mM calcium: WT=12.8, R15L=8.6, $p<0.01$, n=4).

AP2σ2 R15H mutation has no effect on the functional output from the ERK1/2 signalling cascade with respect to SRE-regulated gene transcription.

Following stimulation with 5mM calcium, SRE reporter activity was significantly increased in AP2σ2 WT and R15L cells (mean fold change in reporter activity: WT, 0mM=1.0, 5mM=12.8, $p<0.0001$; R15L, 0mM=1.0, 5mM=8.6, $p<0.0001$; n=4; Figure 5.11C). However, SRE reporter activity was significantly reduced in AP2σ2 R15L cells compared to AP2σ2 WT at 5mM calcium (mean fold change in SRE activity at 5mM calcium: WT=12.8, R15L=8.6, $p<0.01$, n=4, Figure 5.11C).

Western blot analysis showed no significant difference in the amount of CaSR transfected relative to calnexin, used as a loading control for the amount of the total cellular protein content, between AP2σ2 WT and mutant expressing cells (Figure 5.10) used in the luciferase reporter assays.

5.1.3 Characterisation of the effect of cinacalcet on the functional effects of AP2σ2 mutations

Positive allosteric modulators such as the type-II calcimimetic, cinacalcet, have been demonstrated to promote signalling bias at the CaSR, with cinacalcet showing bias towards the IP3 pathway relative to ERK1/2 phosphorylation[96] (section 1.5.5). Recently, cinacalcet has been reported to be therapeutically beneficial in a patient with FHH3 harbouring an AP2σ2 R15L mutation[290] (section 1.10.1.1.4). Thus it was postulated that cinacalcet may modulate the effects of the AP2σ2 mutants on transcription of genes downstream of $G\alpha_{q/11}$ and ERK1/2 signalling pathways. The effects on gene transcription were assessed using NFAT and SRE dual-luciferase reporter assays, as described in sections 3.2.5.4 and 3.2.5.4.1.

5.1.3.1 Optimisation of the luciferase reporter assay conditions

Studies using NFAT and SRE reporter assays to assess the effect of cinacalcet on the extracellular Ca^{2+}-mediated response in HEK293 cells have not previously been performed. The EC_{50} of cinacalcet in HEK293 cells is 51nM at 0.5mM calcium[71] and studies performed in HEK293 cells investigating pERK1/2, IP3 and plasma membrane ruffling have used a concentration of 100nM cinacalcet.[96] Luciferase reporter assays assessing newly developed calcimimetics have exposed Chinese hamster ovary (CHO) cells to the active drug for 5 hours at 2mM calcium.[308] Additionally, the Academic Endocrinology Unit, University of Oxford, has successfully used concentrations of 10-30nM cinacalcet to rectify the loss-of-function observed in intracellular Ca^{2+} responses associated with the AP2σ2 mutations *in vitro* (unpublished data). Due to these experimental differences within the literature and to optimise conditions for my specific assay, a preliminary experiment was performed in HEK293 cells transiently transfected with CaSR to determine the concentration and duration of treatment with cinacalcet. Cells were treated with 0-30nM cinacalcet at 5mM calcium for 6 or 24 hours and NFAT reporter activity assessed.

A significant increase in the NFAT reporter activity was observed following treatment of HEK293 cells transiently expressing CaSR with 10-30nM cinacalcet at 5mM calcium for 6 hours (mean fold change: 0nM, 1.0, 10nM=15.5, 20nM=19.1, 30nM=18.9; 0nM vs 10nM, $p<0.0001$; n=4), with a concentration-dependent increase as the concentration of cinacalcet increased from 10 to 20nM ($p<0.0001$, Figure 5.12A). There was a significant increase in the NFAT reporter gene expression following treatment with 10-30nM cinacalcet at 5mM calcium for 24 hours (mean

fold change: 0nM, 1.0, 10nM=6.1, 20nM=3.9, 30nM=3.2; 0nM vs 10nM, $p<0.0001$; n=4), however these increases were significantly less than those seen at 6 hours ($p<0.0001$, Figure 5.12A). Expression of CaSR in the transfected cells was confirmed by Western blot analysis (Figure 5.12B). These findings were used to generate a protocol of cell treatment with 20nM cinacalcet for 6 hours for subsequent experiments.

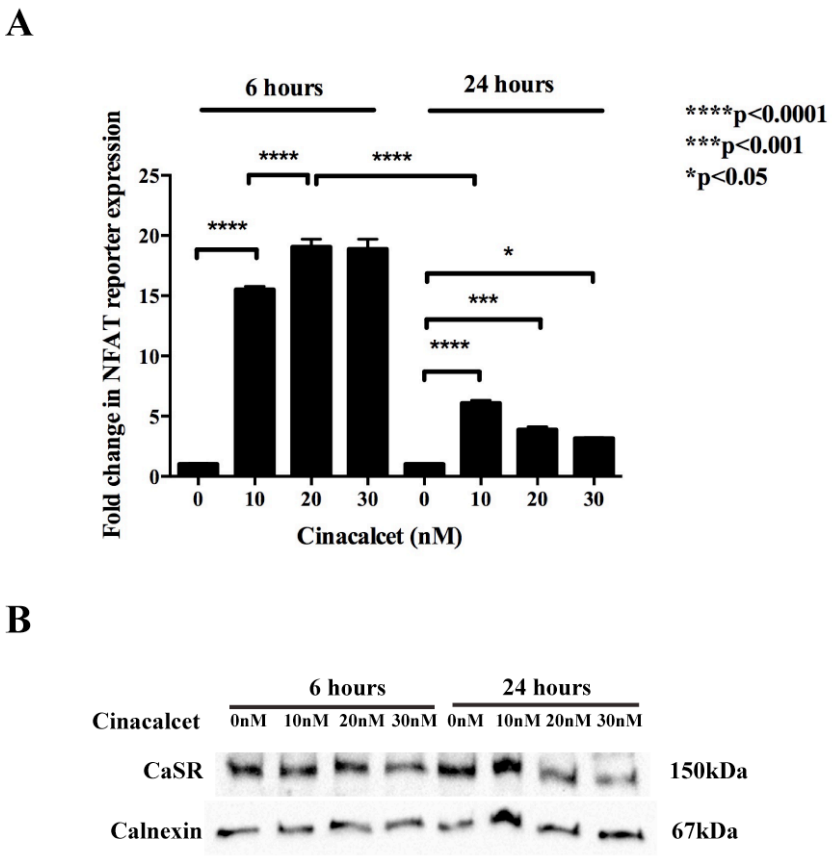


Figure 5.12. Preliminary experiment to determine the effect of cinacalcet concentration and duration of treatment on NFAT reporter gene expression in HEK293 cells transiently transfected with CaSR assessed by dual-luciferase reporter gene assay.

HEK293 cells were transiently transfected with CaSR 48 hours prior to treatment with 0-30nM cinacalcet for either 6 or 24 hours at 5mM calcium. (**A**) Bar chart represents mean fold change in NFAT luciferase reporter gene expression relative to baseline. There was a significant increase in the NFAT reporter gene expression following treatment with 10-30nM cinacalcet at 5mM calcium for 6 hours (mean fold change: 0nM=1.0, 10nM=15.5, 20nM=19.1, 30nM=18.9; 0nM vs 10nM, $p<0.0001$; n=4). NFAT reporter gene expression was significantly reduced in cells treated with cinacalcet for 24 hours compared to 6 hours at all concentrations ($p<0.0001$, n=4 for each data set). Error bars indicate SEM. (**B**) Representative Western blot analysis showing expression of CaSR in transfected cells and calnexin, used as a loading control for the amount of cellular protein content.

5.1.3.2 Effect of cinacalcet on the functional effects of AP2σ2 mutations

To investigate if cinacalcet could rectify the functional effects observed in association with AP2σ2 mutations, HEK293 cells stably expressing AP2σ2 WT or mutants were transiently transfected with CaSR and treated with 20nM cinacalcet at 5mM calcium for 6 hours prior to measurement of NFAT and SRE reporter gene activity. A significant increase in NFAT reporter activity was observed for AP2σ2 WT and mutant cells following treatment with 20nM cinacalcet compared to WT (mean fold change in reporter activity: WT, 0nM=1.0, 20nM=6.7, $p<0.0001$; R15C, 0nM=1.0, 20nM=5.4, $p<0.0001$; R15H, 0nM=1.0, 20nM=2.5, $p<0.001$; R15L, 0nM=1.3, 20nM=7.7, $p<0.0001$; Figure 5.13A). There was no significant difference in NFAT reporter gene expression at 20nM between AP2σ2 WT and R15L expressing cells but NFAT activity was significantly reduced in AP2σ2 R15C and R15H expressing cells compared with WT at 20nM (WT vs R15C, $p<0.001$; WT vs R15H, $p<0.0001$; Figure 5.13A).

A significant increase in SRE reporter activity for AP2σ2 WT and all mutants following treatment with 20nM cinacalcet at 5mM calcium was observed (mean fold change in reporter activity: WT, 0nM=1.0, 20nM=37.8, $p<0.01$; R15C, 0mM=1.0, 5mM=26.0, $p<0.01$; R15H, 0mM=1.0, 5mM=32.3, $p<0.01$; R15L, 0mM=1.2, 5mM= 44.6, $p<0.001$; Figure 5.13B). There was no significant difference in the level of SRE reporter activity between AP2σ2 WT and mutant cells at 20nM cinacalcet, indicating cinacalcet rectifies the loss of SRE activity observed. Expression of CaSR in the transfected cells was confirmed by Western blot analysis (Figure 5.13C). The ERK1/2

signalling cascade is a convergence point for multiple G-protein signalling pathways and can exert effects on gene transcription through SRE (section 1.5).

Cinacalcet was able to rectify the functional effects observed in association with the R15L mutation in both the IP3 and ERK1/2 pathways, suggesting the R15L cells are mediating their effects through downregulation of both pathways. Cinacalcet, however, was unable to fully rectify the effect seen in the IP3 pathway in the R15C and R15H cells, which are likely to be mediating additional effects through another Gα protein-coupled pathway that converges on the MAPK cascade.

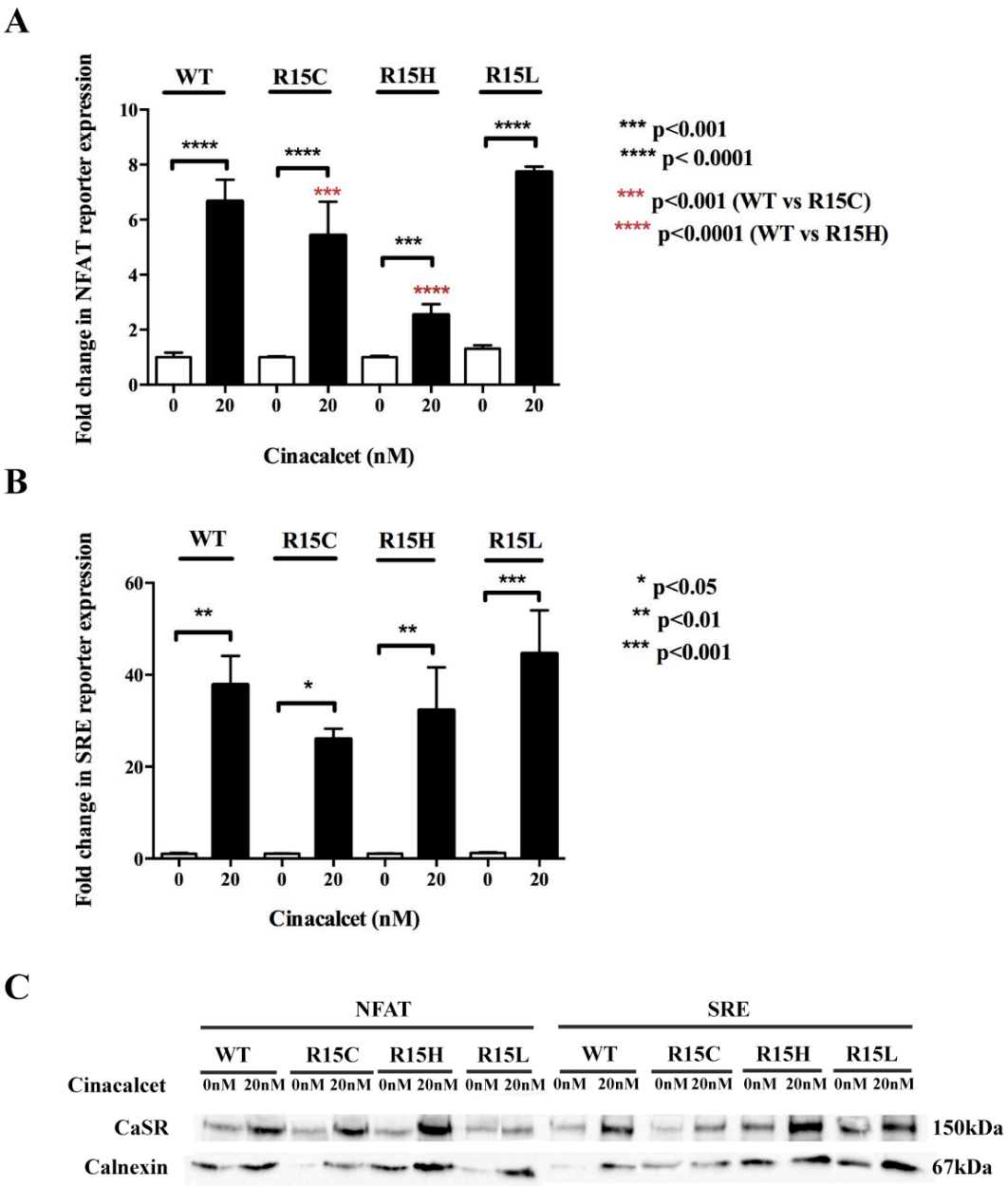


Figure 5.13. The effect of 20nM cinacalcet on NFAT and SRE reporter gene expression in AP2σ2 WT and mutant cells assessed by luciferase reporter gene assay.

HEK293 cells stably expressing either AP2σ2 WT, R15C, R15H or R15L were transiently transfected with CaSR 48 hours prior to treatment with 20nM cinacalcet for 6 hours at 5mM calcium. (**A-B**) Bar charts represent mean fold change in luciferase reporter gene expression relative to WT and n=4 biological replicate for each data set, error bars indicate ± SEM. (**A**) Treatment with 20nM cinacalcet produced a significant increase in NFAT reporter gene expression for AP2σ2 WT, R15C, R15H and R15L expressing cells ($p<0.001$, n=4). However, there was a significant difference in the increase in the NFAT reporter gene expression following treatment with cinacalcet between AP2σ2 WT and R15C ($p<0.001$, represented by red asterisks) and between WT and R15H ($p<0.0001$, represented by red asterisks). (**B**) Treatment with 20nM cinacalcet produced a significant increase in SRE reporter gene expression for AP2σ2 WT, R15C, R15H and R15L expressing cells ($p<0.05$, n=4). There was no significant difference in the increase in the SRE reporter gene expression following treatment between AP2σ2 WT and the AP2σ2 mutant cells. (**C**) Representative Western blot analysis showing expression of CaSR in transfected cells and calnexin, used as a loading control for the amount of cellular protein content. Each band represents a pooled sample of 4 biological replicates.

5.1.4 Discussion and future studies

These studies have demonstrated that FHH3-associated AP2σ2 mutations result in loss of activating phosphorylation events in the ERK1/2 signalling pathway. When pERK1/2 responses were normalised for total ERK1/2 (section 5.1.1.2.4), AP2σ2 R15C and R15L mutants demonstrated downregulation of the ERK1/2 signalling pathway compared to WT (Table 7). R15H showed severely impaired pERK1/2 responses compared to WT (Table 7). The downregulation of the ERK1/2 signalling pathway by AP2σ2 R15C and R15L mutations demonstrated by the AlphaScreen assays is supported by the finding of significantly reduced SRE reporter activity observed by AP2σ2 R15C and R15L mutants compared to WT (Table 7), suggestive of a consequent reduction in MAPK-regulated gene transcription.

AP2σ2 R15H cells showed no downregulation in MAPK-regulated gene transcription compared to WT. This is in contrast to the findings of the AlphaScreen assay that demonstrated a loss of function phenotype for R15H in phosphorylated ERK1/2 responses. This discrepancy could be explained by the complexity of CaSR signalling. Whilst MAPK pathways are the predominant mediators of SRE transcription, there is complex cross-talk between different signalling pathways downstream of CaSR which may have an effect on SRE. Furthermore, these differences may highlight a feature of the R15H residue change, that signalling in the presence of R15H favours coupling to a different G-protein (e.g. $G\alpha_{i/o}$ or $G\alpha_{12/13}$). A greater understanding of the effect of R15H mutations on the $G\alpha_{i/o}$ and $G\alpha_{12/13}$ pathways would provide further evidence for this.

Table 7. Differential effects of AP2σ2 mutations on signalling pathways and gene transcription relative to AP2σ2 WT

AP2σ2 mutation	pERK1/2 response (normalised to total ERK)	Intracellular Ca^{2+} signalling (NFAT)	ERK1/2 signalling (SRE)
R15C	Downregulated (🡻)	Downregulated (🡻)	Downregulated (🡻)
R15H	Severely impaired (🡻🡻)	Severely impaired (🡻🡻)	Unaffected (➔)
R15L	Downregulated (🡻)	Severely impaired (🡻🡻)	Downregulated (🡻)

These studies also highlight the complexity of signalling downstream of a single G-protein. A naïve view of G-protein coupling would assume that $G\alpha_{q/11}$ has similar effects on intracellular calcium and pERK1/2. However, our studies, and those from other groups focussing on CaSR mutations,[110] indicate that this is not the case. The AP2σ2 R15C mutation resulted in downregulation of NFAT transcription, whilst R15H and R15L mutants severely impaired this pathway (Table 7). Previous studies of intracellular calcium responses in these cells indicated that all three mutations caused a reduction in responses.[130] It would therefore be expected that NFAT, which occurs directly downstream of intracellular calcium, would be similarly reduced in all three mutations. The differences identified could again highlight cross-talk with other G-protein pathways. It may be that R15H and R15L prevent coupling to the intracellular calcium pathway, favouring other G-protein pathways, whereas R15C which is still able to signal via intracellular calcium, does not switch preferences for signalling pathways and thus has reduced signalling by both intracellular calcium and MAPK pathways. It could be suggested that R15H is unable to utilise intracellular calcium pathways so switches preference completely, as highlighted in the SRE responses, that are not different to WT. Furthermore, R15L may represent an intermediate of the two, that is unable to signal via the intracellular calcium pathway, but cannot fully compensate for this using MAPK signalling.

Comparing the normalised signalling responses to equimolar concentrations of extracellular Ca^{2+} from the NFAT and SRE dual-luciferase reporter assays, a bias plot was generated to demonstrate the differential coupling of CaSR to downstream signalling pathways in the presence of AP2σ2 mutations[110] and the findings are in agreement with my preliminary hypotheses (Figure 5.14). Overexpression of AP2σ2 WT favoured coupling of CaSR to ERK1/2 phosphorylation slightly more than intracellular Ca^{2+} release (Figure 5.14). The AP2σ2 R15C mutation favoured CaSR coupling to intracellular Ca^{2+} mobilisation (Figure 5.14). Conversely, AP2σ2 R15H and R15L mutations shifted the coupling of CaSR away from mobilisation of intracellular Ca^{2+} towards ERK1/2 phosphorylation, with the R15H mutation showing a greater bias towards ERK1/2 signalling than the R15L mutation (Figure 5.14). Further studies of these mutations in other signalling pathways could highlight where there is G-protein bias in association with these mutations.

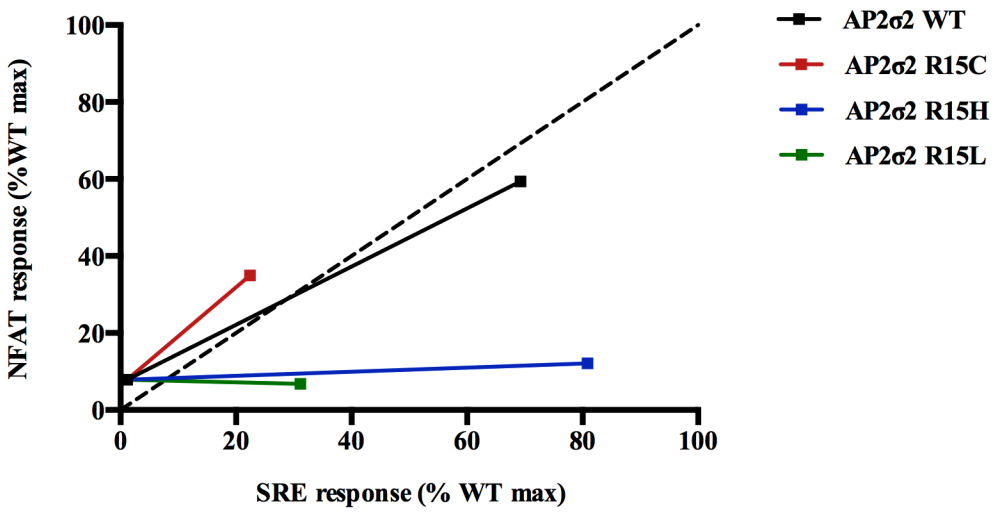


Figure 5.14. Bias plot showing the effects of the AP2σ2 mutations on differential coupling of the CaSR.

The mean responses, expressed as percentages of maximum WT response, to equimolar concentrations of extracellular calcium are plotted for NFAT (y-axis) and SRE (x-axis) reporter gene activity. Data is shown for AP2σ2 WT (black), R15C (red), R15H (blue) and R15L (green) cells. If there is no preference for either pathway, the data points will overlap with the line of identity (represented by the hashed line).[110] However, if signalling bias is present, the points will lie on the side of the line toward the favoured pathway.[110] Overexpression of AP2σ2 WT favours coupling to ERK1/2 signalling whilst R15H and R15L mutations greatly shift the coupling of the CaSR away from mobilisation of intracellular calcium towards ERK1/2 phosphorylation. The AP2σ2 R15C mutation favoured CaSR coupling to intracellular Ca^{2+} mobilisation.

To elucidate the effect of AP2σ2 mutations on the coupling of CaSR to other Gα signalling pathways including $G\alpha_{i/o}$ and $G\alpha_{12/13}$, dual-luciferase reporter studies measuring CRE and SRF reporter activity, respectively could be performed in HEK293 cells stably expressing AP2σ2 WT and mutant cells in response to extracellular calcium. The experiments would be performed as described in section 3.2.5.4. Additionally, all the dual-luciferase experiments would be performed over a range of concentrations to generate a dose-response curve for each reporter gene measured to include the physiological extracellular Ca^{2+} concentrations (1-3mM[10]) and higher Ca^{2+} concentrations to include those seen in the bone microenvironment (>6mM[164]) enabling investigation of the bone phenotype seen in FHH3 probands. *Ex*

vivo studies using bone cells derived from a knock-in AP2σ2 R15L mutant mouse could also be used for the dual-luciferase assays to elucidate the mechanisms occurring *in vivo*.

In future studies, the protocol would not include continuous exposure of cells to calcium in the presence or absence of compounds for 6 hours (sections 5.1.2.1 and 5.1.3.1). This protocol did not consider the effect of continuous ADIS in the presence of prolonged exposure of CaSR to agonist. Possible depletion of intracellular pools of mature receptor leading to decreased CaSR cell surface expression with a subsequent downregulation in intracellular signalling and gene transcription may have occurred. Subsequent time course studies performed by Dr C.M. Gorvin revealed that SRE rises sharply within the first 4 hours of exposure to calcium, with subsequent rapid reduction in responses to baseline by 7 hours (data unpublished). Thus it is likely cell lysis at 6 hours used in my studies was not optimal as SRE responses may have been in decline when assessed. Additionally, it did not take into consideration the possible effects of the AP2σ2 mutants on phosphorylation of ERK1/2 through non-canonical pathways (Section 1.8.1 and Figure 1.21). Thus, the protocol requires further optimisation to include exposure of cells to extracellular calcium with or without compound for 5 minutes followed by a 6 hour incubation period in serum-free media to allow gene transcription to occur prior to cell lysis. These experiments are currently being performed.

Allosteric modulators are known to modify the signalling preferences of the CaSR and cinacalcet has been shown to favour coupling of CaSR to signalling through mobilisation of intracellular Ca^{2+} rather than the ERK1/2 cascade.[96] Treatment of

HEK293 cells stably expressing AP2σ2 WT or mutant with cinacalcet demonstrated differential effects of cinacalcet on the mutation-induced defects in intracellular calcium and ERK1/2-mediated gene transcription (Table 8). Cinacalcet rectified the impaired NFAT-mediated gene transcription to WT levels in AP2σ2 R15L cells but failed to do so in R15C and R15H cells. Conversely cinacalcet rectified all three mutation effects on SRE transcription. These findings are partially consistent with my signalling results and reveal further insights into the effect of different mutations within the same residue of signalling pathways. Thus, it is likely that the R15H mutation prevents intracellular calcium responses occurring, biasing the pathway towards a MAPK-mediated response. This explains the inability of cinacalcet to rectify NFAT responses, while SRE responses are similar to WT. R15L, whilst also favouring MAPK responses over intracellular calcium in the normal state, is still able to use both pathways. Thus, cinacalcet is able to rectify responses in both pathways. The R15C results are more complicated to explain. NFAT responses are almost normalised in these cells, but are significantly lower than in WT cells. This could be because the number of replicates needs to be increased in my studies as the variation in my biological replicates is quite large, or that the time at which luciferase responses are assessed requires optimisation as alluded to earlier.

Table 8. Differential effects of cinacalcet on AP2σ2 mutations

AP2σ2 mutation	Effect of cinacalcet on mutation-induced signalling defect	
	$G\alpha_{q/11}$ signalling defect	ERK1/2 signalling defect
R15C	Failed to rectify	Rectified
R15H	Failed to rectify	Rectified
R15L	Rectified	Rectified

The *in vivo* significance of these results is yet to be fully determined. Cinacalcet has been shown to be clinically beneficial in 4 patients harbouring AP2σ2 mutations, showing improvement in symptoms and reductions in adjusted serum calcium levels.[290 309] The metabolic effects of therapy require further investigation. The mouse model of FHH3 I am developing could be beneficial for *in vivo* drug studies to assess the efficacy and metabolic effects of the compound. Additionally, cells isolated from such a model could be used to assess the signalling pathways discussed further, and the effects of allosteric modulators determined.

While these studies have provided insights into signalling bias they have not determined the mechanism by which AP2σ2 mutations cause these changes in the CaSR signalling pathway. Previous preliminary studies have suggested that AP2σ2 mutations reduce CaSR internalisation. However, if this were to be the case then it would be expected that CaSR signalling would be increased due to retention of the receptor at the plasma membrane surface. Within the Thakker group, new studies of AP2σ2 mutations on CaSR measuring the ADIS response and receptor endocytosis simultaneously have revealed that AP2σ2 mutations reduced receptor internalisation (Dr C. M. Gorvin, *Personal Communication*). In combination with my studies that reveal reduced receptor signal this has helped to form a hypothesis that, similar to the

PTH1R and B_2AR, CaSR may be able to signal via a non-canonical pathway (Figure 1.21).

Therefore, my future studies would focus on elucidating these pathways further. For example, it is not known whether the CaSR is trafficked to the pre-early endosome or the early endosome (Figure 1.16 and section 1.8.1). This could be studied using live confocal imaging of HEK293 cells stably expressing FLAG-tagged CaSR and transiently transfected with AP2σ2 WT or mutants to allow for real-time visualisation of receptor internalisation and postendocytic receptor sorting.[135] Measurement of endosome size in combination with co-localisation of the endosome with markers of distinct endosomal compartments would identify the precise endosomal location of CaSR in the presence of AP2σ2 WT and mutants.[135] Furthermore, assessment of signalling responses over a longer time course (for example, 30-60 minutes) could reveal whether there is a second endosomal, non-canonical response in CaSR, and whether this is impaired in AP2σ2 mutants. The preliminary time course studies for the pERK1/2 AlphaScreen assays were suggestive of a possible second pERK1/2 response but require further investigation and refinement (Figure 5.2). For example, pERK1/2 responses could be assessed by AlphaScreen over a longer time period, and luciferase responses assessed similarly. I would perform these studies in WT cells initially, to determine if such second, endosomal responses did occur before moving on to determining the effect of AP2σ2 mutations.

In summary, these studies have revealed that AP2σ2 mutations cause reduced MAPK responses but that these may be due to differential effects on CaSR coupling to different signalling pathways.

Ap2s1 mouse models

6 *Ap2s1* mouse models

6.1.1 Strategy for the generation of *Ap2s1* mouse models

There are currently no published mouse models with *Ap2s1* mutations or gene knockout (section 1.11.3.1). However, knockout of AP2σ2 in *Arabidopsis thaliana* results in defective auxin transport, reduced plant growth and impaired fertility.[310] In addition, mouse models have been generated where the μ2 and β2 subunits of AP-2 were successfully knocked out. [250 251] In both these models, the heterozygous mice were phenotypically normal.[250 251] The μ2 subunit homozygous knockout mice were embryonic lethal whilst the β2 subunit knockout mice had cleft palate deformities and died in the postnatal period.[250 251]

It was decided to establish a strategy to generate *Ap2s1* mouse models to: study the pleiotropic effects of the AP2σ2 mutations *in vivo*; establish primary cell lines of various origins including renal, bone, and parathyroid, expressing AP2σ2 mutations for *in vitro* signalling and trafficking studies; and study the effects of novel therapeutics at the animal and cellular level. The strategy involved using the existing MRC Harwell N-ethyl-N-nitrosourea (ENU) archive to identify mutations and to generate an *Ap2s1* R15L mouse model using transcription activator-like effector nucleases (TALENs) technology.

6.1.2 *Ap2s1* mutations identified from the MRC Harwell ENU-induced DNA archive screen

Five *Ap2s1* mutations (Figure 6.1) were identified from a genotype-driven screen of the MRC Harwell ENU-induced DNA archive. This archive consists of more than 12,000 samples from individual mice paralleled by frozen sperm samples, thereby facilitating re-derivation of mutant progeny by *in vitro* fertilisation of normal females.[237] Two mutations were located within the exons, c.58T>A and c.386T>A, which were predicted to result in missense amino acid substitutions of Tyr for Asn at residue 20 (Tyr20Asn) and Ile for Asn at residue 123 (Ile123Asn), respectively (Figure 6.1). Three intronic mutations were also identified: IVS2-22T>C, IVS2+2T>C and IVS5-17C>T (Figure 6.1). To determine which *Ap2s1* mutations should undergo functional characterisation, studies were performed to predict the possible consequences of the mutations identified.

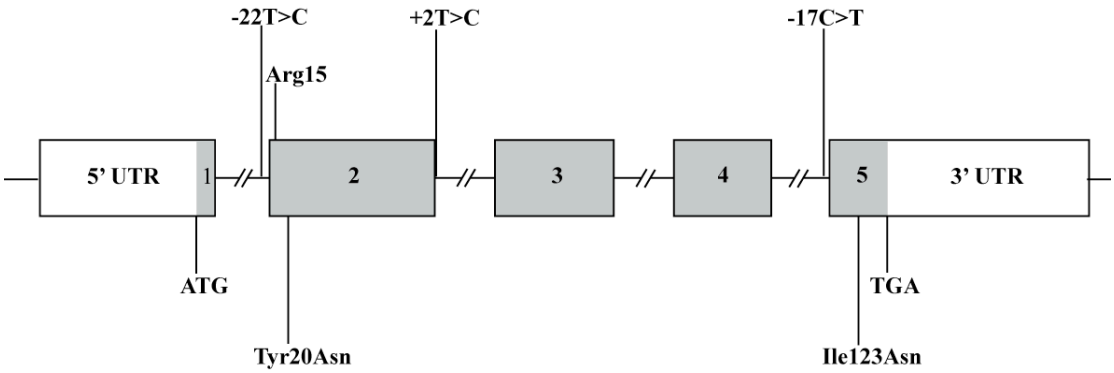


Figure 6.1. Schematic diagram showing the *Ap2s1* mutations identified by a genotype-driven screen of the MRC Harwell ENU-induced DNA archive.

The coding region (represented by the grey boxes) of *Ap2s1* is homologous to *AP2S1*. A screen of the MRC Harwell DNA archive identified 2 exonic mutations (Tyr20Asn and Ile123Asn) and 3 intronic mutations (IVS2-22T>C, IVS2+2T>C and IVS5-17C>T) in *Ap2s1*.

6.1.3 Prediction of the possible consequences of the *Ap2s1* mutations identified

To determine the possible effects of the missense amino acid substitution on the AP2σ2 protein structure, structural modelling of the mutant AP2σ2 subunit compared to WT was performed using Phyre2 protein structure prediction software.[311] Structural modelling predicted mutation of Tyr20 to Asn20 to have no effect on the tertiary structure of AP2σ2 (Figure 6.2B). Similarly, mutation of Ile123 to Asn123 was predicted to have no effect on the tertiary structure of AP2σ2 (Figure 6.2).

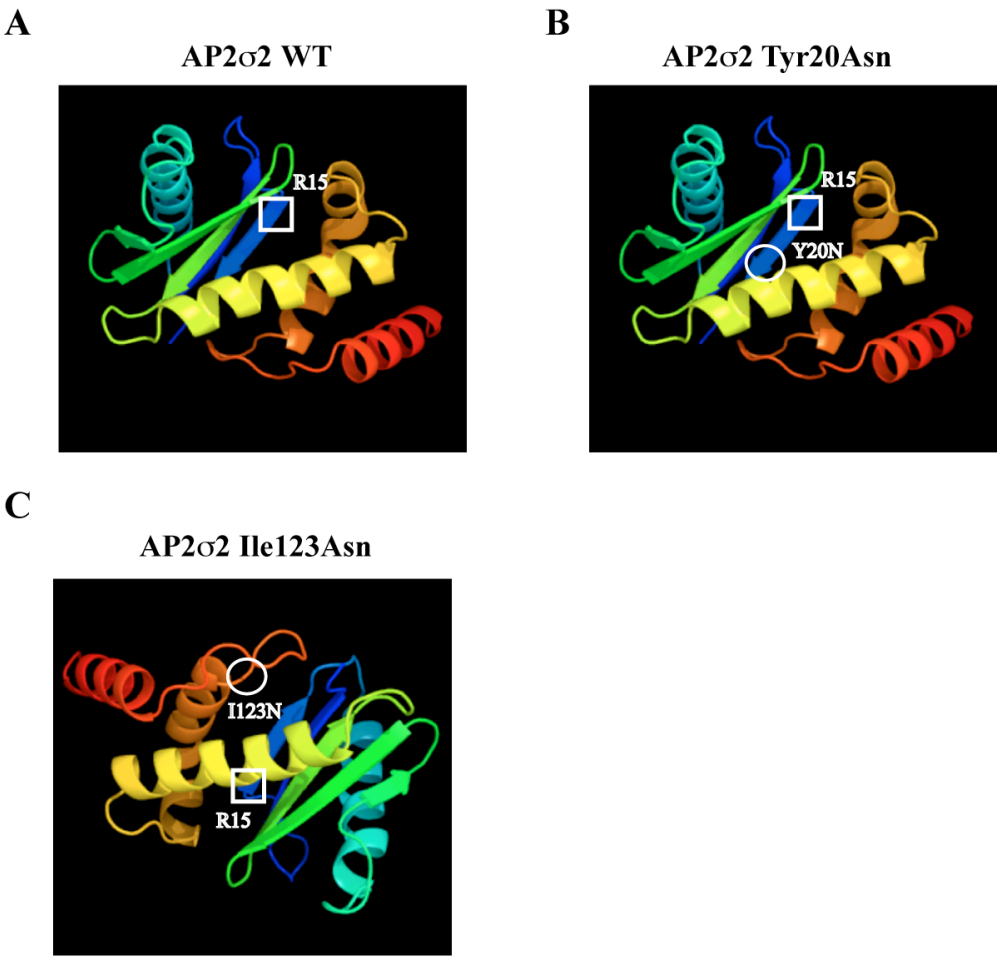


Figure 6.2. Structural modelling of AP2σ2 WT, AP2σ2 Tyr20Asn and AP2σ2 Ile123Asn.

(**A-C**) Structural modelling of AP2σ2 with protein coloured by the rainbow from N to C terminus and position of Arg15 within a beta sheet marked by white box. (**A**) AP2σ2 WT. (**B**) AP2σ2 Tyr20Asn with position of residue 20 marked by white circle. Tyr20Asn is predicted to have no effect on the tertiary structure of AP2σ2. (**C**) AP2σ2 Ile123Asn with position of residue 123 marked by white circle. Ile123Asn is predicted to have no effect on the tertiary structure of AP2σ2.

Residue Tyr20 is highly conserved across vertebrate AP2σ2 subunit orthologues and AP2σ paralogues (Table 9) with no variants identified. However, residue Ile123 is conserved across AP2σ2 orthologues but not across AP2σ paralogues (Table 9). As the predicted Tyr20Asn mutation was in close proximity to the FHH3 Arg15 residue and residue Tyr20 was highly conserved, the mutation was selected for *in vitro* functional characterisation (described in section 6.1.4).

Table 9. Evolutionary conservation of residues 20 and 123 of the AP2σ subunit across vertebrate orthologues and paralogues.

		AP2σ residue	
		Residue 20	**Residue 123**
Orthologue	*Mus musculus*	Tyr	Ile
	Homo sapiens	Tyr	Ile
	Bos Taurus	Tyr	Ile
	Pan troglodytes	Tyr	Ile
	Canis lupus familiaris	Tyr	Ile
Paralogue	AP4σ1	Tyr	Ile
	AP1σ3	Tyr	Ile
	AP1σ2	Tyr	Val
	AP1σ1	Tyr	Val

The possible effects of the intronic mutations on their respective splice sites were predicted using the splice site prediction programs, Berkeley Drosophila Genome Project (BDGP)[287] and GeneSplicer[288]. These programs predicted *Ap2s1* IVS 2+2T>C to result in loss of the donor splice site at the 5' end of intron 2 of *Ap2s1*, which is approximately 3.9kb in length. The possible outcomes of loss of this splice site are: skipping of exon 2 (Figure 6.3); activation of a cryptic splice site 222 bases from the 5' end of intron 2 which is predicted to result in a truncated protein lacking 50 of the 142 amino acids (from exons 3, 4 and 5) due to the incorporation of an in-frame stop

codon 111 bases upstream of the cryptic GT site (Figure 6.3); and intron retention which is also predicted to produce a truncated protein due to the presence of the in-frame stop codon 111 bases from the 5' end of intron 2 (Figure 6.3). On the basis of this prediction, the *Ap2s1* IVS 2+2T>C ENU-induced mutant mouse was selected for re-derivation for phenotypic studies (described in section 6.1.5). *Ap2s1* IVS 2-22C>T and IVS 5-17C>T were predicted to have no effect on splicing and therefore, these mutations were not investigated further.

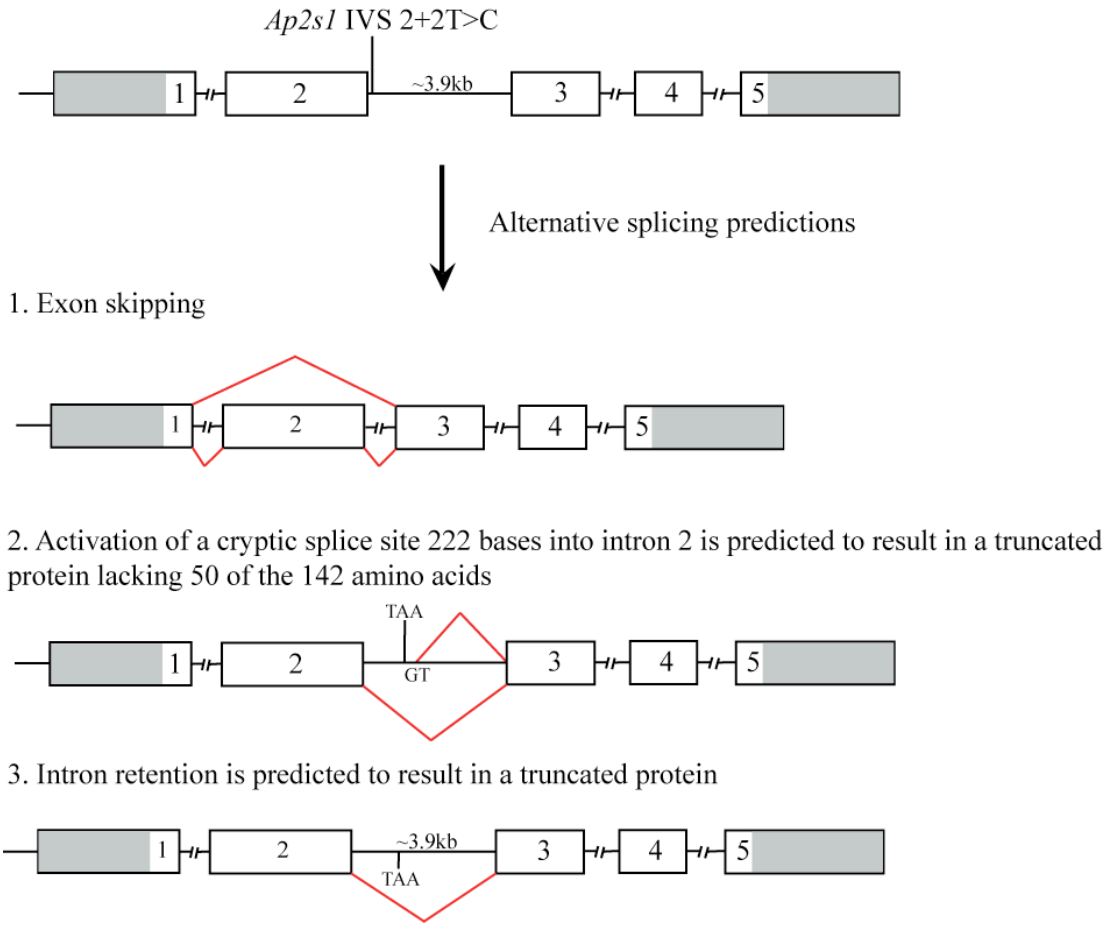


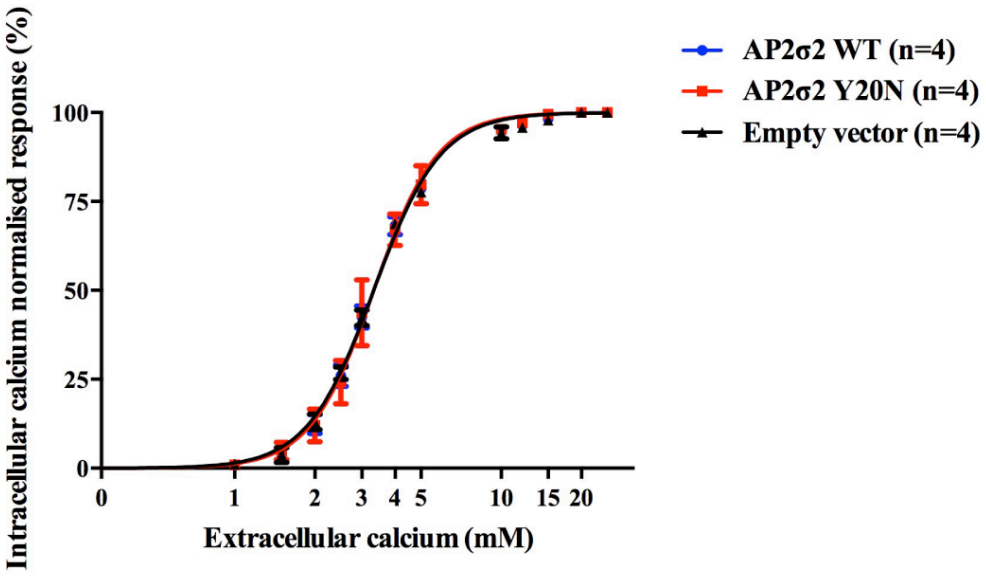
Figure 6.3. Predicted consequences of the *Ap2s1* IVS 2+2T>C mutation.

Ap2s1 IVS 2+2T>C mutation is predicted to result in loss of the donor splice site at the 5' end of intron 2 of *Ap2s1*, which is approximately 3.9kb in length. Loss of this splice site could be predicted to result in exon skipping, activation of a cryptic splice site or intron retention. Red lines indicate alternatively spliced regions.

6.1.4 Characterisation of the functional effects of the AP2σ2 Tyr20Asn mutation

To investigate the functional effects of the AP2σ2 Tyr20Asn (Y20N) mutation, flow cytometry using the calcium-binding dye, Indo-1-AM, and increasing concentrations of extracellular calcium to measure intracellular calcium response was used to generate dose-response curves. HEK293-CaSR cells transiently expressing pBI-CMV4 (empty), pBI-CMV4-AP2σ2 WT, or pBI-CMV4-AP2σ2 Y20N were used for these studies. Intracellular calcium responses increased in a dose-dependent manner in both WT and Y20N cells and there was no significant difference in the EC_{50} values (AP2σ2 WT EC_{50} = 3.32 (95% confidence interval (CI) = 3.25-3.40), AP2σ2 Y20N EC_{50} = 3.33 (95% CI = 3.18-3.48), empty-pBI-CMV4 EC_{50} = 3.32 (95% CI = 3.26-3.39), WT vs. Y20N p= 0.99, n = 4 biological replicates) (Figure 6.4). Thus, the AP2σ2 Y20N mutation failed to produce a rightward shift in the dose-response curve, suggesting the mutation would not give rise to a phenotype consistent with FHH.

A



B

	EC_{50}	95% CI
AP2σ2 WT	3.32	3.25-3.40
AP2σ2 Y20N	3.33	3.18-3.48
Empty vector	3.32	3.26-3.39

Figure 6.4. Intracellular calcium responses to changes in extracellular calcium of HEK293-CaSR cells transfected with AP2σ2 WT, Y20N or empty vector, pBI-CMV4-RFP.

HEK293-CaSR cells were transiently transfected with either AP2σ2 WT (blue), Y20N (red) or empty vector, pBI-CMV4-RFP (black). Forty-eight hours later, cells were labelled with Indo-1-AM and treated with 0-10mM calcium. Transfected cells were selected by flow cytometry based on red fluorescence and the intracellular Ca^{2+} measured at each extracellular Ca^{2+} concentration. (**A**) Dose-response curves displaying mean ± SEM of n=4 biological replicates are shown. (**B**) There was no significant difference in the concentration of calcium required to produce a half maximal response (EC_{50}) of the AP2σ2 Y20N variant compared to WT.

6.1.5 Investigation of the functional effects of *Ap2s1* IVS 2+2T>C mutation *in vivo*

To investigate the functional effects of the *Ap2s1* IVS 2+2T>C mutation *in vivo*, mice were generated by *in vitro* fertilisation of C3H female mice with spermatozoa harbouring the *Ap2s1* IVS 2+2T>C mutation derived from the first generation (G1) male offspring of the ENU-treated male mice (GO) bred at MRC Harwell. Offspring heterozygous for the *Ap2s1* IVS 2+2T>C mutation ($Ap2s1^{+/-}$) were crossed to C3H females to generate the second generation (G2) and G2 $Ap2s1^{+/-}$ mice were then intercrossed to generate the third generation (G3) (Figure 6.7).

6.1.5.1 Investigation of the effects of *Ap2s1* IVS 2+2T>C mutation at the genomic level

Whilst the breeding programme was being established, ear tissue was obtained from 11 week old $Ap2s1^{+/+}$ and $Ap2s1^{+/-}$ mice and RT-PCR performed on extracted RNA (sections 3.2.3.1 and 3.2.3.2) to determine the effect of the splice site mutation at the genomic level. A mutant cDNA product of ~220bp (Figure 6.5A) was cloned into pCR-Blunt II-TOPO (sections 3.2.2.3 and 3.2.2.4, Figure 10.4) and Sanger sequencing performed (section 3.2.2.3). Sequencing revealed the *Ap2s1* IVS 2+2T>C mutation to result in loss of the donor splice site of *Ap2s1* exon 2 as predicted and activation of an in-frame cryptic splice site 51 bases upstream of the 3' end of exon 2 (Figure 6.5B). This was predicted to produce a mutant AP2σ2 protein lacking 17 of the 50 amino acids encoded by exon 2 (Figure 6.5C).

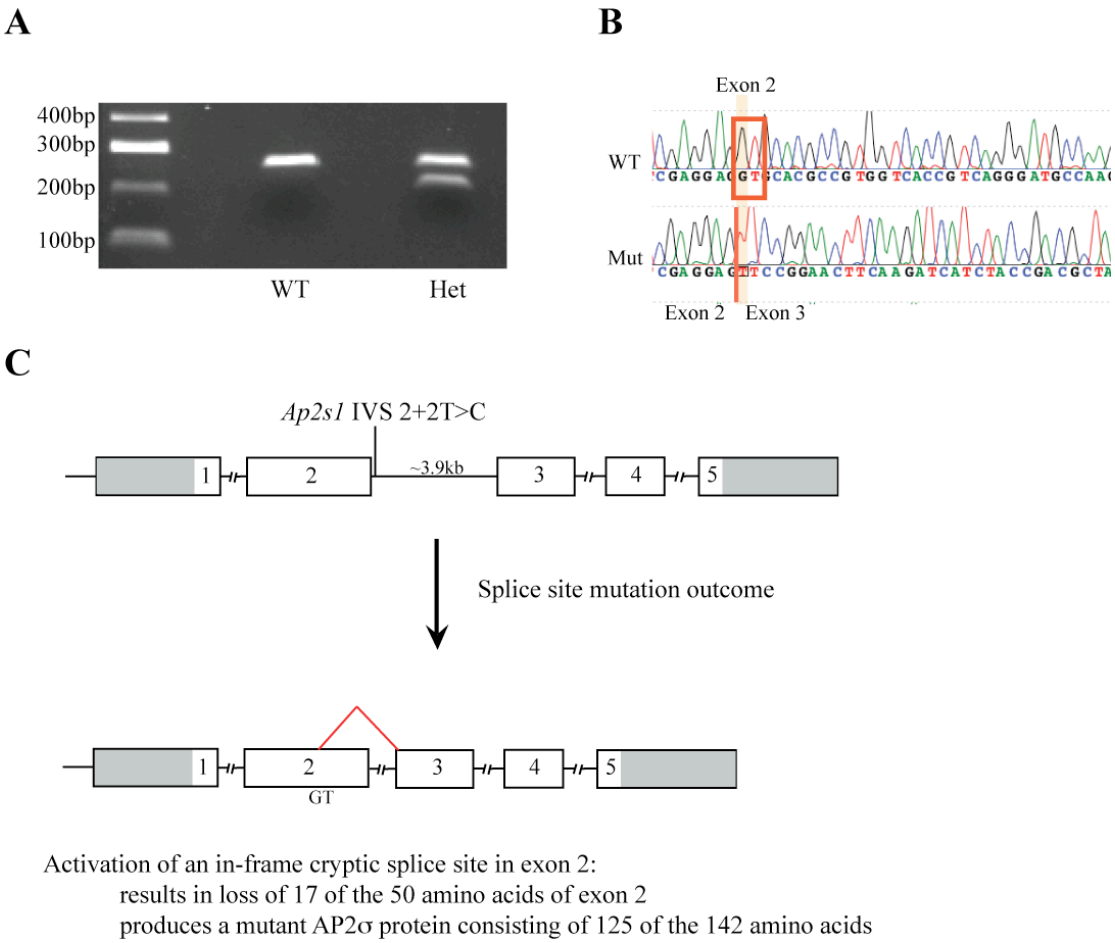


Figure 6.5. Outcome of the *Ap2s1* IVS 2+2T>C mutation at the genomic level in the heterozygous ENU-mutagenised mice.

(**A**) PCR and agarose gel electrophoresis was performed using cDNA obtained from RNA extracted from ear tissue of 11 week old *Ap2s1*$^{+/+}$ (WT) and *Ap2s1*$^{+/-}$ (Het) mice. This revealed two bands for the Het mouse, one equating to the WT PCR product and a smaller band of approximately 220bp. (**B**) The approximately 220bp mutant PCR product from the Het mouse was cloned into pCR-Blunt II-TOPO and Sanger sequencing was performed. Dideoxynucleotide sequence analysis of the WT and mutant (Mut) PCR products revealed that loss of the donor splice site at the 5' end of intron 2 of *Ap2s1* resulted in activation of an in-frame cryptic splice site (shown by the red box) 51 bases upstream of the 3' end of exon 2. The horizontal red line represents the 5' end of exon 3. (**C**) Schematic representation of the predicted effect of the splice site mutation on *Ap2s1*. The mutant AP2σ2 protein produced is predicted to lack 17 amino acids from the 3' end of exon 2. Red lines indicate spliced regions.

Structural modelling of the mutant AP2σ2 protein, using the Phyre2 protein structure prediction software[311], revealed an altered tertiary structure compared to WT comprising loss of an alpha helix at the C terminus and its replacement by a short beta sheet (Figure 6.6), which is likely to have significant effects on its function and ability to interact with the other subunits of AP-2. Thus it was predicted that mice homozygous for the *Ap2s1* IVS 2+2T>C mutation (*Ap2s1*$^{-/-}$) would be *Ap2s1* functional knock-outs.

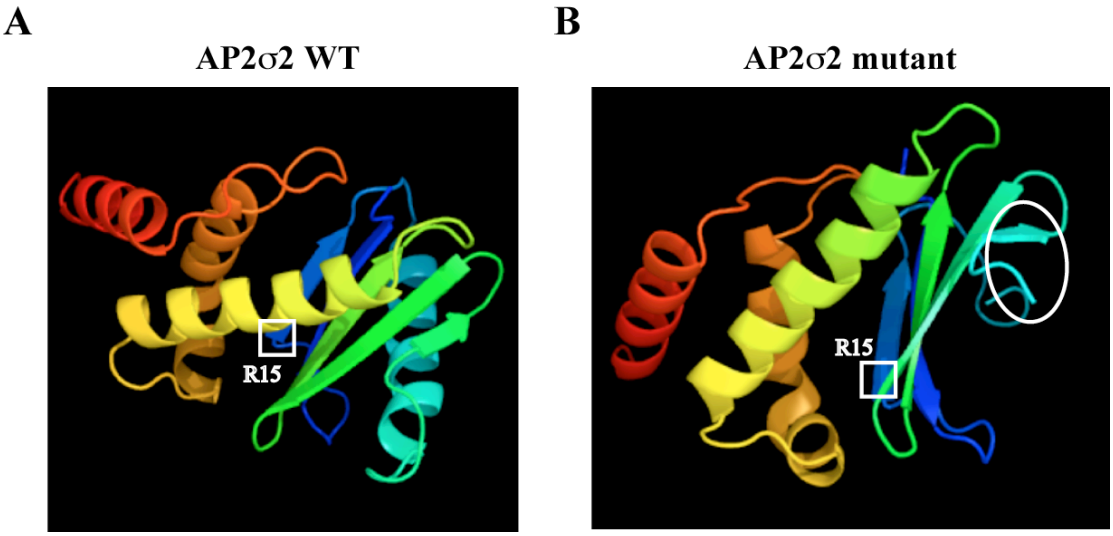


Figure 6.6. Structural modelling of AP2σ2 WT and AP2σ2 splice site mutant proteins.

(**A-C**) Structural modelling of AP2σ2 was performed using the Phyre2 protein structure prediction software[311] and the protein coloured by the rainbow from N to C terminus. (**A**) AP2σ2 WT with position of Arg15 within a beta sheet marked by white box. (**B**) *Ap2s1* IVS 2+2T>C mutation results in a mutant AP2σ2 lacking 17 of the 50 amino acids from exon 2 which is predicted to have a significant effect on the tertiary structure of AP2σ2, comprising loss of an alpha helix at the C terminus and replacement by a short beta sheet (highlighted in white circle).

6.1.5.2 Biochemical and phenotypic analysis of *Ap2s1* IVS 2+2T>C ENU-mutagenised mice

To investigate the pleiotropic effects of the *Ap2s1* IVS 2+2T>C mutation *in vivo*, G2 *Ap2s1*$^{+/+}$ and *Ap2s1*$^{+/-}$ mice (Figure 6.7) underwent phenotypic and biochemical analysis.

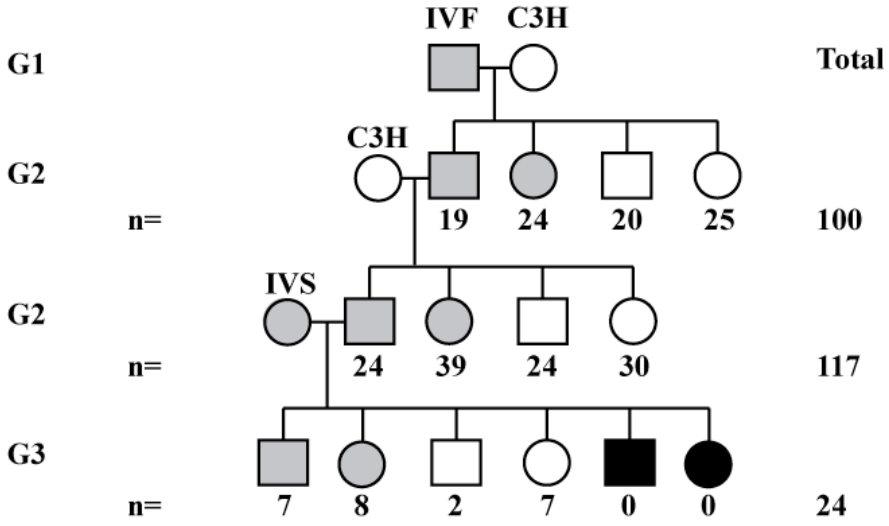


Figure 6.7. Pedigree of *Ap2s1* IVS 2+2T>C mice.

Pedigree of *Ap2s1* IVS 2+2T>C mice showing three generations (G1, G2 and G3). G2: 20.5% wild type (*Ap2s1*$^{+/+}$) males (n=24); 26% *Ap2s1*$^{+/+}$ females (n=30); 20.5% *Ap2s1* heterozygous ($^{+/-}$) males (n=24); 33% *Ap2s1*$^{+/-}$ females (n=39) (G2 mice included in analysis, n= 117). G3: ~8% *Ap2s1*$^{+/+}$ males (n=2); ~29% *Ap2s1*$^{+/+}$ females (n=7); ~29% *Ap2s1*$^{+/-}$ males (n=7); ~33% *Ap2s1*$^{+/-}$ females (n=8); no *Ap2s1* homozygous (*Ap2s1*$^{-/-}$) mice were seen (total, n=24), which deviated from a Mendelian pattern of inheritance. Male, square; female, circle; *Ap2s1*$^{+/+}$, white; *Ap2s1*$^{+/-}$, grey; *Ap2s1*$^{-/-}$, black.

An autosomal dominant pattern of inheritance was seen amongst *Ap2s1*$^{+/+}$ and *Ap2s1*$^{+/-}$ mice born in G2 (Table 10), yielding 117 progeny (48 males and 69 females) of which 54 were *Ap2s1*$^{+/+}$ and 63 were *Ap2s1*$^{+/-}$, suggesting that the *Ap2s1*$^{+/-}$ mice

were viable. The *Ap2s1*$^{+/-}$ mice showed no evidence of perinatal lethality and appeared phenotypically normal in comparison to WT littermates.

Table 10. Observed and expected numbers of mice as predicted by Mendelian inheritance of the *Ap2s1* IVS 2+2T>C mutation in the second generation of mice.

Ap2s1 IVS 2+2T>C genotype	Observed number of mice	Expected number of mice
Ap2s1$^{+/+}$	54	58.5
Ap2s1$^{+/-}$	63	58.5
Total number of mice	117	117

p=0.41 (Ratios of genotypes were tested for goodness of fit to expected Mendelian segregation (1:1) by χ^2 analysis, calculated for two degrees of freedom).

6.1.5.2.1 Metabolic cage studies in *Ap2s1* IVS 2+2T>C ENU-mutagenised mice

Twelve week old *Ap2s1*$^{+/+}$ and *Ap2s1*$^{+/-}$ mice underwent metabolic cage studies to assess the effects of the *Ap2s1* IVS 2+2T>C mutation on mineral homeostasis and renal function *in vivo*. The *Ap2s1* IVS 2+2T>C mutation had no effect on plasma concentrations of albumin-adjusted calcium, phosphate, PTH, vitamin D, magnesium and creatinine (Table 11 and Figure 6.8). There was also no significant difference in the sex-matched total plasma alkaline phosphatase activity, which may be of hepatic, renal, or bone origin, between *Ap2s1*$^{+/-}$ and *Ap2s1*$^{+/+}$ mice (Table 11). Dynamic histomorphometry was not performed on these mice to assess bone remodelling as no abnormalities in plasma biochemistry were detected compared to WT littermates to suggest a disorder of calcium or phosphate homeostasis. Additionally, plasma sodium, potassium, urea, chloride, total bilirubin, alanine transaminase, total cholesterol and glucose showed no significant difference between *Ap2s1*$^{+/-}$ and *Ap2s1*$^{+/+}$ mice (Table 11). Urinary excretion of calcium, phosphate, magnesium, sodium, potassium and chloride were not significantly different between *Ap2s1*$^{+/-}$ and *Ap2s1*$^{+/+}$ littermates

(Table 11 and Figure 6.9). *Ap2s1*$^{+/-}$ mice were not polydipsic or polyuric in comparison to *Ap2s1*$^{+/+}$ mice (Figure 6.9).

Table 11. Biochemistry of 12 week old *Ap2s1*$^{+/+}$ and *Ap2s1*$^{+/-}$ mice obtained through metabolic cage studies.

		Mean plasma concentrations (SEM)														
		Adj. calcium [a] (mmol/l)	Phosphate (mmol/l) [b]	PTH[c] (pg/ml)	Mg[d] (mmol/l)	25OHD[e] (pmol/l)	Creatinine (µmol/l)[f]	ALP (U/l)[g]	Sodium [h] (mmol/l)	Potassium (mmol/l)[i]	Urea (mmol/l)[j]	Chloride (mmol/L)[k]	Total bilirubin (µmol/l)[l]	ALT [m] (U/l)	Total cholesterol (mmol/l)[n]	Glucose [o] (mmol/l)
	WT	2.48	1.89	292	0.79	64.8	16.0	100.8	151	5.5	12.4	114	1.78	53.7	2.3	10.5
Male	(n=12)	(0.02)	(0.07)	(42)	(0.03)	(4.0)	(0.4)	(3.6)	(0.3)	(0.1)	(0.4)	(0.4)	(0.1)	(7.7)	(0.1)	(0.5)
	Het	2.46	1.94	351	0.73	64.3	15.8	100.8	151	5.2	12.9	114	1.65	69.8	2.5	9.2
	(n=10)	(0.01)	(0.06)	(58)	(0.02)	(6.5)	(0.8)	(4.1)	(0.2)	(0.1)	(0.4)	(0.5)	(0.1)	(13.1)	(0.1)	(0.8)
	WT	2.50	2.09	296	0.79	88.7	14.1	146.1	149	4.7	8.6	113	1.64	37.2	2.8	13.3
Female	(n=10)	(0.01)	(0.08)	(58)	(0.02)	(6.5)	(0.7)	(4.1)	(0.5)	(0.1)	(0.5)	(0.3)	(0.1)	(1.5)	(0.1)	(0.7)
	Het	2.49	2.04	303	0.81	85.9	14.4	147	149	4.7	8.5	112	1.84	38.0	2.6	13.1
	(n=12)	(0.01)	(0.07)	(24)	(0.02)	(6.8)	(0.4)	(6.6)	(0.4)	(0.1)	(0.2)	(0.2)	(0.1)	(2.0)	(0.1)	(0.5)

		Mean urine measurements (SEM)					
		CCCR[p]	$FePO_4$[q]	FeMg[r]	FeK[s]	FeNa[t]	FeCl[u]	Urine volume (ml/24hr)[v]
	WT	0.002	0.04	0.07	0.29	0.008	0.015	1.84
Male	(n=12)	(0.0001)	(0.007)	(0.01)	(0.01)	(0.0003)	(0.0006)	(0.13)
	Het	0.002	0.04	0.07	0.29	0.008	0.014	1.90
	(n=10)	(0.0002)	(0.01)	(0.02)	(0.01)	(0.0004)	(0.0009)	(0.13)
	WT	0.002	0.02	0.06	0.27	0.007	0.013	1.85
Female	(n=10)	(0.0003)	(0.009)	(0.01)	(0.02)	(0.0003)	(0.0008)	(0.16)
	Het	0.003	0.02	0.08	0.28	0.007	0.014	2.12
	(n=12)	(0.0002)	(0.006)	(0.01)	(0.01)	(0.0003)	(0.0004)	(0.11)

All serum and urine samples were taken following 72 hours of acclimatisation in metabolic cages: [a] albumin-adjusted calcium, mmol/l; [b] phosphate, mmol/l, [c] PTH, pg/ml; [d] magnesium, mmol/l; [e] 25-hydroxyvitamin D (25OHD), pmol/l; [f] creatinine, µmol/l; [g] alkaline phosphatase (ALP) activity, U/L; [h] sodium, mmol/l; [i] potassium, mmol/l; [j] urea, mmol; [k] chloride, mmol/l; [l] total bilirubin, mmol/l; [m] alanine transaminase (ALT), U/l; [n] total cholesterol, mmol/l; [o] glucose, mmol/l; [p] calcium to creatinine clearance ratio (CCCR) ; [q] fractional excretion of phosphate ($FePO_4$); [r] fractional excretion of magnesium (FeMg); [s] fractional excretion of potassium (FeK); [t] fractional excretion of sodium (FeNa); [u] fractional excretion of chloride (FeCl); [v] urine volume (ml/24 hours). Urine measurements were calculated as described in section 3.2.6.2.1. No sex-matched differences were observed between genotypes on statistical analysis using unpaired Mann-Whitney tests. Animals included in study: WT males, n=12; Het males, n=10; WT females, n=10; Het females, n=12.

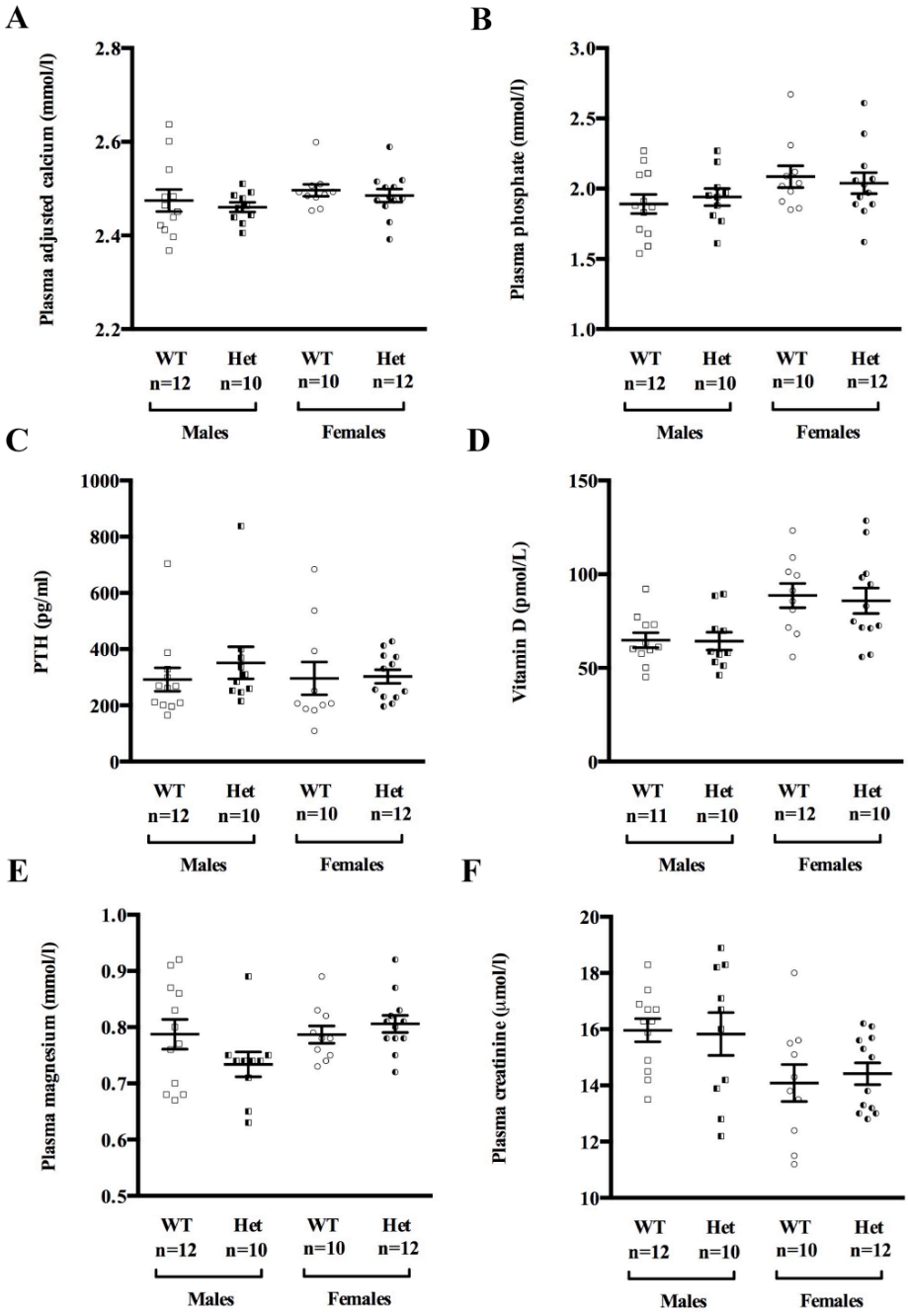


Figure 6.8. Plasma biochemistry of 12 week old *Ap2s1* IVS 2+2T>C *Ap2s1*$^{+/+}$ and *Ap2s1*$^{+/-}$ mice from metabolic cage studies.

(A-F) 12 week old mice were individually housed in metabolic cages and fed on standard chow. Blood collection was undertaken by cardiac puncture after terminal anaesthesia. Mean ± SEM are represented by horizontal lines and error bars, respectively. Sex-matched groups were compared using unpaired Mann-Whitney tests. A value of $p<0.05$ was considered to be statistically significant. No significant difference was identified between *Ap2s1*$^{+/+}$ (WT) and *Ap2s1*$^{+/-}$ (het) sex-matched mice for the following biochemical parameters: (**A**) Plasma albumin-adjusted calcium (mmol/l). (**B**) Plasma phosphate (mmol/l). (**C**) Plasma PTH (pg/ml). (**D**) Plasma vitamin D (pmol/l). (**E**) Plasma magnesium (mmol/l). (**F**) Plasma creatinine (µmol/l).

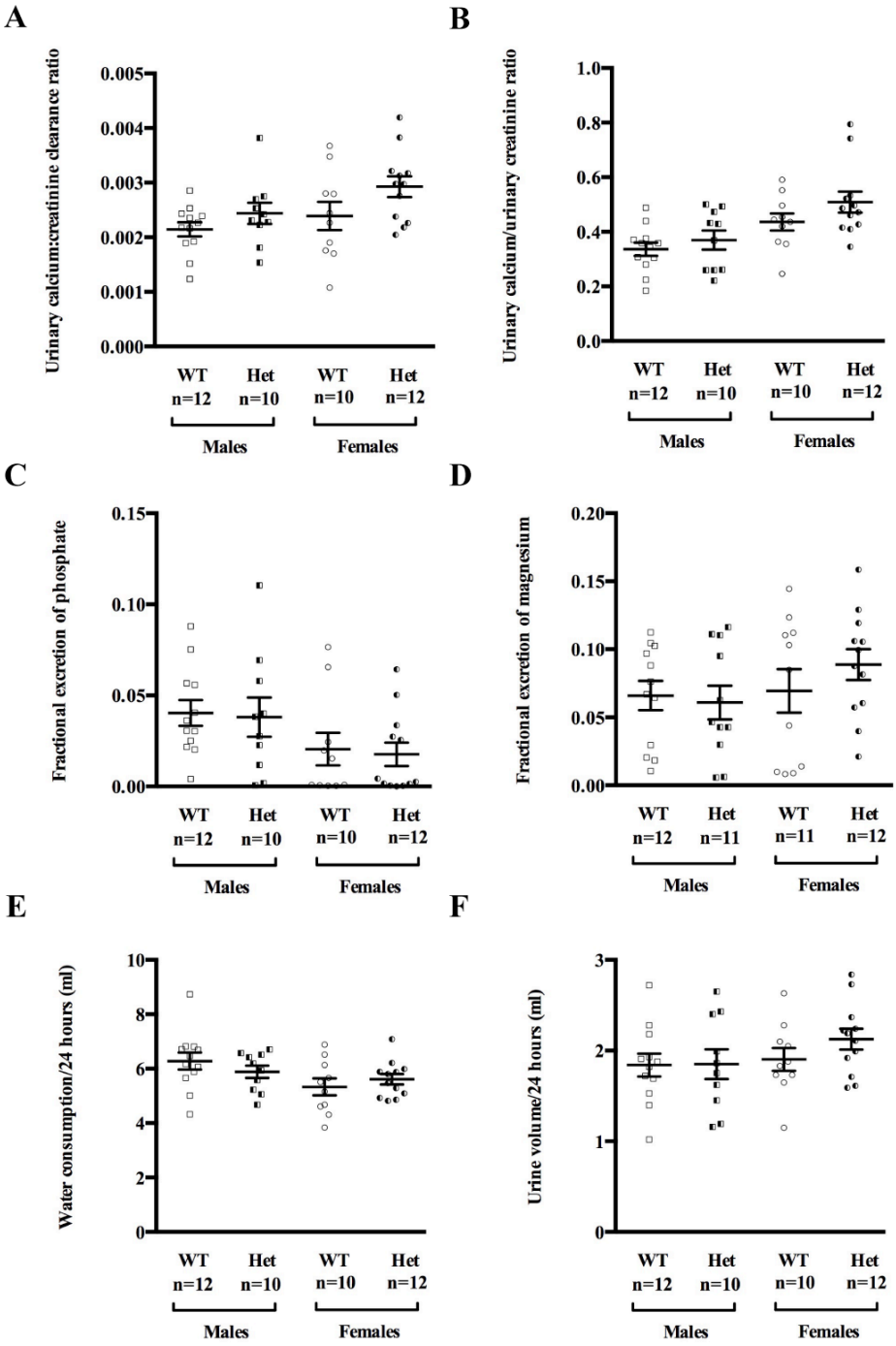


Figure 6.9. Urinary biochemistry of *Ap2s1* IVS 2+2T>C *Ap2s1*$^{+/+}$ and *Ap2s1*$^{+/-}$ mice at 12 weeks of age obtained from metabolic cage studies.

(**A-F**) 12 week old mice were individually housed in metabolic cages and fed on standard chow. 24 hour water consumption and urine volume were recorded. Urine samples were taken for analysis. Mean ± SEM are represented by horizontal lines and error bars respectively. Sex-matched groups were compared using an unpaired Mann-Whitney test. A value of $p<0.05$ was considered to be statistically significant. No significant difference was identified between *Ap2s1*$^{+/+}$ (WT) and *Ap2s1*$^{+/-}$ (het) sex-matched mice for the following parameters: (**A**) CCCR. (**B**) Urinary calcium-to-urinary creatinine ratio. (**C**) Fractional excretion of phosphate. (**D**) Fractional excretion of magnesium. (**E**) 24 hour water consumption (ml) (**F**) 24 hour urine volume (ml).

6.1.5.3 Expression of AP-2 subunits in *Ap2s1* IVS 2+2T>C ENU-mutagenised mice

To investigate the effects of the *Ap2s1* IVS 2+2T>C mutation on the expression of the AP-2 subunits at the RNA and protein level, RT-qPCR and Western blot analysis were performed using lysates extracted from the kidneys of 12 week old $Ap2s1^{+/+}$ and $Ap2s1^{+/-}$ mice (males, n=2 for each genotype; females, n=2 for each genotype; described in sections 3.2.3.3 and 3.2.4.3). No differences were demonstrated in the levels of RNA expression of the AP-2 subunit genes, *Ap2a1* encoding AP2α, *Ap2b1* encoding AP2β2, *Ap2m1* encoding AP2μ2 and *Ap2s1* encoding AP2σ2, in the $Ap2s1^{+/-}$ mice compared with $Ap2s1^{+/+}$ mice (Figure 6.10). Consistent with this result, there was also no difference in the levels of protein expression of the AP-2 subunits, AP2α, AP2β2, AP2μ2 and AP2σ2, in $Ap2s1^{+/-}$ and $Ap2s1^{+/+}$ mice. These findings suggest the stability of AP-2 is not compromised in the heterozygous state.

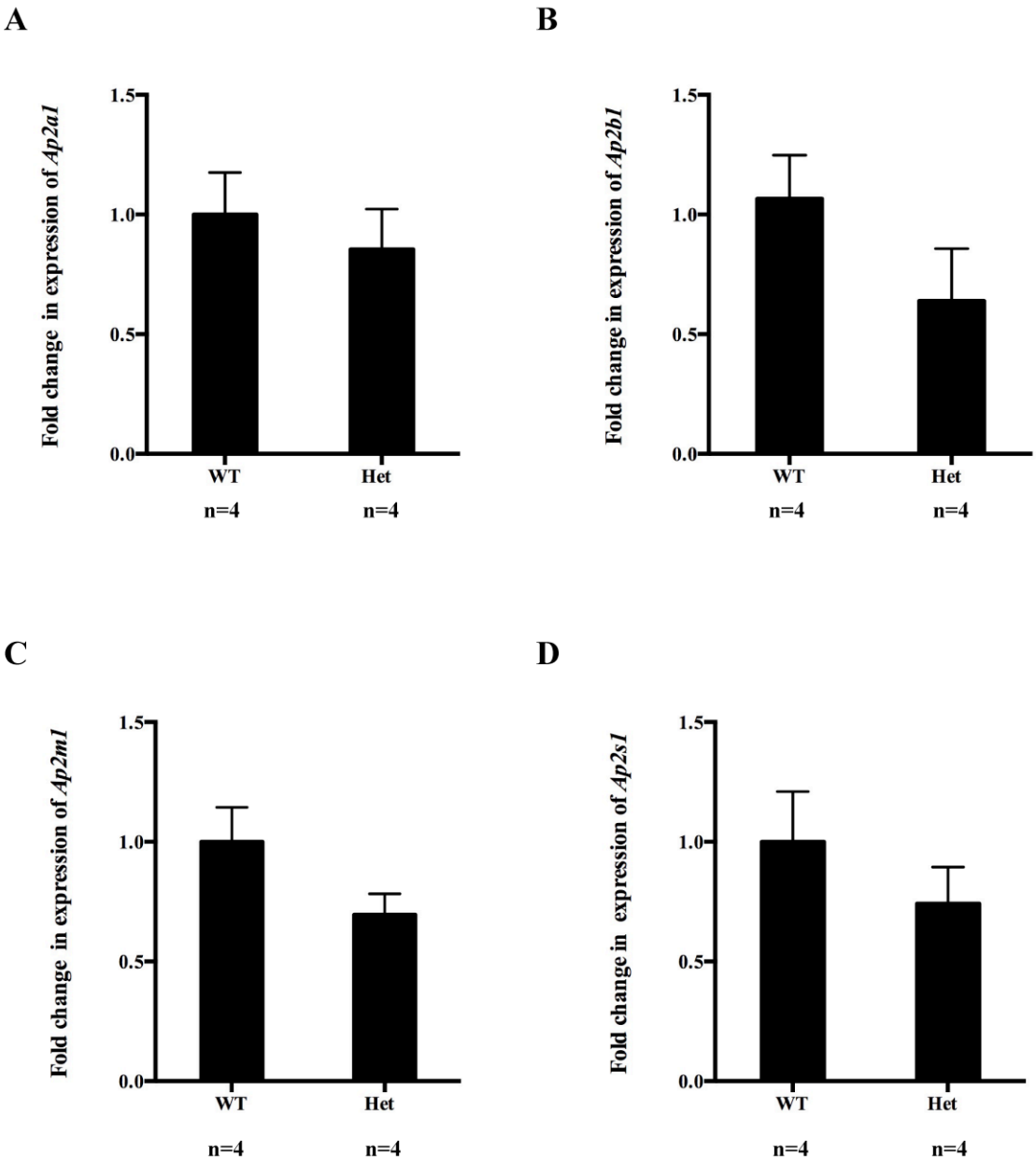


Figure 6.10. RT-qPCR analysis of the AP-2 subunit genes, *Ap2a1*, *Ap2b1*, *Ap2m1* and *Ap2s1*, in the kidney lysates of four *Ap2s1*$^{+/+}$ and *Ap2s1*$^{+/-}$ mice to investigate RNA expression.

The target gene Ct value was expressed relative to the geometric mean Ct value of two housekeeper genes (*Gapdh* and *Act*), and normalised to the mean target gene/housekeeper gene Ct value from the four *Ap2s1*$^{+/+}$ (Wt) mice. (A-D) The mean normalised target gene/housekeeper gene values obtained from a triplicate analysis of each Wt and *Ap2s1*$^{+/-}$ (Het) sample are shown expressed relative to Wt. SEM is represented by the error bar. Results for WT and Het mice were compared using an unpaired Student's *t*-test. A value of $p<0.05$ was considered to be statistically significant. No significant difference was identified between WT and Het mice for any of the AP-2 subunit genes analysed. (**A**) *Ap2a1* (**B**) *Ap2b1* (**C**) *Ap2m1* (**D**) *Ap2s1.*

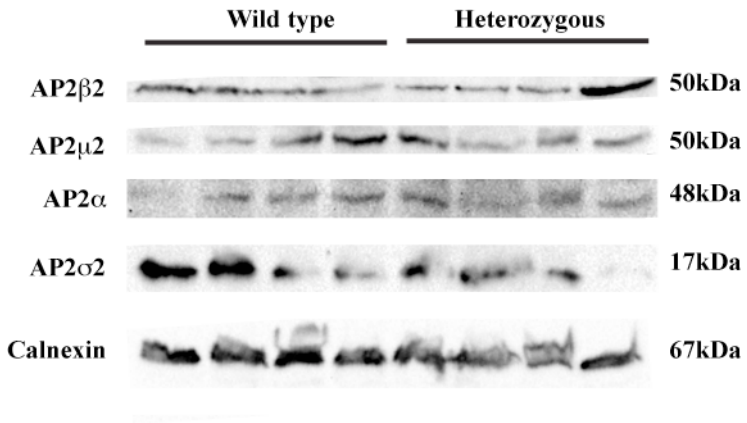


Figure 6.11. Western blot analysis showing expression of the AP-2 subunits in the kidney lysates of four *Ap2s1*$^{+/+}$ and *Ap2s1*$^{+/-}$ mice.

Expression of the β2, μ2, α and σ2 subunits of AP-2 in lysates extracted from the kidneys of four *Ap2s1*$^{+/+}$ (wild type) and *Ap2s1*$^{+/-}$ (heterozygous) mice (n=2 male and n=2 female for each genotype) are shown. Calnexin is used as a loading control for the amount of cellular protein content.

6.1.5.4 Assessment of mice homozygous for the *Ap2s1* IVS 2+2T>C mutation

To investigate the phenotype of mice homozygous for the *Ap2s1* IVS 2+2T>C mutation (*Ap2s1*$^{-/-}$), G2 *Ap2s1*$^{+/-}$ mice were intercrossed to generate G3 mice (Figure 6.7). *Ap2s1*$^{+/-}$ mice showed no evidence of subfertility with 24 live progeny born (Table 12). A Mendelian pattern of inheritance, however, was not seen in G3 with 15 *Ap2s1*$^{+/+}$, 9 *Ap2s1*$^{+/-}$ and no *Ap2s1*$^{-/-}$ progeny born (χ^2 test, $p<0.02$; Table 12). Viability is typically assessed using a minimum of 28 genotype-confirmed, live progeny from heterozygous intercrosses,[312] where zero homozygotes from 28 progeny would give 95% confidence that the probability of homozygote survival was ≤40%, based on binomial probability calculations. However, zero homozygotes from 24 progeny gave 95% confidence that the probability of homozygote survival was ≤50%, based on binomial probability calculations. To determine the developmental stage at which the *Ap2s1*$^{-/-}$ embryos were dying, staged embryo analysis was performed with embryo analysis commencing at E12.5, corresponding to mid-gestation.

Table 12. Observed and expected numbers of mice as predicted by Mendelian inheritance of the *Ap2s1* IVS 2+2T>C mutation in the third generation of mice

Ap2s1 IVS 2+2T>C Genotype	Observed number of mice	Expected number of mice
$Ap2s1^{+/+}$	15	6
$Ap2s1^{+/-}$	9	12
$Ap2s1^{-/-}$	0	6
Total number of mice	24	24

$p<0.02$ (Ratios of genotypes were tested for goodness of fit to expected Mendelian segregation (1:2:1) by χ^2 analysis, calculated for two degrees of freedom).

6.1.5.4.1 Staged embryo analysis

Forty-four embryos were isolated at E12.5 for genotyping and analysis. A loss of Mendelian inheritance at E12.5 was demonstrated with 15 $Ap2s1^{+/+}$ embryos (~34%), 28 $Ap2s1^{+/-}$ embryos (~64%), and 1 $Ap2s1^{-/-}$ embryo genotyped (~2%) (χ^2 test, $p<0.002$) (Table 13).

Table 13. Observed and expected numbers of E12.5 embryos as predicted by Mendelian inheritance of the *Ap2s1* IVS 2+2T>C mutation.

Genotype	Observed number of embryos	Expected number of embryos
$Ap2s1^{+/+}$	15	11
$Ap2s1^{+/-}$	28	22
$Ap2s1^{-/-}$	1	11
Total number of embryos	44	44

$p<0.002$ (Ratios of genotypes were tested for goodness of fit to expected Mendelian segregation (1:2:1) by χ^2 analysis, calculated for two degrees of freedom).

Based on binominal probability calculations, the homozygote survival rate at E12.5 was <20%. Analysis of the E12.5 embryos revealed a resorption rate of 19%. The resorptions were not genotyped. Resorption consists of four stages commencing with

growth retardation, followed by bradycardia and pericardial oedema, overall development ceases and the embryo dies.[313] Resorption of the remnants by the maternal immune cells then occurs.[313] It is likely the resorptions represent mostly dead *Ap2s1*$^{-/-}$ embryos. These findings suggest that the *Ap2s1*$^{-/-}$ embryos were dying at an earlier stage in gestation, and therefore, E9.5 embryos are currently undergoing analysis. Morphological analysis of the E12.5 embryos revealed the *Ap2s1*$^{-/-}$ embryo to be smaller in size and exhibit an overall delay in development compared to the *Ap2s1*$^{+/+}$ embryo (Figure 6.12).

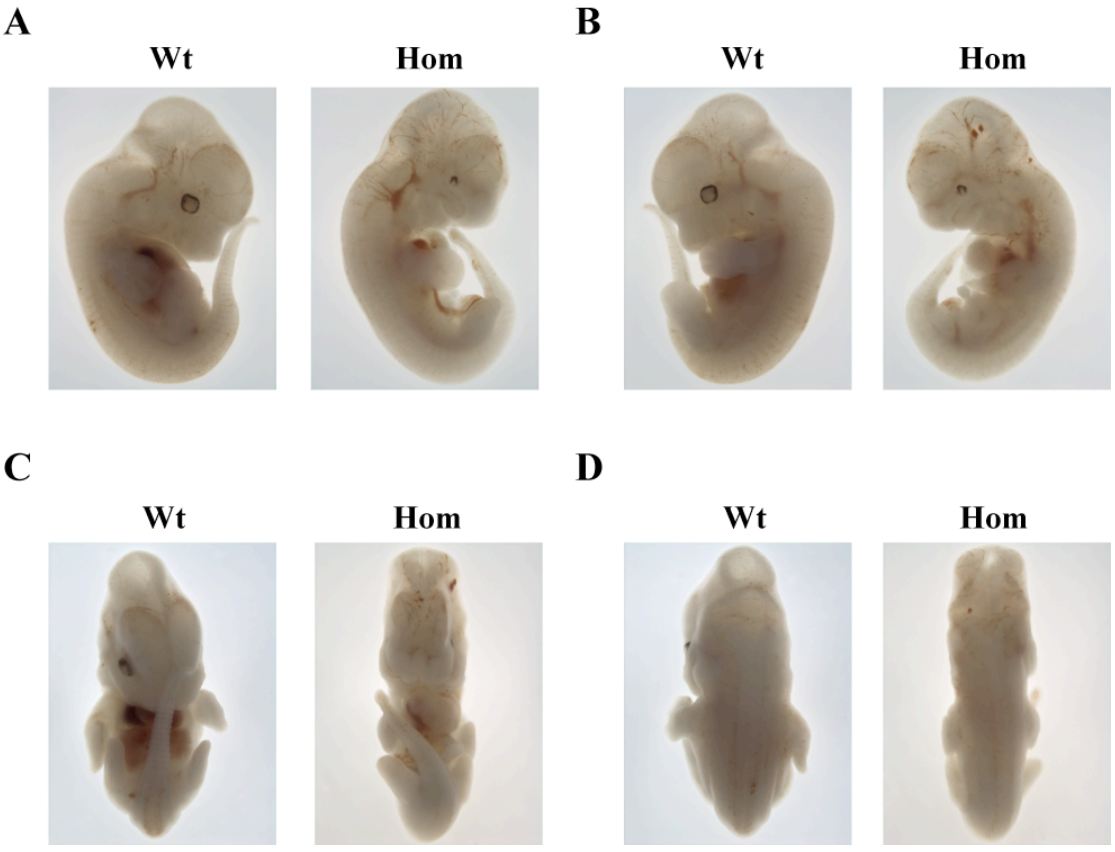


Figure 6.12. Gross morphological appearances of E12.5 *Ap2s1*$^{+/+}$ and *Ap2s1*$^{-/-}$ embryos.

The *Ap2s1*$^{-/-}$ (hom) embryo was smaller in size and exhibited globally delayed development in comparison with the *Ap2s1*$^{+/+}$ (Wt) embryo. (**A**) Right lateral view. (**B**) Left lateral view. (**C**) Ventral view. (**D**) Dorsal view.

6.1.6 Generation of a knock-in mouse model harbouring a heterozygous *Ap2s1* R15L mutation

To investigate the physiological mechanisms underlying FHH3 due to AP2σ2 R15 missense mutations, a mouse model harbouring an *Ap2s1* R15L mutation was generated. The R15L mutation was chosen as preliminary data from the clinical studies had identified probands harbouring AP2σ2 R15L mutations with learning difficulties, short stature, reduced bone mineral density and acute pancreatitis (section 4.1.3.2). Therefore, this mutation was selected to further elucidate the mechanisms underlying the calciotropic and non-calciotropic phenotype seen in these patients, and provide an *in vivo* model for testing of compounds. Generation of a knock-in mouse was initially attempted using transcriptor activator-like effector nucleases (TALENS) technology (section 1.11.2). The TALENs approach is reported to be time- and cost-effective as it involves injection directly into one cell embryos and thus, eliminates the chimera stage.[241] At the time of my study, MRC Harwell were using the TALENs approach to generate mouse models of human disease with good preliminary results.

A TALEN pair was constructed against a sequence comprising exon 2 of *Ap2s1* to bind and cut the target DNA.[238] A repair sequence, used as a donor matrix, to allow incorporation of the *Ap2s1* R15L mutation by homologous recombination but containing 6 silent single nucleotide changes to prevent cutting by the TALEN was also constructed (section 3.2.2.4). The two TALEN mRNAs were microinjected with the *Ap2s1* R15L donor matrix into the pro-nuclei of BL/6J one-cell embryos. The microinjected embryos (approximately 100) were transferred into ten foster mothers and 15 mice obtained from the reimplanted embryos were genotyped to identify

individual founders harbouring the *Ap2s1* R15L mutation. No mice were found to be harbouring the *Ap2s1* R15L mutation. As the C57BL/6J strain is associated with low embryo yields and survival,[238] a second day of microinjections was performed to increase the number of pups born but no mice harbouring the *Ap2s1* R15L mutation were generated from this. Direct mutagenesis with TALENs was therefore abandoned and a clustered regularly interspaced short palindromic repeats (CRISPR)-Cas9 approach adopted (section 1.11.2).

6.1.7 Discussion and future studies

Screening of the MRC Harwell ENU-induced DNA archive yielded the splice site mutation, *Ap2s1* IVS 2+2T>C, predicted to result in a truncated mutant AP2σ2 protein with altered tertiary structure. *In vivo* studies demonstrated that mice heterozygous for the *Ap2s1* IVS 2+2T>C mutation were phenotypically normal and showed no alteration in RNA or protein expression of the AP-2 subunits when compared to WT littermates. This suggested that stable mutant AP-2 complexes were forming *in vivo* and ≤50% WT AP2σ2 function results in a normal phenotype.

Heterozygous intercrosses yielded no live-born homozygous mice and staged embryo analysis demonstrated homozygous mutant embryos were dying before E12.5. Thus the homozygous *Ap2s1* IVS 2+2T>C mutation represents a functional homozygous knock-out of *Ap2s1*. The AP2σ2 functional knock-out has similar characteristics to other animal models where adaptor protein subunits are knocked-out by embryonic stem cell-based gene targeting. In both the AP2β2 and AP2μ2 heterozygous knockout mouse models, the mice were phenotypically normal.[250 251] In homozygous knockout

adaptor protein subunit knockout animals, two phenotypes are seen. The first phenotype is characterised by embryo death early in gestation suggesting the subunits involved are essential for cell viability. Examples include the AP2μ2 homozygous knockout mice, which were embryonic lethal before E3.5[250] and the AP2α homozygous knockout zebrafish, which do not survive beyond 24 hours post-fertilisation due to pleomorphic early patterning and axis formation abnormalities.[314] The second phenotype is characterised by embryos which die later in gestation, suggesting these subunits are required for normal development rather than cell viability. An example includes the AP2β2 homozygous knockout mice which had cleft palate deformities and died in the postnatal period.[251] The preliminary findings from the functional knock-out *Ap2s1* mice suggest that AP2σ2 may be essential for cell viability.

To identify the stage at which the homozygous mutant embryos die, embryo analysis at E9.5 is currently being performed. E9.5 is a critical point in development as both establishment of the chorioallantoic placenta from the mesodermally-derived extraembryonic structures and the development of the circulation within the embryo are occurring.[315] Failure of coordination of these two events can result in embryo death.[315] E9.5 has been chosen as it is likely that the resorptions identified at E12.5 represent homozygous embryos that died after implantation but before or just after establishment of the chorioallantoic placenta. Histopathological assessment of the embryos at E9.5 with examination of placentation and vascularisation will identify if this is the case.

It is probable that the loss of the 17 amino acids upstream of the 3' end of exon 2 of *Ap2s1* is responsible for the phenotype seen in the homozygous knockout mice. APσ is highly conserved amongst orthologues (Figure 6.13A) and paralogues (Figure 6.13B) and the region deleted by the splice site mutation includes several conserved residues (Figure 6.13), suggesting these residues play a significant role in the function of the protein.

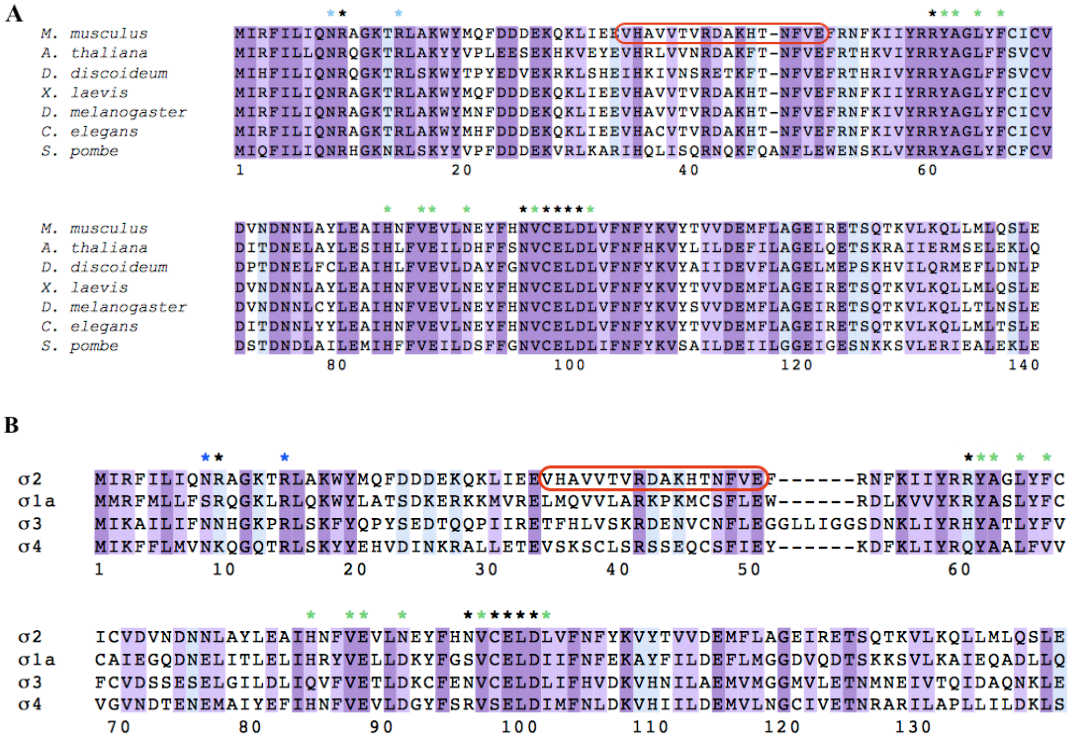


Figure 6.13. Amino acid residue conservation between APσ orthologues and paralogues.

APσ amino acid sequences are aligned to demonstrated conservation of residues between (**A**) AP2σ2 orthologues and (**B**) APσ paralogues. The conservation is displayed as follows: deep purple represents absolute conservation; and light purple represents moderate degree of conservation. The amino acids deleted from AP2σ2 by the splice site mutation are outlined in red (V35 to E51 inclusive). Coloured astericks indicate residues involved in binding to cargo proteins: blue, indicate residues involved in binding to the -4 position peptide residue; green, indicate residues binding to the dileucine motif; and black, indicate residues binding elsewhere. Adapted from Kelly *et al*. 2008.[129]

Additionally, it is predicted that deletion of the residues by the mutation will result in disruption of the two adjacent hydrophobic pockets involved in binding to the dileucine motif of cargo proteins[129] (Figure 6.13). Structural modelling, performed

using the Phyre2 protein structure prediction software[311], predicted the positions of residues known to bind to the dileucine motif of transmembrane proteins[129] in the mutant AP2σ2 to be altered compared to WT (Figure 6.14).

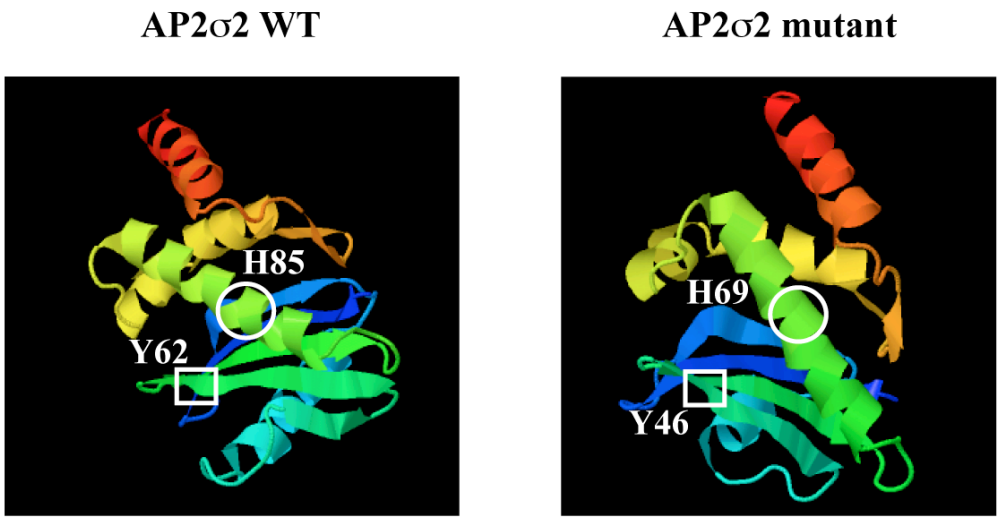


Figure 6.14. Structural modelling of mutant and WT AP2σ2 showing altered positions of the residues involved in binding to the dileucine motifs in transmembrane proteins.

Structural modelling of AP2σ2 was performed using the Phyre2 protein structure prediction software[311] and the protein coloured by the rainbow from N to C terminus. (**A**) AP2σ2 WT with positions of residues Y62 (white square) and H85 (white circle) involved in binding to dileucine motifs shown within the protein. (**B**) The *Ap2s1* IVS 2+2T>C mutation results in a mutant AP2σ2 lacking 17 of the 50 amino acids which alters the positions of the Y and H residues to Y46 and H69, respectively.

Clathrin-mediated endocytosis is essential during embryogenesis, for nutrient uptake into cells and morphogenesis.[252] To investigate global clathrin-mediated endocytosis in the homozygous mutant embryos, mouse embryonic fibroblasts (MEFs) will be established and uptake studies of transferrin and LDL cholesterol performed. This will confirm if the phenotypes observed in the mice are due to nutrient uptake defects (in which case the results of uptake studies are likely to be reduced uptake in mutant cells), or due to specific effects on developmental pathways. For example, clathrin-mediated endocytosis is known to be important in Wnt/Beta-catenin[316] and Notch[317] signalling. Initial investigations into the ability of mutant cells to perform uptake of

global clathrin-mediated endocytic ligands such as transferrin and LDL will then inform whether further investigation of developmental pathways is required.

Little is known regarding the global trafficking of CaSR and how AP2σ2 relates to this. The effect of the mutant AP2σ2 on cellular signalling and trafficking is yet to be elucidated. This mouse model represents an ideal resource from which to study these fundamental concepts. MEFs will be established from the mice and used in studies utilising techniques such as advanced microscopy including TIRF and dynamic live-cell imaging using Förster resonance energy transfer (FRET), and measurement of intracellular Ca^{2+} responses at the single cell level using the calcium-binding dye, Fura-2.[120 318 319] Additionally, the MEFs could be transfected with AP2σ2 WT or mutant with the advantage of their lack of endogenous WT AP2σ2 expression. Knockdown studies using siRNA aim for undetectable levels of AP2σ2 but are often limited by the persistence of a small quantity of endogenous AP2σ2. These cells will be used to investigate the effects of AP2σ2 on trafficking of CaSR using the techniques outlined above. This will provide a 'cleaner' system without the problem of endogenous protein effects on parameters being measured.

The attempt to generate a mouse model harbouring an *Ap2s1* R15L mutation using TALENS technology was unsuccessful. This method of targeted gene editing relies on homology-directed repair and data published predicts the expected mutagenesis rate to be in the range of 10-40%, [238] however this varies depending on the target site in the genome and the amount of RNA injected.[241] The co-injections of TALEN pair RNA and *Ap2s1* R15L donor matrix were reported to be toxic to the single cell embryos initially, which has been seen with both TALENs and ZFNs.[241] A reduction in the

amount of RNA injected to reduce cell toxicity may have reduced the mutagenesis rate resulting in failure of the technique. A CRISPR-Cas9 approach has subsequently been adopted as an alternative method of introducing the *Ap2s1* R15L base change directly into the genome of single-cell embryos. The main disadvantage of this strategy is the risk of off-target mutations occurring at sites with similar sequences to the target site.[241] Consequently, whole genome sequencing will need to be performed on any potential founders to screen for off-target mutations.

Genetics of AP2σ2 mutations in ADH

7 Genetics of AP2σ2 mutations in ADH

Loss-of-function *AP2S1* mutations have been shown to occur in >20% of FHH probands without CaSR mutations (section 4.1.8). ADH can be caused by gain-of-function mutations of *CASR* (ADH1),[209 210 214] which accounts for more than 70% of ADH cases, or gain-of-function mutations of *GNA11* (ADH2), of which two cases have been reported.[197] Gain-of-function *AP2S1* mutations have not been identified to date, and it was hypothesised, by analogy to the situation in ADH1 and ADH2, that such gain-of-function mutations may result in an additional form of ADH. To identify possible gain-of-function *AP2S1* mutations, hypocalcemic probands with phenotypes consistent with ADH or isolated hypoparathyroidism were selected for PCR amplification and Sanger sequencing of the exons, intron-exon boundaries and UTRs of *AP2S1*. Hypocalcaemic probands with mutations in *CASR*, *GNA11*, homolog of Drosophila glial cell missing 2 gene (*GCMB*) encoding the transcription factor GCMB, or *PTH* mutations were excluded from the analysis.

7.1.1 Statistical analysis and determination of ADH proband sample size

As the prevalence of *AP2S1* mutations in hypocalcaemic probands was not known, a binomial probability calculation was performed in which the prevalence of *AP2S1* mutations was varied (Figure 7.1). This showed that if the prevalences of *AP2S1* mutations in hypocalcaemic probands were 5%, 10%, 15%, or 20%, the sample sizes required to detect at least one *AP2S1* mutation with >95% probability, were n=59, n=29, n=19 and n=14, respectively. Therefore, if the prevalence of *AP2S1* mutations in ADH without *CASR* mutations was assumed to be similar to that observed for *AP2S1*

mutations in FHH without *CASR* mutations (i.e. 20%),[130] a sample size of 19 hypocalcaemic probands would result in a >98% likelihood of detecting at least one *AP2S1* mutation.

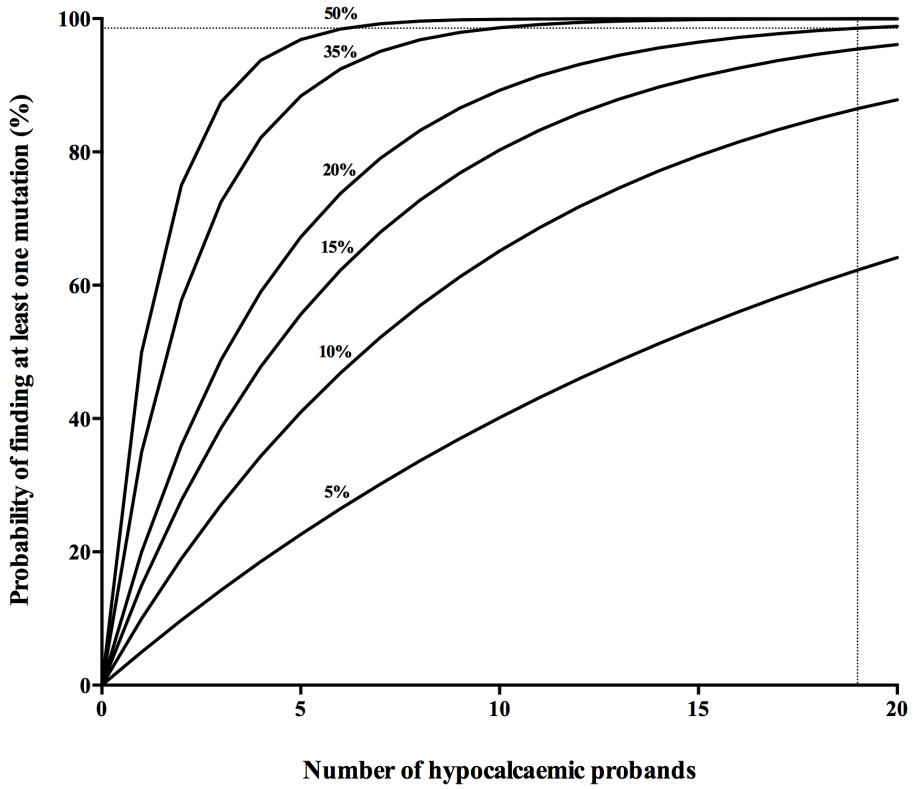


Figure 7.1. Binomial probability analysis to predict sample size required to detect one or more *AP2S1* mutations for different mutation prevalences in hypocalcaemic probands.

The number of probands is shown on the x-axis and the probability of detecting at least one *AP2S1* mutation, at different prevalences ranging from 5% to 50%, is shown on the y-axis. The analysis indicated that a sample size of 19 hypocalcaemic probands (represented by the dotted line) is required to detect at least one *AP2S1* mutation at a 20% prevalence, similar to that observed in FHH without CaSR mutations, with a probability of >98%.

7.1.2 Clinical and biochemical features of probands with ADH

Nineteen unrelated probands (13 males and 6 females) with hypocalcaemia consistent with isolated hypoparathyroidism were included in the study (Table 14). Previous sequence analysis of *CASR*, *GNA11, GCMB* and *PTH* had not identified any mutations. The probands did not have features of autoimmune disease, immunodeficiency, deafness, cardiofacial abnormalities, or a history of neck surgery. As the probands had non-syndromic hypoparathyroidism, fluorescent-*in situ*-hybridisation to detect deletions and translocations of chromosome 22q associated with DiGeorge syndrome was not performed.

More than 65% of probands presented with hypocalcaemic symptoms, with ages at diagnosis or presentation that ranged from the neonatal period to 60 years (Table 14). Over 70% of the probands had severe hypocalcaemia (defined as adjusted serum calcium <1.90 mmol/L; normal range 2.10-2.60 mmol/L). Six probands (~33%) had a family history of hypocalcaemia (Table 14). Approximately 85% of probands had serum PTH concentrations that were either below or within the normal range (normal range: 10-65 ng/L; 1.3-7.6 pmol/L). More than 60% of the probands had elevated serum phosphate concentrations and 25% had serum phosphate concentrations in the high normal range. Hypomagnesaemia was found in 30% of probands (mean serum magnesium±SEM= 0.77±0.03mmol/L, n=16) and serum alkaline phosphatase activity was within the normal range in 80% probands (n=18). Urinary calcium excretion was inappropriately elevated in 30% of probands (mean CCCR±SEM= 0.02±0.005, n=12). These findings are similar to those reported in ADH1 probands.[320 321]

Table 14. Clinical and biochemical findings in the 19 hypocalcaemic probands.

					Serum							Urine
Patient	**Sex**	**Family history**	**Age (years)**	**Clinical features at presentation/ diagnosis**	**Calcium (mmol/L)[a]**	**Phosphate (mmol/L)[b-c]**	**ALP (U/L)[d,e]**	**Mg (mmol/L)[f]**	**Creatinine (µmol/L)[g]**	**PTH [h,i]**	**25OHD (nmol/L)[j]**	**CCCR[k-m]**
15/01	M	No	55	Asymptomatic	1.99	1.28[b]	95[d]	0.8	180	2.0[h]	-	0.01[k]
07/02	M	Sons affected	46	Cataracts	1.35	1.9[b]	49[d]	-	49	5.0[h]	-	-
08/03	M	No	60	Asymptomatic	1.63	1.38[b]	104[e]	0.93	-	1.6[i]	-	0.003[k]
05/04	F	Yes[n]	Neonate	Seizures	1.62	3.10[c]	228[e]	0.65	49	0.8[i]	-	0.004[k]
13/04	F	Son affected	53	Asymptomatic	1.93	0.87[b]	53[d]	0.86	81	4.7[i]	77.5	0.018[k]
05/05	M	Mother and sister affected	3	Asymptomatic	2.03	1.91[c]	129[e]	0.97	49	1.1[i]	85	0.05[k]
16/07	M	No	9	Seizures	1.86	2.77[b]	336[e]	0.7	49	5.6[i]	105	0.04[k]
01/08	M	No[o]	2	Seizures	0.94	2.20[c]	432[e]	0.73	47	2.6[i]	<18	0.02[k]
19/09	F	No	68	Asymptomatic	1.91	1.21[b]	91[d]	0.68	75	18[h]	64	0.004[k]
19/10	M	-	1 mth	Seizures	1.63	3.29[c]	104[d]	0.68	30	3.6[i]	43	-
01/12	F	No[o]	2 mths	Seizures	1.25	2.52[c]	388[e]	0.57	<18	1.4[i]	101	1.25[l]
09/12	M	No[o]	2 mths	Seizures	1.30	2.35[c]	-	-	25	<0.3[i]	17	0.001[k]
16/12	M	Father affected	31	Carpopedal spasm	1.88	1.73[b]	52[d]	-	88	0.7[i]	35	0.008[k]
04/13	M	No	62	Paraesthesia	1.64	1.43[b]	53[d]	0.76	104	22[h]	29	13.5[m]
07/13	M	No	2	Seizures	1.37	3.74[c]	125[e]	1.03	38	1.6[i]	36	0.006[k]
10/13	F	No	25	Tetany	1.53	1.55[b]	131[e]	0.70	61	<0.3[i]	50	-
15/13	M	Father affected	57	Polyuria	1.94	0.96[b]	74[d]	0.93	84	26[h]	86	8.94[m]
19/13	F	No	9	Seizures	1.35	3.32[c]	166[e]	0.64	52	<0.3[i]	18	0.05[k]
25/13	M	No	31	Tetany, cataracts	1.31	1.20[b]	155[e]	0.73	80	0.3	27	0.03[m]

All serum and urine estimations were undertaken at a time when the probands were not being treated with vitamin D preparations or calcium supplementation. Normal serum ranges [322]: albumin-adjusted calcium [a]2.10-2.60 mmol/L; phosphate [b]0.70-1.40 mmol/L, [c]1.20-2.10 mmol/L; alkaline phosphatase (ALP) activity [d]30-130 U/L, [e]70-330 U/L; magnesium (Mg) [f]0.70-1.05 mmol/L; creatinine [g]54-145 µmol/L; PTH [h]10-65 ng/L, [i]1.3-7.6 pmol/L; 25-hydroxyvitamin D (25OHD) [j] >50 nmol/L. Normal urine ranges [322]: calcium to creatinine clearance ratio (CCCR) [k] >0.02; calcium to creatinine ratio [l] 0.1-0.7; 24-hour urine calcium excretion [m] >4.0 mmol/24 hours. [n]Details of affected members not available. [o]Patient is the offspring of consanguineous unaffected parents. M, male; F, female; not known, -. Thirteen probands were White Europeans and six probands (01/08, 19/10, 01/12, 9/12, 16/12, 25/13) were of Asian or Middle Eastern origin. The age at presentation or diagnosis is provided. 50% of ADH patients are asymptomatic and hence the age of presentation is the same as that at diagnosis; however, if the age at presentation and diagnosis are not the same, then the age at diagnosis is provided. Other family members were unavailable for studies.

7.1.3 Dideoxynucleotide sequence analysis in the ADH probands

Dideoxynucleotide sequence analysis of the 429 bp coding region of *AP2S1* and the 8 intron-exon boundaries in the 19 hypocalcaemic probands (Table 15) did not detect any point mutations, deletions, insertions or unreported SNPs. Additionally, an examination of the four reported synonymous *AP2S1* SNPs (rs201984742 (Ile5Ile), rs150080027 (Asp25Asp), rs151335841 (Phe87Phe), and rs143384246 (Asn92Asn)), the non-synonymous *AP2S1* SNPs (rs76488045 (Tyr59Ser) and rs11550738 (Cys68Ser)) and the splice donor variant (rs112326072) revealed the presence of only the major alleles in the hypocalcaemic probands. These findings suggest that *AP2S1* gain-of-function mutations are unlikely to be a major cause of ADH.

CASR dideoxynucleotide sequence analysis identified 7 probands harbouring 3 known non-synonymous *CASR* SNPs located in exon 7 (Table 15). The effects of the 3 *CASR* SNPs on CaSR protein function were predicted to be benign by Polyphen-2.[286] *GNA11* dideoxynucleotide sequence analysis identified 8 probands harbouring 3 known *GNA11* SNPs (Table 15): rs4900, a synonymous SNP located in exon 6; rs11085000, located in intron 2; and rs308046, located in intron 5. The intronic SNPs were predicted to have no effect on their respective splice sites by the splice site prediction programs, Berkeley Drosphilia Genome Project (BDGP)[287] and GeneSplicer.[288]

Table 15. ***CASR*** **and** ***GNA11*** **heterozygous SNPs identified in hypocalcemic probands.**

Proband	*CASR*				*GNA11*			
	rs number	**cDNA change (protein change)**	**Exon**	**MAF (%)**	**rs number**	**cDNA change (protein change)**	**Exon/Intron**	**MAF (%)**
05/05		-	-	-	rs308046	c.736-20T>G	Intron 5	18.4
					rs4900	c.771C>T	Exon 6	38.2
01/08	-	c.3031G>C (Glu1011Gln)	Exon 7	8.2		-	-	-
01/12	rs1801725	c.2956G>T (Ala986Ser)	Exon 7	11.2	rs4900	c.771C>T	Exon 6	38.2
09/12	rs1801725	c.2956G>T (Ala986Ser)	Exon 7	11.2		-	-	-
16/12	rs1042636	c.2968A>G (Arg990Gly)	Exon 7	6.3	rs11085000	c.321+18T>G	Intron 2	36.6
					rs4900	c.771C>T	Exon 6	38.2
04/13		-	-	-	rs4900	c.771C>T	Exon 6	38.2
07/13	-	c.3031G>C (Glu1011Gln)	Exon 7	8.2		-	-	-
10/13		-	-	-	rs4900	c.771C>T	Exon 6	38.2
15/13		-	-	-	rs4900	c.771C>T	Exon 6	38.2
19/13	rs1042636	c.2968A>G (Arg990Gly)	Exon 7	6.3		-	-	-
25/13	rs1801725	c.2956G>T (Ala986Ser)	Exon 7	11.2		-	-	-

Variants are numbered in relation to the *CASR* and *GNA11* cDNA reference sequence (GenBank accession numbers NM_000388.3 and NM_002067.3, respectively), whereby nucleotide +1 corresponds to A of the ATG-translation initiation codon. The amino acid changes for non-synonymous SNPs are provided in parentheses.

7.1.4 Discussion and future studies

Coding region *AP2S1* mutations were not identified in the hypocalcemic probands who had clinical features consistent with isolated hypoparathyroidism, in whom no genetic cause had previously been identified. Thus, *AP2S1* mutations are unlikely to be a cause of ADH. This finding is consistent with a larger study of 60 probands (10 familial and 50 sporadic cases) with isolated hypoparathyroidism without *CASR, GCMB* and T-box transcription factor gene (*TBX1*) mutations, which identified no mutations in *AP2S1*.[323] It remains possible that these probands may harbour mutations in the non-coding regulatory regions of *AP2S1* that result in a gain of CaSR function and hypocalcaemia. However, as AP-2 is a heterotetrameric complex, it is difficult to predict how a mutation in a single subunit would result in a gain-of-function in the complex. Only loss-of-function mutations of other adaptor protein complexes have been reported to date.[253 324] Loss-of-function mutations of *AP3B1*, which encodes the β3A subunit of AP-3, have been identified in probands with Hermansky-Pudlak syndrome, which is associated with oculocutaneous albinism, platelet dysfunction and abnormalities of lysosomal storage.[253] Additionally, a homozygous splice site mutation of *AP1S1*, which encodes the σ subunit of AP-1, is associated with a syndrome characterised by mental retardation, enteropathy, deafness, peripheral neuropathy, ichthyosis and keratoderma (MEDNIK).[324]

To identify the genetic causes in the remaining <30% of ADH probands, unrelated individuals and families with ADH without *CASR, GNA11, GCMB* and *PTH* mutations will be analysed by whole genome or whole exome sequencing. The families are not large enough for gene localisation using linkage analysis and a candidate gene approach is unfeasible given the large number of potential pathway components. This project is currently underway.

8 Summary

The aim of this thesis was to increase understanding of the role of AP2σ2 in calcium homeostasis. This was achieved using a combination of genetic and phenotypic studies in FHH3 probands, *in vitro* and *in vivo* studies.

AP2σ2 mutational analysis in FHH probands identified an additional 9 FHH3 probands harbouring AP2σ2 mutations, demonstrating that AP2σ2 mutations account for ~7% of all FHH mutations. The AP2σ2 mutations identified only affected the R15 residue, reflecting the importance of this residue in forming polar contacts with a putative dileucine motif in CaSR to give rise to a disorder of calcium homeostasis. Evidence of mutation bias at R15 was demonstrated, with only the heterozygous missense mutations R15C, R15H, and R15L, identified. The other possible amino acid codon changes at the R15 residue have been demonstrated to result in loss of CaSR function *in vitro* but have not been observed in FHH3 probands and the explanation for this is yet to be elucidated. Phenotypic studies of FHH3 probands have demonstrated the occurrence of *de novo* AP2σ2 mutations and revealed that FHH3 probands may present with a non-calciotropic phenotype comprising learning difficulties and acute pancreatitis. Additionally, a bone phenotype not seen in FHH1 comprising reduced BMD is suggestive of abnormal bone remodelling. Studies on EBV-transformed lymphoblastoid cells from FHH3 patients demonstrated harbouring a heterozygous missense AP2σ2 R15C mutation had no effect on the stability of the AP-2 complex *in vivo*.

The CaSR activates its downstream signalling pathways, including the MAPK pathway, through coupling with its associated G-proteins. The AP2σ2 mutations were demonstrated to result in loss of activating phosphorylation events in the MAPK pathway. This suggests a role for AP2σ2 in MAPK-mediated CaSR signalling.

Additionally, the AP2σ2 R15C, R15H, and R15L mutations were revealed to exert differential effects on the $G\alpha_{q/11}$ and MAPK signalling pathways, suggesting mutation-bias signalling: the AP2σ2 R15C mutation was demonstrated to result in downregulation of the $G\alpha_{q/11}$ and MAPK signalling pathways; the AP2σ2 R15H mutation resulted in severe impairment of the $G\alpha_{q/11}$ signalling pathway whereas the MAPK signalling pathway was unaffected; and the AP2σ2 R15L mutation caused severe impairment of the $G\alpha_{q/11}$ signalling pathway and downregulation of the MAPK signalling pathway. Understanding the effects of the AP2σ2 mutations on the other Gα signalling pathways will elucidate the mechanisms underlying the role of AP2σ2 in CaSR signalling.

Clathrin-mediated endocytosis is crucial during embryogenesis, with roles including nutrient uptake and sensing morphogen gradients essential for patterning. This thesis has demonstrated that mice heterozygous for the *Ap2s1* splice site mutation, predicted to produce a truncated AP2σ2 protein lacking 17 amino acids, were phenotypically normal. It was demonstrated that the mutant AP-2 complex had no effect on protein complex formation *in vivo*. However, mice homozygous for an *Ap2s1* splice site mutation, were lethal before E12.5, suggesting AP2σ2 is essential for cell viability in the developing embryo. The exact stage of embryo death is yet to be elucidated. MEFs from homozygous embryos will be used to study the role of AP2σ2 in CaSR trafficking. Additionally, the AP2σ2 R15L knock-in mouse model, generated using Cas9-CRISPR technology, will be studied using metabolic cage analysis, behavioural tasks, immunohistochemistry, DXA, microCT, and primary cell lines will be established to study CaSR signalling *in vitro*.

Much remains to be elucidated regarding the post-endocytic sorting of the CaSR and the role of AP2σ2. It is now widely recognised that GPCRs can signal via non-canonical pathways[116 319] and that this can be closely linked to their endosomal location.[135] Future studies to elucidate the post-endocytic sorting of the CaSR and the role of AP2σ2 and the MAPK pathway in non-canonical CaSR signalling are required. MEFs from homozygous *Ap2s1* embryos will be essential to study the role of AP2σ2 in CaSR signalling and trafficking studies. The β-arrestins have been demonstrated to activate signalling pathways downstream of β_2AR independently of G-protein activation by acting as a scaffold for the assembly of proteins including those involved in the ERK1/2 pathway (Figure 1.21).[137] The interactions between β-arrestins, AP2σ2 and the ERK1/2 pathway for CaSR are yet to be elucidated and this is another area for future studies.

Finally, postulating that as gain-of-function CaSR and Gα11 mutations cause ADH1 and ADH2, respectively, a sample of 19 hypocalcaemic probands with isolated hypoparathyroidism and ADH were investigated for the presence of AP2σ2 mutations. My study demonstrated the absence of AP2σ2 mutations in isolated hypoparathyroidism and ADH. As the mutation is unknown in ~30% of cases of ADH, whole exome and whole genome studies should be performed.

In conclusion, this thesis has shown that probands with FHH3 have a broader phenotype compared to that seen in FHH1. The studies are the first to demonstrate a role for AP2σ2 in CaSR signalling through the MAPK signalling pathway. Furthermore, the establishment of the homozygous *Ap2s1* splice site mutation mouse model is the first to show that AP2σ2 is essential for normal embryogenesis.

9 References

1. Brown EM. Extracellular Ca2+ sensing, regulation of parathyroid cell function, and role of Ca2+ and other ions as extracellular (first) messengers. Physiol Rev 1991;**71**(2):371-411.
2. Berridge MJ. Elementary and global aspects of calcium signalling. J Physiol 1997;**499 (Pt 2)**:291-306.
3. Carafoli E. The calcium-signalling saga: tap water and protein crystals. Nat Rev Mol Cell Biol 2003;**4**(4):326-32.
4. Ringer S. A further Contribution regarding the influence of the different Constituents of the Blood on the Contraction of the Heart. J Physiol 1883;**4**(1):29-42 3.
5. Arnold WH, Gaengler P. Quantitative analysis of the calcium and phosphorus content of developing and permanent human teeth. Ann Anat 2007;**189**(2):183-90.
6. Pang ZP, Sudhof TC. Cell biology of Ca2+-triggered exocytosis. Curr Opin Cell Biol 2010;**22**(4):496-505.
7. Ciapa B, Chiri S. Egg activation: upstream of the fertilization calcium signal. Biol Cell 2000;**92**(3-4):215-33.
8. Liu M. The biology and dynamics of mammalian cortical granules. Reprod Biol Endocrinol 2011;**9**:149.
9. Whitaker M. Calcium at fertilization and in early development. Physiol Rev 2006;**86**(1):25-88.
10. Brown EM. The extracellular Ca2+-sensing receptor: central mediator of systemic calcium homeostasis. Annu Rev Nutr 2000;**20**:507-33.
11. Hirsch PF, Baruch H. Is calcitonin an important physiological substance? Endocrine 2003;**21**(3):201-8.
12. Brown EM. Mechanisms underlying the regulation of parathyroid hormone secretion in vivo and in vitro. Current opinion in nephrology and hypertension 1993;**2**(4):541-51.
13. Mannstadt M, Juppner H, Gardella TJ. Receptors for PTH and PTHrP: their biological importance and functional properties. The American journal of physiology 1999;**277**(5 Pt 2):F665-75.
14. Brown EM. Role of the calcium-sensing receptor in extracellular calcium homeostasis. Best Pract Res Clin Endocrinol Metab 2013;**27**(3):333-43.
15. Bilezikian JP, Canfield RE, Jacobs TP, et al. Response of 1alpha,25-dihydroxyvitamin D3 to hypocalcemia in human subjects. N Engl J Med 1978;**299**(9):437-41.
16. Dusso AS, Brown AJ, Slatopolsky E. Vitamin D. Am J Physiol Renal Physiol 2005;**289**(1):F8-28.
17. DeLuca HF. Overview of general physiologic features and functions of vitamin D. Am J Clin Nutr 2004;**80**(6 Suppl):1689S-96S.
18. Riccardi D, Brown EM. Physiology and pathophysiology of the calcium-sensing receptor in the kidney. Am J Physiol Renal Physiol 2010;**298**(3):F485-99.
19. Brown EM, Gardner DG, Brennan MF, et al. Calcium-regulated parathyroid hormone release in primary hyperparathyroidism: studies in vitro with dispersed parathyroid cells. Am J Med 1979;**66**(6):923-31.

20. Brown EM, Wilson RE, Eastman RC, et al. Abnormal regulation of parathyroid hormone release by calcium in secondary hyperparathyroidism due to chronic renal failure. J Clin Endocrinol Metab 1982;**54**(1):172-9.
21. Bas S, Aguilera-Tejero E, Bas A, et al. The influence of the progression of secondary hyperparathyroidism on the set point of the parathyroid hormone-calcium curve. J Endocrinol 2005;**184**(1):241-7.
22. Moallem E, Kilav R, Silver J, et al. RNA-Protein binding and post-transcriptional regulation of parathyroid hormone gene expression by calcium and phosphate. J Biol Chem 1998;**273**(9):5253-9.
23. Naveh-Many T, Rahamimov R, Livni N, et al. Parathyroid cell proliferation in normal and chronic renal failure rats. The effects of calcium, phosphate, and vitamin D. J Clin Invest 1995;**96**(4):1786-93.
24. Li J, Ning Y, Hedley W, et al. The Molecule Pages database. Nature 2002;**420**(6916):716-7.
25. Dixon RA, Kobilka BK, Strader DJ, et al. Cloning of the gene and cDNA for mammalian beta-adrenergic receptor and homology with rhodopsin. Nature 1986;**321**(6065):75-9.
26. Cerione RA, Sibley DR, Codina J, et al. Reconstitution of a hormone-sensitive adenylate cyclase system. The pure beta-adrenergic receptor and guanine nucleotide regulatory protein confer hormone responsiveness on the resolved catalytic unit. J Biol Chem 1984;**259**(16):9979-82.
27. Lerea CL, Somers DE, Hurley JB, et al. Identification of specific transducin alpha subunits in retinal rod and cone photoreceptors. Science 1986;**234**(4772):77-80.
28. Oldham WM, Hamm HE. Heterotrimeric G protein activation by G-protein-coupled receptors. Nat Rev Mol Cell Biol 2008;**9**(1):60-71.
29. Bunemann M, Frank M, Lohse MJ. Gi protein activation in intact cells involves subunit rearrangement rather than dissociation. Proc Natl Acad Sci U S A 2003;**100**(26):16077-82.
30. Digby GJ, Lober RM, Sethi PR, et al. Some G protein heterotrimers physically dissociate in living cells. Proc Natl Acad Sci U S A 2006;**103**(47):17789-94.
31. Attwood TK, Findlay JB. Fingerprinting G-protein-coupled receptors. Protein Eng 1994;**7**(2):195-203.
32. Bjarnadottir TK, Gloriam DE, Hellstrand SH, et al. Comprehensive repertoire and phylogenetic analysis of the G protein-coupled receptors in human and mouse. Genomics 2006;**88**(3):263-73.
33. Lagerstrom MC, Schioth HB. Structural diversity of G protein-coupled receptors and significance for drug discovery. Nat Rev Drug Discov 2008;**7**(4):339-57.
34. Brown EM, Gamba G, Riccardi D, et al. Cloning and characterization of an extracellular Ca(2+)-sensing receptor from bovine parathyroid. Nature 1993;**366**(6455):575-80.
35. Kunishima N, Shimada Y, Tsuji Y, et al. Structural basis of glutamate recognition by a dimeric metabotropic glutamate receptor. Nature 2000;**407**(6807):971-7.
36. Muto T, Tsuchiya D, Morikawa K, et al. Structures of the extracellular regions of the group II/III metabotropic glutamate receptors. Proc Natl Acad Sci U S A 2007;**104**(10):3759-64.
37. Dore AS, Okrasa K, Patel JC, et al. Structure of class C GPCR metabotropic glutamate receptor 5 transmembrane domain. Nature 2014;**511**(7511):557-62.
38. Huang Y, Zhou Y, Castiblanco A, et al. Multiple Ca(2+)-binding sites in the extracellular domain of the Ca(2+)-sensing receptor corresponding to cooperative Ca(2+) response. Biochemistry 2009;**48**(2):388-98.

39. Silve C, Petrel C, Leroy C, et al. Delineating a Ca2+ binding pocket within the venus flytrap module of the human calcium-sensing receptor. J Biol Chem 2005;**280**(45):37917-23.
40. Gurevich VV, Gurevich EV. How and why do GPCRs dimerize? Trends Pharmacol Sci 2008;**29**(5):234-40.
41. Zhang Z, Sun S, Quinn SJ, et al. The extracellular calcium-sensing receptor dimerizes through multiple types of intermolecular interactions. J Biol Chem 2001;**276**(7):5316-22.
42. Ward DT, Brown EM, Harris HW. Disulfide bonds in the extracellular calcium-polyvalent cation-sensing receptor correlate with dimer formation and its response to divalent cations in vitro. J Biol Chem 1998;**273**(23):14476-83.
43. Pidasheva S, Grant M, Canaff L, et al. Calcium-sensing receptor dimerizes in the endoplasmic reticulum: biochemical and biophysical characterization of CASR mutants retained intracellularly. Hum Mol Genet 2006;**15**(14):2200-9.
44. Bai M, Trivedi S, Brown EM. Dimerization of the extracellular calcium-sensing receptor (CaR) on the cell surface of CaR-transfected HEK293 cells. J Biol Chem 1998;**273**(36):23605-10.
45. Chun L, Zhang WH, Liu JF. Structure and ligand recognition of class C GPCRs. Acta Pharmacol Sin 2012;**33**(3):312-23.
46. Pollak MR, Brown EM, Chou YH, et al. Mutations in the human Ca(2+)-sensing receptor gene cause familial hypocalciuric hypercalcemia and neonatal severe hyperparathyroidism. Cell 1993;**75**(7):1297-303.
47. Janicic N, Soliman E, Pausova Z, et al. Mapping of the calcium-sensing receptor gene (CASR) to human chromosome 3q13.3-21 by fluorescence in situ hybridization, and localization to rat chromosome 11 and mouse chromosome 16. Mamm Genome 1995;**6**(11):798-801.
48. Garrett JE, Capuano IV, Hammerland LG, et al. Molecular cloning and functional expression of human parathyroid calcium receptor cDNAs. J Biol Chem 1995;**270**(21):12919-25.
49. Canaff L, Hendy GN. Human calcium-sensing receptor gene. Vitamin D response elements in promoters P1 and P2 confer transcriptional responsiveness to 1,25-dihydroxyvitamin D. J Biol Chem 2002;**277**(33):30337-50.
50. Canaff L, Zhou X, Mosesova I, et al. Glial cells missing-2 (GCM2) transactivates the calcium-sensing receptor gene: effect of a dominant-negative GCM2 mutant associated with autosomal dominant hypoparathyroidism. Hum Mutat 2009;**30**(1):85-92.
51. Tsuchiya D, Kunishima N, Kamiya N, et al. Structural views of the ligand-binding cores of a metabotropic glutamate receptor complexed with an antagonist and both glutamate and Gd3+. Proc Natl Acad Sci U S A 2002;**99**(5):2660-5.
52. Hendy GN, Guarnieri V, Canaff L. Calcium-sensing receptor and associated diseases. Prog Mol Biol Transl Sci 2009;**89**:31-95.
53. Galvez T, Duthey B, Kniazeff J, et al. Allosteric interactions between GB1 and GB2 subunits are required for optimal GABA(B) receptor function. EMBO J 2001;**20**(9):2152-9.
54. Kniazeff J, Bessis AS, Maurel D, et al. Closed state of both binding domains of homodimeric mGlu receptors is required for full activity. Nat Struct Mol Biol 2004;**11**(8):706-13.
55. Downes GB, Gautam N. The G protein subunit gene families. Genomics 1999;**62**(3):544-52.

56. Simon MI, Strathmann MP, Gautam N. Diversity of G proteins in signal transduction. Science 1991;**252**(5007):802-8.
57. Oldham WM, Hamm HE. Structural basis of function in heterotrimeric G proteins. Q Rev Biophys 2006;**39**(2):117-66.
58. Varrault A, Pena MS, Goldsmith PK, et al. Expression of G protein alpha-subunits in bovine parathyroid. Endocrinology 1995;**136**(10):4390-6.
59. Khan MA, Conigrave AD. Mechanisms of multimodal sensing by extracellular Ca(2+)-sensing receptors: a domain-based survey of requirements for binding and signalling. Br J Pharmacol 2010;**159**(5):1039-50.
60. Kifor O, Diaz R, Butters R, et al. The Ca2+-sensing receptor (CaR) activates phospholipases C, A2, and D in bovine parathyroid and CaR-transfected, human embryonic kidney (HEK293) cells. J Bone Miner Res 1997;**12**(5):715-25.
61. Chang W, Pratt S, Chen TH, et al. Coupling of calcium receptors to inositol phosphate and cyclic AMP generation in mammalian cells and Xenopus laevis oocytes and immunodetection of receptor protein by region-specific antipeptide antisera. J Bone Miner Res 1998;**13**(4):570-80.
62. Chang W, Chen TH, Pratt S, et al. Amino acids in the second and third intracellular loops of the parathyroid Ca2+-sensing receptor mediate efficient coupling to phospholipase C. J Biol Chem 2000;**275**(26):19955-63.
63. Quinn SJ, Ye CP, Diaz R, et al. The Ca2+-sensing receptor: a target for polyamines. The American journal of physiology 1997;**273**(4 Pt 1):C1315-23.
64. Ward DT, Maldonado-Perez D, Hollins L, et al. Aminoglycosides induce acute cell signaling and chronic cell death in renal cells that express the calcium-sensing receptor. J Am Soc Nephrol 2005;**16**(5):1236-44.
65. Nemeth EF. Allosteric modulators of the extracellular calcium receptor. Drug Discov Today Technol 2013;**10**(2):e277-84.
66. Conigrave AD, Quinn SJ, Brown EM. L-amino acid sensing by the extracellular Ca2+-sensing receptor. Proc Natl Acad Sci U S A 2000;**97**(9):4814-9.
67. Cook AE, Mistry SN, Gregory KJ, et al. Biased allosteric modulation at the CaS receptor engendered by structurally diverse calcimimetics. Br J Pharmacol 2015;**172**(1):185-200.
68. Conigrave AD, Ward DT. Calcium-sensing receptor (CaSR): pharmacological properties and signaling pathways. Best Pract Res Clin Endocrinol Metab 2013;**27**(3):315-31.
69. Fox J, Lowe SH, Petty BA, et al. NPS R-568: a type II calcimimetic compound that acts on parathyroid cell calcium receptor of rats to reduce plasma levels of parathyroid hormone and calcium. J Pharmacol Exp Ther 1999;**290**(2):473-9.
70. Fox J, Lowe SH, Conklin RL, et al. Calcimimetic compound NPS R-568 stimulates calcitonin secretion but selectively targets parathyroid gland Ca(2+) receptor in rats. J Pharmacol Exp Ther 1999;**290**(2):480-6.
71. Nemeth EF, Heaton WH, Miller M, et al. Pharmacodynamics of the type II calcimimetic compound cinacalcet HCl. J Pharmacol Exp Ther 2004;**308**(2):627-35.
72. Parfrey PS, Drueke TB, Block GA, et al. The Effects of Cinacalcet in Older and Younger Patients on Hemodialysis: The Evaluation of Cinacalcet HCl Therapy to Lower Cardiovascular Events (EVOLVE) Trial. Clin J Am Soc Nephrol 2015;**10**(5):791-9.
73. Messa P, Alfieri C, Brezzi B. Clinical utilization of cinacalcet in hypercalcemic conditions. Expert Opin Drug Metab Toxicol 2011;**7**(4):517-28.

74. Silverberg SJ, Rubin MR, Faiman C, et al. Cinacalcet hydrochloride reduces the serum calcium concentration in inoperable parathyroid carcinoma. J Clin Endocrinol Metab 2007;**92**(10):3803-8.
75. Tenhola S, Hendy GN, Valta H, et al. Cinacalcet Treatment in an Adolescent With Concurrent 22q11.2 Deletion Syndrome and Familial Hypocalciuric Hypercalcemia Type 3 Caused by AP2S1 Mutation. J Clin Endocrinol Metab 2015;**100**(7):2515-8.
76. Park SY, Mun HC, Eom YS, et al. Identification and characterization of D410E, a novel mutation in the loop 3 domain of CASR, in autosomal dominant hypocalcemia and a therapeutic approach using a novel calcilytic, AXT914. Clin Endocrinol (Oxf) 2013;**78**(5):687-93.
77. Letz S, Haag C, Schulze E, et al. Amino alcohol- (NPS-2143) and quinazolinone-derived calcilytics (ATF936 and AXT914) differentially mitigate excessive signalling of calcium-sensing receptor mutants causing Bartter syndrome Type 5 and autosomal dominant hypocalcemia. PLoS One 2014;**9**(12):e115178.
78. Dong B, Endo I, Ohnishi Y, et al. Calcilytic Ameliorates Abnormalities of Mutant Calcium-Sensing Receptor (CaSR) Knock-in Mice Mimicking Autosomal Dominant Hypocalcemia (ADH). J Bone Miner Res 2015.
79. Hannan FM, Walls GV, Babinsky VN, et al. The calcilytic agent NPS 2143 rectifies hypocalcemia in a mouse model with an activating calcium-sensing-receptor (CaSR) mutation: relevance to autosomal dominant hypocalcemia type 1 (ADH1). Endocrinology 2015:en20151269.
80. Mamillapalli R, VanHouten J, Zawalich W, et al. Switching of G-protein usage by the calcium-sensing receptor reverses its effect on parathyroid hormone-related protein secretion in normal versus malignant breast cells. J Biol Chem 2008;**283**(36):24435-47.
81. Godwin SL, Soltoff SP. Calcium-sensing receptor-mediated activation of phospholipase C-gamma1 is downstream of phospholipase C-beta and protein kinase C in MC3T3-E1 osteoblasts. Bone 2002;**30**(4):559-66.
82. Hofer AM, Brown EM. Extracellular calcium sensing and signalling. Nature reviews Molecular cell biology 2003;**4**(7):530-8.
83. Yanez M, Gil-Longo J, Campos-Toimil M. Calcium binding proteins. Adv Exp Med Biol 2012;**740**:461-82.
84. Kursula P. The many structural faces of calmodulin: a multitasking molecular jackknife. Amino Acids 2014;**46**(10):2295-304.
85. Kifor O, MacLeod RJ, Diaz R, et al. Regulation of MAP kinase by calcium-sensing receptor in bovine parathyroid and CaR-transfected HEK293 cells. Am J Physiol Renal Physiol 2001;**280**(2):F291-302.
86. Whitmarsh AJ. Regulation of gene transcription by mitogen-activated protein kinase signaling pathways. Biochim Biophys Acta 2007;**1773**(8):1285-98.
87. Chang L, Karin M. Mammalian MAP kinase signalling cascades. Nature 2001;**410**(6824):37-40.
88. Crabtree GR, Olson EN. NFAT signaling: choreographing the social lives of cells. Cell 2002;**109 Suppl**:S67-79.
89. Treisman R. The serum response element. Trends Biochem Sci 1992;**17**(10):423-6.
90. Cheng Z, Garvin D, Paguio A, et al. Luciferase Reporter Assay System for Deciphering GPCR Pathways. Curr Chem Genomics 2010;**4**:84-91.
91. Wang J, Stern PH. Osteoclastogenic activity and RANKL expression are inhibited in osteoblastic cells expressing constitutively active Galpha(12) or constitutively active RhoA. J Cell Biochem 2010;**111**(6):1531-6.

92. Singh AT, Gilchrist A, Voyno-Yasenetskaya T, et al. G alpha12/G alpha13 subunits of heterotrimeric G proteins mediate parathyroid hormone activation of phospholipase D in UMR-106 osteoblastic cells. Endocrinology 2005;**146**(5):2171-5.
93. Brennan TC, Rybchyn MS, Green W, et al. Osteoblasts play key roles in the mechanisms of action of strontium ranelate. Br J Pharmacol 2009;**157**(7):1291-300.
94. Wu M, Deng L, Zhu G, et al. G Protein and its signaling pathway in bone development and disease. Front Biosci (Landmark Ed) 2010;**15**:957-85.
95. Wennerberg K, Rossman KL, Der CJ. The Ras superfamily at a glance. J Cell Sci 2005;**118**(Pt 5):843-6.
96. Davey AE, Leach K, Valant C, et al. Positive and negative allosteric modulators promote biased signaling at the calcium-sensing receptor. Endocrinology 2012;**153**(3):1232-41.
97. Jiang LI, Collins J, Davis R, et al. Regulation of cAMP responses by the G12/13 pathway converges on adenylyl cyclase VII. J Biol Chem 2008;**283**(34):23429-39.
98. Spencer JA, Misra RP. Expression of the SRF gene occurs through a Ras/Sp/SRF-mediated-mechanism in response to serum growth signals. Oncogene 1999;**18**(51):7319-27.
99. Choudhary S, Kumar A, Kale RK, et al. Extracellular calcium induces COX-2 in osteoblasts via a PKA pathway. Biochem Biophys Res Commun 2004;**322**(2):395-402.
100. Fimia GM, Sassone-Corsi P. Cyclic AMP signalling. J Cell Sci 2001;**114**(Pt 11):1971-2.
101. Mamillapalli R, Wysolmerski J. The calcium-sensing receptor couples to Galpha(s) and regulates PTHrP and ACTH secretion in pituitary cells. J Endocrinol 2010;**204**(3):287-97.
102. Leach K, Conigrave AD, Sexton PM, et al. Towards tissue-specific pharmacology: insights from the calcium-sensing receptor as a paradigm for GPCR (patho)physiological bias. Trends Pharmacol Sci 2015;**36**(4):215-25.
103. Thomsen AR, Hvidtfeldt M, Brauner-Osborne H. Biased agonism of the calcium-sensing receptor. Cell Calcium 2012;**51**(2):107-16.
104. Wootten D, Christopoulos A, Sexton PM. Emerging paradigms in GPCR allostery: implications for drug discovery. Nat Rev Drug Discov 2013;**12**(8):630-44.
105. Broadhead GK, Mun HC, Avlani VA, et al. Allosteric modulation of the calcium-sensing receptor by gamma-glutamyl peptides: inhibition of PTH secretion, suppression of intracellular cAMP levels, and a common mechanism of action with L-amino acids. J Biol Chem 2011;**286**(11):8786-97.
106. Rey O, Young SH, Yuan J, et al. Amino acid-stimulated Ca2+ oscillations produced by the Ca2+-sensing receptor are mediated by a phospholipase C/inositol 1,4,5-trisphosphate-independent pathway that requires G12, Rho, filamin-A, and the actin cytoskeleton. J Biol Chem 2005;**280**(24):22875-82.
107. Henley C, 3rd, Yang Y, Davis J, et al. Discovery of a calcimimetic with differential effects on parathyroid hormone and calcitonin secretion. J Pharmacol Exp Ther 2011;**337**(3):681-91.
108. Hendy GN, D'Souza-Li L, Yang B, et al. Mutations of the calcium-sensing receptor (CASR) in familial hypocalciuric hypercalcemia, neonatal severe hyperparathyroidism, and autosomal dominant hypocalcemia. Hum Mutat 2000;**16**(4):281-96.
109. Thakker RV. Diseases associated with the extracellular calcium-sensing receptor. Cell Calcium 2004;**35**(3):275-82.

110. Leach K, Wen A, Davey AE, et al. Identification of molecular phenotypes and biased signaling induced by naturally occurring mutations of the human calcium-sensing receptor. Endocrinology 2012;**153**(9):4304-16.
111. Hannan FM, Nesbit MA, Zhang C, et al. Identification of 70 calcium-sensing receptor mutations in hyper- and hypo-calcaemic patients: evidence for clustering of extracellular domain mutations at calcium-binding sites. Hum Mol Genet 2012;**21**(12):2768-78.
112. Zhang L, Sports CD, Osawa S, et al. Rhodopsin phosphorylation sites and their role in arrestin binding. J Biol Chem 1997;**272**(23):14762-8.
113. Pi M, Oakley RH, Gesty-Palmer D, et al. Beta-arrestin- and G protein receptor kinase-mediated calcium-sensing receptor desensitization. Mol Endocrinol 2005;**19**(4):1078-87.
114. Luttrell LM, Lefkowitz RJ. The role of beta-arrestins in the termination and transduction of G-protein-coupled receptor signals. J Cell Sci 2002;**115**(Pt 3):455-65.
115. Lin FT, Miller WE, Luttrell LM, et al. Feedback regulation of beta-arrestin1 function by extracellular signal-regulated kinases. J Biol Chem 1999;**274**(23):15971-4.
116. Lin FT, Chen W, Shenoy S, et al. Phosphorylation of beta-arrestin2 regulates its function in internalization of beta(2)-adrenergic receptors. Biochemistry 2002;**41**(34):10692-9.
117. Bai M, Trivedi S, Lane CR, et al. Protein kinase C phosphorylation of threonine at position 888 in Ca2+o-sensing receptor (CaR) inhibits coupling to Ca2+ store release. J Biol Chem 1998;**273**(33):21267-75.
118. Lorenz S, Frenzel R, Paschke R, et al. Functional desensitization of the extracellular calcium-sensing receptor is regulated via distinct mechanisms: role of G protein-coupled receptor kinases, protein kinase C and beta-arrestins. Endocrinology 2007;**148**(5):2398-404.
119. Davies SL, Ozawa A, McCormick WD, et al. Protein kinase C-mediated phosphorylation of the calcium-sensing receptor is stimulated by receptor activation and attenuated by calyculin-sensitive phosphatase activity. J Biol Chem 2007;**282**(20):15048-56.
120. Grant MP, Stepanchick A, Cavanaugh A, et al. Agonist-driven maturation and plasma membrane insertion of calcium-sensing receptors dynamically control signal amplitude. Sci Signal 2011;**4**(200):ra78.
121. Schmid EM, McMahon HT. Integrating molecular and network biology to decode endocytosis. Nature 2007;**448**(7156):883-8.
122. McMahon HT, Boucrot E. Molecular mechanism and physiological functions of clathrin-mediated endocytosis. Nat Rev Mol Cell Biol 2011;**12**(8):517-33.
123. Drake MT, Shenoy SK, Lefkowitz RJ. Trafficking of G protein-coupled receptors. Circ Res 2006;**99**(6):570-82.
124. Zhuang X, Northup JK, Ray K. Large putative PEST-like sequence motif at the carboxyl tail of human calcium receptor directs lysosomal degradation and regulates cell surface receptor level. J Biol Chem 2012;**287**(6):4165-76.
125. Holstein DM, Berg KA, Leeb-Lundberg LM, et al. Calcium-sensing receptor-mediated ERK1/2 activation requires Galphai2 coupling and dynamin-independent receptor internalization. J Biol Chem 2004;**279**(11):10060-9.
126. Collins BM, McCoy AJ, Kent HM, et al. Molecular architecture and functional model of the endocytic AP2 complex. Cell 2002;**109**(4):523-35.
127. Laporte SA, Oakley RH, Holt JA, et al. The interaction of beta-arrestin with the AP-2 adaptor is required for the clustering of beta 2-adrenergic receptor into clathrin-coated pits. J Biol Chem 2000;**275**(30):23120-6.

128. Jackson LP, Kelly BT, McCoy AJ, et al. A large-scale conformational change couples membrane recruitment to cargo binding in the AP2 clathrin adaptor complex. Cell 2010;**141**(7):1220-9.
129. Kelly BT, McCoy AJ, Spate K, et al. A structural explanation for the binding of endocytic dileucine motifs by the AP2 complex. Nature 2008;**456**(7224):976-79.
130. Nesbit MA, Hannan FM, Howles SA, et al. Mutations in AP2S1 cause familial hypocalciuric hypercalcemia type 3. Nature genetics 2013;**45**(1):93-7.
131. Zhang J, Ferguson SS, Barak LS, et al. Dynamin and beta-arrestin reveal distinct mechanisms for G protein-coupled receptor internalization. J Biol Chem 1996;**271**(31):18302-5.
132. Sweitzer SM, Hinshaw JE. Dynamin undergoes a GTP-dependent conformational change causing vesiculation. Cell 1998;**93**(6):1021-9.
133. Massol RH, Boll W, Griffin AM, et al. A burst of auxilin recruitment determines the onset of clathrin-coated vesicle uncoating. Proc Natl Acad Sci U S A 2006;**103**(27):10265-70.
134. Vitaliano GD, Vitaliano F, Rios JD, et al. New clathrin-based nanoplatforms for magnetic resonance imaging. PLoS One 2012;**7**(5):e35821.
135. Jean-Alphonse F, Bowersox S, Chen S, et al. Spatially restricted G protein-coupled receptor activity via divergent endocytic compartments. J Biol Chem 2014;**289**(7):3960-77.
136. Hanyaloglu AC, von Zastrow M. Regulation of GPCRs by endocytic membrane trafficking and its potential implications. Annu Rev Pharmacol Toxicol 2008;**48**:537-68.
137. DeWire SM, Ahn S, Lefkowitz RJ, et al. Beta-arrestins and cell signaling. Annu Rev Physiol 2007;**69**:483-510.
138. Calebiro D, Nikolaev VO, Persani L, et al. Signaling by internalized G-protein-coupled receptors. Trends Pharmacol Sci 2010;**31**(5):221-8.
139. Huang Y, Niwa J, Sobue G, et al. Calcium-sensing receptor ubiquitination and degradation mediated by the E3 ubiquitin ligase dorfin. J Biol Chem 2006;**281**(17):11610-7.
140. Stepanchick A, Breitwieser GE. The cargo receptor p24A facilitates calcium sensing receptor maturation and stabilization in the early secretory pathway. Biochem Biophys Res Commun 2010;**395**(1):136-40.
141. Bouschet T, Martin S, Henley JM. Receptor-activity-modifying proteins are required for forward trafficking of the calcium-sensing receptor to the plasma membrane. J Cell Sci 2005;**118**(Pt 20):4709-20.
142. Zhuang X, Adipietro KA, Datta S, et al. Rab1 small GTP-binding protein regulates cell surface trafficking of the human calcium-sensing receptor. Endocrinology 2010;**151**(11):5114-23.
143. Huang Y, Zhou Y, Wong HC, et al. Calmodulin regulates Ca2+-sensing receptor-mediated Ca2+ signaling and its cell surface expression. J Biol Chem 2010;**285**(46):35919-31.
144. Lopez-Fernandez I, Schepelmann M, Brennan SC, et al. The calcium-sensing receptor: one of a kind. Exp Physiol 2015.
145. Riccardi D, Kemp PJ. The calcium-sensing receptor beyond extracellular calcium homeostasis: conception, development, adult physiology, and disease. Annu Rev Physiol 2012;**74**:271-97.
146. Quinn SJ, Kifor O, Kifor I, et al. Role of the cytoskeleton in extracellular calcium-regulated PTH release. Biochem Biophys Res Commun 2007;**354**(1):8-13.

147. Galitzer H, Lavi-Moshayoff V, Nechama M, et al. The calcium-sensing receptor regulates parathyroid hormone gene expression in transfected HEK293 cells. BMC Biol 2009;**7**:17.
148. Wada M, Furuya Y, Sakiyama J, et al. The calcimimetic compound NPS R-568 suppresses parathyroid cell proliferation in rats with renal insufficiency. Control of parathyroid cell growth via a calcium receptor. J Clin Invest 1997;**100**(12):2977-83.
149. Ho C, Conner DA, Pollak MR, et al. A mouse model of human familial hypocalciuric hypercalcemia and neonatal severe hyperparathyroidism. Nature genetics 1995;**11**(4):389-94.
150. Alagaratnam S, Brain C, Spoudeas H, et al. Surgical treatment of children with hyperparathyroidism: single centre experience. J Pediatr Surg 2014;**49**(11):1539-43.
151. Mallya SM, Arnold A. Cyclin D1 in parathyroid disease. Front Biosci 2000;**5**:D367-71.
152. Cozzolino M, Brancaccio D, Gallieni M, et al. Pathogenesis of parathyroid hyperplasia in renal failure. J Nephrol 2005;**18**(1):5-8.
153. Riccardi D, Lee WS, Lee K, et al. Localization of the extracellular Ca(2+)-sensing receptor and PTH/PTHrP receptor in rat kidney. The American journal of physiology 1996;**271**(4 Pt 2):F951-6.
154. Riccardi D, Hall AE, Chattopadhyay N, et al. Localization of the extracellular Ca2+/polyvalent cation-sensing protein in rat kidney. The American journal of physiology 1998;**274**(3 Pt 2):F611-22.
155. Maiti A, Beckman MJ. Extracellular calcium is a direct effecter of VDR levels in proximal tubule epithelial cells that counter-balances effects of PTH on renal Vitamin D metabolism. J Steroid Biochem Mol Biol 2007;**103**(3-5):504-8.
156. Ba J, Brown D, Friedman PA. Calcium-sensing receptor regulation of PTH-inhibitable proximal tubule phosphate transport. Am J Physiol Renal Physiol 2003;**285**(6):F1233-43.
157. Wang WH, Lu M, Hebert SC. Cytochrome P-450 metabolites mediate extracellular Ca(2+)-induced inhibition of apical K+ channels in the TAL. The American journal of physiology 1996;**271**(1 Pt 1):C103-11.
158. Vargas-Poussou R, Huang C, Hulin P, et al. Functional characterization of a calcium-sensing receptor mutation in severe autosomal dominant hypocalcemia with a Bartter-like syndrome. J Am Soc Nephrol 2002;**13**(9):2259-66.
159. Motoyama HI, Friedman PA. Calcium-sensing receptor regulation of PTH-dependent calcium absorption by mouse cortical ascending limbs. Am J Physiol Renal Physiol 2002;**283**(3):F399-406.
160. Blankenship KA, Williams JJ, Lawrence MS, et al. The calcium-sensing receptor regulates calcium absorption in MDCK cells by inhibition of PMCA. Am J Physiol Renal Physiol 2001;**280**(5):F815-22.
161. Topala CN, Schoeber JP, Searchfield LE, et al. Activation of the Ca2+-sensing receptor stimulates the activity of the epithelial Ca2+ channel TRPV5. Cell Calcium 2009;**45**(4):331-9.
162. Sands JM, Naruse M, Baum M, et al. Apical extracellular calcium/polyvalent cation-sensing receptor regulates vasopressin-elicited water permeability in rat kidney inner medullary collecting duct. J Clin Invest 1997;**99**(6):1399-405.
163. Marie PJ. The calcium-sensing receptor in bone cells: a potential therapeutic target in osteoporosis. Bone 2010;**46**(3):571-6.
164. Goltzman D, Hendy GN. The calcium-sensing receptor in bone--mechanistic and therapeutic insights. Nat Rev Endocrinol 2015;**11**(5):298-307.

165. Brown EM, Chattopadhyay N, Yano S. Calcium-sensing receptors in bone cells. J Musculoskelet Neuronal Interact 2004;**4**(4):412-3.
166. Fromigue O, Hay E, Barbara A, et al. Calcium sensing receptor-dependent and receptor-independent activation of osteoblast replication and survival by strontium ranelate. J Cell Mol Med 2009;**13**(8B):2189-99.
167. Dvorak MM, Siddiqua A, Ward DT, et al. Physiological changes in extracellular calcium concentration directly control osteoblast function in the absence of calciotropic hormones. Proc Natl Acad Sci U S A 2004;**101**(14):5140-5.
168. Sugimoto T, Kanatani M, Kano J, et al. Effects of high calcium concentration on the functions and interactions of osteoblastic cells and monocytes and on the formation of osteoclast-like cells. J Bone Miner Res 1993;**8**(12):1445-52.
169. Mentaverri R, Yano S, Chattopadhyay N, et al. The calcium sensing receptor is directly involved in both osteoclast differentiation and apoptosis. FASEB J 2006;**20**(14):2562-4.
170. Dvorak MM, Chen TH, Orwoll B, et al. Constitutive activity of the osteoblast Ca2+-sensing receptor promotes loss of cancellous bone. Endocrinology 2007;**148**(7):3156-63.
171. Xue Y, Xiao Y, Liu J, et al. The calcium-sensing receptor complements parathyroid hormone-induced bone turnover in discrete skeletal compartments in mice. Am J Physiol Endocrinol Metab 2012;**302**(7):E841-51.
172. Smajilovic S, Yano S, Jabbari R, et al. The calcium-sensing receptor and calcimimetics in blood pressure modulation. Br J Pharmacol 2011;**164**(3):884-93.
173. Alam MU, Kirton JP, Wilkinson FL, et al. Calcification is associated with loss of functional calcium-sensing receptor in vascular smooth muscle cells. Cardiovasc Res 2009;**81**(2):260-8.
174. Huybrechts KF, Caro JJ, London GM. Modeling the implications of changes in vascular calcification in patients on hemodialysis. Kidney Int 2005;**67**(4):1532-8.
175. Yarova PL, Stewart AL, Sathish V, et al. Calcium-sensing receptor antagonists abrogate airway hyperresponsiveness and inflammation in allergic asthma. Sci Transl Med 2015;**7**(284):284ra60.
176. Finney BA, del Moral PM, Wilkinson WJ, et al. Regulation of mouse lung development by the extracellular calcium-sensing receptor, CaR. J Physiol 2008;**586**(Pt 24):6007-19.
177. Vizard TN, O'Keeffe GW, Gutierrez H, et al. Regulation of axonal and dendritic growth by the extracellular calcium-sensing receptor. Nat Neurosci 2008;**11**(3):285-91.
178. Riccardi D, Finney BA, Wilkinson WJ, et al. Novel regulatory aspects of the extracellular Ca2+-sensing receptor, CaR. Pflugers Arch 2009;**458**(6):1007-22.
179. Kovacs CS, Kronenberg HM. Maternal-fetal calcium and bone metabolism during pregnancy, puerperium, and lactation. Endocr Rev 1997;**18**(6):832-72.
180. Chang W, Tu C, Chen TH, et al. The extracellular calcium-sensing receptor (CaSR) is a critical modulator of skeletal development. Sci Signal 2008;**1**(35):ra1.
181. Warburton D, El-Hashash A, Carraro G, et al. Lung organogenesis. Curr Top Dev Biol 2010;**90**:73-158.
182. Ferry S, Traiffort E, Stinnakre J, et al. Developmental and adult expression of rat calcium-sensing receptor transcripts in neurons and oligodendrocytes. Eur J Neurosci 2000;**12**(3):872-84.
183. Jackson CE, Boonstra CE. Hereditary Hypercalcemia and Parathyroid Hyperplasia without Definite Hyperparathyroidism. J Lab Clin Med 1966;**68**(5):883-&.
184. Foley TP, Jr., Harrison HC, Arnaud CD, et al. Familial benign hypercalcemia. J Pediatr 1972;**81**(6):1060-7.

185. Marx SJ, Attie MF, Levine MA, et al. The hypocalciuric or benign variant of familial hypercalcemia: clinical and biochemical features in fifteen kindreds. Medicine (Baltimore) 1981;**60**(6):397-412.
186. Law WM, Jr., Heath H, 3rd. Familial benign hypercalcemia (hypocalciuric hypercalcemia). Clinical and pathogenetic studies in 21 families. Ann Intern Med 1985;**102**(4):511-9.
187. Pearce SH, Wooding C, Davies M, et al. Calcium-sensing receptor mutations in familial hypocalciuric hypercalcaemia with recurrent pancreatitis. Clin Endocrinol (Oxf) 1996;**45**(6):675-80.
188. Chou YH, Brown EM, Levi T, et al. The gene responsible for familial hypocalciuric hypercalcemia maps to chromosome 3q in four unrelated families. Nature genetics 1992;**1**(4):295-300.
189. Heath H, 3rd, Jackson CE, Otterud B, et al. Genetic linkage analysis in familial benign (hypocalciuric) hypercalcemia: evidence for locus heterogeneity. American journal of human genetics 1993;**53**(1):193-200.
190. Lloyd SE, Pannett AA, Dixon PH, et al. Localization of familial benign hypercalcemia, Oklahoma variant (FBHOk), to chromosome 19q13. American journal of human genetics 1999;**64**(1):189-95.
191. Nesbit MA, Hannan FM, Graham U, et al. Identification of a second kindred with familial hypocalciuric hypercalcemia type 3 (FHH3) narrows localization to a <3.5 megabase pair region on chromosome 19q13.3. J Clin Endocrinol Metab 2010;**95**(4):1947-54.
192. Pearce SH, Trump D, Wooding C, et al. Calcium-sensing receptor mutations in familial benign hypercalcemia and neonatal hyperparathyroidism. J Clin Invest 1995;**96**(6):2683-92.
193. Hannan FM, Thakker RV. Calcium-sensing receptor (CaSR) mutations and disorders of calcium, electrolyte and water metabolism. Best Pract Res Clin Endocrinol Metab 2013;**27**(3):359-71.
194. Ward BK, Magno AL, Blitvich BJ, et al. Novel mutations in the calcium-sensing receptor gene associated with biochemical and functional differences in familial hypocalciuric hypercalcaemia. Clin Endocrinol (Oxf) 2006;**64**(5):580-7.
195. Nissen PH, Christensen SE, Heickendorff L, et al. Molecular genetic analysis of the calcium sensing receptor gene in patients clinically suspected to have familial hypocalciuric hypercalcemia: phenotypic variation and mutation spectrum in a Danish population. J Clin Endocrinol Metab 2007;**92**(11):4373-9.
196. D'Souza-Li L, Canaff L, Janicic N, et al. An acceptor splice site mutation in the calcium-sensing receptor (CASR) gene in familial hypocalciuric hypercalcemia and neonatal severe hyperparathyroidism. Hum Mutat 2001;**18**(5):411-21.
197. Nesbit MA, Hannan FM, Howles SA, et al. Mutations affecting G-protein subunit alpha11 in hypercalcemia and hypocalcemia. N Engl J Med 2013;**368**(26):2476-86.
198. Gunganah K, Grossman A, Druce M. Recurrent pancreatitis in a patient with familial hypocalciuric hypercalcaemia treated successfully with cinacalcet. Endocrinol Diabetes Metab Case Rep 2014;**2014**:140050.
199. Alon US, VandeVoorde RG. Beneficial effect of cinacalcet in a child with familial hypocalciuric hypercalcemia. Pediatr Nephrol 2010;**25**(9):1747-50.
200. Timmers HJ, Karperien M, Hamdy NA, et al. Normalization of serum calcium by cinacalcet in a patient with hypercalcaemia due to a de novo inactivating mutation of the calcium-sensing receptor. J Intern Med 2006;**260**(2):177-82.

201. Marx SJ, Attie MF, Spiegel AM, et al. An association between neonatal severe primary hyperparathyroidism and familial hypocalciuric hypercalcemia in three kindreds. N Engl J Med 1982;**306**(5):257-64.
202. Marx SJ, Fraser D, Rapoport A. Familial hypocalciuric hypercalcemia. Mild expression of the gene in heterozygotes and severe expression in homozygotes. Am J Med 1985;**78**(1):15-22.
203. Eftekhari F, Yousefzadeh DK. Primary infantile hyperparathyroidism: clinical, laboratory, and radiographic features in 21 cases. Skeletal Radiol 1982;**8**(3):201-8.
204. Bai M, Pearce SH, Kifor O, et al. In vivo and in vitro characterization of neonatal hyperparathyroidism resulting from a de novo, heterozygous mutation in the Ca2+-sensing receptor gene: normal maternal calcium homeostasis as a cause of secondary hyperparathyroidism in familial benign hypocalciuric hypercalcemia. J Clin Invest 1997;**99**(1):88-96.
205. Egbuna OI, Brown EM. Hypercalcaemic and hypocalcaemic conditions due to calcium-sensing receptor mutations. Best Pract Res Clin Rheumatol 2008;**22**(1):129-48.
206. Reh CM, Hendy GN, Cole DE, et al. Neonatal hyperparathyroidism with a heterozygous calcium-sensing receptor (CASR) R185Q mutation: clinical benefit from cinacalcet. J Clin Endocrinol Metab 2011;**96**(4):E707-12.
207. Atay Z, Bereket A, Haliloglu B, et al. Novel homozygous inactivating mutation of the calcium-sensing receptor gene (CASR) in neonatal severe hyperparathyroidism-lack of effect of cinacalcet. Bone 2014;**64**:102-7.
208. Kifor O, McElduff A, LeBoff MS, et al. Activating antibodies to the calcium-sensing receptor in two patients with autoimmune hypoparathyroidism. J Clin Endocrinol Metab 2004;**89**(2):548-56.
209. Raue F, Pichl J, Dorr HG, et al. Activating mutations in the calcium-sensing receptor: genetic and clinical spectrum in 25 patients with autosomal dominant hypocalcaemia - a German survey. Clinical endocrinology 2011;**75**(6):760-5.
210. Pearce SH, Williamson C, Kifor O, et al. A familial syndrome of hypocalcemia with hypercalciuria due to mutations in the calcium-sensing receptor. N Engl J Med 1996;**335**(15):1115-22.
211. D'Souza-Li L, Yang B, Canaff L, et al. Identification and functional characterization of novel calcium-sensing receptor mutations in familial hypocalciuric hypercalcemia and autosomal dominant hypocalcemia. J Clin Endocrinol Metab 2002;**87**(3):1309-18.
212. Rogers A, Nesbit MA, Hannan FM, et al. Mutational analysis of the adaptor protein 2 sigma subunit (AP2S1) gene: search for autosomal dominant hypocalcemia type 3 (ADH3). J Clin Endocrinol Metab 2014;**99**(7):E1300-5.
213. Yamamoto M, Akatsu T, Nagase T, et al. Comparison of hypocalcemic hypercalciuria between patients with idiopathic hypoparathyroidism and those with gain-of-function mutations in the calcium-sensing receptor: is it possible to differentiate the two disorders? J Clin Endocrinol Metab 2000;**85**(12):4583-91.
214. Pollak MR, Brown EM, Estep HL, et al. Autosomal dominant hypocalcaemia caused by a Ca(2+)-sensing receptor gene mutation. Nature genetics 1994;**8**(3):303-7.
215. Okazaki R, Chikatsu N, Nakatsu M, et al. A novel activating mutation in calcium-sensing receptor gene associated with a family of autosomal dominant hypocalcemia. J Clin Endocrinol Metab 1999;**84**(1):363-6.
216. De Luca F, Ray K, Mancilla EE, et al. Sporadic hypoparathyroidism caused by de Novo gain-of-function mutations of the Ca(2+)-sensing receptor. J Clin Endocrinol Metab 1997;**82**(8):2710-5.

217. Lienhardt A, Garabedian M, Bai M, et al. A large homozygous or heterozygous in-frame deletion within the calcium-sensing receptor's carboxylterminal cytoplasmic tail that causes autosomal dominant hypocalcemia. J Clin Endocrinol Metab 2000;**85**(4):1695-702.
218. Conley YP, Finegold DN, Peters DG, et al. Three novel activating mutations in the calcium-sensing receptor responsible for autosomal dominant hypocalcemia. Mol Genet Metab 2000;**71**(4):591-8.
219. Hirai H, Nakajima S, Miyauchi A, et al. A novel activating mutation (C129S) in the calcium-sensing receptor gene in a Japanese family with autosomal dominant hypocalcemia. J Hum Genet 2001;**46**(1):41-4.
220. Nagase T, Murakami T, Tsukada T, et al. A family of autosomal dominant hypocalcemia with a positive correlation between serum calcium and magnesium: identification of a novel gain of function mutation (Ser(820)Phe) in the calcium-sensing receptor. J Clin Endocrinol Metab 2002;**87**(6):2681-7.
221. Sato K, Hasegawa Y, Nakae J, et al. Hydrochlorothiazide effectively reduces urinary calcium excretion in two Japanese patients with gain-of-function mutations of the calcium-sensing receptor gene. J Clin Endocrinol Metab 2002;**87**(7):3068-73.
222. Guarnieri V, Valentina D'Elia A, Baorda F, et al. CASR gene activating mutations in two families with autosomal dominant hypocalcemia. Mol Genet Metab 2012;**107**(3):548-52.
223. Lazarus S, Pretorius CJ, Khafagi F, et al. A novel mutation of the primary protein kinase C phosphorylation site in the calcium-sensing receptor causes autosomal dominant hypocalcemia. Eur J Endocrinol 2011;**164**(3):429-35.
224. Kim MY, Tan AH, Ki CS, et al. Autosomal dominant hypocalcemia caused by an activating mutation of the calcium-sensing receptor gene: the first case report in Korea. J Korean Med Sci 2010;**25**(2):317-20.
225. Mittelman SD, Hendy GN, Fefferman RA, et al. A hypocalcemic child with a novel activating mutation of the calcium-sensing receptor gene: successful treatment with recombinant human parathyroid hormone. J Clin Endocrinol Metab 2006;**91**(7):2474-9.
226. Uckun-Kitapci A, Underwood LE, Zhang J, et al. A novel mutation (E767K) in the second extracellular loop of the calcium sensing receptor in a family with autosomal dominant hypocalcemia. Am J Med Genet A 2005;**132A**(2):125-9.
227. Hu J, Mora S, Weber G, et al. Autosomal dominant hypocalcemia in monozygotic twins caused by a de novo germline mutation near the amino-terminus of the human calcium receptor. J Bone Miner Res 2004;**19**(4):578-86.
228. Chikatsu N, Watanabe S, Takeuchi Y, et al. A family of autosomal dominant hypocalcemia with an activating mutation of calcium-sensing receptor gene. Endocr J 2003;**50**(1):91-6.
229. Gonzales MC, Lieb DC, Richardson DW, et al. Recombinant human parathyroid hormone therapy (1-34) in an adult patient with a gain-of-function mutation in the calcium-sensing receptor-a case report. Endocr Pract 2013;**19**(1):e24-8.
230. Theman TA, Collins MT, Dempster DW, et al. PTH(1-34) replacement therapy in a child with hypoparathyroidism caused by a sporadic calcium receptor mutation. J Bone Miner Res 2009;**24**(5):964-73.
231. Vezzoli G, Arcidiacono T, Paloschi V, et al. Autosomal dominant hypocalcemia with mild type 5 Bartter syndrome. J Nephrol 2006;**19**(4):525-8.
232. Watanabe S, Fukumoto S, Chang H, et al. Association between activating mutations of calcium-sensing receptor and Bartter's syndrome. Lancet 2002;**360**(9334):692-4.

233. Nishioka Y. The origin of common laboratory mice. Genome 1995;**38**(1):1-7.
234. Keane TM, Goodstadt L, Danecek P, et al. Mouse genomic variation and its effect on phenotypes and gene regulation. Nature 2011;**477**(7364):289-94.
235. Mouse Genome Sequencing C, Waterston RH, Lindblad-Toh K, et al. Initial sequencing and comparative analysis of the mouse genome. Nature 2002;**420**(6915):520-62.
236. Piret SE, Thakker RV. Mouse models for inherited endocrine and metabolic disorders. J Endocrinol 2011;**211**(3):211-30.
237. Coghill EL, Hugill A, Parkinson N, et al. A gene-driven approach to the identification of ENU mutants in the mouse. Nature genetics 2002;**30**(3):255-6.
238. Wefers B, Panda SK, Ortiz O, et al. Generation of targeted mouse mutants by embryo microinjection of TALEN mRNA. Nat Protoc 2013;**8**(12):2355-79.
239. Wefers B, Meyer M, Ortiz O, et al. Direct production of mouse disease models by embryo microinjection of TALENs and oligodeoxynucleotides. Proc Natl Acad Sci U S A 2013;**110**(10):3782-7.
240. Platt RJ, Chen S, Zhou Y, et al. CRISPR-Cas9 knockin mice for genome editing and cancer modeling. Cell 2014;**159**(2):440-55.
241. Gupta RM, Musunuru K. Expanding the genetic editing tool kit: ZFNs, TALENs, and CRISPR-Cas9. J Clin Invest 2014;**124**(10):4154-61.
242. Joung JK, Sander JD. TALENs: a widely applicable technology for targeted genome editing. Nat Rev Mol Cell Biol 2013;**14**(1):49-55.
243. Jones JM, Meisler MH. Modeling human epilepsy by TALEN targeting of mouse sodium channel Scn8a. Genesis 2014;**52**(2):141-8.
244. Larcher T, Lafoux A, Tesson L, et al. Characterization of dystrophin deficient rats: a new model for Duchenne muscular dystrophy. PLoS One 2014;**9**(10):e110371.
245. Liu C, Xiao L, Li F, et al. Generation of outbred Ace2 knockout mice by RNA transfection of TALENs displaying colitis reminiscent pathophysiology and inflammation. Transgenic Res 2015;**24**(3):433-46.
246. Mali P, Yang L, Esvelt KM, et al. RNA-guided human genome engineering via Cas9. Science 2013;**339**(6121):823-6.
247. Cong L, Ran FA, Cox D, et al. Multiplex genome engineering using CRISPR/Cas systems. Science 2013;**339**(6121):819-23.
248. Toka HR, Al-Romaih K, Koshy JM, et al. Deficiency of the calcium-sensing receptor in the kidney causes parathyroid hormone-independent hypocalciuria. J Am Soc Nephrol 2012;**23**(11):1879-90.
249. Hough TA, Bogani D, Cheeseman MT, et al. Activating calcium-sensing receptor mutation in the mouse is associated with cataracts and ectopic calcification. Proc Natl Acad Sci U S A 2004;**101**(37):13566-71.
250. Mitsunari T, Nakatsu F, Shioda N, et al. Clathrin adaptor AP-2 is essential for early embryonal development. Mol Cell Biol 2005;**25**(21):9318-23.
251. Li W, Puertollano R, Bonifacino JS, et al. Disruption of the murine Ap2beta1 gene causes nonsyndromic cleft palate. Cleft Palate Craniofac J 2010;**47**(6):566-73.
252. Bokel C, Brand M. Endocytosis and signaling during development. Cold Spring Harb Perspect Biol 2014;**6**(3).
253. Dell'Angelica EC, Shotelersuk V, Aguilar RC, et al. Altered trafficking of lysosomal proteins in Hermansky-Pudlak syndrome due to mutations in the beta 3A subunit of the AP-3 adaptor. Mol Cell 1999;**3**(1):11-21.
254. Peden AA, Rudge RE, Lui WW, et al. Assembly and function of AP-3 complexes in cells expressing mutant subunits. J Cell Biol 2002;**156**(2):327-36.

255. Boucrot E, Saffarian S, Zhang R, et al. Roles of AP-2 in clathrin-mediated endocytosis. PLoS One 2010;**5**(5):e10597.
256. Saiki RK, Gelfand DH, Stoffel S, et al. Primer-directed enzymatic amplification of DNA with a thermostable DNA polymerase. Science 1988;**239**(4839):487-91.
257. Sanger F, Nicklen S, Coulson AR. DNA sequencing with chain-terminating inhibitors. Proc Natl Acad Sci U S A 1977;**74**(12):5463-7.
258. Flicek P, Amode MR, Barrell D, et al. Ensembl 2011. Nucleic Acids Res 2011;**39**(Database issue):D800-6.
259. Jackson DA, Symons RH, Berg P. Biochemical method for inserting new genetic information into DNA of Simian Virus 40: circular SV40 DNA molecules containing lambda phage genes and the galactose operon of Escherichia coli. Proc Natl Acad Sci U S A 1972;**69**(10):2904-9.
260. Bentley L, Esapa CT, Nesbit MA, et al. An N-ethyl-N-nitrosourea induced corticotropin-releasing hormone promoter mutation provides a mouse model for endogenous glucocorticoid excess. Endocrinology 2014;**155**(3):908-22.
261. Wilfinger WW, Mackey K, Chomczynski P. Effect of pH and ionic strength on the spectrophotometric assessment of nucleic acid purity. Biotechniques 1997;**22**(3):474-6, 78-81.
262. Chiang PW, Song WJ, Wu KY, et al. Use of a fluorescent-PCR reaction to detect genomic sequence copy number and transcriptional abundance. Genome Res 1996;**6**(10):1013-26.
263. VanGuilder HD, Vrana KE, Freeman WM. Twenty-five years of quantitative PCR for gene expression analysis. Biotechniques 2008;**44**(5):619-26.
264. Pfaffl MW. A new mathematical model for relative quantification in real-time RT-PCR. Nucleic Acids Res 2001;**29**(9):e45.
265. Van Baal J, Yu A, Hartog A, et al. Localization and regulation by vitamin D of calcium transport proteins in rabbit cortical collecting system. The American journal of physiology 1996;**271**(5 Pt 2):F985-93.
266. Blancher C, Jones A. SDS -PAGE and Western Blotting Techniques. Methods Mol Med 2001;**57**:145-62.
267. Loh NY, Bentley L, Dimke H, et al. Autosomal dominant hypercalciuria in a mouse model due to a mutation of the epithelial calcium channel, TRPV5. PLoS One 2013;**8**(1):e55412.
268. Towbin H, Staehelin T, Gordon J. Electrophoretic transfer of proteins from polyacrylamide gels to nitrocellulose sheets: procedure and some applications. Proc Natl Acad Sci U S A 1979;**76**(9):4350-4.
269. Trump D, Whyte MP, Wooding C, et al. Linkage studies in a kindred from Oklahoma, with familial benign (hypocalciuric) hypercalcaemia (FBH) and developmental elevations in serum parathyroid hormone levels, indicate a third locus for FBH. Human genetics 1995;**96**(2):183-7.
270. Hui-Yuen J, McAllister S, Koganti S, et al. Establishment of Epstein-Barr virus growth-transformed lymphoblastoid cell lines. J Vis Exp 2011(57).
271. Felgner PL, Gadek TR, Holm M, et al. Lipofection: a highly efficient, lipid-mediated DNA-transfection procedure. Proc Natl Acad Sci U S A 1987;**84**(21):7413-7.
272. Reed AA, Loh NY, Terryn S, et al. CLC-5 and KIF3B interact to facilitate CLC-5 plasma membrane expression, endocytosis and microtubular transport: relevance to pathophysiology of Dent's disease. Am J Physiol Renal Physiol 2009.
273. Pearce SH, Bai M, Quinn SJ, et al. Functional characterization of calcium-sensing receptor mutations expressed in human embryonic kidney cells. J Clin Invest 1996;**98**(8):1860-6.

274. Luckhoff A. Measuring cytosolic free calcium concentration in endothelial cells with indo-1: the pitfall of using the ratio of two fluorescence intensities recorded at different wavelengths. Cell Calcium 1986;**7**(4):233-48.
275. Ullman EF, Kirakossian H, Singh S, et al. Luminescent oxygen channeling immunoassay: measurement of particle binding kinetics by chemiluminescence. Proc Natl Acad Sci U S A 1994;**91**(12):5426-30.
276. Newey PJ, Gorvin CM, Cleland SJ, et al. Mutant prolactin receptor and familial hyperprolactinemia. N Engl J Med 2013;**369**(21):2012-20.
277. Hampf M, Gossen M. A protocol for combined Photinus and Renilla luciferase quantification compatible with protein assays. Anal Biochem 2006;**356**(1):94-9.
278. Stechman MJ, Ahmad BN, Loh NY, et al. Establishing normal plasma and 24-hour urinary biochemistry ranges in C3H, BALB/c and C57BL/6J mice following acclimatization in metabolic cages. Lab Anim 2010;**44**(3):218-25.
279. Fujisawa Y, Yamaguchi R, Satake E, et al. Identification of AP2S1 mutation and effects of low calcium formula in an infant with hypercalcemia and hypercalciuria. J Clin Endocrinol Metab 2013;**98**(12):E2022-7.
280. Hendy GN, Canaff L, Newfield RS, et al. Codon Arg15 mutations of the AP2S1 gene: common occurrence in familial hypocalciuric hypercalcemia cases negative for calcium-sensing receptor (CASR) mutations. J Clin Endocrinol Metab 2014;**99**(7):E1311-5.
281. Lynch M. Rate, molecular spectrum, and consequences of human mutation. Proc Natl Acad Sci U S A 2010;**107**(3):961-8.
282. Hannan FM, Howles SA, Rogers A, et al. Adaptor protein-2 sigma subunit mutations causing familial hypocalciuric hypercalcaemia type 3 (FHH3) demonstrate genotype-phenotype correlations, codon bias and dominant-negative effects. Hum Mol Genet 2015.
283. Binkovitz LA, Henwood MJ. Pediatric DXA: technique and interpretation. Pediatr Radiol 2007;**37**(1):21-31.
284. McMurtry CT, Schranck FW, Walkenhorst DA, et al. Significant developmental elevation in serum parathyroid hormone levels in a large kindred with familial benign (hypocalciuric) hypercalcemia. Am J Med 1992;**93**(3):247-58.
285. Bhambri R, Naik V, Malhotra N, et al. Changes in bone mineral density following treatment of osteomalacia. J Clin Densitom 2006;**9**(1):120-7.
286. Adzhubei IA, Schmidt S, Peshkin L, et al. A method and server for predicting damaging missense mutations. Nat Methods 2010;**7**(4):248-9.
287. Reese MG, Eeckman FH, Kulp D, et al. Improved splice site detection in Genie. J Comput Biol 1997;**4**(3):311-23.
288. Pertea M, Lin X, Salzberg SL. GeneSplicer: a new computational method for splice site prediction. Nucleic Acids Res 2001;**29**(5):1185-90.
289. Motley A, Bright NA, Seaman MN, et al. Clathrin-mediated endocytosis in AP-2-depleted cells. J Cell Biol 2003;**162**(5):909-18.
290. Tenhola S, Hendy GN, Valta H, et al. Cinacalcet Treatment in an Adolescent with Concurrent 22q11.2 Deletion Syndrome and FHH3 caused by AP2S1 Mutation. J Clin Endocrinol Metab 2015:jc20151518.
291. Taki K, Kogai T, Sakumoto J, et al. Familial hypocalciuric hypercalcemia with a de novo heterozygous mutation of calcium-sensing receptor. Endocrinol Diabetes Metab Case Rep 2015;**2015**:150016.
292. Fujita T, Watanabe N, Fukase M, et al. Familial hypocalciuric hypercalcemia involving four members of a kindred including a girl with severe neonatal primary hyperparathyroidism. Miner Electrolyte Metab 1983;**9**(1):51-4.

293. Law WM, Jr., Wahner HW, Heath H, 3rd. Bone mineral density and skeletal fractures in familial benign hypercalcemia (hypocalciuric hypercalcemia). Mayo Clin Proc 1984;**59**(12):811-5.
294. Abugassa S, Nordenstrom J, Jarhult J. Bone mineral density in patients with familial hypocalciuric hypercalcaemia (FHH). Eur J Surg 1992;**158**(8):397-402.
295. Christensen SE, Nissen PH, Vestergaard P, et al. Skeletal consequences of familial hypocalciuric hypercalcaemia vs. primary hyperparathyroidism. Clin Endocrinol (Oxf) 2009;**71**(6):798-807.
296. Jakobsen NF, Rolighed L, Moser E, et al. Increased trabecular volumetric bone mass density in Familial Hypocalciuric Hypercalcemia (FHH) type 1: a cross-sectional study. Calcif Tissue Int 2014;**95**(2):141-52.
297. Li D, Opas EE, Tuluc F, et al. Autosomal dominant hypoparathyroidism caused by germline mutation in GNA11: phenotypic and molecular characterization. J Clin Endocrinol Metab 2014;**99**(9):E1774-83.
298. Felderbauer P, Klein W, Bulut K, et al. Mutations in the calcium-sensing receptor: a new genetic risk factor for chronic pancreatitis? Scand J Gastroenterol 2006;**41**(3):343-8.
299. Das I, Reeves RH. The use of mouse models to understand and improve cognitive deficits in Down syndrome. Dis Model Mech 2011;**4**(5):596-606.
300. Borck G, Molla-Herman A, Boddaert N, et al. Clinical, cellular, and neuropathological consequences of AP1S2 mutations: further delineation of a recognizable X-linked mental retardation syndrome. Hum Mutat 2008;**29**(7):966-74.
301. Motley AM, Berg N, Taylor MJ, et al. Functional analysis of AP-2 alpha and mu2 subunits. Mol Biol Cell 2006;**17**(12):5298-308.
302. O'Seaghdha CM, Yang Q, Glazer NL, et al. Common variants in the calcium-sensing receptor gene are associated with total serum calcium levels. Hum Mol Genet 2010;**19**(21):4296-303.
303. Kifor O, Kifor I, Moore FD, Jr., et al. Decreased expression of caveolin-1 and altered regulation of mitogen-activated protein kinase in cultured bovine parathyroid cells and human parathyroid adenomas. J Clin Endocrinol Metab 2003;**88**(9):4455-64.
304. Wagener BM, Marjon NA, Revankar CM, et al. Adaptor protein-2 interaction with arrestin regulates GPCR recycling and apoptosis. Traffic 2009;**10**(9):1286-300.
305. Gesty-Palmer D, Chen M, Reiter E, et al. Distinct beta-arrestin- and G protein-dependent pathways for parathyroid hormone receptor-stimulated ERK1/2 activation. J Biol Chem 2006;**281**(16):10856-64.
306. Pi M, Quarles LD. Osteoblast calcium-sensing receptor has characteristics of ANF/7TM receptors. J Cell Biochem 2005;**95**(6):1081-92.
307. Winslow MM, Pan M, Starbuck M, et al. Calcineurin/NFAT signaling in osteoblasts regulates bone mass. Dev Cell 2006;**10**(6):771-82.
308. Temal T, Jary H, Auberval M, et al. New potent calcimimetics: I. Discovery of a series of novel trisubstituted ureas. Bioorg Med Chem Lett 2013;**23**(8):2451-4.
309. Howles SAH, F. M. Babinsky, V.N. Rogers, A. Rust, N. Richardson, T. McKenna, M.J, Nesbit, M.A.N. Thakker, R.V. . Cinacalcet is an effective therapy for familial hypocalciuric hypercalcaemia type 3 (FHH3) caused by AP2S1 mutations. Endocrine Society's 97th Annual Meeting and Expo. San Diego, 2015.
310. Fan L, Hao H, Xue Y, et al. Dynamic analysis of Arabidopsis AP2 sigma subunit reveals a key role in clathrin-mediated endocytosis and plant development. Development 2013;**140**(18):3826-37.
311. Kelley LA, Sternberg MJ. Protein structure prediction on the Web: a case study using the Phyre server. Nat Protoc 2009;**4**(3):363-71.

312. White JK, Gerdin AK, Karp NA, et al. Genome-wide generation and systematic phenotyping of knockout mice reveals new roles for many genes. Cell 2013;**154**(2):452-64.
313. Flores LE, Hildebrandt TB, Kuhl AA, et al. Early detection and staging of spontaneous embryo resorption by ultrasound biomicroscopy in murine pregnancy. Reprod Biol Endocrinol 2014;**12**:38.
314. Umasankar PK, Sanker S, Thieman JR, et al. Distinct and separable activities of the endocytic clathrin-coat components Fcho1/2 and AP-2 in developmental patterning. Nat Cell Biol 2012;**14**(5):488-501.
315. Papaioannou VE, Behringer RR. Early embryonic lethality in genetically engineered mice: diagnosis and phenotypic analysis. Vet Pathol 2012;**49**(1):64-70.
316. Liu CC, Kanekiyo T, Roth B, et al. Tyrosine-based signal mediates LRP6 receptor endocytosis and desensitization of Wnt/beta-catenin pathway signaling. J Biol Chem 2014;**289**(40):27562-70.
317. Kandachar V, Roegiers F. Endocytosis and control of Notch signaling. Curr Opin Cell Biol 2012;**24**(4):534-40.
318. Feinstein TN, Yui N, Webber MJ, et al. Noncanonical control of vasopressin receptor type 2 signaling by retromer and arrestin. J Biol Chem 2013;**288**(39):27849-60.
319. Wehbi VL, Stevenson HP, Feinstein TN, et al. Noncanonical GPCR signaling arising from a PTH receptor-arrestin-Gbetagamma complex. Proc Natl Acad Sci U S A 2013;**110**(4):1530-5.
320. Pearce SH, Williamson C, Kifor O, et al. A familial syndrome of hypocalcemia with hypercalciuria due to mutations in the calcium-sensing receptor. The New England journal of medicine 1996;**335**(15):1115-22.
321. Raue F, Pichl J, Dorr HG, et al. Activating mutations in the calcium-sensing receptor: genetic and clinical spectrum in 25 patients with autosomal dominant hypocalcaemia - a German survey. Clinical endocrinology 2011;**75**(6):760-5.
322. Pearce SH, Trump D, Wooding C, et al. Calcium-sensing receptor mutations in familial benign hypercalcemia and neonatal hyperparathyroidism. J Clin Invest 1995;**96**(6):2683-92.
323. Lambert AS, Grybek V, Francou B, et al. Analysis of AP2S1, a calcium-sensing receptor regulator, in familial and sporadic isolated hypoparathyroidism. J Clin Endocrinol Metab 2014;**99**(3):E469-73.
324. Montpetit A, Cote S, Brustein E, et al. Disruption of AP1S1, causing a novel neurocutaneous syndrome, perturbs development of the skin and spinal cord. PLoS Genet 2008;**4**(12):e1000296.

Appendix

10 Appendix

10.1 Vector maps

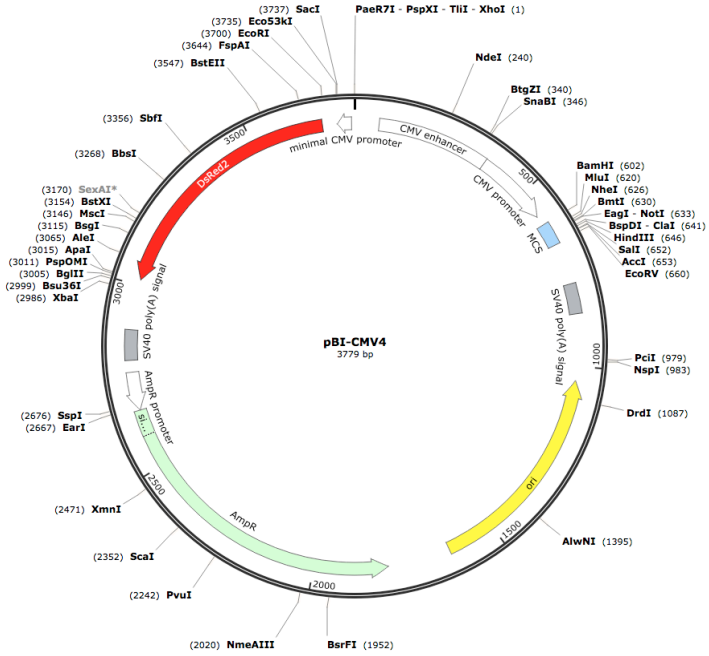


Figure 10.1. Vector map for pBI-CMV4-RFP.

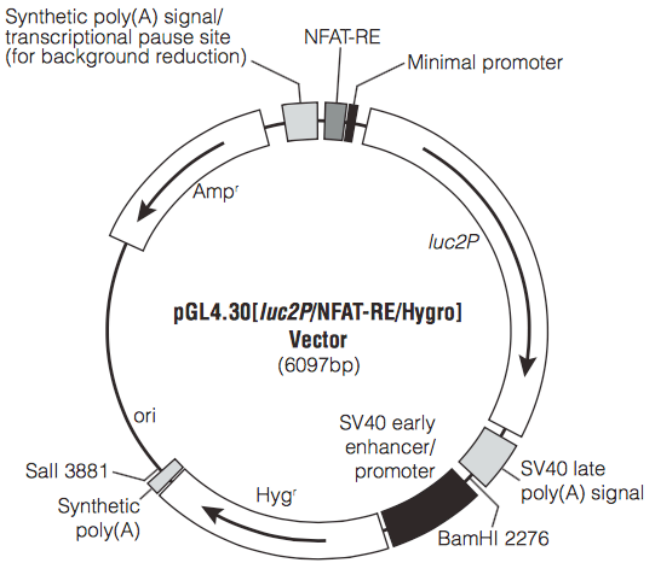


Figure 10.2. Vector map for pGL4.30[*luc2P*/NFAT-RE/Hydro].

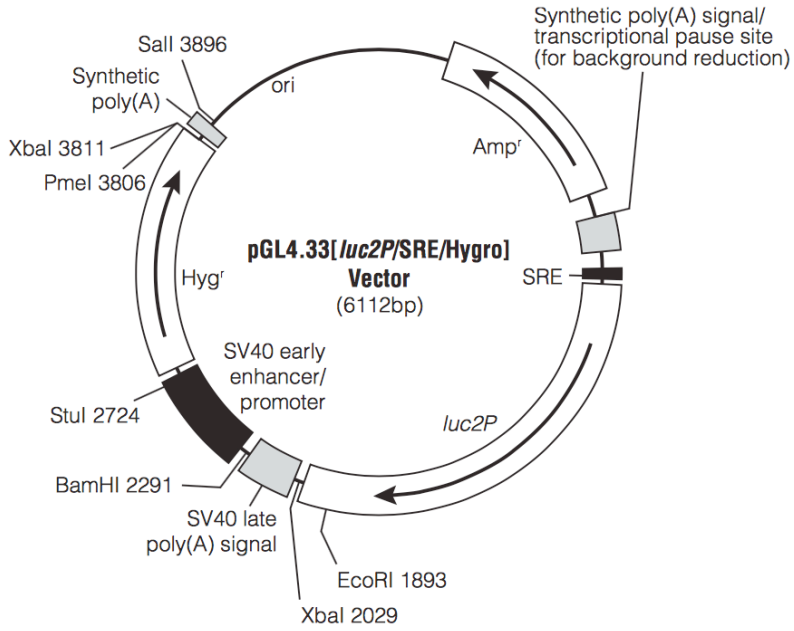


Figure 10.3. Vector map for pGL4.33[*luc2P*/SRE/Hydro].

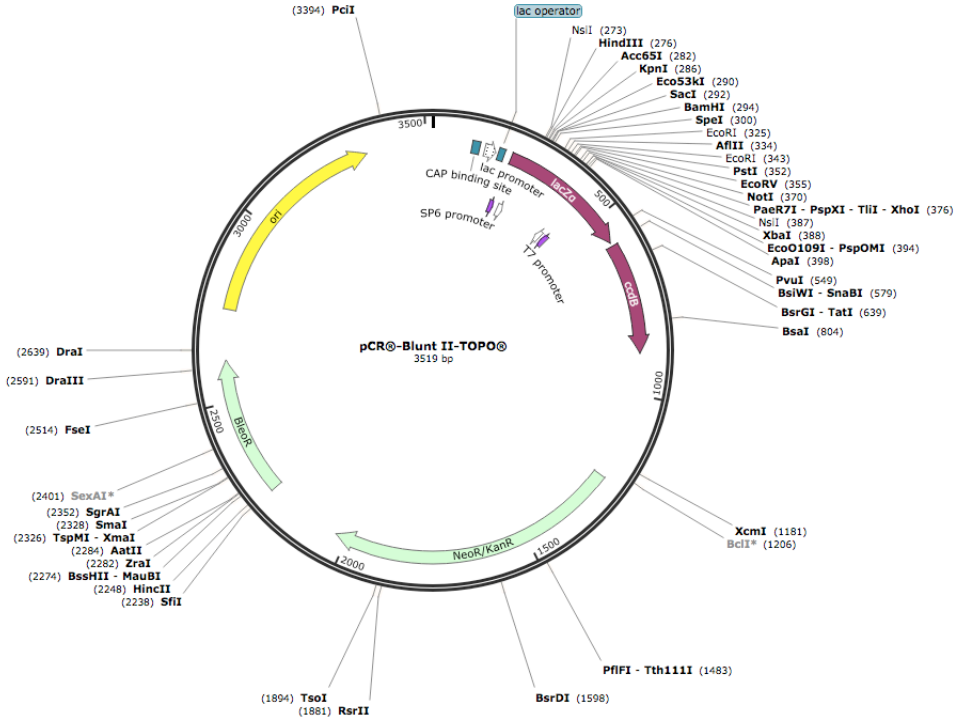


Figure 10.4. Vector map for pCR-Blunt II-TOPO.

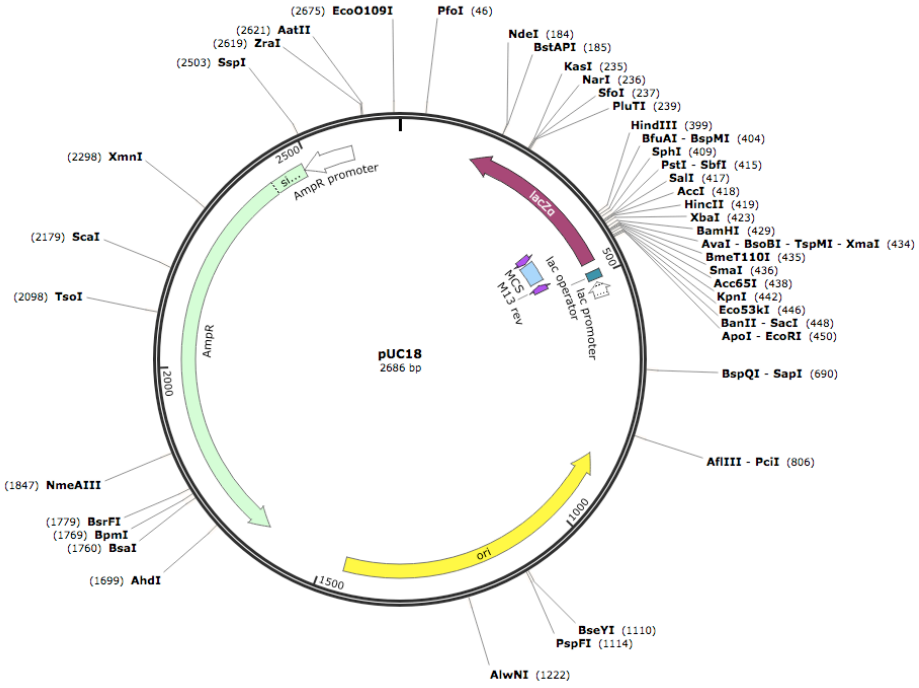


Figure 10.5. Vector map for pUC18.

10.2 Primer sequences

10.2.1 Primers for PCR amplification and sequencing of human *AP2S1*

Exon	Primer sequence	Annealing temperature (°C)
Exon 1	F: CTGGTTCTTCAGCATCTCG R: CAGAGAAGGGACTTGTCAGC	58
Exon 2	F: AGCCCTATCTCCCCTCTGG R: GAAGCAAGCAAGCTCAAAGC	59
Exon 3	F: GAGTGAAGGAGTGAATGTTTTGG R: AAGAAATGGAGAGGGAGAGTCC	61
Exon 4	F: TTGCTGTCTCTCTTTCTGATGACC R: AGCTGGGACACAGACCTCAG	61.5
Exon 5	F: ATCAGAGCCCCAGCTTCC R: GAAGGACTGCTGGGTTGG	61.5

10.2.2 Primers for PCR amplification and sequencing of human *GNA11*

Exon	Primer sequence	Annealing temperature (°C)
Exon 1	F: CCAGCCTGCTAGGTTGTCC R: ACTCACCGAGCAGCAGCAG	62
Exon 2	F: GCAGGGTCTGGGTAAGAGG R: ATGGATGACCAGGGGTAGC	61
Exon 3	F: CGAGCTCTCGACGTCTCC R: CCTTCCCGAAGGGTCCCA	61
Exon 4	F: GTGCTGTGTCCCTGTCCTG R: GGGCAAATGAGCCTCTCAG	61.5
Exon 5	F: GCCAGGTGGCTGAGTCCT R: CACTGCACACAGCCCAAG	64
Exon 6	F: CTTGGGCTGTGTGCAGTG R: ATGAGCCCCTCTCCCATATC	60
Exon 7	F: ACAAAGGGGCCCACGAGT R: GTGTCTCCATCCCGTCTC	60

10.2.3 Primers for PCR of mouse *AP2S1* cDNA

Exon	Primer sequence	Annealing temperature (°C)
Exon 1-2 boundary	F: GATCCGATTCATCCTTATCC	60
Exon 2-3 boundary	R: CCTCGAGATAGGCCAGATTGT	60

10.2.4 Primers for genotyping of splice site *Ap2s1* mouse model

Primer sequence	Annealing temperature (°C)
F: TCTCCCATAGAATGTCTCGT	60
R: CAACGAGCCACATCCACAAC	60

10.2.5 Primers for sequencing pCR-Blunt II-TOPO construct

Primer sequence
M13F: GTAAAACGACGGCCAG
M13R: CAGGAAACAGCTATGAC

10.2.6 Primers for sequencing pBI-CMV4 *AP2S1* construct

Primer sequence
VF: CAACGGGACTTTCCAAAATG
VR: GCTCAGTCACTCGCTCCTTC
AP2S1 F: TATCCTCATCCAGAACCGGG
AP2S1 R: GTTTCAGCACCTTCGTCTGG

10.2.7 Primers for sequencing pBI-CMV4 *GNA11* constructs

Primer sequences
VF: CAACGGGACTTTCCAAAATG
VR: GCTCAGTCACTCGCTCCTTC
GNA11 1F: CGATGACTCTGGAGTCC
GNA11 3R: TCCACCAGGTGCGAGTACAGG

10.2.8 Primers used for site-directed mutagenesis in pBI-CMV4 *GNA11* construct

Mutation	Primer sequence
Met87Val	GGATCATGGCCTGCACGGCGGTGAAGATGTT
	AACATCTTCACCGCCGTGCAGGCCATGATCC

10.2.8.1 Primers used to construct the TALENs donor matrix

Mutation/s	Primer sequence
6 silent mutations to prevent TALEN cutting donor matrix	CCGATTCATCCTGATTCAGAATCGGGCAGGCAAG
	GACGCGCCTGGCAAAATGGTATATGCAGTTCGAT
Arg15Leu	CGGGCAGGCAAGACGCTCCTGGCAAAATGGT
	ACCATTTTGCCAGGAGCGTCTTGCCTGCCCG

10.3 Antibodies

10.3.1 Primary

Primary antibody	Manufacturer	Dilution
Mouse monoclonal anti-human CaSR	Abcam, ab19347	1:1000
Rabbit monoclonal anti-human/mouse AP2σ2	Abcam, ab128950	1:1000
Rabbit monoclonal anti-mouse AP2α	Abcam, ab108311	1:250
Rabbit polyclonal anti-mouse AP2β2	Abcam, ab82711	1:250
Rabbit monoclonal anti-human/mouse AP2μ2	Abcam, ab75995	1:250
Rabbit polyclonal anti-human/mouse calnexin	Merck Millipore, AB2301	1:1000

10.3.2 Secondary

Secondary antibody	Manufacturer	Dilution
Goat anti-rabbit IgG-HRP	BioRad, 1706515	1:3000
Goat anti-mouse IgG-HRP	SantaCruz, sc-2005	1:3000

10.4 Publications

Rogers A*, Nesbit MA*, Hannan FM*, *et al*. Mutational analysis of the adaptor protein 2 sigma subunit (*AP2S1*) gene: search for autosomal dominant hypocalcemia type 3 (ADH3). *The Journal of Clinical Endocrinology and Metabolism*. 2014;99(7):E1300-5.

Hannan FM*, Howles SA*, **Rogers A***, *et al*. Adaptor protein-2 sigma subunit mutations causing familial hypocalciuric hypercalcaemia type 3 (FHH3) demonstrate genotype-phenotype correlations, codon bias and dominant-negative effects. *Human Molecular Genetics* 2015; doi: 10.1093/hmg/ddv226.

Howles SA*, Hannan FM*, Babinsky VN, **Rogers A**, *et al*. Cinacalcet rectifies symptomatic hypercalcemia caused by *AP2S1* mutations. *NEJM*. 2016; 374: 1396-8.

* Joint first author

Mutational Analysis of the Adaptor Protein 2 Sigma Subunit (*AP2S1*) Gene: Search for Autosomal Dominant Hypocalcemia Type 3 (ADH3)

Angela Rogers,* M. Andrew Nesbit,* Fadil M. Hannan,* Sarah A. Howles, Caroline M. Gorvin, Treena Cranston, Jeremy Allgrove, John S. Bevan, Gul Bano, Caroline Brain, Vipan Datta, Ashley B. Grossman, Shirley V. Hodgson, Louise Izatt, Lynne Millar-Jones, Simon H. Pearce, Lisa Robertson, Peter L. Selby, Brian Shine, Katie Snape, Justin Warner, and Rajesh V. Thakker†

Context: Autosomal dominant hypocalcemia (ADH) types 1 and 2 are due to calcium-sensing receptor (*CASR*) and G-protein subunit-α11 (*GNA11*) gain-of-function mutations, respectively, whereas *CASR* and *GNA11* loss-of-function mutations result in familial hypocalciuric hypercalcemia (FHH) types 1 and 2, respectively. Loss-of-function mutations of adaptor protein-2 sigma subunit (AP2σ 2), encoded by *AP2S1*, cause FHH3, and we therefore sought for gain-of-function *AP2S1* mutations that may cause an additional form of ADH, which we designated ADH3.

Objective: The objective of the study was to investigate the hypothesis that gain-of-function *AP2S1* mutations may cause ADH3.

Design: The sample size required for the detection of at least one mutation with a greater than 95% likelihood was determined by binomial probability analysis. Nineteen patients (including six familial cases) with hypocalcemia in association with low or normal serum PTH concentrations, consistent with ADH, but who did not have *CASR* or *GNA11* mutations, were ascertained. Leukocyte DNA was used for sequence and copy number variation analysis of *AP2S1*.

Results: Binomial probability analysis, using the assumption that *AP2S1* mutations would occur in hypocalcemic patients at a prevalence of 20%, which is observed in FHH patients without *CASR* or *GNA11* mutations, indicated that the likelihood of detecting at least one *AP2S1* mutation was greater than 95% and greater than 98% in sample sizes of 14 and 19 hypocalcemic patients, respectively. *AP2S1* mutations and copy number variations were not detected in the 19 hypocalcemic patients.

Conclusion: The absence of *AP2S1* abnormalities in hypocalcemic patients, suggests that ADH3 may not occur or otherwise represents a rare hypocalcemic disorder. **(*J Clin Endocrinol Metab* 99: E1300–E1305, 2014)**

Hypocalcemia is usually associated with either undetectable serum PTH concentrations, as occurring in hypoparathyroidism, or elevated serum PTH concentrations, as occurring in secondary hyperparathyroidism, whose causes include vitamin D deficiency or chronic renal failure, or pseudohypoparathyroidism, which is due to PTH resistance (1). However, hypocalcemia may also occasionally occur in association with normal or low serum PTH concentrations, as in autosomal dominant hypocalcemia [ADH; online inheritance in man (OMIM) number 601198 and number 615361]. ADH may be associated with either of the following: 1) gain-of-function mutations of the calcium-sensing receptor (CaSR) (2–5), a guanine-nucleotide protein (G protein)-coupled receptor, which is

ISSN Print 0021-972X ISSN Online 1945-7197
Printed in U.S.A.
Copyright © 2014 by the Endocrine Society
Received October 25, 2013. Accepted March 18, 2014.
First Published Online April 7, 2014

* A.R., M.A.N., and F.M.H. contributed equally to this study.
†Author affiliations are shown at the bottom of the next page.
Abbreviations: ADH, autosomal dominant hypocalcemia; ADH1, ADH type 1; ADH2, ADH type 2; ADH3, ADH type 3; AP2σ2, adaptor protein-2 sigma subunit; Ca^{2+}_o, extracellular calcium; CaSR, calcium-sensing receptor; CNV, copy number variation; C_T, threshold cycle; FHH, familial hypocalciuric hypercalcemia; *GNA11*, gene encoding G-protein-α11 subunit; OMIM, Online Mendelian Inheritance in Man; SNP, single-nucleotide polymorphism.

The Endocrine Society. Downloaded from press.endocrine.org by [${individualUser.displayName}] on 14 September 2015. at 06:34 For personal use only. No other uses without permission. . All rights reserved.

encoded by *CASR* (6) and referred to as ADH type 1 (ADH1; OMIM number 601198); or 2) gain-of-function mutations of the G-protein subunit-α11 which is encoded by *GNA11* and referred to as ADH2 (OMIM number 615361) (7). *GNA11* mutations have also been reported in two families with isolated hypoparathyroidism, and these could be referred to as ADH2 because the hypocalcemia was associated with either serum PTH concentrations within the reference range (in ~40% of patients) or below the lower limit of the reference range (in ~60% of patients), similar to the situation in ADH patients (8). Thus, in ADH1 patients, the hypocalcemia may be mild (2.00–2.20 mmol/L) or severe (<1.90 mmol/L) and associated with serum PTH concentrations within the reference range in greater than 40% of ADH1 patients and below the lower limit of the reference range in the remaining less than 60% of ADH1 patients (3, 9).

The hypocalcemia in ADH1 patients may be associated with symptoms that include paraesthesia, carpopedal spasm, and seizures in approximately 50% of patients (3, 9), whereas the remaining 50% of ADH1 patients have asymptomatic hypocalcemia. Serum phosphate concentrations in ADH1 patients may be elevated or in the upper-normal range (2), and serum magnesium concentrations may be low or in the low-normal range (3). Approximately 10% of ADH1 patients have an absolute hypercalciuria, which may be associated with nephrocalcinosis or kidney stones (3, 10). Vitamin D preparations and calcium supplements to correct the hypocalcemia may worsen the hypercalciuria and lead to renal impairment (11). Ectopic calcifications in sites such as the basal ganglia may be found in greater than 35% of ADH1 patients (3). Approximately 20% of ADH1 probands may not have a family history because they have de novo *CASR* mutations (7). The clinical features of the reported hypocalcemic patients and families with *GNA11* mutations (7, 8) seem to be similar to those of ADH1 patients, although this extrapolation requires cautious interpretation because only four such patients and families have been reported to date (7, 8). The *CASR* and *GNA11* mutations that are associated with ADH1 and ADH2, respectively, result in an increased sensitivity of cells expressing CaSRs to extracellular calcium (Ca^{2+}_o) and are thus representations of gain-of-function mutations, in contrast to the loss-of-function mutations of the *CASR* and *GNA11*, which are associated with familial hypocalciuric hypercalcemia (FHH) type 1 (OMIM number 145980) and FHH2 (OMIM number 145981), respectively (5, 7, 12).

A recent study has shown that FHH3 is due to loss-of-function mutations of the *AP2S1* gene, which encodes the adaptor protein-2 sigma subunit (AP2σ2) (13). Indeed, such *AP2S1* mutations were found to occur in greater than 20% of FHH patients without *CASR* mutations and were shown to decrease the sensitivity of the CaSR-expressing cells to Ca^{2+}_o, consistent with a loss-of-function (13). Gain-of-function *AP2S1* mutations have not been identified to date, and we postulated, by analogy to the situation in ADH1 and ADH2, that such gain-of-function mutations may result in an additional form of ADH, which we have designated ADH3. We sought to identify gain-of-function *AP2S1* mutations in hypocalcemic patients who were considered to have ADH or isolated hypoparathyroidism but did not have *CASR*, *GNA11*, *GCMB*, or *PTH* mutations, which may occur in approximately 50% of such patients.

Materials and Methods

Patients

Informed consent was obtained from individuals, using protocols approved by the local and national ethics committees (MREC/02/2/93). Nineteen unrelated patients (13 males and six females) with hypocalcemia, likely due to isolated hypoparathyroidism, were ascertained, and six patients had a family history of hypocalcemia (Table 1). These patients did not have features of autoimmune disease, immunodeficiency, deafness, cardiofacial abnormalities, or a history of neck surgery, and because the patients had isolated (nonsyndromic) hypoparathyroidism, fluorescent in situ hybridization to detect deletions and translocations of chromosome 22q, which would be found in the DiGeorge syndrome, was not performed. Previous mutational analysis of *CASR*, *GNA11*, *GCMB*, and *PTH* genes by Sanger DNA sequencing, and alignment to the corresponding reference sequences, had not identified any abnormalities of the coding regions and exon-intron boundaries of these genes. All serum and urine estimations were undertaken at a time when the patients were not being treated with vitamin D preparations or calcium supplementation.

Academic Endocrine Unit (A.R., M.A.N., F.M.H., S.A.H., C.M.G., R.V.T.), Nuffield Department of Clinical Medicine, and Academic Endocrine Unit (A.R., M.A.N., F.M.H., S.A.H., C.M.G., R.V.T.), Radcliffe Department of Medicine, University of Oxford, Oxford OX3 7LJ, United Kingdom; Oxford Molecular Genetics Laboratory (T.C.) and Oxford Centre for Diabetes, Endocrinology, and Metabolism (A.B.G.), Churchill Hospital, Oxford OX3 7LJ, United Kingdom; Department of Paediatric Endocrinology (J.A., C.B.), Great Ormond Street Hospital, London WC1N 3JH, United Kingdom; Department of Paediatric Endocrinology (J.A.), Royal London Hospital, London E1 1BB, United Kingdom; Department of Endocrinology (J.S.B.), Aberdeen Royal Infirmary, Aberdeen AB25 2ZN, United Kingdom; Departments of Diabetes and Endocrinology (G.B.) and Clinical Genetics (S.V.H., K.S.), St George's Hospital, London SW17 0RE, United Kingdom; Jenny Lind Children's Department (V.D.), Norfolk and Norwich University Hospitals National Health Service Foundation Trust, Norfolk NR4 7UY, United Kingdom; Department of Clinical Genetics (L.I.), Guy's and St Thomas' Foundation Trust, Guy's Hospital, London SE1 9RT, United Kingdom; Department of Paediatrics (L.M.-J.), Royal Glamorgan Hospital, Glamorgan CF72 8XR, United Kingdom; Endocrine Unit (S.H.P.), Royal Victoria Infirmary, Newcastle upon Tyne NE1 4LP, United Kingdom; Department of Clinical Genetics (L.R.), Leicester Royal Infirmary, Leicester LE1 5WW, United Kingdom; Department of Medicine (P.L.S.), Manchester Royal Infirmary, Manchester M13 9WL, United Kingdom; Department of Clinical Biochemistry (B.S.), John Radcliffe Hospital, Oxford OX3 9DU, United Kingdom; and Department of Paediatrics (J.W.), University Hospital of Wales, Cardiff CF14 4XW, United Kingdom

The Endocrine Society. Downloaded from press.endocrine.org by [${individualUser.displayName}] on 14 September 2015. at 06:34 For personal use only. No other uses without permission. . All rights reserved.

Table 1. Clinical and Biochemical Findings in the Hypocalcemic Patients, Considered as Having ADH but Without *CASR* or *GNA11* Mutations

					Serum							Urine
Patient	Sex	Family History	Age	Clinical Features at Presentation/ Diagnosis	Calcium, mmol/L[a]	Phosphate, mmol/L[b,c]	ALP, U/L[d,e]	Mg, mmol/L[f]	Creatinine, μmol/L[g]	PTH[h,i]	25OHD, nmol/L[j]	CCCR[k,l,m]
15/01	M	No	55 y	Asymptomatic	1.99	1.28[b]	95[d]	0.8	180	2.0[h]	—	0.01[k]
07/02	M	Sons affected	46 y	Cataracts	1.35	1.9[b]	49[d]	—	49	5.0[h]	—	—
08/03	M	No	60 y	Asymptomatic	1.63	1.38[b]	104[e]	0.93	—	1.6[i]	—	0.003[k]
05/04	F	Yes[n]	Neonate	Seizures	1.62	3.10[c]	228[e]	0.65	49	0.8[i]	—	0.004[k]
13/04	F	Son affected	53 y	Asymptomatic	1.93	0.87[b]	53[d]	0.86	81	4.7[i]	77.5	0.018[k]
05/05	M	Mother and sister affected	3 y	Asymptomatic	2.03	1.91[c]	129[e]	0.97	49	1.1[i]	85	0.05[k]
16/07	M	No	9 y	Seizures	1.86	2.77[b]	336[e]	0.7	49	5.6[i]	105	0.04[k]
01/08	M	No[o]	2 y	Seizures	0.94	2.20[c]	432[e]	0.73	47	2.6[i]	<18	0.02[k]
19/09	F	No	68 y	Asymptomatic	1.91	1.21[b]	91[d]	0.68	75	18[h]	64	0.004[k]
19/10	M	—	1 mo	Seizures	1.63	3.29[c]	104[d]	0.68	30	3.6[i]	43	—
01/12	F	No[o]	2 mo	Seizures	1.25	2.52[c]	388[e]	0.57	<18	1.4[i]	101	1.25[l]
09/12	M	No[o]	2 mo	Seizures	1.30	2.35[c]	—	—	25	<0.3[i]	17	0.001[k]
16/12	M	Father affected	31 y	Carpopedal spasm	1.88	1.73[b]	52[d]	—	88	0.7[i]	35	0.008[k]
04/13	M	No	62 y	Paraesthesia	1.64	1.43[b]	53[d]	0.76	104	22[h]	29	13.5[m]
07/13	M	No	2 y	Seizures	1.37	3.74[c]	125[e]	1.03	38	1.6[i]	36	0.006[k]
10/13	F	No	25 y	Tetany	1.53	1.55[b]	131[e]	0.70	61	<0.3[i]	50	—
15/13	M	Father affected	57 y	Polyuria	1.94	0.96[b]	74[d]	0.93	84	26[h]	86	8.94[m]
19/13	F	No	9 y	Seizures	1.35	3.32[c]	166[e]	0.64	52	<0.3[i]	18	0.05[k]
25/13	M	No	31 y	Tetany, cataracts	1.31	1.20[b]	155[e]	0.73	80	0.3	27	0.03[m]

Abbreviations: ALP, alkaline phosphatase activity; CCCR, calcium to creatinine clearance ratio; F, female; M, male; —, not known; 25OHD, 25-hydroxyvitamin D. All serum and urine estimations were undertaken at a time when the patients were not being treated with vitamin D preparations or calcium supplementation. Thirteen patients were white Europeans and six patients (01/08, 19/10, 01/12, 9/12, 16/12, 25/13) were of Asian or Middle Eastern origin. The age at presentation or diagnosis is provided. Fifty percent of ADH patients are asymptomatic, and hence, the age of presentation is the same as that at diagnosis; however, if the age at presentation and diagnosis are not the same, then the age at diagnosis is provided. Other family members were unavailable for studies.

Normal serum ranges listed below are reported elsewhere (12).

[a] Albumin-adjusted calcium, 2.10–2.60 mmol/L.

[b] Phosphate, 0.70–1.40 mmol/L.

[c] Phosphate, 1.20–2.10 mmol/L.

[d] ALP activity, 30–130 U/L.

[e] ALP activity, 70–330 U/L.

[f] Magnesium (Mg), 0.70–1.05 mmol/L.

[g] Creatinine, 54–145 μmol/L.

[h] PTH, 10–65 ng/L.

[i] PTH, 1.3–7.6 pmol/L.

[j] 25OHD, greater than 50 nmol/L.

[k] CCCR, greater than 0.02.

[l] Urine calcium to creatinine ratio, 0.1–0.7 per 24 hours.

[m] Urine calcium excretion, Greater than 4.0 mmol per 24 hours.

[n] Details of affected members are not available.

[o] Patient is the offspring of consanguineous unaffected parents.

Statistical analysis

It is unclear whether gain-of-function *AP2S1* mutations may be associated with ADH. To establish whether the study was sufficiently powered to detect at least one *AP2S1* mutation with a greater than 95% likelihood, the sample size required was determined by binomial probability analysis (Microsoft Excel), as previously reported (14). Because FHH1 and ADH1 are associated with a similar prevalence of *CASR* mutations, approximately 65% and greater than 70%, respectively (2, 3, 5, 9, 15), the binomial analysis was based on a 20% prevalence for *AP2S1* mutations in hypocalcemic patients without *CASR*, *GNA11*, *GCMB*, or *PTH* mutations, which would be similar to that observed for *AP2S1* loss-of-function mutations in FHH patients (13) and less than the prevalence of greater than 70% for gain-of-function *CASR* mutations observed in ADH patients (2, 3, 9, 15). The binomial distribution probability was calculated using the following formula:

Binomial distribution probability = $b(x;n,p)$, where

$$b(x;n,p) = \binom{n}{x} p^x(1-p)^{n-x}$$

where n = sample size, x = number of probands harboring mutations; n-x = number of probands with no mutation; and p = prevalence of *AP2S1* mutations in the cohort.

The Endocrine Society. Downloaded from press.endocrine.org by [${individualUser.displayName}] on 14 September 2015. at 06:34 For personal use only. No other uses without permission. . All rights reserved.

Mutational analysis

Leukocyte DNA was extracted from venous blood samples (14) and quantified using the high-sensitivity Qubit system (Invitrogen). *AP2S1*-specific primers were used to perform PCR amplification of the five exons and eight exon-intron boundaries of the *AP2S1* gene, as previously reported (13). DNA sequence analysis of the PCR products was performed using the BigDye Terminator version 3.1 cycle sequencing kit (Life Technologies) and an ABI automated capillary sequencer (Applied Biosystems), as reported (5). The DNA sequences were aligned to the corresponding genomic sequence (ENST00000263270) from Ensembl (www.ensembl.org) to detect any mutations. An assessment of single-nucleotide polymorphisms (SNPs) was undertaken using the NCBI database single nucleotide polymorphism (dbSNP) (http://ncbi.nlm.nih.gov/SNP/) and Exome Variant Server (http://evs.gs.washington.edu/EVS/) databases (16). The occurrence of *AP2S1* deletions or duplications was assessed by estimating the *AP2S1* copy number variations (CNVs) in DNA from hypocalcemic patients and normocalcemic controls using quantitative PCR and the Rotorgene SYBR green kit (QIAGEN) (17). Samples were assessed in triplicate using primers specific for *AP2S1* and TATA-box binding protein 1 (*TBP1*), as a reference gene. Threshold cycle (C_T) values were obtained and analyzed, as described (13, 17). *AP2S1* Ct values were expressed relative to *TBP1* Ct values and normalized to the mean *AP2S1/TBPI* Ct value from four normocalcemic controls.

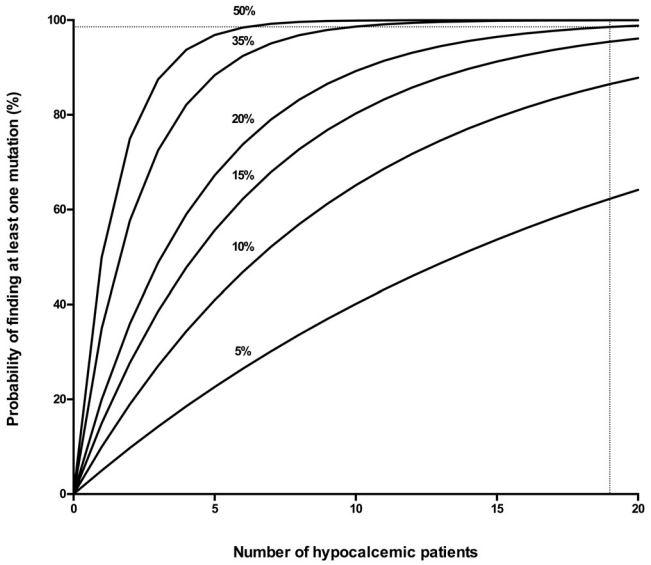


Figure 1. Binomial probability analysis to predict the sample size required to detect one or more *AP2S1* mutations for different mutation prevalences in hypocalcemic patients. The number of patients is shown on the x-axis, and the probability of detecting at least one *AP2S1* mutation, at different prevalences ranging from 5% to 50%, is shown on the y-axis. The analysis indicated that a sample size of 19 hypocalcemic patients (represented by the dotted line) is required to detect at least one *AP2S1* mutation at a 20% prevalence, which is observed in FHH3, with a probability of greater than 98%.

Results

Patients

The 19 hypocalcemic patients comprised 13 males and six females with ages at diagnosis or presentation that ranged from the neonatal period to 68 years (Table 1), and greater than 65% of the patients had presented with hypocalcemic symptoms. More than 70% of the patients had severe hypocalcemia; serum PTH concentrations were either below the lower limit of normal, in the low normal range, or in the high normal range in 40%, greater than 40%, and greater than 15% of the patients, respectively (n = 19); more than 60% of the patients (n = 19) had elevated serum phosphate concentrations and 25% had serum phosphate concentrations in the high normal range. Hypomagnesemia was found in 30% of 16 patients and serum alkaline phosphatase activity was within the normal range in 80% of 18 patients. The urinary calcium to creatinine clearance ratio was high in 30% of 12 patients. These findings are similar to those reported in ADH1 patients (3, 9).

Power calculation and sample size

The prevalence of *AP2S1* mutations in hypocalcemic patients is not known, and a binomial probability analysis in which the prevalence of *AP2S1* mutations was varied was performed (Figure 1). This showed that if the prevalences of *AP2S1* mutations in hypocalcemic patients were 5%, 10%, 15%, or 20%, then the sample sizes to detect at least one *AP2S1* mutation in a hypocalcemic patient with a greater than 95% probability, who had been previously shown to not have *CASR*, *GNA11*, *GCMB*, or *PTH* mutations, were n = 59, n = 29, n = 19, and n = 14, respectively. Thus, if the prevalence of *AP2S1* mutations in ADH was similar to that observed for *AP2S1* mutations in FHH (ie, 20%), then a sample size of 14 hypocalcemic patients would have a greater than 95% probability of detecting at least one *AP2S1* mutation, and the sample size of 19 hypocalcemic patients, used in this study, would have a greater than 98% and greater than 95% likelihood of detecting at least one *AP2S1* mutation, assuming a mutation prevalence of 20% and 15%, respectively.

AP2S1 mutational analysis

DNA sequence analysis of the 429-bp coding region of the *AP2S1* gene and the eight intron-exon boundaries in the 19 hypocalcemic patients (Table 1) did not detect any point mutations, deletions, insertions, or unreported SNPs. Furthermore, an examination of the four reported synonymous *AP2S1* SNPs (rs201984742 (I5I), rs150080027 (D25D), rs151335841 (F87F), and rs143384246 (N92N)), the nonsynonymous *AP2S1* SNP (rs11550738 (C68S), and the splice donor variant (rs112326072) revealed the presence of only the major (ie, more frequent) alleles in the hypocalcemic patients. *AP2S1* CNVs were not detected, indicating the absence of deletions, insertions, or duplications (Supplemental

The Endocrine Society. Downloaded from press.endocrine.org by [${individualUser.displayName}] on 14 September 2015. at 06:34 For personal use only. No other uses without permission. . All rights reserved.

Figure 1). Finally, 11 probands were found to have known *CASR* and/or *GNA11* SNPs (Supplemental Table 1). Thus, *AP2S1* mutations, deletions, or duplications were not identified in any of the hypocalcemic patients analyzed in this study.

Discussion

Our study has not identified *AP2S1* mutations in hypocalcemic patients who had clinical features consistent with ADH and did not have *CASR*, *GNA11*, *GCMB*, or *PTH* mutations. These results suggest that *AP2S1* gain-of-function mutations are unlikely to be a major cause of ADH. In addition, CNVs such as gene duplications that may lead to overexpression of *AP2S1* were not identified. However, our study analyzed both familial and nonfamilial hypocalcemic cases because ADH has been reported to occur in both familial and sporadic forms (7), and it is possible that the likelihood of detecting an *AP2S1* mutation may have been higher if a group of solely familial hypocalcemic patients were analyzed. Moreover, our study analyzed the coding region and exon-intron boundaries only, and it remains possible that these patients may harbor mutations in the noncoding regulatory regions of the *AP2S1* gene that lead to an increased expression of the AP2σ2 subunit and enhance the sensitivity of cells expressing CaSR to $Ca^{2+}{}_o$, thereby resulting in a gain of CaSR function and hypocalcemia. However, the noncoding regulatory *AP2S1* regions remain to be defined, thereby precluding their current analysis, and of note, noncoding mutations of the *CASR* and *GNA11* genes have not been reported in ADH1 or ADH2, respectively (4, 5, 7).

Adaptor proteins are heterotetrameric complexes, and a mutation in one of the constituent subunits may lead to loss of function, but it is less clear how it would lead to a gain-of-function mutation, and it seems possible that *AP2S1* gain-of-function mutations may not occur. Indeed, to date only loss-of-function mutations of other adaptor protein complexes have been reported (18, 19). These comprise a homozygous splice site mutation of the *AP1S1* gene, which is predicted to disrupt the sigma subunit of the adaptor protein-1 complex and is associated with the mental retardation, enteropathy, deafness, peripheral neuropathy, ichthyosis, and keratoderma syndrome (19), and loss-of-function mutations of the *AP3B1* gene, which encodes the β3A-subunit of the adaptor protein-3 complex, have been identified in patients with Hermansky-Pudlak syndrome, which is associated with oculocutaneous albinism, platelet dysfunction, and abnormalities of lysosomal storage (18).

In summary, we did not find any *AP2S1* abnormalities in hypocalcemic patients. We conclude that *AP2S1* abnormalities are unlikely to be a cause of ADH and that ADH3, caused by gain-of-function *AP2S1* mutations, may not occur or otherwise represents a rare hypocalcemic disorder.

Acknowledgments

Address all correspondence and requests for reprints to: Rajesh V. Thakker, MD, FRCP, FRCPath FMedSci, Academic Endocrine Unit, Radcliffe Department of Medicine, Oxford Centre for Diabetes, Endocrinology, and Metabolism, Churchill Hospital, Oxford OX3 7LJ, United Kingdom. E-mail: rajesh.thakker@ndm.ox.ac.uk.

This work was supported by United Kingdom Medical Research Council Program Grants G9825289 and G1000467 (to M.A.N., F.M.H., and R.V.T.) and National Institute for Health Research Oxford Biomedical Research Centre Programme (to M.A.N. and R.V.T.). A.R. and S.A.H. are Wellcome Trust Clinical Training Fellows.

Disclosure Summary: The authors have nothing to disclose.

References

1. **Hannan FM, Thakker RV.** Investigating hypocalcaemia. *BMJ*. 2013;346:f2213.
2. **Pollak MR, Brown EM, Estep HL, et al.** Autosomal dominant hypocalcaemia caused by a Ca(2+)-sensing receptor gene mutation. *Nat Genet*. 1994;8:303–307.
3. **Pearce SH, Williamson C, Kifor O, et al.** A familial syndrome of hypocalcemia with hypercalciuria due to mutations in the calcium-sensing receptor. *N Engl J Med*. 1996;335:1115–1122.
4. **Hannan FM, Thakker RV.** Calcium-sensing receptor (CaSR) mutations and disorders of calcium, electrolyte and water metabolism. *Best Pract Res Clin Endocrinol Metab*. 2013;27:359–371.
5. **Hannan FM, Nesbit MA, Zhang C, et al.** Identification of 70 calcium-sensing receptor mutations in hyper- and hypo-calcaemic patients: evidence for clustering of extracellular domain mutations at calcium-binding sites. *Hum Mol Genet*. 2012;21:2768–2778.
6. **Brown EM, Gamba G, Riccardi D, et al.** Cloning and characterization of an extracellular Ca(2+)-sensing receptor from bovine parathyroid. *Nature*. 1993;366:575–580.
7. **Nesbit MA, Hannan FM, Howles SA, et al.** Mutations affecting G-protein subunit α11 in hypercalcemia and hypocalcemia. *N Engl J Med*. 2013;368:2476–2486.
8. **Mannstadt M, Harris M, Bravenboer B, et al.** Germline mutations affecting Gα11 in hypoparathyroidism. *N Engl J Med*. 2013;368:2532–2534.
9. **Raue F, Pichl J, Dorr HG, et al.** Activating mutations in the calcium-sensing receptor: genetic and clinical spectrum in 25 patients with autosomal dominant hypocalcaemia—a German survey. *Clin Endocrinol (Oxf)*. 2011;75:760–765.
10. **Yamamoto M, Akatsu T, Nagase T, Ogata E.** Comparison of hypocalcemic hypercalciuria between patients with idiopathic hypoparathyroidism and those with gain-of-function mutations in the calcium-sensing receptor: is it possible to differentiate the two disorders? *J Clin Endocrinol Metab*. 2000;85:4583–4591.
11. **Thakker RV.** Genetic developments in hypoparathyroidism. *Lancet*. 2001;357:974–976.
12. **Pearce SH, Trump D, Wooding C, et al.** Calcium-sensing receptor

The Endocrine Society. Downloaded from press.endocrine.org by [${individualUser.displayName}] on 14 September 2015. at 06:34 For personal use only. No other uses without permission. . All rights reserved.

mutations in familial benign hypercalcemia and neonatal hyperparathyroidism. *J Clin Invest*. 1995;96:2683–2692.
13. **Nesbit MA, Hannan FM, Howles SA, et al.** Mutations in AP2S1 cause familial hypocalciuric hypercalcemia type 3. *Nat Genet*. 2013; 45:93–97.
14. **Newey PJ, Nesbit MA, Rimmer AJ, et al.** Whole-exome sequencing studies of nonhereditary (sporadic) parathyroid adenomas. *J Clin Endocrinol Metab*. 2012;97:E1995–E2005.
15. **D'Souza-Li L, Yang B, Canaff L, et al.** Identification and functional characterization of novel calcium-sensing receptor mutations in familial hypocalciuric hypercalcemia and autosomal dominant hypocalcemia. *J Clin Endocrinol Metab*. 2002;87:1309–1318.
16. **Fu W, O'Connor TD, Jun G, et al.** Analysis of 6,515 exomes reveals the recent origin of most human protein-coding variants. *Nature*. 2013;493:216–220.
17. **Pfaffl MW.** A new mathematical model for relative quantification in real-time RT-PCR. *Nucleic Acids Res*. 2001;29:e45.
18. **Dell'Angelica EC, Shotelersuk V, Aguilar RC, Gahl WA, Bonifacino JS.** Altered trafficking of lysosomal proteins in Hermansky-Pudlak syndrome due to mutations in the β3A subunit of the AP-3 adaptor. *Mol Cell*. 1999;3:11–21.
19. **Montpetit A, Cote S, Brustein E, et al.** Disruption of AP1S1, causing a novel neurocutaneous syndrome, perturbs development of the skin and spinal cord. *PLoS Genet*. 2008;4:e1000296.

ENDOCRINE SOCIETY

Members receive free electronic delivery of
FDA **drug safety alerts** from the PDR Network.

endocrine.org/FDA

The Endocrine Society. Downloaded from press.endocrine.org by [${individualUser.displayName}] on 14 September 2015. at 06:34 For personal use only. No other uses without permission. . All rights reserved.

Human Molecular Genetics, 2015, Vol. 24, No. 18 5079–5092

doi: 10.1093/hmg/ddv226
Advance Access Publication Date: 16 June 2015
Original Article

ORIGINAL ARTICLE

Adaptor protein-2 sigma subunit mutations causing familial hypocalciuric hypercalcaemia type 3 (FHH3) demonstrate genotype–phenotype correlations, codon bias and dominant-negative effects

Fadil M. Hannan[1,†,‡], Sarah A. Howles[1,†], Angela Rogers[1,†], Treena Cranston[2,†], Caroline M. Gorvin[1], Valerie N. Babinsky[1], Anita A. Reed[1], Clare E. Thakker[1], Detlef Bockenhauer[3], Rosalind S. Brown[4], John M. Connell[5], Jacqueline Cook[6], Ken Darzy[7], Sarah Ehtisham[8], Una Graham[9], Tony Hulse[10], Steven J. Hunter[9], Louise Izatt[11], Dhavendra Kumar[12], Malachi J. McKenna[13], John A. McKnight[14], Patrick J. Morrison[15,16], M. Zulf Mughal[8], Domhnall O'Halloran[17], Simon H. Pearce[18], Mary E. Porteous[19], Mushtaqur Rahman[20], Tristan Richardson[21], Robert Robinson[22], Isabelle Scheers[23], Haroon Siddique[24], William G. van't Hoff[3], Timothy Wang[25], Michael P. Whyte[26], M. Andrew Nesbit[1,¶] and Rajesh V. Thakker[1,*]

[1]Academic Endocrine Unit, Radcliffe Department of Medicine, University of Oxford, Oxford, UK, [2]Oxford Molecular Genetics Laboratory, Churchill Hospital, Oxford, UK, [3]Renal Unit, Great Ormond Street Hospital for Children NHS Foundation Trust and UCL Institute of Child Health, London, UK, [4]Division of Endocrinology, Boston Children's Hospital, Boston, MA, USA, [5]School of Medicine, Ninewells Hospital, University of Dundee, Dundee, UK, [6]Clinical Genetics Department, Sheffield Children's Hospital NHS Foundation Trust, Sheffield, UK, [7]Queen Elizabeth II Hospital, Welwyn Garden City, UK, [8]Department of Paediatric Endocrinology, Royal Manchester Children's Hospital, Manchester, UK, [9]Regional Centre for Endocrinology and Diabetes, Royal Victoria Hospital, Belfast, UK, [10]Department of Paediatrics, Evelina London Children's Hospital, St. Thomas' Hospital, London, UK, [11]Department of Clinical Genetics, Guy's Hospital, London, UK, [12]Institute of Cancer and Genetics, University Hospital of Wales, Cardiff, UK, [13]Department of Endocrinology, St. Vincent's University Hospital, Dublin, Ireland, [14]Metabolic Unit, Western General Hospital, NHS Lothian and University of Edinburgh, Edinburgh, UK, [15]Centre for Cancer Research and Cell Biology, Queens University of Belfast, Belfast, UK, [16]Department of Genetic Medicine,

[†]The authors wish it to be known that, in their opinion, the first four authors should be regarded as joint First Authors.
[‡]Present address: Department of Musculoskeletal Biology, Institute of Ageing and Chronic Disease, University of Liverpool, Liverpool, UK.
[¶]Present address: Biomedical Sciences Research Institute, Ulster University, Coleraine, UK.
Received: May 1, 2015. **Revised and Accepted:** June 12, 2015

© The Author 2015. Published by Oxford University Press.
This is an Open Access article distributed under the terms of the Creative Commons Attribution License (http://creativecommons.org/licenses/by/4.0/), which permits unrestricted reuse, distribution, and reproduction in any medium, provided the original work is properly cited.

Downloaded from http://hmg.oxfordjournals.org/ at Oxford University on September 14, 2015

Belfast HSC Trust, Belfast, UK, [17]Department of Endocrinology, Cork University Hospital, Cork, Ireland, [18]Institute of Genetic Medicine, Newcastle University, Newcastle upon Tyne, UK, [19]SE Scotland Genetic Service, Western General Hospital, Edinburgh, UK, [20]Department of Endocrinology, Northwick Park Hospital, London, UK, [21]Diabetes and Endocrine Centre, Royal Bournemouth Hospital, Bournemouth, UK, [22]Department of Endocrinology, Chesterfield Royal Hospital NHS Foundation Trust, Derbyshire, UK, [23]Pediatric Gastroenterology, Hepatology and Nutrition Unit, Cliniques Universitaires Saint-Luc, Brussels, Belgium, [24]Department of Endocrinology, Russells Hall Hospital, Dudley, UK, [25]Department of Clinical Biochemistry, Frimley Park Hospital, Surrey, UK and [26]Center for Metabolic Bone Disease and Molecular Research, Shriners Hospital for Children, St. Louis, Missouri, USA

*To whom correspondence should be addressed at: Academic Endocrine Unit, Radcliffe Department of Medicine, Oxford Centre for Diabetes, Endocrinology and Metabolism (OCDEM), Churchill Hospital, Oxford OX3 7LJ, UK. Tel: +44-1865857501; Fax: +44-1865857502. Email: rajesh.thakker@ndm.ox.ac.uk

Abstract

The adaptor protein-2 sigma subunit (AP2σ2) is pivotal for clathrin-mediated endocytosis of plasma membrane constituents such as the calcium-sensing receptor (CaSR). Mutations of the AP2σ2 Arg15 residue result in familial hypocalciuric hypercalcaemia type 3 (FHH3), a disorder of extracellular calcium (Ca^{2+}_o) homeostasis. To elucidate the role of AP2σ2 in Ca^{2+}_o regulation, we investigated 65 FHH probands, without other FHH-associated mutations, for AP2σ2 mutations, characterized their functional consequences and investigated the genetic mechanisms leading to FHH3. AP2σ2 mutations were identified in 17 probands, comprising 5 Arg15Cys, 4 Arg15His and 8 Arg15Leu mutations. A genotype–phenotype correlation was observed with the Arg15Leu mutation leading to marked hypercalcaemia. FHH3 probands harboured additional phenotypes such as cognitive dysfunction. All three FHH3-causing AP2σ2 mutations impaired CaSR signal transduction in a dominant-negative manner. Mutational bias was observed at the AP2σ2 Arg15 residue as other predicted missense substitutions (Arg15Gly, Arg15Pro and Arg15Ser), which also caused CaSR loss-of-function, were not detected in FHH probands, and these mutations were found to reduce the numbers of CaSR-expressing cells. FHH3 probands had significantly greater serum calcium (sCa) and magnesium (sMg) concentrations with reduced urinary calcium to creatinine clearance ratios (CCCR) in comparison with FHH1 probands with CaSR mutations, and a calculated index of sCa × sMg/100 × CCCR, which was ≥ 5.0, had a diagnostic sensitivity and specificity of 83 and 86%, respectively, for FHH3. Thus, our studies demonstrate AP2σ2 mutations to result in a more severe FHH phenotype with genotype–phenotype correlations, and a dominant-negative mechanism of action with mutational bias at the Arg15 residue.

Downloaded from http://hmg.oxfordjournals.org/ at Oxford University on September 14, 2015

Introduction

Familial hypocalciuric hypercalcaemia (FHH) is an autosomal dominant disorder of extracellular calcium (Ca^{2+}_o) homeostasis characterized by lifelong mild-to-moderate elevations of serum calcium concentrations, mild hypermagnesaemia, normal or elevated circulating parathyroid hormone (PTH) concentrations and inappropriately low urinary calcium excretion [mean urinary calcium to creatinine clearance ratio (CCCR) <0.01] (1–4). FHH is a genetically heterogeneous disorder comprising three reported variants. FHH types 1 and 2 (FHH1, OMIM #145980; FHH2, OMIM #145981) are due to heterozygous loss-of-function mutations of the calcium-sensing receptor (CaSR) and G-protein, $G\alpha_{11}$, encoded by the *CASR* and *GNA11* genes, respectively (5–9). CaSR and $G\alpha_{11}$ are widely expressed, including in the parathyroid glands and kidneys, and play a pivotal role in Ca^{2+}_o homeostasis by detecting alterations in Ca^{2+}_o concentrations and initiating multiple intracellular signalling cascades that include phospholipase C-mediated accumulation of inositol 1,4,5-trisphosphate and increases in intracellular calcium (Ca^{2+}_i) concentrations (10), which in turn lead to alterations in PTH secretion and urinary calcium excretion. FHH type 3 (FHH3, OMIM #600740) is associated with heterozygous loss-of-function mutations of *AP2S1*, located on chromosome 19q13.3 (11–14).

AP2S1 encodes the σ2-subunit of the ubiquitously expressed heterotetrameric adaptor protein-2 (AP2) complex, which also comprises α-, β2- and μ2-subunits. The AP2 complex is a central component of clathrin-coated vesicles and facilitates the endocytosis of plasma membrane constituents such as G-protein-coupled receptors (GPCRs) (15–17). *AP2S1* mutations have been reported in 19 FHH patients and families to date, and these all comprise heterozygous missense substitutions of the AP2 σ2-subunit (AP2σ2) Arg15 residue (Arg15Cys, Arg15His and Arg15Leu) (11,12,14). This Arg residue is located in a positively charged region of AP2σ2 that binds to specific peptide motifs on membrane cargo proteins (18). It is predicted that FHH3-causing Arg15 mutations disrupt binding of the AP2 complex to the intracellular carboxyl terminus of the CaSR, thereby impairing endocytosis of this GPCR (11). This hypothesis is supported by *in vitro* expression studies that have demonstrated *AP2S1* mutations to affect CaSR cell-surface expression and signal transduction (11). These studies of *AP2S1* mutations have highlighted a role for the AP2 endocytic complex in Ca^{2+}_o homeostasis. To date, 19 FHH3 patients have been reported with AP2σ2 mutations, comprising 8 Arg15Cys, 4 Arg15His and 7 Arg15Leu. To further elucidate the role and spectrum of AP2σ2 mutations in the aetiology of the phenotypic features of FHH3, we conducted studies to characterise the structural/functional consequences of AP2σ2 mutations together with their underlying genetic mechanisms in additional FHH patients, who did not have *CASR* or *GNA11* mutations. Our study identified AP2σ2 mutations in 17 hypercalcaemic probands and their families, and further analysis of these AP2σ2 mutants has revealed the presence of a genotype–phenotype correlation, a mutational bias of the AP2σ2 Arg15 residue with a

likely dominant-negative action and a clinical approach to differentiate patients with FHH3 from those with FHH1.

Results

AP2S1 mutations and clinical phenotypes

DNA sequence analysis of the entire *AP2S1* 429-bp coding region and 8 exon–intron boundaries was undertaken in 65 unrelated FHH probands without *CASR* or *GNA11* mutations (22 males and 43 females). This revealed the presence of *AP2S1* mutations in 17 probands (7 males and 10 females), thereby representing a >25% *AP2S1* mutation detection rate in this cohort of FHH patients without *CASR* and *GNA11* mutations. The FHH3-associated mutations only affected the AP2σ2 Arg15 (R15) residue and consisted of five Arg15Cys (R15C), four Arg15His (R15H) and eight Arg15Leu (R15L) mutations (Table 1), all of which had previously been reported to represent pathogenic mutations (11). Two unrelated FHH3 female probands, aged 7 and 15 years, harboured Arg15Leu mutations that were demonstrated to be absent in both of their parents, and hence likely to be arising *de novo* (Fig. 1). Four FHH3 subjects had symptoms attributable to hypercalcaemia, including lethargy, constipation, widespread musculoskeletal pain and polydipsia (Table 1). Eleven FHH3 probands had clinical features in addition to hypercalcaemia and hypocalciuria (Table 1). In particular, bone mineral density (BMD) was noted to be low (T-score < –1.0 or Z-score < –2.0) at the lumbar spine or femoral neck in 5 of 10 patients aged 14 to 64 years (Table 1). The low BMD in all five patients was not associated with renal dysfunction, hyperparathyroidism, vitamin D deficiency or thyrotoxicosis. Furthermore, seven FHH3 patients (aged 3–37 years) were noted to have learning disabilities characterized by cognitive deficits and/or behavioural disturbances (Table 1). In addition, the father of a proband with learning disabilities (06/13a, Table 1) also had a cognitive deficit in association with hypercalcaemia. Two of the Arg15Leu probands with cognitive deficits (02/03 and 02/11, Table 1) had short stature with height at or below the third centile, and one of these probands (02/03, Table 1) was found to harbour an atrial septal defect, whereas the other individual (02/11, Table 1) suffered from recurrent episodes of pancreatitis. The pancreatitis in this patient was not due to gallstones or alcohol abuse, and analysis of genes known to be associated with pancreatitis, such as *SPINK1*, *CFTR*, *PRSS1* and *CTRC* (19), did not reveal any mutations.

Genotype–phenotype correlations at the AP2σ2 Arg15 residue

We examined for phenotypic differences between patients with Arg15Cys, Arg15His or Arg15Leu *AP2S1* mutations. Analysis of biochemical and clinical data available for a total of 27 FHH3 probands [17 from this study and 10 from our previously reported study (11)] revealed that patients with the Arg15Leu mutation had significantly greater elevations of serum albumin adjusted-calcium concentrations when compared with those with the Arg15Cys and Arg15His AP2σ2 mutations (3.06 ± 0.04 mmol/l for Arg15Leu versus 2.83 ± 0.03 mmol/l for Arg15Cys and 2.74 ± 0.03 mmol/l for Arg15His, $P < 0.01$). Moreover, patients with the Arg15Cys mutation had a significantly greater hypercalcaemia ($P < 0.05$) than patients harbouring the Arg15His mutation. Such differences were not observed for other biochemical indices of mineral metabolism (Fig. 2).

Table 1. Clinical and biochemical findings in 17 FHH probands with *AP2S1* mutations

Mutation	Patient	Sex	Family history	Age at presentation/ diagnosis (years)	Associated clinical features	Serum Ca[a,b]	Pi[c]	Mg[d]	ALP[e,f]	PTH[g,h]	Urine CCCR[i,j]	BMD LS	FN
Arg15Cys													
	19/12a	M	Yes	48	Nil	2.94[a]	–	0.82	110[e]	45.0[g]	0.009[i]	–1.0[k]	–2.9[k]
	03/13a	M	Yes	22	H	2.96[a]	0.82	–	98[e]	41.0[g]	0.004[i]	–	–
	16/13	M	Yes	37	H, L	2.80[a]	0.76	1.02	68[e]	50.0[g]	0.003[i]	–1.6[k]	–0.2[k]
	07/14	F	Yes	16	B	1.50[b]	1.22	0.95	39[e]	44.0[g]	0.004[i]	–1.2[k]	–1.4[k]
	11/14	M	–	3	L	2.90[a]	1.09	0.91	368[f]	60.0[g]	0.004[i]	–	–
Arg15His													
	08/11	F	Yes	33	H	2.76[a]	0.85	0.99	74[e]	7.4[h]	0.010[i]	–2.1[k]	–1.7[k]
	03/12	F	Yes	44	Nil	2.80[a]	0.86	–	65[e]	5.2[h]	0.009[i]	0.0[k]	–0.4[k]
	19/12b	F	–	19	–	2.74[a]	0.65	–	104[e]	4.6[h]	0.005[i]	–	–
	03/13b	M	Yes	64	Nil	2.72[a]	–	–	103[e]	6.0[h]	–	–0.6[l]	–1.1[l,m]
Arg15Leu													
	02/03	F	No	15	A, L, S	2.90[a]	0.86	1.03	–	4.7[h]	0.015[i]	–4.6[k]	–
	13/08	F	No	<1[o]	L	3.01[a]	0.99	–	242[f]	15.0[g]	–	–	–
	02/11	F	–	14	L, P, S	3.20[a]	1.2	1.02	88[e]	31.0[g]	0.005[i]	–3.0[k]	–2.5[k]
	04/11	M	–	11	L	3.00[a]	0.60	0.89	314[f]	50[g]	0.004[i]	–1.4[k]	–1.4[k]
	09/12	F	–	9	–	2.81[a]	1.0	0.97	298[f]	96[g]	0.002[i]		
	06/13a	M	Yes	9	L	3.10[a]	0.78	–	249[f]	38[g]	0.27[j]	–	–
	06/13b	F	No	7	Nil	3.03[a]	0.87	0.95	285[f]	40.5[g]	0.001[i]	–1.3[k,n]	N
	02/14	F	No	26	H	2.95[a]	1.17	0.98	–	4.0[h]	0.008[i]	–	–

Normal serum ranges (6): albumin adjusted-calcium, [a]2.10–2.60 mmol/l; ionized calcium, [b]1.19–1.35 mmol/l; phosphate (Pi), [c]0.70–1.40 mmol/l; magnesium (Mg), [d]0.70–1.0 mmol/l; total alkaline phosphatase (ALP) activity, [e]30–130 U/l, [f]70–330 U/l; PTH, [g]10–65 ng/l; [h]1.3–7.6 pmol/l. Normal urine ranges; calcium-to-creatinine clearance ratio (CCCR), [i]>0.02; calcium-to-creatinine ratio, [j]0.3–0.7. [k]BMD Z-scores are provided for subjects of <50 years old and [l]BMD T-scores are provided for subjects of >50 years old; [m]forearm BMD T-score = –2.5 for proband 03/13b; [n]whole-body BMD Z-score = –2.0 for proband 06/13b; [o]diagnosed in early infancy. A, atrial septal defect; B, irritable bowel syndrome co-segregating with hypercalcaemia in family 07/14; FN, femoral neck; H, hypercalcaemic symptoms; L, mild-to-moderate learning disability; LS, lumbar spine; N, normal; S, short stature (height <third centile); P, pancreatitis; —, not known.

Downloaded from http://hmg.oxfordjournals.org/ at Oxford University on September 14, 2015

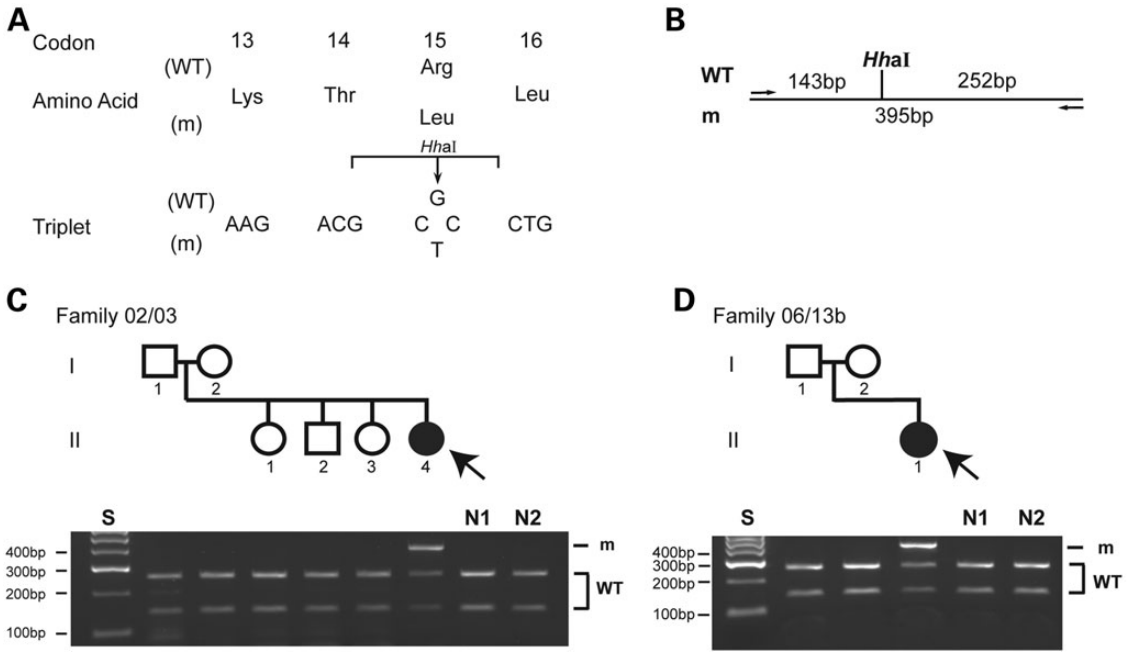


Figure 1. Detection of *de novo AP2S1* mutations in families 02/03 and 06/13b. (**A**) DNA sequence analyses of the probands (arrowed) revealed a G-to-T transversion at codon 15, predicted to result in a missense amino acid substitution of Arg to Leu, and loss of a *Hha*I restriction endonuclease site. (**B**) Restriction map showing that *Hha*I digestion would result in two products of 143 and 252 bp from the wild-type (WT) sequence, but would not affect the mutant (m) sequence. PCR and *Hha*I digestion revealed the probands [individual II.4 of family 02/03 (**C**) and individual II.1 of family 06/13b (**D**)] to be heterozygous for the Arg15Leu mutation. The absence of the Arg15Leu mutation in the unaffected parents of both probands is consistent with the mutation arising *de novo*.

Phenotypic differences between FHH3 and FHH1

To determine whether FHH3 is associated with any differences in the biochemical phenotype when compared with FHH1, we analysed the serum and urine biochemistry from 51 FHH3 subjects that included affected members of the previously reported multi-generational FHH3 kindreds from Oklahoma (FHH_{OK}) and Northern Ireland (FHH_{NI}) (20–23), and 43 previously reported FHH1 probands, who all harboured *CASR* mutations (8). This revealed FHH3 patients to have a greater degree of hypercalcaemia than the FHH1 patients (serum adjusted-calcium = 2.87 ± 0.02 mmol/l for FHH3 versus 2.76 ± 0.02 mmol/l for FHH1, $P < 0.001$) (Fig. 3). FHH3 patients when compared with FHH1 patients also had significantly marked hypermagnesaemia (serum magnesium = 1.04 ± 0.02 mmol/l for FHH3 versus 0.95 ± 0.02 mmol/l for FHH1, $P < 0.01$) and hypocalciuria (CCCR = 0.004 ± 0.001 for FHH3 versus 0.007 ± 0.001 for FHH1, $P < 0.01$) (Fig. 3). There were no significant differences in the serum concentrations of phosphate, alkaline phosphatase (ALP) activity or PTH between the FHH3 and FHH1 patients (Fig. 3). As serum adjusted-calcium, serum magnesium and CCCR values were significantly different between FHH3 and FHH1 patients, we investigated whether the combined use of these biochemical parameters could be utilized to discriminate between these two hypercalcaemic disorders. Based on the observation that serum adjusted-calcium (sCa) and serum magnesium (sMg) values are elevated, whereas CCCR is reduced in FHH3, a calculated index (sCa × sMg/100 × CCCR), designated CMCR, was determined for each of the subjects in the FHH1 and FHH3 groups (Fig. 3) with all biochemical parameters being measured in millimole per litre. Receiver–operator curve (ROC) analysis of the CMCR index (Fig. 3) revealed an area-under-the curve (AUC) of 0.85 ($P < 0.001$) and an optimal cut-off value of 5.0 for discriminating between FHH3 and FHH1, which provides a diagnostic sensitivity of 83% [95% confidence interval (CI) = 61–95] and specificity of 86% (95% CI = 57–98), and positive and negative predictive values of 90% (95% CI = 70–98) and 80% (95% CI = 52–95), respectively.

Analysis of AP2σ2 codon 15 mutation bias

The present study has identified 17 hypercalcaemic patients with *AP2S1* mutations that all affected the AP2σ2 Arg15 residue, and previous studies have reported 19 *AP2S1* mutations that all affect the Arg15 residue (11,12,14) yielding a total of 36 FHH3-causing mutations identified to date. These 36 *AP2S1* mutations involving substitutions of Arg15 comprise 13 Arg15Cys, 8 Arg15His and 15 Arg15Leu. Analysis of the DNA sequence of the Arg15 codon reveals it to be CGC indicating that missense substitutions affecting the first or second nucleotides would be predicted to be non-synonymous and lead to one of six possible amino acid substitutions, which comprise Cys, Gly, His, Leu, Pro and Ser (Fig. 4). This expected observation of six different amino acid substitutions contrasts significantly ($P < 0.0001$, Chi-squared test) with the three Arg15-mutant substitutions observed in FHH3 patients.

To investigate the potential occurrence of the Arg15Cys, Arg15His and Arg15Leu, and the absence of Arg15Gly, Arg15Pro and Arg15Ser variants, we assessed the effects of all six potential Arg15 mutants on the structure and function of AP2. Analysis of the AP2 complex crystal structure predicted that all the six Arg15 missense substitutions, including the Arg15Gly, Arg15Pro and Arg15Ser variants that have not been observed in FHH3, would impair AP2 complex function by disrupting a key polar contact between the AP2 complex and the cargo protein dileucine recognition motif (Fig. 4). Thus, all the six Arg15 missense substitutions would significantly alter the structure, and we therefore determined their functional consequences on CaSR activity, by expressing them in HEK293 cells that stably expressed the CaSR

Downloaded from http://hmg.oxfordjournals.org/ at Oxford University on September 14, 2015

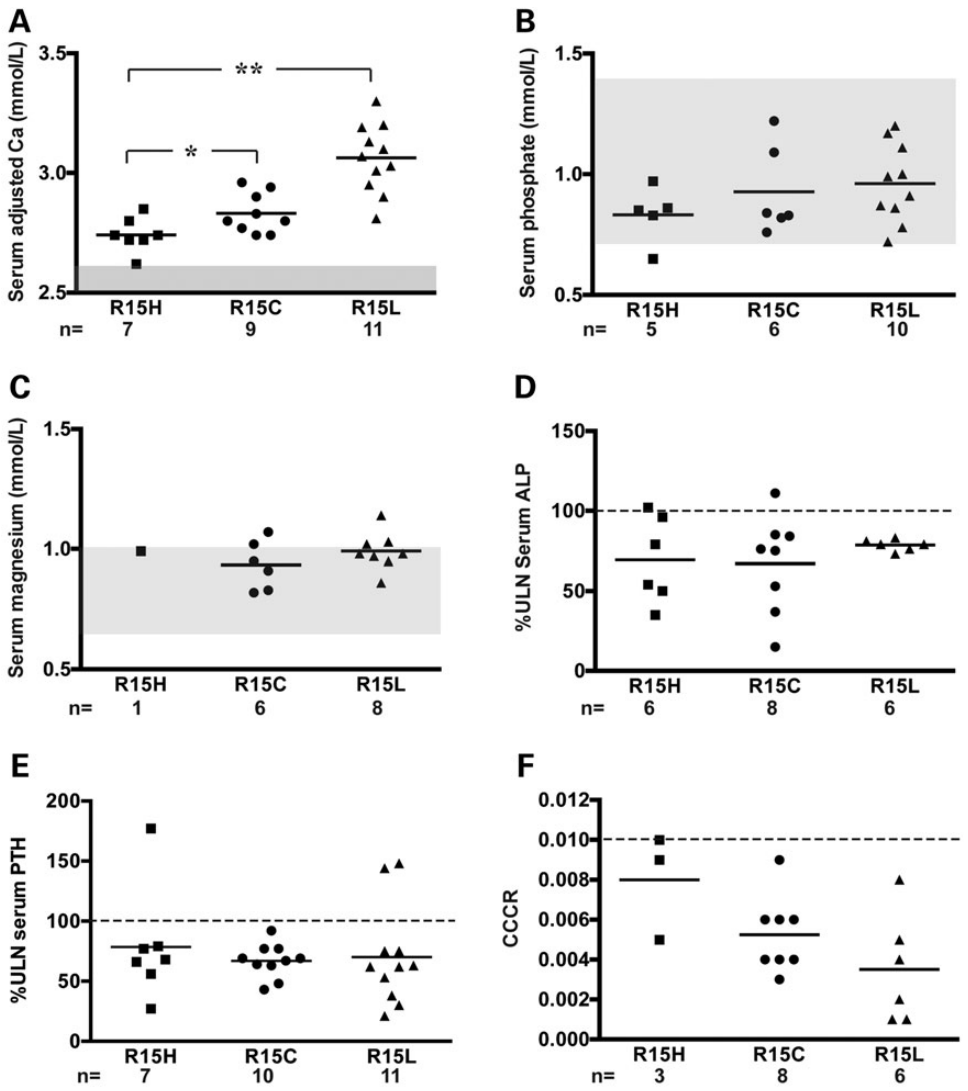


Figure 2. Assessment of genotype–phenotype correlations between probands harbouring Arg15His (R15H), Arg15Cys (R15C) or Arg15Leu (R15L) *AP2S1* mutations. Serum and urine biochemical values are shown as scatter plots. (**A**) Probands with R15L mutations had significantly greater elevations of serum adjusted-calcium concentrations than probands with R15C or R15H mutations. Probands with R15C mutations were significantly more hypercalcaemic than probands with R15H mutations. (**B–F**) No significant differences in serum concentrations of phosphate, magnesium, ALP activity, PTH or urinary CCCR were observed between probands harbouring each of the three *AP2S1* R15 mutations. Mean values for the respective groups are indicated by horizontal solid lines. The normal ranges [mean ± 2 standard deviations (SDs)] for serum calcium, phosphate and magnesium are indicated by the grey areas. The upper limit of normal (ULN) for the assay that was used for serum ALP activity and PTH concentrations are represented by the broken line. For CCCR, the lower limit (<0.01) for the consideration of hypocalciuria is represented by the broken line. *$P < 0.05$, **$P < 0.01$.

(HEK-CaSR) (9,11). Transient transfection of the wild-type or mutant *AP2S1*-pBI-CMV4-RFP expression constructs, or vector containing the red fluorescence protein (RFP) reporter gene alone, was undertaken in the HEK-CaSR cells (9,11). Expression of the CaSR and RFP, which represents a surrogate of AP2σ2 expression, was detected by immunofluorescence and western blotting of whole-cell lysates (Fig. 5), and the responses of $Ca^{2+}{}_i$ concentrations to alterations in $Ca^{2+}{}_o$ concentrations were then assayed by flow cytometry (9,11).

HEK-CaSR cells expressing each of the six Arg15 missense AP2σ2 variants (i.e. the three observed Arg15Cys, Arg15His and Arg15Leu and the three non-observed Arg15Gly, Arg15Pro and Arg15Ser AP2σ2 variants) were found to have half-maximal effective concentration (EC_{50}) values that were significantly higher ($P < 0.0001$) than cells expressing the wild-type AP2σ2 protein. Thus, the three non-observed Arg15 AP2σ2 variants decreased the sensitivity of HEK-CaSR cells to $Ca^{2+}{}_o$ concentrations in a similar manner to the three FHH3-causing AP2σ2 mutations (Fig. 5 and Table 2). However, cells expressing the non-observed Arg15Gly, Arg15Pro or Arg15Ser AP2σ2 mutants were found to have significantly reduced increases in cell numbers over a 24-h period, when compared with cells expressing wild-type or FHH3-mutant AP2σ2 proteins (Fig. 5). These results indicate that the Arg15Gly, Arg15Pro and Arg15Ser AP2σ2 mutants are likely not observed as they are associated with an impairment of cell growth, when compared with wild-type or the FHH3-associated mutant AP2σ2 proteins (Fig. 5 and Supplementary Material, Fig. S1).

Downloaded from http://hmg.oxfordjournals.org/ at Oxford University on September 14, 2015

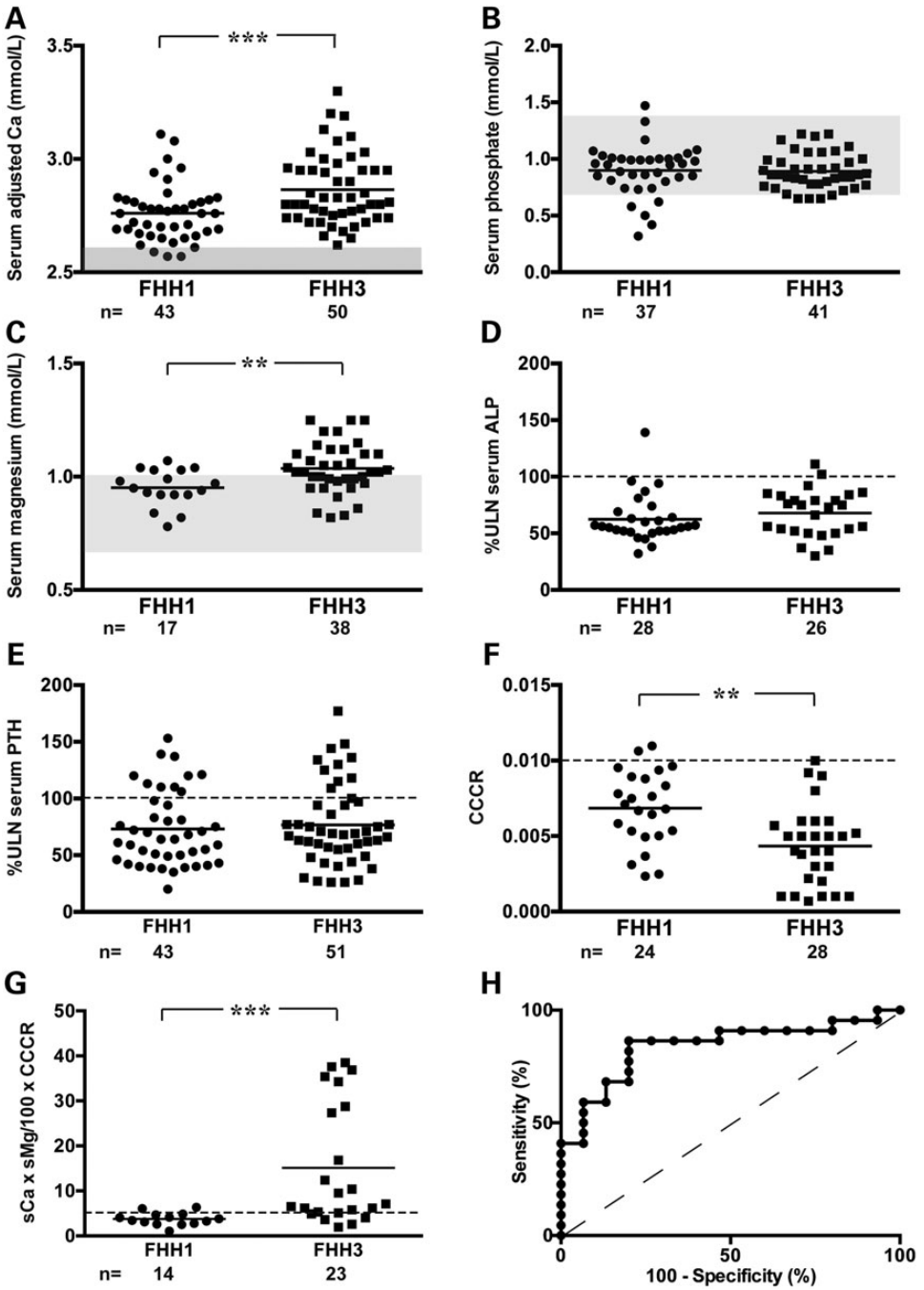


Figure 3. Comparison of biochemical phenotypes between FHH1 and FHH3. Scatter plots of serum concentrations of (**A**) adjusted-calcium, (**B**) phosphate, (**C**) magnesium, (**D**) ALP activity, (**E**) PTH, (**F**) urinary CCCR and (**G**) CMCR index, which is calculated as sCa × sMg/100 × CCCR, for FHH3 probands are shown. Such biochemical values are also provided for an age- and gender-matched cohort of previously reported FHH1 probands with CASR mutations (8). All biochemical parameters comprising the CMCR index were measured in millimole per litre. FHH3 probands, when compared with FHH1 probands, had significantly greater elevations of serum adjusted-calcium and magnesium concentrations, reduced CCCR values and elevated CMCR. Mean values for the respective groups are indicated by horizontal solid lines. The normal ranges (mean ± 2 SDs) for serum calcium, phosphate and magnesium are indicated by the grey areas. The ULN for the assay that was used for serum ALP activity and PTH concentrations are represented by the broken line. For CCCR, the lower limit (<0.01) for the consideration of hypocalciuria is represented by the broken line. For CMCR index, the cut-off value of 5.0, above which a diagnosis of FHH3 should be considered, is represented by the broken line. (**H**) ROC of discriminatory power of CMCR index to distinguish between FHH3 and FHH1. The CMCR had an AUC of 0.85, which was significantly greater than that of the reference line ($P < 0.001$). $^{**}P < 0.01$, $^{***}P < 0.001$.

Dominant-negative effects of AP2S1 mutations

FHH3 is associated with heterozygous loss-of-function AP2σ2 mutations, and these could be causing the disease by either haploinsufficiency (i.e. a reduced dosage of the wild-type AP2σ2 protein) or dominant-negative effects on the heterotetrameric AP2 complex. To investigate these genetic mechanisms, we studied the effects of altering the dosage of wild-type and mutant

Downloaded from http://hmg.oxfordjournals.org/ at Oxford University on September 14, 2015

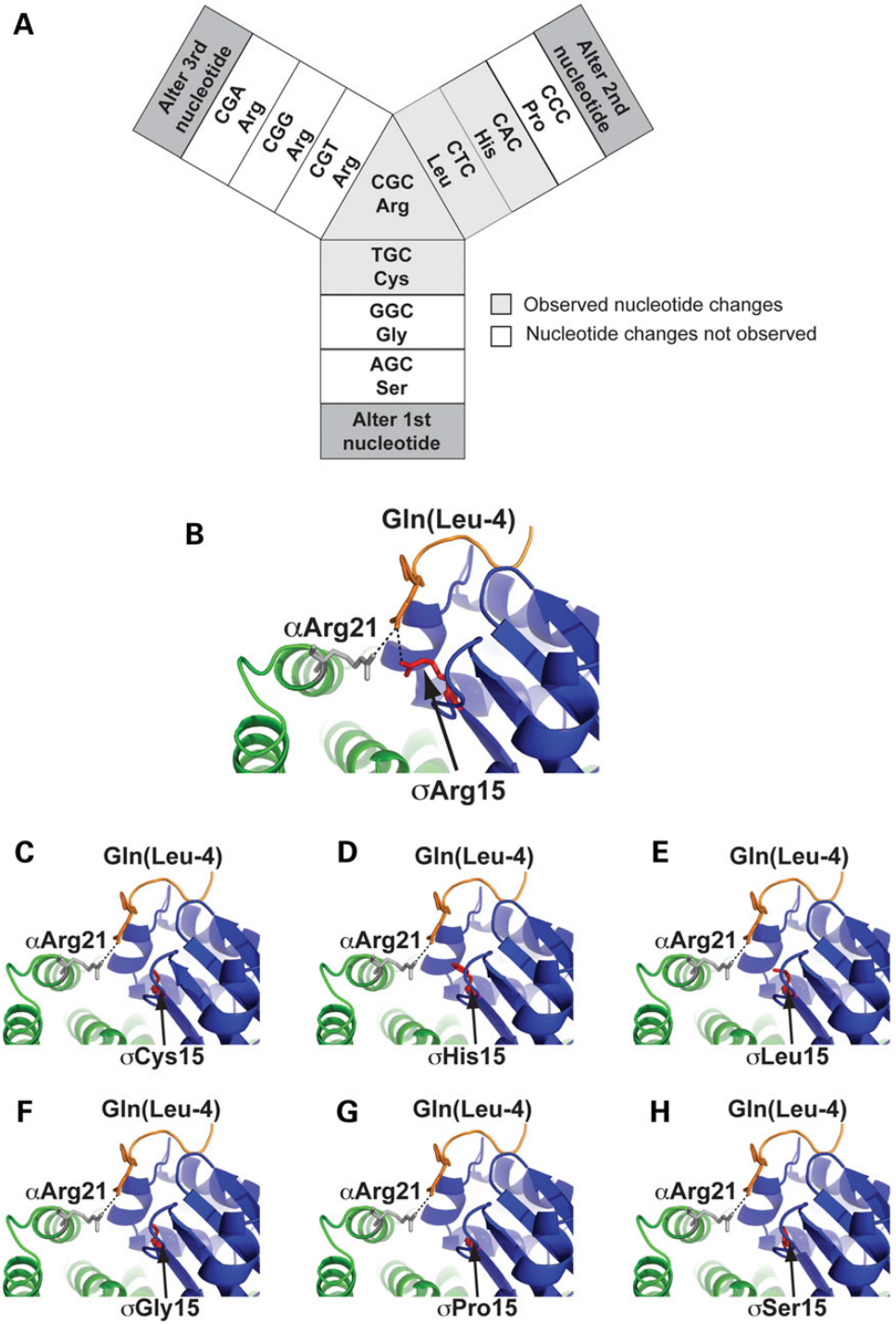


Figure 4. Observed and predicted mutations at the *AP2S1* Arg15 (R15) residue. **(A)** Schematic representation of possible nucleotide and amino acid substitutions affecting codon 15. Substitutions affecting the first or second nucleotide of codon 15 (CGC) are predicted to lead to one of six possible non-synonymous mutations or variants, which are Cys15 (TGC), Gly15 (GGC), His15 (CAC), Leu15 (CTC), Pro15 (CCC) or Ser15 (AGC). Substitutions affecting the third nucleotide of the CGC triplet are predicted to lead to synonymous variants only. **(B)** Crystal structure of the α-subunit (green) and σ2-subunit (blue) of the AP2 heterotetrameric complex bound to an acidic (Gln-containing) dileucine cargo protein motif [PDB file 2JKR (18)]. The key polar contacts (black dashed lines) between the σ2-subunit Arg15 residue (σArg15, red) and α-subunit Arg21 residue (αArg21, grey), and a Gln residue located four residues from the first Leu residue of the acidic dileucine motif [Gln(Leu-4), orange], are shown. **(C–G)** Structural analysis of six potential Arg15 mutations demonstrating that the observed mutants (Cys15, His15 and Leu15) and non-observed mutants (Gly15, Pro15 and Ser15) are all predicted to result in the loss of the key polar contact with the cargo protein Gln (Leu-4) residue.

AP2σ2 proteins on the EC_{50} responses of HEK-CaSR cells that were transiently transfected with wild-type or mutant *AP2S1*-pBI-CMV4-RFP expression constructs. We used the bidirectional *AP2S1*-pBI-CMV4-RFP vector as it expresses RFP and AP2σ2 at equivalent levels, thereby enabling RFP expression to be used as a surrogate for AP2σ2 expression (9). We selected populations of

Downloaded from http://hmg.oxfordjournals.org/ at Oxford University on September 14, 2015

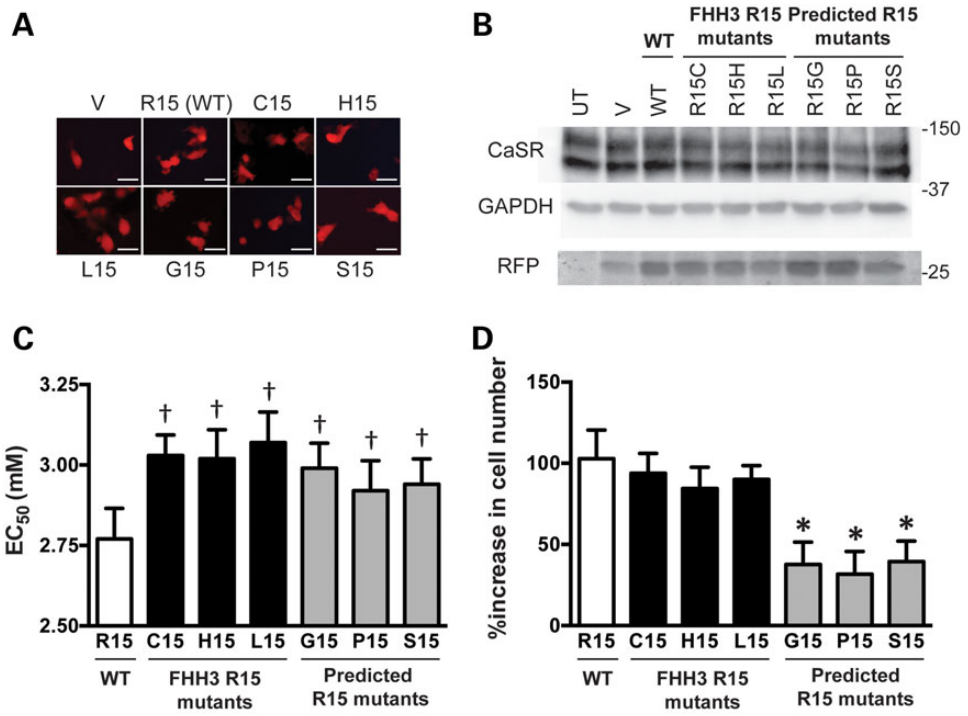


Figure 5. Functional expression of *AP2S1* Arg15 (R15) mutants. (**A**) Fluorescence microscopy of HEK293 cells stably transfected with CaSR and transiently transfected with wild-type R15 (WT-R15), and FHH3-associated mutants (Cys15, C15; His15, H15; Leu15, L15) or other possible R15 mutants (Fig. 4) (Gly15, G15; Pro15, P15; Ser15, S15), or pBI-CMV4-RFP expression vector only (V). RFP expression in these cells indicates successful transfection and expression by these constructs. Bar indicates 20 μm. (**B**) Western blot analysis of whole-cell lysates using anti-CaSR, anti-GAPDH and anti-RFP antibodies. The FHH3-mutant AP2σ2 and predicted possible R15 mutant proteins were expressed at similar levels. UT, untransfected cells. (**C**) Measurement of $Ca^{2+}{}_i$ responses following stimulation with varying $Ca^{2+}{}_o$ concentrations revealed cells expressing observed FHH3-associated mutants or the non-observed possible R15 mutants (Fig. 4) to have significantly raised EC_{50} values when compared with cells expressing the wild-type AP2σ2 (WT-R15) protein. Results are from eight to ten assays and three independent transfections. (**D**) Growth of cells expressing WT or mutant AP2σ2 proteins. Cells expressing the non-observed possible R15 mutants showed a significantly reduced percentage increase in cell numbers over a 24-h period when compared with cells expressing WT or FHH3-associated mutant AP2σ2 proteins, consistent with an impairment of proliferation. Results are from 11 to 18 assays and 4 independent transfections. $^{*}P < 0.05$ and $^{\dagger}P < 0.0001$.

Table 2. EC_{50} values of observed and non-observed AP2σ2 Arg15 mutants

AP2σ2 construct	EC_{50} (mM) Mean value	95% CI	*N*	*P*-value (versus WT)
pBI-CMV4 vector	2.85	2.80–2.89	10	NS
Wild-type AP2σ2	2.77	2.74–2.81	10	—
Observed AP2σ2 mutants				
Arg15His	3.02	2.96–3.08	9	<0.0001
Arg15Cys	3.03	2.98–3.07	10	<0.0001
Arg15Leu	3.07	3.01–3.13	10	<0.0001
Non-observed AP2σ2 mutants				
Arg15Gly	2.99	2.94–3.04	9	<0.0001
Arg15Pro	2.92	2.85–2.98	8	<0.0001
Arg15Ser	2.94	2.89–3.00	8	<0.0001

The number (*N*) of replicate experiments from three independent transfections is indicated.
NS, not significant; CI, confidence interval.

cells with increasing levels of RFP expression by flow cytometry (Fig. 6) and assessed the effects of altering wild-type and mutant AP2σ2 dosage by measuring the $Ca^{2+}{}_i$ responses of the HEK-CaSR cells to changes in $Ca^{2+}{}_o$ concentrations, and determining the linear regression of mean EC_{50} values against expression levels of wild-type and mutant AP2σ2 proteins. In this experiment, loss-of-function mutations with dominant-negative actions, which would exert greater effects with increasing protein concentrations, will show a positive correlation between mutant protein concentration and EC_{50}. However, loss-of-function mutations associated with haploinsufficiency would not exert effects on the wild-type protein, whose concentration would remain constant, and hence there would be absent correlation between mutant protein concentrations and EC_{50} values (Fig. 6).

The results of such linear regression analyses revealed that increased expression levels of FHH3-causing Arg15-mutant AP2σ2 proteins progressively impaired the sensitivity of HEK-CaSR cells, as highlighted by a significantly positive relationship

Downloaded from http://hmg.oxfordjournals.org/ at Oxford University on September 14, 2015

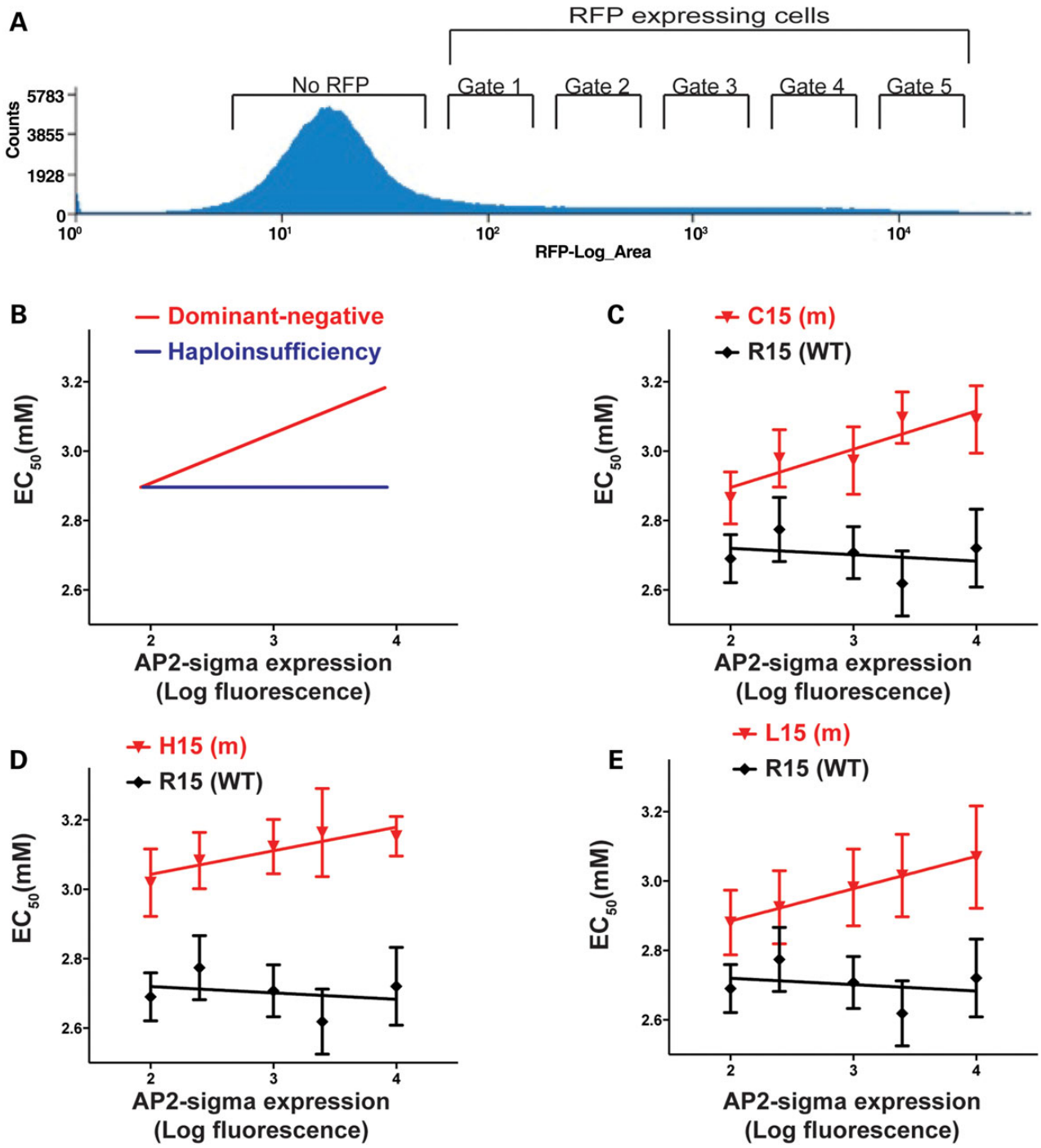


Figure 6. Comparison of EC_{50} values for HEK-CaSR cells transfected with increasing amounts of wild-type (WT) or mutant *AP2S1*-pBI-CMV4-RFP expression constructs. (**A**) During flow cytometry, fluorescence over a 1–10 000 range can be detected. The first large peak represents cells not expressing RFP but displaying low levels of auto-fluorescence. Cells displaying increased fluorescence with respect to this population reflect those expressing RFP. Cells from five different RFP fluorescences were selected on the basis of mean fluorescence (gate 1 log mean fluorescence = 50–100, gate 2 log mean fluorescence = 125–250, gate 3 log mean fluorescence = 500–1000, gate 4 log mean fluorescence = 1250–2500 and gate 5 log mean fluorescence = 5000–10000), consistent with a fluorescence ranging from between 1- and 100-fold over baseline, i.e. between gate 1 and gate 5, which represent the lowest and the highest levels of RFP fluorescence, and therefore AP2σ2, respectively. (**B**) Predicted linear regressions of mean EC_{50} with effects owing to dominant-negative and haploinsufficiency mutants. Loss-of-function mutants with dominant-negative effects on the WT protein will exert greater effects on EC_{50} values with increasing concentrations (red line), whereas loss-of-function mutants associated with haploinsufficiency of the WT protein will not affect the EC_{50} values with increasing concentrations as the EC_{50} will depend on the concentration of WT protein, which will remain constant (blue line). (**C–E**) Linear regression of the mean EC_{50} of cells with increasing levels of AP2σ2 expression demonstrate no significant deviation from zero in cells transfected with the WT-R15 *AP2S1*-pBI-CMV4-RFP expression construct ($r^2 = 0.07$, $P = 0.67$), whereas a significantly positive incline to the slope is observed in cells transfected with the mutant *AP2S1*-pBI-CMV4-RFP expression constructs (C15 $r^2 = 0.82$, $P < 0.05$; H15 $r^2 = 0.84$, $P < 0.05$; L15 $r^2 = 0.99$, $P < 0.0001$), thereby indicating that FHH3-associated AP2σ2 mutations may act in a dominant-negative manner. All experiments were conducted on $N = 8$ separate occasions.

Downloaded from http://hmg.oxfordjournals.org/ at Oxford University on September 14, 2015

between the expression levels of all three AP2σ2 mutants and the mean cellular EC_{50} responses (Cys15 $r^2 = 0.82$, $P < 0.05$; His15 $r^2 = 0.84$, $P < 0.05$; Leu15 $r^2 = 0.99$, $P < 0.0001$), but that increased expression levels of wild-type AP2σ2 had no effect on EC_{50} values ($r^2 = 0.07$, $P = 0.67$) (Fig. 6). These findings indicate a potential dominant-negative effect of the FHH3-causing Arg15 AP2σ2 mutants.

Discussion

Our results, which have identified *AP2S1* mutations that only result in missense substitutions of the Arg15 residue in 17 additional FHH probands, have helped to establish a genotype–phenotype correlation between AP2σ2 mutants and the severity of hypercalcaemia; devise an index based on measurements of plasma calcium and magnesium concentrations and urinary clearances of calcium and creatinine to differentiate between FHH1 and FHH3; elucidate the occurrence of a mutational bias at the AP2σ2 Arg15 residue in FHH3 patients and define the likely genetic mechanism for AP2σ2 mutations as being a dominant-negative action in causing FHH3. In addition, our study shows that FHH3 can be associated with *de novo AP2S1* mutations, consistent with a previous report (12), thereby indicating that patients may not have a family history of the disorder and that *AP2S1* mutations may be associated with non-familial forms of hypercalcaemia and hypocalciuria.

The identification by this study of *AP2S1* mutations in 17 additional probands with FHH3, together with ours and other previous reports (11,12,14), yields a total of 36 probands with such AP2σ2 mutations, which all involve the Arg15 residue and result in 1 of 3 missense substitutions comprising Arg15Cys, Arg15His and Arg15Leu. Our analyses of these subjects reveal genotype–phenotype correlations for these AP2σ2 mutations, in which the Arg15Leu mutation is associated with the most pronounced hypercalcaemia, whereas Arg15His is associated with the mildest increase in serum calcium concentrations. This is surprising and the mechanisms underlying these genotype–phenotype correlations are unclear, as three-dimensional modelling and *in vitro* functional expression studies indicate that all three Arg15 AP2σ2 mutations disrupt CaSR activity to a similar extent (11), and the basis for the differences between our *in vivo* clinical observations and *in vitro* results remains to be elucidated.

Our study has also revealed phenotypic differences between FHH1 and FHH3. In particular, FHH3 was associated with significantly greater elevations of serum calcium, and >20% of FHH3 patients in this cohort had symptomatic hypercalcaemia. These findings are not typical of FHH, which is considered to be a benign and asymptomatic disorder, and in general associated with serum calcium concentrations that remain within 10% of the upper limit of the normal range (1). In addition to the more severe hypercalcaemia, FHH3 was associated with more pronounced suppression of urinary calcium excretion than FHH1. The more marked serum and urinary calcium phenotype of FHH3 contrasts with the results of *in vitro* studies that indicate FHH3-causing *AP2S1* mutations to lead to a milder shift in the set point of CaSR-expressing cells when compared with FHH1-causing *CASR* mutations (11). These findings suggest that AP2σ2 mutations may influence Ca^{2+}_o homeostasis through effects on cell membrane proteins other than the CaSR. Indeed, the renal thick ascending limb $Na^+/K^+/2Cl^-$ (NKCC2) transporter, which is pivotal for urinary calcium reabsorption, has been demonstrated to be regulated by clathrin-mediated endocytosis (24). Other phenotypic differences between FHH3 and FHH1 included the occurrence of low BMD and cognitive dysfunction in FHH3. Low BMD occurred in five FHH3 probands with *AP2S1* mutations whereas patients with FHH1, owing to *CASR* mutations, have been reported to have normal bone resorption rates and BMD measurements at the spine, hip and forearm (25). Cognitive dysfunction was observed in seven FHH3 probands, four of which presented with serum calcium concentrations of >3.0 mmol/l, and exposure to marked hypercalcaemia in infancy or childhood may have led to developmental delay and adversely affected neurological development in these individuals (26). It is also possible that expression of mutant AP2σ2 subunits within the brain may directly influence neurological development, consistent with the role of the AP2 complex in mediating receptor trafficking within neuronal synapses of the hippocampus (27), a region of the brain required for memory acquisition and spatial orientation. The Arg15Leu *AP2S1* mutation was also associated with recurrent pancreatitis in one FHH3 proband, a finding consistent with FHH1, in which recurrent pancreatitis has occasionally been reported (28). However, FHH1 probands with pancreatitis typically harbour heterozygous mutations of both the *CASR* and serine protease inhibitor, Kazal type 1 (*SPINK1*) genes (29). In contrast, the affected FHH3 proband did not harbour a mutation of *SPINK1* or other genes associated with pancreatitis (19), and this proband's marked hypercalcaemia may have been sufficient to disrupt pancreatic function. Given these possible phenotypic differences between FHH3 and FHH1, we sought to design an index based on clinical biochemistry tests of serum and urine that would help to differentiate the two disorders. The findings that FHH3 is associated with greater elevations in serum calcium and magnesium concentrations, and reductions in urinary calcium excretion, when compared with FHH1, led us to design the calcium–magnesium–calcium clearance ratio (CMCR), calculated as sCa × sMg/100 × CCCR. Assessment of the performance characteristics of this index indicated that FHH patients with CMCR ≥5.0 were significantly more likely to have FHH3. Thus, the CMCR index may have utility in the clinical setting for directing FHH patients for either *CASR* or *AP2S1* gene analysis, with patients having a CMCR value of ≥5.0 being prioritized for *AP2S1* analysis (Fig. 7). However, ∼30% of FHH3 patients have CMCR values that overlap with that of FHH1 patients (Fig. 3), and combined analysis of the *CASR*, *AP2S1* and *GNA11* genes is suggested in individuals with CMCR values of <5.0 (Fig. 7). No correlation was observed between the CMCR index and codon 15 genotype of the FHH3 patients. The CMCR index requires further validation in studies of other populations and using alternate biochemical assays.

The finding that all the 36 reported FHH3 patients, of which 17 are from this study, harbour either an Arg15Cys, Arg15His or Arg15Leu mutation, highlights the importance of this evolutionary conserved residue for AP2-mediated Ca^{2+}_o homeostasis (11,12,14). Furthermore, the absence of the other possible missense substitutions at this codon (Arg15Gly, Arg15Pro or Arg15Ser) indicates mutation bias at the AP2σ2 Arg15 residue. Our *in vitro* characterization of the non-observed Gly15, Pro15 or Ser15 mutations demonstrated these mutant AP2σ2 proteins to be expressed and to result in an impairment of CaSR activity. However, the Gly15, Pro15 or Ser15 mutants had additional deleterious effects that led to a reduction in the numbers of cells expressing these mutants. These findings indicate a potential role for the AP2 complex in cell growth or viability and are consistent with a previously reported study of mice harbouring a germline ablation of the AP2μ2 subunit, which led to early embryonic lethality, thus highlighting the involvement of the ubiquitously expressed AP2 complex in mammalian development (30). Thus, a possible explanation for the absence of the Arg15Gly, Arg15Pro and Arg15Ser AP2σ2 mutations in patients

Downloaded from http://hmg.oxfordjournals.org/ at Oxford University on September 14, 2015

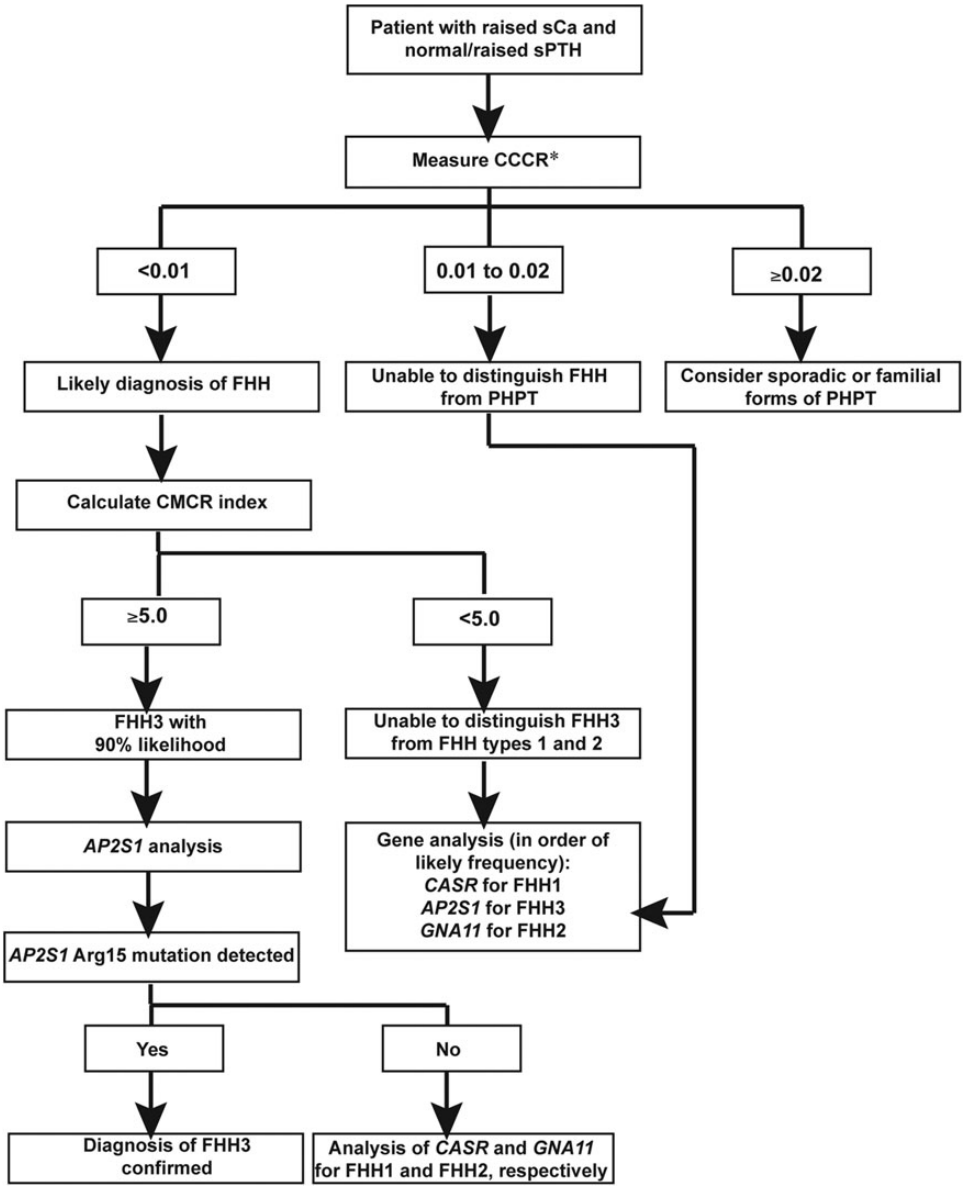


Figure 7. Clinical approach to distinguishing between FHH1 and FHH3 in a hypercalcaemic patient. sCa, serum calcium; sMg, serum magnesium; sPTH, serum PTH; CCCR, calcium to creatinine clearance ratio; CMCR = sCa × sMg/100 × CCCR; PHPT; primary hyperparathyroidism. *In a hypercalcaemic patient with normal/raised sPTH, a CCCR of <0.01 is consistent with a diagnosis of FHH, provided that thiazide diuretic use, vitamin D deficiency and renal impairment have been excluded.

is that these deleterious mutations likely result in embryonic lethality, whereas the FHH3-causing AP2σ2 mutations Arg15Cys, Arg15His and Arg15Leu are observed in patients, as these mutations are not associated with deleterious effects on cell growth, but are tolerated and compatible with embryonic and post-natal survival.

Our findings of a likely dominant-negative effect of FHH3-causing Arg15 AP2σ2 mutations are consistent with previous mutagenesis studies of the AP2 complex (31). Indeed, overexpression of a mutated μ2-subunit (AP2μ2), which displayed diminished capacity to bind to some cargo proteins, has been reported to inhibit receptor trafficking in a dominant-negative manner (31). The precise mechanisms of such dominant-negative actions remain to be established but three possibilities are (1) the incorporation of a mutant σ2 subunit may impair the assembly of the tetrameric complex, (2) incorporation of the mutant σ2 subunit may alter the structure of the AP2 complex and hinder the efficiency of wild-type AP2α, AP2β and AP2μ subunits (32) and (3) the mutant AP2 complex may potentially sequester the CaSR at the plasma membrane and prevent wild-type AP2 molecules from effectively trafficking this GPCR.

In summary, our studies of *AP2S1* mutations, which highlight FHH3 as a distinct disorder of Ca^{2+}_o homeostasis and demonstrate the importance of the AP2σ2 Arg15 residue for AP2 function, have revealed genotype–phenotype correlations with mutation bias at the Arg15 residue, as well as a likely dominant-negative mechanism of action.

Materials and Methods

Subjects

Informed consent was obtained from individuals, using protocols approved by the local and national ethics committees (MREC/02/

Downloaded from http://hmg.oxfordjournals.org/ at Oxford University on September 14, 2015

2/93). Sixty-five unrelated probands (22 males and 43 females) were ascertained. The age at diagnosis or presentation ranged from early infancy to 76 years, and all probands had hypercalcaemia with normal or elevated PTH concentrations, in association with inappropriately low urinary calcium excretion. Previous mutational analysis of *CASR* and *GNA11* had not identified any abnormalities of the coding regions and exon–intron boundaries of these genes (8,9).

DNA sequence analysis

Leukocyte DNA was extracted from venous blood samples and quantified using the High sensitivity Qubit system (Invitrogen) (11). *AP2S1*-specific primers were used to perform PCR amplification of the five exons and eight intron-exon boundaries of the *AP2S1* gene, as previously reported (11). DNA sequence analysis of the PCR products was performed using the BigDye Terminator v3.1 Cycle Sequencing Kit (Life Technologies) and an ABI automated capillary sequencer (Applied Biosystems), as reported (8). DNA sequence abnormalities and co-segregation in families were confirmed by restriction endonuclease analysis (New England Biolabs), as described (11).

Computer modelling of the AP2 structure

The crystal structure of the AP2 heterotetramer bound to an acidic dileucine peptide has been reported previously (18). The PyMOL Molecular Graphics System (version 1.2r3pre, Schrödinger) was used to model the effect of the FHH3-associated AP2σ2 mutations on the interaction with the acidic dileucine motif peptide using the three-dimensional structure of AP2 archived in the Protein Data Bank at the European Bioinformatics Institute with the accession number 2JKR (8,9,11,18). The effect of the Arg15Cys, Arg15Leu, Arg15His, Arg15Pro, Arg15Ser and Arg15Gly mutations on the interaction of AP2σ2 subunit with the acidic dileucine peptide was modelled using PyMod plug-in and Modeller.21 (9).

Generation of *AP2S1* expression constructs

An AP2σ2 expression construct was generated by cloning the full-length *AP2S1* coding region into the bidirectional cloning vector pBI-CMV4-RFP (Clontech), which allows for co-expression of AP2σ2 and RFP at equivalent levels (11,33). The use of RFP minimized overlap between the emission spectra of this reporter gene and the indo-1-AM Ca^{2+}-binding fluorophore. *AP2S1* mutations were introduced into the construct by site-directed mutagenesis (QuikChange Lightning, Stratagene) and confirmed by DNA sequence analysis, as described (8,11).

Cell culture and transfection

Functional studies of *AP2S1* mutations were performed in HEK293 cells that stably expressed the CaSR (11). HEK293 cells were used because suitable parathyroid and renal tubular cells are not available, and HEK293 cells have been established as a model for such studies (8,9,11,34). The reported stably CaSR-transfected HEK293 cell line (HEK-CaSR) (9,11) was cultured in high-glucose DMEM (Invitrogen) supplemented with 10% fetal bovine serum and 1% geneticin (11). A high level of CaSR expression in these cells was confirmed by western blot analysis of whole-cell protein extract using a mouse monoclonal antibody to human CaSR (ADD; Abcam, ab19347, 1:1000) (9,11). The wild-type and mutant AP2σ2 constructs were transiently transfected into HEK-CaSR cells using Lipofectamine 2000 (Invitrogen) (9,11). Expression of RFP was used as a surrogate for AP2σ2 expression as it is expressed at equivalent levels to AP2σ2 by the pBI-CMV4-RFP bidirectional vector (11). Western blot analysis of cellular protein extract was undertaken using a rabbit polyclonal antibody to RFP (Thermo Scientific, PA1-986, 1:500) (11). The membrane was re-probed with mouse anti-GAPDH antibody (Abcam, ab8245, 1:3000) as a loading control. Successful transfection was also confirmed by visualising RFP fluorescence using an Eclipse E400 fluorescence microscope with an epifluorescence filter, and images were captured using a DXM1200C digital camera and NIS Elements software (Nikon) (9,11). The effect of mutant AP2σ2 proteins on cell growth was assessed by determining the percentage increase in cell numbers over a 24-h period, as follows. Twenty-four hours after transfection, equal numbers of cells were seeded into a 96-well plate, and the cells were imaged, at 48 and 72 h, using fluorescence microscopy, as mentioned above (9,11). Following blinding to both transfection and time point, the numbers of transfected cells were counted manually at 48 and 72 h post-transfection, and the percentage increase in cells determined using Microsoft Excel and statistical analysis undertaken in GraphPad Prism (GraphPad) (9,11).

Measurement of Ca^{2+}_i responses

The effect of mutant AP2σ2 proteins on CaSR-mediated Ca^{2+}_i responses were assessed by determining EC_{50} values (i.e. $[Ca^{2+}]_o$ required for 50% of the maximal response) and comparing these to the wild-type EC_{50}, as reported (8,9,11). Briefly, 48 h after transfection, the cells were harvested, washed in calcium- and magnesium-free Hank's balanced salt solution (HBSS) (Invitrogen) and loaded with 1 μg/ml indo-1-acetoxymethylester (Indo-1-am) (Molecular Probes) for 1 h at 37 °C (8,9,11). After the removal of free dye, the cells were resuspended in calcium- and magnesium-free HBSS and maintained at 37°C. Flow cytometry was performed with a Beckman Coulter MoFlo XDP equipped with JDSUY Xcyte UV Laser and a Coherent Sapphire 488 Laser using a 550LP dichroic mirror and 580/30 bandpass filter. Single cells were isolated from debris on the basis of morphology using forward scatter and side scatter readings (8,9,11). Cells were stimulated by sequentially adding calcium to the calcium- and magnesium-free HBSS to progressively increase the $[Ca^{2+}]_o$ from 0 to 15 mM. The baseline fluorescence ratio was measured for 2 min, the fluorescence ratio compared with the time was recorded and data were collected for 2 min at each $[Ca^{2+}]_o$. Cytomation Summit software was used to determine the peak mean fluorescence ratio of the transient response after each individual stimulus expressed as a normalized response (8,9,11). Analysis of five separate populations of cells gated for increasing RFP as a concordant surrogate for increasing AP2σ2 expression was undertaken and concentration–response curves generated using the normalized response at each of nine different $[Ca^{2+}]_o$ (0–15 mM) for each separate experiment. Nonlinear regression of the concentration–response curves was performed with GraphPad Prism (GraphPad) to calculate the EC_{50} for each separate experiment (9,11). Subsequent linear regression of the mean EC_{50} ($N = 8$ experiments) for each *AP2S1*-pBI-CMV4-RFP expression vector was undertaken with GraphPad Prism (GraphPad) (9,11).

Statistical analyses

The phenotypic data from this study were pooled with those of our previous studies of FHH3 patients and families (11,20,23). To undertake a comparison of phenotypes between FHH3 and FHH1, we used data from 43 previously reported unrelated

Downloaded from http://hmg.oxfordjournals.org/ at Oxford University on September 14, 2015

FHH1 probands (13 males and 30 females, aged 1–84 years) who had germline heterozygous *CASR* mutations (8). Comparisons of continuous variables between two groups were undertaken using the Mann–Whitney *U* test, and the Kruskal–Wallis test was used to compare multiple groups. Categorical variables were analysed using the Chi-squared test. ROC analysis using values of the CMCR sensitivity and specificity was performed to study the discriminatory power of the CMCR index to distinguish between FHH1 and FHH3. Comparisons of EC_{50} values were performed using the *F* test, as described (9,11). The Mann–Whitney *U* test was used to compare the proliferation rates of cells expressing wild-type or mutant AP2σ2 proteins. All analyses were undertaken using GraphPad Prism (GraphPad) and are presented as mean ± SEM unless otherwise stated. A value of $P < 0.05$ was considered significant for all analyses.

Supplementary Material

Supplementary Material is available at *HMG* online.

Conflict of Interest statement. None declared.

Funding

This work was supported by the United Kingdom Medical Research Council (MRC) programme grants—G9825289 and G1000467 (to M.A.N., F.M.H. and R.V.T.) and National Institute for Health Research (NIHR) Oxford Biomedical Research Centre Programme (to M.A.N. and R.V.T.). S.A.H. and A.R. are Wellcome Trust Clinical Training Fellows. Funding to pay the Open Access publication charges for this article was provided by Medical Research Council (MRC), UK and Wellcome Trust Open Access Block Grants.

References

1. Hannan, F.M. and Thakker, R.V. (2013) Calcium-sensing receptor (CaSR) mutations and disorders of calcium, electrolyte and water metabolism. *Best. Pract. Res. Clin. Endocrinol. Metab.*, **27**, 359–371.
2. Marx, S.J., Spiegel, A.M., Brown, E.M., Koehler, J.O., Gardner, D. G., Brennan, M.F. and Aurbach, G.D. (1978) Divalent cation metabolism. Familial hypocalciuric hypercalcemia versus typical primary hyperparathyroidism. *Am. J. Med.*, **65**, 235–242.
3. Christensen, S.E., Nissen, P.H., Vestergaard, P., Heickendorff, L., Brixen, K. and Mosekilde, L. (2008) Discriminative power of three indices of renal calcium excretion for the distinction between familial hypocalciuric hypercalcaemia and primary hyperparathyroidism: a follow-up study on methods. *Clin. Endocrinol. (Oxf)*, **69**, 713–720.
4. Christensen, S.E., Nissen, P.H., Vestergaard, P., Heickendorff, L., Rejnmark, L., Brixen, K. and Mosekilde, L. (2008) Plasma 25-hydroxyvitamin D, 1,25-dihydroxyvitamin D, and parathyroid hormone in familial hypocalciuric hypercalcemia and primary hyperparathyroidism. *Eur. J. Endocrinol.*, **159**, 719–727.
5. Pollak, M.R., Brown, E.M., Chou, Y.H., Hebert, S.C., Marx, S.J., Steinmann, B., Levi, T., Seidman, C.E. and Seidman, J.G. (1993) Mutations in the human Ca(2+)-sensing receptor gene cause familial hypocalciuric hypercalcemia and neonatal severe hyperparathyroidism. *Cell*, **75**, 1297–1303.
6. Pearce, S.H., Trump, D., Wooding, C., Besser, G.M., Chew, S.L., Grant, D.B., Heath, D.A., Hughes, I.A., Paterson, C.R., Whyte, M.P. *et al.* (1995) Calcium-sensing receptor mutations in familial benign hypercalcemia and neonatal hyperparathyroidism. *J. Clin. Invest.*, **96**, 2683–2692.
7. Pearce, S.H., Bai, M., Quinn, S.J., Kifor, O., Brown, E.M. and Thakker, R.V. (1996) Functional characterization of calcium-sensing receptor mutations expressed in human embryonic kidney cells. *J. Clin. Invest.*, **98**, 1860–1866.
8. Hannan, F.M., Nesbit, M.A., Zhang, C., Cranston, T., Curley, A.J., Harding, B., Fratter, C., Rust, N., Christie, P.T., Turner, J.J. *et al.* (2012) Identification of 70 calcium-sensing receptor mutations in hyper- and hypo-calcaemic patients: evidence for clustering of extracellular domain mutations at calcium-binding sites. *Hum. Mol. Genet.*, **21**, 2768–2778.
9. Nesbit, M.A., Hannan, F.M., Howles, S.A., Babinsky, V.N., Head, R.A., Cranston, T., Rust, N., Hobbs, M.R., Heath, H. 3rd and Thakker, R.V. (2013) Mutations affecting G-protein subunit alpha11 in hypercalcemia and hypocalcemia. *N. Engl. J. Med.*, **368**, 2476–2486.
10. Hofer, A.M. and Brown, E.M. (2003) Extracellular calcium sensing and signalling. *Nat. Rev. Mol. Cell. Biol.*, **4**, 530–538.
11. Nesbit, M.A., Hannan, F.M., Howles, S.A., Reed, A.A., Cranston, T., Thakker, C.E., Gregory, L., Rimmer, A.J., Rust, N., Graham, U. *et al.* (2013) Mutations in AP2S1 cause familial hypocalciuric hypercalcemia type 3. *Nat. Genet.*, **45**, 93–97.
12. Fujisawa, Y., Yamaguchi, R., Satake, E., Ohtaka, K., Nakanishi, T., Ozono, K. and Ogata, T. (2013) Identification of AP2S1 mutation and effects of low calcium formula in an infant with hypercalcemia and hypercalciuria. *J. Clin. Endocrinol. Metab.*, **98**, E2022–E2027.
13. Hendy, G.N. and Cole, D.E. (2013) Ruling in a suspect: the role of AP2S1 mutations in familial hypocalciuric hypercalcemia type 3. *J. Clin. Endocrinol. Metab.*, **98**, 4666–4669.
14. Hendy, G.N., Canaff, L., Newfield, R.S., Tripto-Shkolnik, L., Wong, B.Y., Lee, B.S. and Cole, D.E. (2014) Codon Arg15 mutations of the AP2S1 gene: common occurrence in familial hypocalciuric hypercalcemia cases negative for calcium-sensing receptor (CASR) mutations. *J. Clin. Endocrinol. Metab.*, **99**, E1311–E1315.
15. Collins, B.M., McCoy, A.J., Kent, H.M., Evans, P.R. and Owen, D. J. (2002) Molecular architecture and functional model of the endocytic AP2 complex. *Cell*, **109**, 523–535.
16. Edeling, M.A., Mishra, S.K., Keyel, P.A., Steinhauser, A.L., Collins, B.M., Roth, R., Heuser, J.E., Owen, D.J. and Traub, L.M. (2006) Molecular switches involving the AP-2 beta2 appendage regulate endocytic cargo selection and clathrin coat assembly. *Dev. Cell.*, **10**, 329–342.
17. Ohno, H. (2006) Physiological roles of clathrin adaptor AP complexes: lessons from mutant animals. *J. Biochem.*, **139**, 943–948.
18. Kelly, B.T., McCoy, A.J., Spate, K., Miller, S.E., Evans, P.R., Honing, S. and Owen, D.J. (2008) A structural explanation for the binding of endocytic dileucine motifs by the AP2 complex. *Nature*, **456**, 976–979.
19. Whitcomb, D.C. (2010) Genetic aspects of pancreatitis. *Ann. Rev. Med.*, **61**, 413–424.
20. McMurtry, C.T., Schranck, F.W., Walkenhorst, D.A., Murphy, W.A., Kocher, D.B., Teitelbaum, S.L., Rupich, R.C. and Whyte, M.P. (1992) Significant developmental elevation in serum parathyroid hormone levels in a large kindred with familial benign (hypocalciuric) hypercalcemia. *Am. J. Med.*, **93**, 247–258.
21. Lloyd, S.E., Pannett, A.A., Dixon, P.H., Whyte, M.P. and Thakker, R.V. (1999) Localization of familial benign hypercalcemia, Oklahoma variant (FBHOk), to chromosome 19q13. *Am. J. Hum. Genet.*, **64**, 189–195.

Downloaded from http://hmg.oxfordjournals.org/ at Oxford University on September 14, 2015

22. Hannan, F.M., Nesbit, M.A., Turner, J.J., Stacey, J.M., Cianferotti, L., Christie, P.T., Conigrave, A.D., Whyte, M.P. and Thakker, R.V. (2010) Comparison of human chromosome 19q13 and syntenic region on mouse chromosome 7 reveals absence, in man, of 11.6 Mb containing four mouse calcium-sensing receptor-related sequences: relevance to familial benign hypocalciuric hypercalcaemia type 3. *Eur. J. Hum. Genet.*, **18**, 442–447.
23. Nesbit, M.A., Hannan, F.M., Graham, U., Whyte, M.P., Morrison, P.J., Hunter, S.J. and Thakker, R.V. (2010) Identification of a second kindred with familial hypocalciuric hypercalcemia type 3 (FHH3) narrows localization to a <3.5 megabase pair region on chromosome 19q13.3. *J. Clin. Endocrinol. Metab.*, **95**, 1947–1954.
24. Ares, G.R. and Ortiz, P.A. (2012) Dynamin2, clathrin, and lipid rafts mediate endocytosis of the apical Na/K/2Cl cotransporter NKCC2 in thick ascending limbs. *J. Biol. Chem.*, **287**, 37824–37834.
25. Christensen, S.E., Nissen, P.H., Vestergaard, P., Heickendorff, L., Rejnmark, L., Brixen, K. and Mosekilde, L. (2009) Skeletal consequences of familial hypocalciuric hypercalcaemia versus primary Hyperparathyroidism. *Clin. Endocrinol. (Oxf)*, **71**, 798–807.
26. Cole, D., Forsythe, C.R., Dooley, J.M., Grantmyre, E.B. and Salisbury, S.R. (1990) Primary neonatal hyperparathyroidism: a devastating neurodevelopmental disorder if left untreated. *J. Craniofac. Genet. Dev. Biol.*, **10**, 205–214.
27. Lee, S.H., Liu, L., Wang, Y.T. and Sheng, M. (2002) Clathrin adaptor AP2 and NSF interact with overlapping sites of GluR2 and play distinct roles in AMPA receptor trafficking and hippocampal LTD. *Neuron*, **36**, 661–674.
28. Pearce, S.H., Wooding, C., Davies, M., Tollefsen, S.E., Whyte, M.P. and Thakker, R.V. (1996) Calcium-sensing receptor mutations in familial hypocalciuric hypercalcaemia with recurrent pancreatitis. *Clin. Endocrinol. (Oxf)*, **45**, 675–680.
29. Felderbauer, P., Klein, W., Bulut, K., Ansorge, N., Dekomien, G., Werner, I., Epplen, J.T., Schmitz, F. and Schmidt, W.E. (2006) Mutations in the calcium-sensing receptor: a new genetic risk factor for chronic pancreatitis? *Scand. J. Gastroenterol.*, **41**, 343–348.
30. Mitsunari, T., Nakatsu, F., Shioda, N., Love, P.E., Grinberg, A., Bonifacino, J.S. and Ohno, H. (2005) Clathrin adaptor AP-2 is essential for early embryonal development. *Mol. Cell. Biol.*, **25**, 9318–9323.
31. Nesterov, A., Carter, R.E., Sorkina, T., Gill, G.N. and Sorkin, A. (1999) Inhibition of the receptor-binding function of clathrin adaptor protein AP-2 by dominant-negative mutant mu2 subunit and its effects on endocytosis. *EMBO*, **18**, 2489–2499.
32. Veitia, R.A. (2009) Dominant negative factors in health and disease. *J. Pathol.*, **218**, 409–418.
33. Fang, Y., Huang, C.C., Kain, S.R. and Li, X. (1999) Use of coexpressed enhanced green fluorescent protein as a marker for identifying transfected cells. *Method Enzymol.*, **302**, 207–212.
34. Leach, K., Wen, A., Davey, A.E., Sexton, P.M., Conigrave, A.D. and Christopoulos, A. (2012) Identification of molecular phenotypes and biased signaling induced by naturally occurring mutations of the human calcium-sensing receptor. *Endocrinology*, **153**, 4304–4316.

Downloaded from http://hmg.oxfordjournals.org/ at Oxford University on September 14, 2015

Cinacalcet for Symptomatic Hypercalcemia Caused by *AP2S1* Mutations

TO THE EDITOR: Familial hypocalciuric hypercalcemia is a genetically heterogeneous disorder with three variants: types 1, 2, and 3. Type 1 is caused by calcium-sensing receptor (*CASR*) mutations,[1] and type 2 is caused by guanine nucleotide–binding protein (G-protein) subunit α_{11} (*GNA11*) mutations.[2] Type 3, which is the most severe variant clinically, is caused by adaptor-related protein complex 2 (AP2), sigma 1 subunit (*AP2S1*) heterozygous mutations. *AP2S1* mutations cause Arg15Cys, Arg15His, and Arg15Leu substitutions, and the mutant AP2-sigma proteins result in impaired calcium-sensing receptor–mediated signal transduction.[3,4]

There is currently no effective therapy for familial hypocalciuric hypercalcemia type 3. We therefore evaluated the usefulness of cinacalcet, a licensed calcium-sensing receptor allosteric activator,[5] in correcting signaling defects due to *AP2S1* mutations and in ameliorating symptomatic hypercalcemia.

We evaluated three previously unreported cases of familial hypocalciuric hypercalcemia type 3. Each of the three probands had an *AP2S1* mutation causing an Arg15Cys, Arg15His, or Arg15Leu substitution (Fig. 1A). The probands included a 34-year-old woman who had a 12-year history of hypercalcemia. She presented with fatigue, headaches, and persistent generalized aches that did not resolve after parathyroidectomy. In addition, a 22-year-old man presented with hypercalcemia, fatigue, and generalized rib pain, and a 52-year-old woman who had an approximately 20-year history of hypercalcemia presented with headaches, abdominal pain, vomiting, fatigue, and musculoskeletal pain that did not resolve after pamidronate infusion or parathyroidectomy (Fig. 1A and 1B).

The in vitro effects of cinacalcet on the signaling responses of cells expressing the calcium-sensing receptor and familial hypocalciuric hypercalcemia type 3–associated AP2-sigma mutants were assessed by measurement of intracellular calcium concentrations and of the activity of the mitogen-activated protein kinase (MAPK)–serum response element reporter in response to alterations in extracellular calcium (see the Methods section in the Supplementary Appendix, available with the full text of this letter at NEJM.org). Cinacalcet (at a concentration of 10 nM) corrected the abnormal intracellular calcium signaling and MAPK responses to extracellular calcium in cells expressing the Cys15, His15, or Leu15 AP2-sigma mutants (Fig. S1 and S2 in the Supplementary Appendix).

Oral cinacalcet (at a dose of 30 to 60 mg daily) was administered to the three probands with familial hypocalciuric hypercalcemia type 3 over a 33-to-45-month period. This treatment led to more than 20% reductions in serum calcium concentrations (Fig. 1B) and abatement of symptoms. Cinacalcet also increased serum phosphate concentrations and reduced serum parathyroid hormone concentrations, although these values remained within the normal range (Fig. 1B).

Adverse effects such as nausea, vomiting, and hypocalcemia did not develop in any of the probands. However, long-term surveillance will be required to assess safety and monitor for hypocalcemia.

Our results show that cinacalcet-mediated allosteric modulation of the calcium-sensing receptor can correct the loss of function of *AP2S1* mutations. In addition, in the short term, cinacalcet can reduce the symptoms of familial hypocalciuric hypercalcemia type 3 associated with all three *AP2S1* mutations.

Figure 1 (facing page). Cinacalcet for Hypercalcemia Associated with *AP2S1* Mutations.

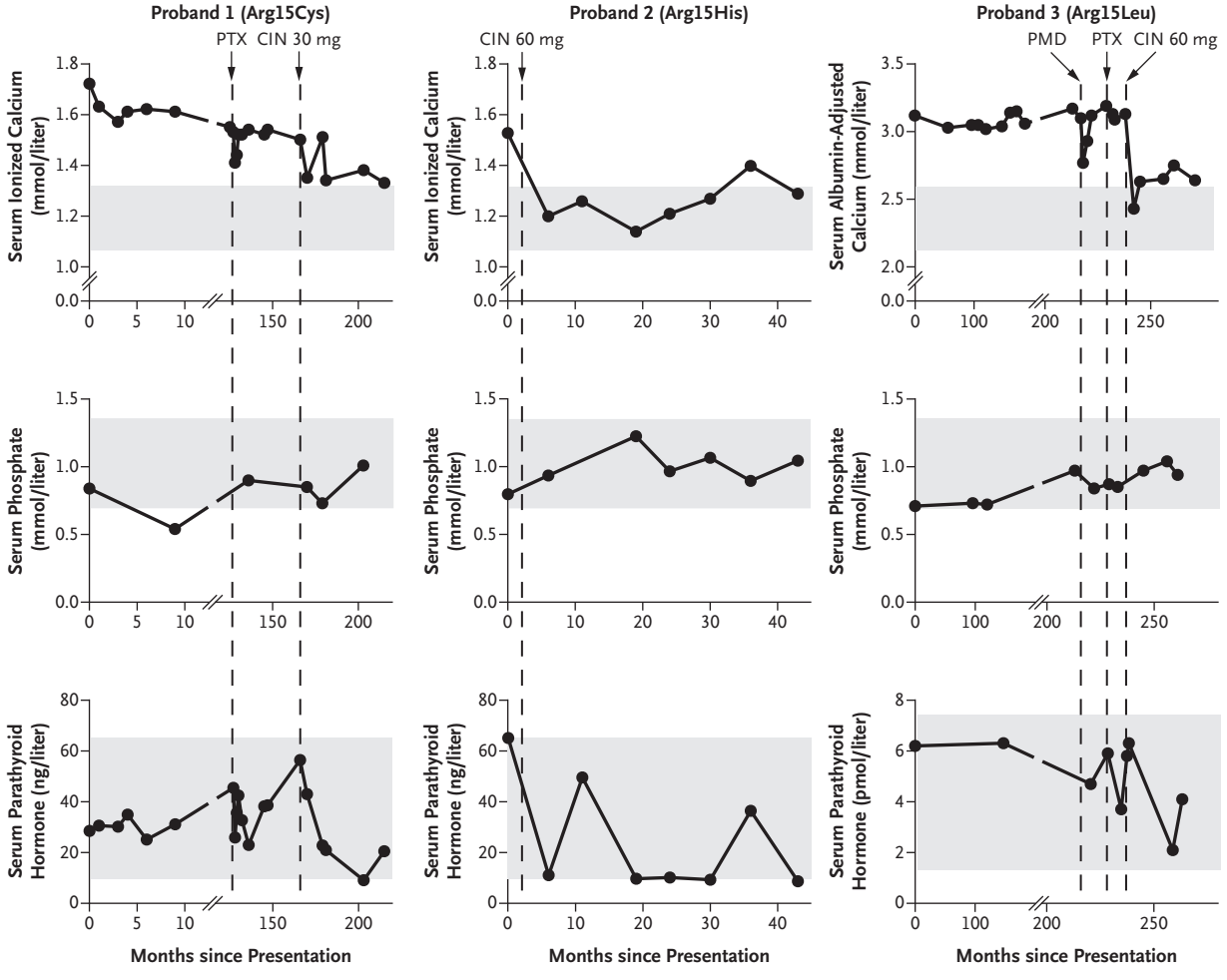
Panel A shows the clinical and biochemical findings at presentation in three unrelated probands with familial hypocalciuric hypercalcemia who had heterozygous adaptor-related protein complex 2 (AP2), sigma 1 subunit (*AP2S1*) mutations resulting in Arg15Cys, Arg15His, or Arg15Leu substitutions in the AP2-sigma mutant proteins. Reference ranges are from Nesbit et al.[2] Panel B shows the effect of cinacalcet on serum concentrations of calcium, phosphate, and parathyroid hormone in the three probands. Vertical dashed lines indicate initiation of cinacalcet (CIN) therapy, pamidronate (PMD) infusion, or parathyroidectomy (PTX). Shaded gray areas indicate reference ranges.

The New England Journal of Medicine
Downloaded from nejm.org at the Bodleian Libraries of the University of Oxford on May 4, 2016. For personal use only. No other uses without permission.
Copyright © 2016 Massachusetts Medical Society. All rights reserved.

A

Variable	Reference Range	Proband 1	Proband 2	Proband 3
Sex		Female	Male	Female
Age at presentation — yr		22	22	32
Family history of hypercalcemia		Yes	Yes	No
Associated clinical features		Fatigue, headaches, generalized musculoskeletal pain	Fatigue, rib pain	Fatigue, headaches, vomiting, abdominal and musculoskeletal pain
Serum measurements				
Calcium — mmol/liter				
Ionized	1.10–1.30	1.72	1.53	—
Albumin-adjusted	2.10–2.60	—	—	3.07
Phosphate — mmol/liter	0.70–1.40	1.00	0.80	0.95
Alkaline phosphatase				
Total — U/liter	30–130	55.0	—	81.0
Bone-specific — μg/liter	3.7–20.9	—	20.6	—
Magnesium — mmol/liter	0.70–1.40	0.97	—	0.98
Parathyroid hormone				
Base units	10–65 ng/liter	28.5	65.1	—
SI units	1.3–7.6 pmol/liter	—	—	6.2
Urinary calcium-to-creatinine clearance ratio	>0.02	0.001	0.002	0.001
AP2S1 mutation		Arg15Cys	Arg15His	Arg15Leu

B



The New England Journal of Medicine
Downloaded from nejm.org at the Bodleian Libraries of the University of Oxford on May 4, 2016. For personal use only. No other uses without permission.
Copyright © 2016 Massachusetts Medical Society. All rights reserved.

Sarah A. Howles, D.Phil.
Fadil M. Hannan, D.Phil.
Valerie N. Babinsky, D.Phil.
Angela Rogers, M.B., B.S.
Caroline M. Gorvin, D.Phil.
Nigel Rust, B.Sc.

University of Oxford
Oxford, United Kingdom

Tristan Richardson, M.B., B.S.

Royal Bournemouth Hospital
Bournemouth, United Kingdom

Malachi J. McKenna, M.D.

St. Vincent's University Hospital
Dublin, Ireland

M. Andrew Nesbit, Ph.D.
Rajesh V. Thakker, M.D.

University of Oxford
Oxford, United Kingdom
rajesh.thakker@ndm.ox.ac.uk

Drs. Howles and Hannan contributed equally to this letter.

A complete list of authors is available with the full text of this letter at NEJM.org.

Supported by program grants (G9825289 and G1000467, to Drs. Hannan, Gorvin, Nesbit, and Thakker) from the United Kingdom Medical Research Council, a grant (to Drs. Nesbit and Thakker) from the National Institute for Health Research (NIHR) Oxford Biomedical Research Centre Programme, a grant (FP7-264663, to Dr. Babinsky) from the European Commission Seventh Framework Program, Wellcome Trust clinical training fellowships (to Drs. Howles and Rogers), a Wellcome Trust Investigator Award (to Dr. Thakker), and an NIHR Senior Investigator Award (to Dr. Thakker).

Disclosure forms provided by the authors are available with the full text of this letter at NEJM.org.

1. Hannan FM, Nesbit MA, Zhang C, et al. Identification of 70 calcium-sensing receptor mutations in hyper- and hypo-calcaemic patients: evidence for clustering of extracellular domain mutations at calcium-binding sites. Hum Mol Genet 2012;21:2768-78.
2. Nesbit MA, Hannan FM, Howles SA, et al. Mutations affecting G-protein subunit α11 in hypercalcemia and hypocalcemia. N Engl J Med 2013;368:2476-86.
3. Nesbit MA, Hannan FM, Howles SA, et al. Mutations in AP2S1 cause familial hypocalciuric hypercalcemia type 3. Nat Genet 2013;45:93-7.
4. Hannan FM, Howles SA, Rogers A, et al. Adaptor protein-2 sigma subunit mutations causing familial hypocalciuric hypercalcaemia type 3 (FHH3) demonstrate genotype-phenotype correlations, codon bias and dominant-negative effects. Hum Mol Genet 2015;24:5079-92.
5. Nemeth EF, Shoback D. Calcimimetic and calcilytic drugs for treating bone and mineral-related disorders. Best Pract Res Clin Endocrinol Metab 2013;27:373-84.

DOI: 10.1056/NEJMc1511646
Correspondence Copyright © 2015 Massachusetts Medical Society.

The New England Journal of Medicine
Downloaded from nejm.org at the Bodleian Libraries of the University of Oxford on May 4, 2016. For personal use only. No other uses without permission.
Copyright © 2016 Massachusetts Medical Society. All rights reserved.